Geochemistry of Gold One tailings and associated contaminant transport into the Randfontein area, Witwatersrand Basin.

By

Jamie-Leigh Robin Abrahams

A thesis submitted in partial fulfillment of the requirements for the degree of Master of Science in Applied Geology in the Department of Earth Science, University of the Western Cape.

Supervisor: Prof. C. Okujeni November 2017

Declaration

I declare that "***Geochemistry of Gold One tailings and associated contaminant transport into the Randfontein area, Witwatersrand Basin."*** is my own work, that it has not been submitted for any degree or examination at any other university and that all the sources I have used have been indicated and acknowledged in complete references.

……...
Jamie-Leigh Robin Abrahams

November 2017

Abstract

The city of Randfontein, in the Witwatersrand, hosts several slimes and tailings storage facilities which pose potential threat to the environment in the form of acid mine drainage (AMD). The latter, readily scavenges toxic metals, contaminating surrounding soils and water resources, thereby potentially compromising the overall environmental- and public health of the area. To this end, three slimes sections (section T001, T002 and T003) from the Gold One Millsite Slimes Complex were investigated, with the aim of understanding metal release from the slimes dam into the Randfontein area. To achieve this, the mineralogical and geochemical factors controlling metal release were investigated using combined core log analysis, cluster and discriminant analysis, x-ray diffraction analysis, bulk geochemical analysis, acid base accounting methods and selective sequential extraction procedures.

This study distinguished three weathering zones, namely a 2.2 meter thick oxidized zone (comprised of upper pale fine sands and lower Fe-mottled fine sands), 1 – 5 meter thick transition zone (comprised of pale red-brown fine sands) and 2 – 4 meter thick reduced zone (comprised of grey fine sands). The slimes mineralogy was found to consist of mainly high quartz (especially dominant in the upper oxidized zone) and minor pyrophyllite-, pyrite-, chlinochlore-, gypsum- and yoshiokaite proportions. Major- and trace element concentrations were notably subdued in the upper oxidized zone of the slimes dam and enriched in the lower oxidized- and reduced zone. The former, is attributed to the flushing/leaching of elements by infiltrating rainwater in the upper oxidized zone while the latter, is the result of metal adsorption to oxides in the reduced zone.

Of the slimes sections investigated, section T003 was determined as the least weathered, showing the highest pyrite contents (approximately 0.42 – 0.64 %) and the earliest onset of grey (reduced) fine sands. Section T001 was determined the most oxidized, showing the lowest pyrite contents (approximately 0.12 – 0.13 %) and lowest overall major- oxide and metal contents. It was noted that the weathering zones (pH) have significant impact on the release of metals as they increased mobility in the oxidized- and transition zones while they showed poor mobility in the reduced zone. As was the case with pH, reactive sulphur (sulphide-sulphur) was found to play a

significant role in metal mobilization, even for metals traditionally considered fairly immobile (Zn, Pb and Au). Using calculated sulphide-sulphur, acid base accounting characterized the slimes dam as largely acid-generating, hosting non-acid generating samples only within the upper oxidized zone. These findings showed good correlation with near undetectable sulphide-sulphur in the upper oxidized zone. Subdued sulphide-sulphur is expected at this depth since the environment is highly oxidizing. Of the metals leached by selective sequential extraction, Ni, Cu, Co and Zn showed the highest concentrations (approximately11 ppm, 5 ppm, 4 ppm and 3 ppm, respectively) yielded in water-soluble, exchangeable and acid soluble phases. This suggests that Ni, Cu, Co and Zn can be easily mobilized by infiltrating rainwater and by the lowering of pH. The results of this study characterize the source- and patterns of heavy metal release in the Gold One Millsite Slimes Complex and show that acid base accounting methods and sequential extraction procedures can be used to assist in the preliminary prediction of AMD generation and monitor the behaviour of metals in response to reclamation efforts.

Keywords: acid mine drainage; acid generating potential; sequential extraction procedures

Acknowledgements

Above all, I would thank the Lord Jesus for having seen me through the past two years, allowing me to deliver this dissertation.

Furthermore, I owe many thanks to the people who have helped me during the completion of my thesis.

- To my supervisor, Prof. Charles Okujeni, thank you for your excellent guidance and countless hours spent reviewing my work.
- To my co-supervisor, Dr. Abdi Siad, thank you for assisting me where you could.
- To my colleagues, Mr. Oluseyi Abegunde and Mrs. Iris Wu, thank you for welcoming me on this project and allowing me to make use of your data. Thank you for your efforts in the laboratory and for having provided me with extra literature.
- To Mr. Adrian Williams, thank you for having analyzed my data and for your constant willingness to assist me during the compilation of this thesis. Your attention to detail in the laboratory has helped me produce work I am proud of.
- To Mr. Tshipeng Mwenze, thank you for accommodating me in your busy schedule and always being available for extra assistance and advice.
- To Mrs. Yafay Williams, thank you for your constant willingness to assist wherever possible.
- To Ms. Janine Becorney, thank you for your assistance in the geochemical laboratory.
- To Mr. Peter Meyer, thank you for having assisted me in the production of my thin sections. Thank you for having allowed me into the laboratory with you to gain some hands-on experience.
- Lastly, to the Abrahams family, and friends, thank you for all your prayers, love and support during the past two years. All of your encouragements have made the submission of this thesis possible. Thank you!

List of Figures

List of Tables

Table of Contents

CHAPTER ONE: Introduction

The old gold mining district of Randfontein in the Witwatersrand, hosts a number of tailings and slimes storage facilities. Tailings and slimes dams pose potential threat to the environment in the form of acid mine drainage. Acid mine drainage forms largely as a result of pyrite oxidation and is typically sourced from tailings and slimes produced during the mining process. Heavy metals are readily mobilized under the acidic conditions and migrate from tailings into surrounding soils, groundwater, and streams draining the area (McGowen and Basta, 2001). In terms of environmental impact, the mobilization of excessive heavy metal concentrations seemingly poses greater threat than the acidity (Kleinman, 1990; Fyson et al., 1994; Clarke, 1996; Kuyucak, 2002; Filipek et al., 2003) and as a result, may contaminate soils and water resources, thereby threatening the overall environmental- and socio-economic wellbeing of the area.

Gold in the Witwatersrand was first discovered during 1886, in the conglomerates of the Witwatersrand Supergroup (Robb & Robb, 1998). Mineral processing of the auriferous conglomerate rock typically involved reduction in mineral sizes and subsequent separation of individual minerals. During the first stage of mineral processing, blocks of hard Au ore, nearly one meter in diameter, are reduced to only a few millimeters or even microns in size (Lottermoser, 2013). To achieve this, the ore is first crushed then put through a process of grinding and milling. The process of crushing is a dry one while the grinding process, requires abrasion of water suspended particles. The goal of size reduction is to break down the Au ore enough as to release ore minerals from the gangue phases (Lottermoser, 2013).

The second stage of mineral processing involves the separation of ore minerals from the gangue minerals. Several methods may be employed during this stage and typically include the use of specific gravimetric-, electric-, magnetic- and surface properties of the ore and gangue phases. As a result, the end-products of ore processing are (i) a concentrate of the valuable commodity and (ii) a quantity of residual wastes, termed tailings or slimes (Lottermoser, 2013). In general, the residual wastes are mixed with process water and discharged into dams as coarse-grained (> 63 μm) sediment-water slurries termed tailings dams or fine-grained (< 63 μm) sediment-water

slurries termed slimes dams (Bosch, 1987). Slimes dams are generally comprised of very fine-grained material and as a result are often highly compacted (Bosch, 1987).

In the mining of metal ores, only a minor fraction of the entire rock mass is represented by the liberated ore minerals, while the remaining mined material is deposited on the surface as tailings or slimes (Lottermoser, 2013). These surface deposits may comprise up to 99 % of the originally mined material. Since the recovery of 100 % of the mined ore is near impossible, tailings and slimes potentially host minor quantities of valuable ore along with elevated heavy metal concentrations. The latter, is often susceptible to leaching by surface- and groundwater (Caboi et al., 1993; Fanfani et al., 1997; He et al., 2005). In general, the mineralogy of tailings and slimes is dominated by ground gangue minerals from which most of the valuable ore has been extracted (Lottermoser, 2013). Remnant solids typically consist of silicate-, carbonate-, oxide-, hydroxide- and sulphide minerals (Lottermoser, 2013). Minor sulphide mineral concentrations occur in nearly all tailings and slimes deposits (Dold, 2005).

Overtime, tailings and slimes deposits become complex hydrogeological environments and as a result, facilitate several sulphide-related weathering reactions (Table 1, after Kleinmann et al., 1981; Nordstrom, 1982; Blowes and Ptacek, 1994; Nordstrom and Alpers, 1999; Plumlee, 1999; White et al., 1999; Bigham and Nordstrom, 2000). Of these, the oxidation of sulphide minerals (primarily pyrite) is of the greatest environmental concern (Heikkinen, 2009). Sulphide minerals occur as MS_2 varieties such as pyrite and MS varieties such as chalcocite (Cu_2S), covellite (CuS), galena (PbS) and sphalerite (ZnS). MS_2 and MS sulphides react differently when exposed to the atmosphere (Eby, 2004). While the hydrolysis of MS sulphides may release H^+ ions into solution, its impact on overall acidity is minor compared to that generated by MS_2 sulphides (pyrite) when undergoing oxidation (Eby, 2004). When exposed to air and water, MS_2 sulphide minerals such as pyrite oxidize to form sulphuric acid.

Table 1: A summary of the key chemical reactions associated with sulphide weathering in tailing/slimes, compiled by Heikkinen, 2009 (after Kleinmann et al., 1981; Nordstrom, 1982; Blowes and Ptacek, 1994; Nordstrom and Alpers, 1999; Plumlee, 1999; White et al., 1999; Bigham and Nordstrom, 2000).

Reaction	Reaction formula
Sulphide oxidation	Pyrite: $FeS_{2(s)} + 7/2O_{2(g)} + H_2O_{(l)} \rightarrow Fe^{2+}{}_{(aq)} + 2SO_4^{2-}{}_{(aq)} + 2H^+{}_{(aq)}$
	Pyrite: $FeS_{2(s)} + 14Fe^{3+}{}_{(aq)} + 8H_2O_{(aq)} \rightarrow 15Fe^{2+}(aq) + 2SO_4^{2-}{}_{(aq)} + 16H^+{}_{(aq)}$ (pH < 4.5)
	Overall reactions of pyrite oxidation:
	$FeS_{2(s)} + 15/4O_{2(g)} + 7/2H_2O_{(l)} \rightarrow Fe(OH)_{3(s)} + 2H_2SO_{4(aq)}$
Oxidation of Fe(II)	$Fe^{2+}{}_{(aq)} + 1/4O_{2(g)} + H^+{}_{(aq)} \rightarrow Fe^{3+}{}_{(aq)} + 1/2H_2O_{(l)}$
Hydrolysis of Al and Fe; precipitation of secondary Fe minerals	$Al^{3+}{}_{(aq)} + H_2O_{(l)} \leftrightarrow Al(OH)^{2+}{}_{(aq)} + H^+{}_{(aq)}$
	Amorphous Fe hydroxide: $Fe^{3+}{}_{(aq)} + 3H_2O_{(l)} \leftrightarrow Fe(OH)_{3(s)} + 3H^+{}_{(aq)}$
	Goethite: $Fe_{3+(aq)} + 2H_2O_{(l)} \rightarrow FeOOH(s) + 3H^+{}_{(aq)}$
	Jarosite: $3Fe^{3+}{}_{(aq)} + K^+{}_{(aq)} + 2SO_4^{2-}{}_{(aq)} + 6H_2O_{(l)} \rightarrow KFe_3(SO_4)_2(OH)_{6(s)} + 6H^+{}_{(aq)}$
	Schwertmannite: $8Fe^{3+}{}_{(aq)} + SO_4^{2-}{}_{(aq)} + 14H_2O_{(l)} \rightarrow Fe_8O_8(OH)_6(SO_4)_{(s)} + 22H^+{}_{(aq)}$
Carbonate dissolution	Calcite: $CaCO_{3\,(s)} + H^+{}_{(aq)} \leftrightarrow Ca^{2+}{}_{(aq)} + HCO_3^-{}_{(aq)}$
	Dolomite: $CaMg(CO_3)_{2(s)} + 2H^+{}_{(aq)} \leftrightarrow Ca^{2+}{}_{(aq)} + Mg^{2+}{}_{(aq)} + 2HCO_3^-{}_{(aq)}$
Silicate dissolution/hydrolysis	Olivine: $Mg_2SiO_{4(s)} + 4H^+{}_{(aq)} \rightarrow Mg^{2+}{}_{(aq)} + H_4SiO_{4(aq)}$
	Anorthite: $CaAl_2Si_2O_{8(s)} + 2H^+{}_{(aq)} + H_2O \rightarrow Ca^{2+}{}_{(aq)} + Al_2Si_2O_5(OH)_{4(s)}$
	K-feldspar: $KAlSi_3O_{8(s)} + 4H^+{}_{(aq)} + 4H_2O_{(l)} \leftrightarrow Al^{3+}{}_{(aq)} + 3Si(OH)_{4(aq)} + K^+{}_{(aq)}$

Singer and Strumm (1970) suggested that the complex reaction of pyrite oxidation can be represented by the following reactions:

$$FeS_2 + 7/2\ O_2 + H_2O \rightarrow Fe^{2+} + 2\ SO_4^{2-} + 2\ H^+ \text{..... (1)}$$

Liberated Fe^{2+}, SO_4^{2-} and H^+ ions are representative of enhanced total dissolved salt and acidity and thus, lowered pH. Under strongly oxidizing conditions, ferrous iron (Fe^{2+}) is largely oxidized to form ferric iron (Fe^{3+}):

$$Fe^{2+} + ¼\ O_2 + H^+ \rightarrow Fe^{3+} + ½\ H_2O \text{..... (2)}$$

Reaction 2 is rate-determining and is influenced by bacterial activity, available oxygen and pH. When pH values in excess of 2.3 – 3.5 are encountered, the ferric iron undergoes precicipitation to form Fe $(OH)_3$. Consequently, Fe^{2+} is largely removed from solution and the pH decreased:

$$Fe^{3+} + 3\ H_2O \rightarrow Fe\ (OH)_3 + 3\ H^+ \ldots\ldots\ldots\ldots\ldots\ldots\ldots\ldots\ (3)$$

Any remaining Fe^{3+} in reaction (2), not precipitated in reaction (3) may contribute to the oxidation of additional pyrite:

$$FeS_2 + 14\ Fe^{3+} + 8\ H_2O \rightarrow 15\ Fe^{2+} + 2\ SO_4^{2-} + 16\ H^+ \ldots.(4)$$

Thus, based on reactions one through three, one mole of pyrite produces four moles of protons. Accompanying the release of these protons, is the production of iron precipitated as $Fe(OH)_3$ i.e. Yellow Boy.

Under typical weathering conditions, sulphide-rich minerals such as pyrite produce acid at a slow enough rate to be readily removed by natural neutralization processes (McCarthy, 2011). However, the extensive fragmentation of rock resulting from mining increases the surface area and thereby increases the overall rate at which acid is produced (McCarthy, 2011). Consequently, as rain falls, sulphuric acid percolates through tailings and slimes dumps, scavenging heavy metals (together with uranium) and ultimately surfaces from the base of the dump where it forms contamination plumes upon meeting with the local groundwater system (McCarthy, 2011). This contaminated water eventually surfaces in the rivers draining the surrounding areas. As a result, the rivers draining tailings/slimes dumps are typically characterized as highly acidic, containing high-sulphate and heavy metal concentrations (McCarthy, 2011). In surrounding soils, heavy metals may accumulate in various geochemical phases. These phases include water-soluble-, exchangeable-, carbonate-bound, Fe-Mn oxide-bound and residual forms (Tessier et al, 1979). Bioavailable phases include water-soluble and exchangeable forms and potentially, oxide-, carbonate- and organic-matter-associated forms; while residual forms are considered non-bioavailable (Pickering, 1986). Bioavailable phases are significant in their influence on heavy metal uptake by plants and groundwater contamination (Pickering, 1986).

To address metal fractionation in soils, various sequential extraction procedures (SEPs) have been developed (Tessier et al, 1979; Clevenger, 1990; El-Demerdashe et al., 1995; McGrath and

Cegarra, 1992) and in recent decades, have been applied to contaminated mine soils (McGregor et al., 1995; Fanfani et al., 1997; McCarthy et al., 1998, Dold, 1999; Leinz et al., 1999, 2000; Dold and Fonbote, 2001; Dold and Fonbote, 2002; Dold, 2003 and Favas et al., 2011). Sequential extraction methods typically make use of a series of digestants, each designed to extract a specific bonding form, thereby liberating the proportion of metals in that bonding form (Zachmann and Block, 1994). In doing so, sequential extraction procedures can provide an understanding of metal mobility, retention and bioavailability in mine contaminated soils, proving useful in acid mine drainage studies.

The subject of acid mine drainage is fairly well-studied in South Africa, with primary focus on environmental impact (Marsden, 1986; Rosner and Schalkwyk, 2000; Naicker et al. 2003) and the development of new and advanced remediation techniques (James, 1966; Groves, 1974; Blight, 1984; Molden and Merrey, 2002; Mphephu and Viljoen, 2002; Van de Venter, 2002; Adler and Rascher, 2007 and Iliso Consulting Ltd., 2008). While remediation studies offer useful treatment methods, not many have investigated the mineralogical and geochemical interactions in tailings or slimes dams in South Africa (Sami and Druczinski, 2003; Bezuidenhout and Rousseau, 2006). Such investigations, according to Dold (2005), are crucial to understanding the factors influencing contaminant distribution in tailings/slimes and the subsequent development of preventative techniques. To this end, the aim of this study was to understand heavy metal release from the Gold One Millsite Slimes Complex into the Randfontein area, in the Witwatersrand, by investigating the mineralogical and geochemical factors influencing metal release.

1.1 Research Aim and Objectives

As stated earlier, the aim of this study was to understand heavy metal release from the Gold One Millsite Slimes Complex into the Randfontein area, Witwatersrand. To fulfill the research aim, the objectives of this study were as follows:

- To assess the influence of mineralogical factors on heavy metal release through core-log reappraisal and the description of trends in x-ray diffraction data.

- To assess the influence of geochemical factors on metal release by describing trends in the bulk geochemical data.
- To determine and model the weathering zones using cluster and discriminant analysis.
- To determine sulphide-sulphur (wt %) and its potential influence on metal mobilization.
- To predict the acid generating potential of slimes samples using the calculated sulphide-sulphur (wt %).
- To determine the leachability of metals using selective sequential extraction.

1.2 Location site

The study site (Fig. 1.1) for this project is the Gold One Millsite Slime Complex (MSC) in Randfontein, Witwatersrand. The Millsite complex together with four other tailings/slimes dams namely, Dump 20 Slimes, Old 4 Tailings, Lindum slimes and Cooke tailings storage facilities form part of the Cooke Surface Operation. The Gold One Millsite Slime Complex (MSC) is situated close to the Krugersdorp Game Reserve and the central business district (CBD) of Randfontein.

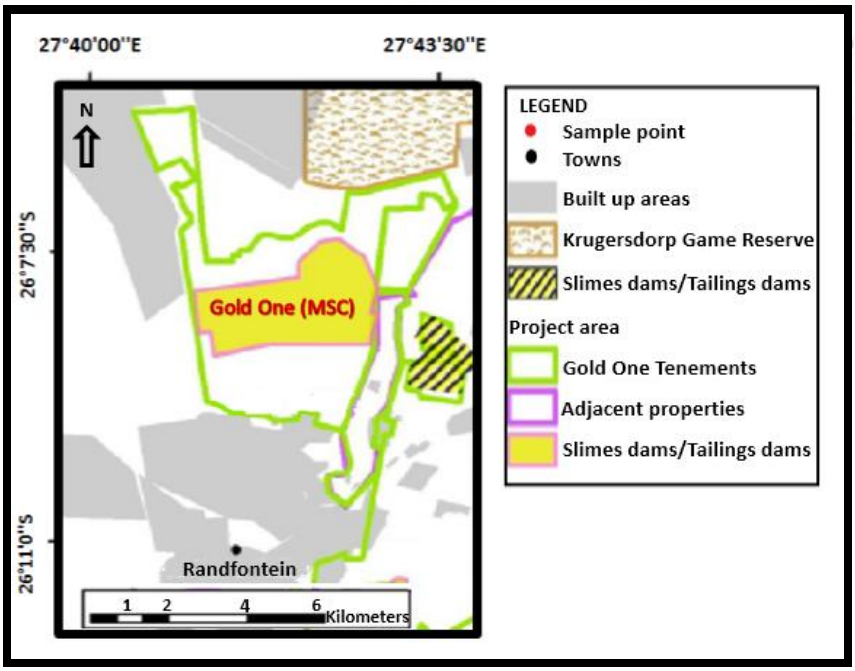

Figure 1. 1: A location map of the Gold One Millsite slimes complex study area

1.2.1 Accessibility and Infrastructure

The project area was very well serviced by the infrastructure within the borders of Randfontein City. Situated between the Millsite Slime Complex and Cooke TSF (tailings storage facility), is the Central Business District (CBD) of Randfontein. Potable water, necessary for operations, was supplied to the site by the municipality of Randfontein. Operations were powered by Eskom (WRDM, 2014).

1.2.2 Climate and rainfall

The Randfontein climate is characterized as mild, and typically warm and temperate (WRDM, 2014). Average midday temperatures in Randfontein may be as low as 16.3 °C in June and reach a high of 26.3 °C in January (Fig. 1.2). The region experiences the lowest temperatures in July, where the average evening temperature plummets to 0.1 °C. The area of Randfontein receives an average of 742 mm of rain per annum, most of which occurs as thunderstorms during the summer months (Fig. 1.2). The lowest rainfall (7 mm) is typically recorded in August and the highest (139 mm) during the month of January (WRDM, 2014).

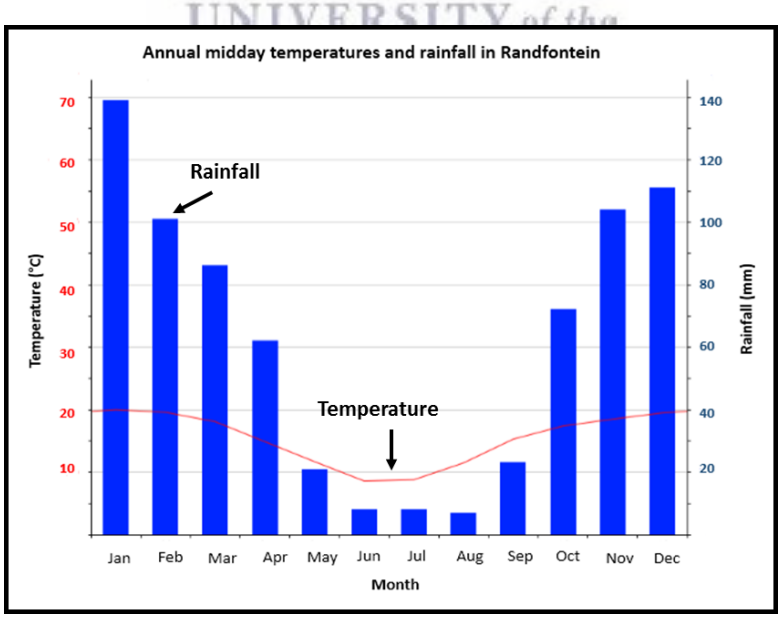

Figure 1. 2: A bar graph showing average annual rainfall and midday temperatures in the city of Randfontein.

1.2.3 Physiography (vegetation and elevation)

The topography of Randfontein is typified by moderately undulated plains and the regions natural vegetation, savannah grassland. The elevation of the project area is between approximately 1600 and 1660m above mean sea level (WRDM, 2014).

1.3. History of the Cooke section and associated Cooke Surface Operations (CSOs)

One of the first mines established in the Witwatersrand was the Randfontein Mine (1886), operated by Randfontein Estates Gold Mining Company Ltd (REGM). The mid 1970's saw the establishment of the Cooke section (section 1 – 3) and Cooke Surface Operation (CSO), as a section of the Randfontein Estates Mine (Yaldywn et al., 2013).

The Cooke section is subdivided into three individual areas, namely Cooke 1, Cooke 2 and Cooke 3, all of which are accompanied by a shaft and necessary underground infrastructure (Yaldywn et al., 2013). In 1973, Cooke 1 commenced underground production, reaching full production in March of the following year. The shaft sinking of Cooke 2 began in January of that same year (1974), with production commencing in 1977. In June 1981, the shaft sinking of Cooke 3 began. Production of the shaft began in 1983 and sunk to approximately 1373 m beneath collar. REGM sold the Cooke (1-3) section to Pamodzi and Harmony Gold Mining Company Ltd, through an established Special Purpose Vehicle (SPV), called Rand Uranium, in December 2007 (Yaldywn et al., 2013). As a result, Harmony owned 40 % of Rand Uranium and the Pamodzi Resources Fund, 60%. In December 2007, through an established SPV, Newshelf 1114 (Pty) Ltd, Gold One bought 100% of Rand Uranium from Pamodzi and Harmony (Yaldywn et al., 2013).

The Cooke Surface Operation (CSO) was established in 1976, as an advanced gold and uranium exploration project located in the vicinity of Randfontein in South Africa, and includes a gold plant for the treatment of approximately 300 ktpm of tailings (Van Zyl et al, 2013). The Cooke Surface assets are located close to processing plants treating ore from the original Randfontein Estates Gold Mine and are owned by Gold One. CSO comprises of five tailings/slimes storage

facilities namely, Dump 20, the Millsite slimes complex, the Old tailings 4, the Lindum tailings and the Cooke tailings (Fig. 1.3).

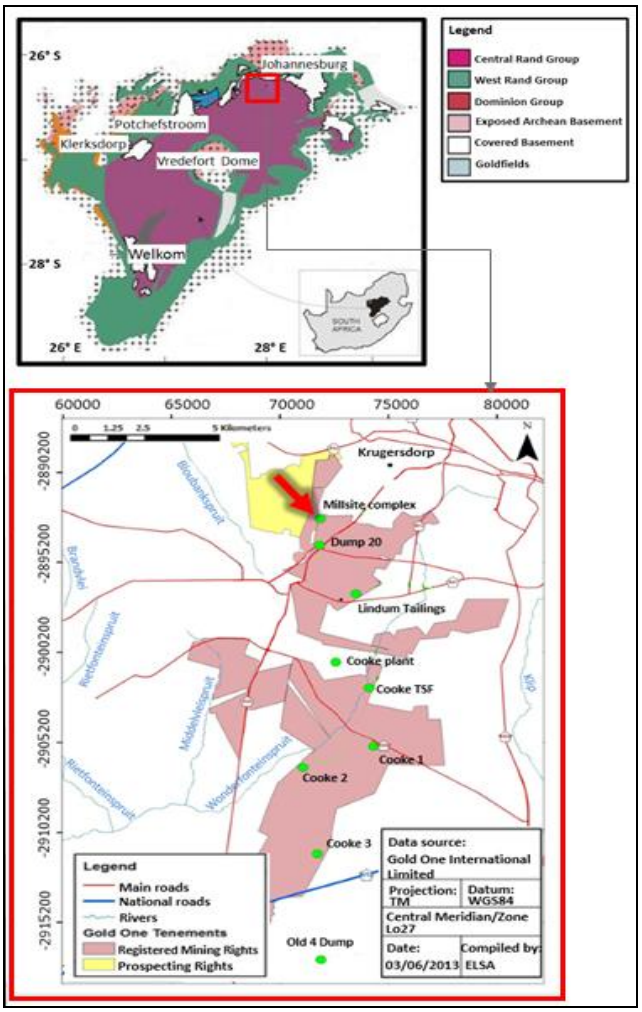

Figure 1. 3: A location map of Gold One tenements at Cooke mining operations which include Dump 20, the Millsite slimes complex (study site), Old 4 tailings, Lindum tailings, Cooke section (1-3) and Cooke TFS.

1.3.1 Dump 20 slime and sand

During the 1890's, Dump 20 Slimes formed in response the pumping of residual slime material, from the original Millsite plant, into the nearby Rietpan. Dump 20 Sand formed due to the stamp milling technology employed at the Millsite Gold Plant. In 1911, the latter was commissioned

(Van Zyl et al, 2013). Tailings Dam 20 was formed when the battery of stamp mills proved ineffective in finely grinding the ore for further exploitation of contained gold. Dump 20 (slime and sand) is processed by the Randfontein Surface Operations, generally at a rate of 300 000 tpm and generates approximately 32 000 ounces annually (Van Zyl et al, 2013).

1.3.2 The Millsite Slime Complex (Study site for this project)

In 1920's, the Millsite Slime Complex (MSC) was established from mining activities on the Main reefs amongst others in the Old Randfontein sections (Van Zyl et al, 2013). These occur north of the Witpoortjie fault.

1.3.3 The Old 4 Tailings

Old 4 Tailings ("Dump 4") was formed from mining activities on the Venterdorp Contact Reef, Upper Elsburg reefs and Middle Elsburg reefs (Van Zyl et al, 2013). The latter, is found in the northern portions of the old Western Areas Gold mine.

1.3.4 The Lindum Tailings

In the early 1900s, the Lindum slimes dams were established from the mining of the Main Reef conglomerates (Van Zyl et al, 2013). The conglomerates are situated in the southern sections of Randfontein Estates. In the mid-1990s, further mining of the Lindum Reefs Mine resulted in the deposition of additional material onto the Lindum site (Van Zyl et al, 2013).

1.3.5 The Cooke tailings

The Cooke tailings ("TFS") was established in 1976 from the extensive mining of the Elsburg reefs in the vicinity of the Cooke shafts, all of which were rich carriers of uranium (Van Zyl et al, 2013).

Since some of the reefs are gold and uranium-rich, it stands that tailings and slimes storage facilities serve as residual sources of minor economically viable gold and uranium concentrations. Thus, deeming these deposits potentially profitable acquisitions.

CHAPTER TWO: Geological Setting

2.1 Regional setting of the Witwatersrand Basin

The Witwatersrand Basin (Fig. 2.1) is a sedimentary basin located within the central region of the Archean Kaapvaal craton (Pretorius, 1974). The basin is approximately 350 kilometers in length and 200 kilometers in width and is comprised of mainly arenaceous, argillaceous, and minor rudaceous units (Pretorius, 1974). The oldest rocks of the Witwatersrand basin are Archean basement rocks. The Archean basement is overlain by rock from the Dominion Group. Overlying the Dominion Group is the Witwatersrand Supergroup (Pretorius, 1974). The Witwatersrand Supergroup consists of approximately 7400 m of sediments. Stratigraphically, the Witwatersrand Supergroup consists of two separate groups: an upper quartzite and conglomerate- dominated Central Rand Group and a lower shale-dominated West Rand Group (Pretorius, 1974).

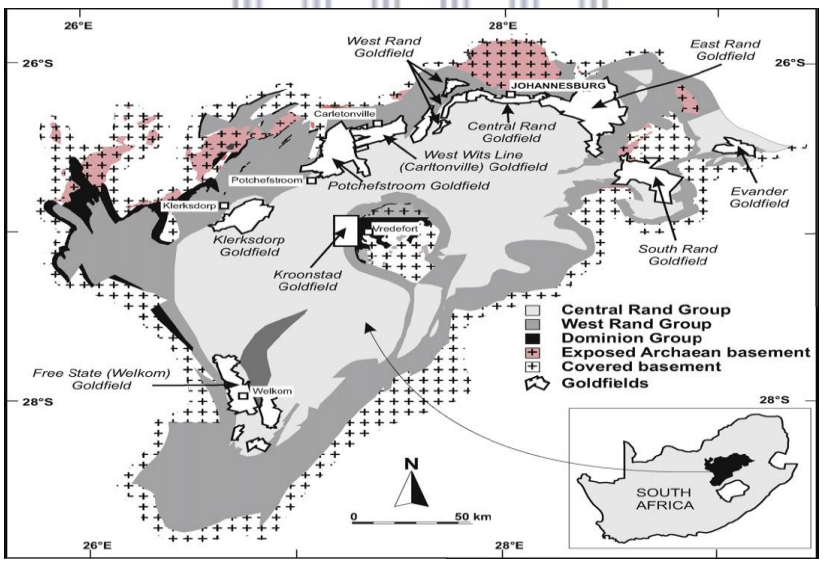

Figure 2. 1: A schematic geological map of the Witwatersrand Basin with the Ventersdorp Supergroup, Transvaal Basin sequences and Karoo Supergroup cover removed (modified after Pretorius et al., 1986), the distribution of Archean basement and location of goldfields after (Pretorius et al., 1986).

2.1.1 Geology

U-Pb dating techniques employed by Kositcin and Krapez (2004) date the Witwatersrand basin as Archean, having developed between ca. 2985 and 2849 Ma. Deposition of the underlying Dominion took place over a relatively short period, between 3086 +- 3 Ma (the approximate age of the underlying Westerdam granite) and 3074 +- 6 Ma (U-Pb detrital zircon SHRIMP), the approximate age of lavas underlain by Dominion sediments ca. (Myers et al., 1989). Detrital zircon and monzanite grains obtained from the Dominion Reef provide the maximum age of deposition, between 3191 and 3105 Ma (Robb & Meyer, 1995). The minimum age of the overlying West Rand is given by the Crown lava beneath the West Rand–Central Rand transition, dated at 2914 +- 8 Ma.

The maximum age was determined by detrital grains extracted from the Orange Grove quartzite and Promise Reef occurring in the West Rand Group. Successive deposition of the Central Rand was initiated prior to 2914 Ma, following the extrusion of the Crown lava and may have commenced as late as 2894 Ma, at which the youngest detrital zircon grain obtained from the Elsburg reef is dated. Separating the upper portion of Central Rand from the overlying Ventersdorp Supergroup (ca. 2.72 – 2.63 Ga), is the Ventersdorp Contact Reef belonging to the larger Venterspost Formation (ca. 2729 +- 19 Ma; Kositcin and Krapez, 2004; U-Pb detrital zircon SHRIMP). The Black Reef Formation marks the onset of the overlying Transvaal Supergroup (ca. 2588 +- 6 Ma; Jolley et al., 2004; Krapez, 1985; Vos, 1975). The Tranvaal Supergroup is in turn overlain by sequences of the Karoo Basin (190 – 180 Ma, Ar/Ar and K/Ar, Fitch and Miller, 1984; Duncan and Marsh, 2007). As a result, only a portion of the Witwatersrand Supergroup is exposed (Dankert and Hein, 2010).

2.1.2 Tectonic evolution of the Witwatersrand region

Initially, the Witwatersrand Basin was thought to have been deposited in an extensional half-graben environment during the early-Proterozoic era (Pretorius, 1976). The theory of plate tectonics later led to a dramatic shift in perception, suggesting the basin developed in response to various processes linked to plate tectonics during the late-Archean (Coward, 1995). Based on the

age constraints given above, it is clear that the Witwatersrand Basin is representative of a single, long-lived geological cycle leading to the formation of an early continental nucleus, termed the Kaapvaal craton (De Wit et al., 1992). The terminal stages of craton formation are considered to be closely linked to the encroachment of the Zimbabwe and Kaapvaal cratons and the development of the Limpopo orogeny between the two at +- 2700 Ma (De Wit et al., 1992).

Thus, earlier dynamic models considered the Witwatersrand depository a as foreland basin (Burke et al., 1986; Winter, 1987). The concept of a "successor basin" was later proposed for the region by Clendenin et al. (1988). Clendin et al. (1988) suggested the formation of the Dominion-Witwatersrand-Ventersdorp-Transvaal depositional system as a result of alternating extensional and compressive forces localized along sites presenting pre-existing tectono-thermal instability. Stanistreet and McCarthy (1991) later postulated the formation of the Witwatersrand Basin in response to processes related to a Wilson cycle, suggesting that the evolution of the Witwatersrand system occurred in five major stages.

These five stages may be outlined as follows: (1) Structural evolution and distribution of granite greenstone belts resulting in the formation of a structural grain on the Kaapvaal craton (Stanistreet and McCarthy, 1991). (2) Deposition of the Dominion Reef under extensional (rift) conditions, with the flooding of a thick bimodal volcanic pile. (3) Onset of foreland basin tectonics and encroachment of the Zimbabwe craton, in response to thermal collapse, resulting in the extensive epicontinental, subtidal sedimentary sequences comprising the West Rand Group (Stanistreet and McCarthy, 1991). (4) Collision of the Zimbabwe and Kaapvaal craton, development of foreland basin tectonics, and deposition of the Central Rand Group. (5) Extrusion of the basal Ventersdorp (Klipriviersburg) tholeiitic flood basalts and initiation of renewed extensional tectonics resulting in the formation of the overlying Ventersdorp (Platberg) graben-fill layers (Stanistreet and McCarthy, 1991).

De Wit et al., (1992) incorporated many of these notions producing a broader model of the Kaapvaal shield and craton construction. This model considers the craton a collage of sub-terranes each characterized by distinct geological attributes. An important note is the proposition that two distinct terranes constitute the Witwatersrand hinterland, the Amalia terrain to the west

comprising rocks < 3000 Ma and the other north and northwest of the basin comprising crust > 3000 Ma (De Wit et al., 1992). Robb et al., (1991) summarized the major tectonic events related to the development of the Witwatersrand Basin as follows: Intrusion of Westerdam and Coligny plutons amongst others, during the extensional and the thermal collapse phase of the Dominion. Sedimentation of the West Rand (lower wits) and possibly areas of the Central Rand (upper Witwatersrand) following the early foreland basin stage was accompanied by intrusion of S-type granites elsewhere on the craton (Robb et al., 1991). Exposures of these exist in the Barberton area. Between 2840-2702 Ma, the stage of continent-continent collision was accompanied, northwest of the Welkom goldfield, by voluminous Gaborone-Kanye event-, Schweizer-Reneke granite and hydrothermally altered granite emplacement (Robb et al., 1991). Lastly, I-type granite activity accompanied the largely extensional Ventersdorp event, especially in eastern and northern regions of the craton (Robb et al., 1991).

Later studies, employing seismic methods, attempted to map the evolution of thrust systems in and around the depository (Coward et al., 1995). Development of the topographic expression north-west of the basin is shown to be attributed to major thrust systems subsequently controlling the main pathways of sediment input. These thrusts, southeast directed, are shown to migrate and decrease in age further southeast (Coward et al., 1995). This reflects the coeval development and tectonics and accretion along the northwestern edge of the craton. Processes related to craton edges remain poorly constrained at present (Coward et al., 1995). Recent age determinations and sequence stratigraphic correlations pertaining to the Limpopo Belt show the orogeny was longer-lived than initially thought, dating as recent as 2000 Ma (Cheney, 1995; Jaeckel et al., 1995). More work is necessary, particularly on the timing and sequence of events, to determine the specific role of the Limpopo orogeny in the evolution of the Witwatersrand Basin.

2.1.3 Stratigraphy

The Witwatersrand Supergroup (ca. 2985 – 2849 Ma; Kositcin and Krapez, 2004) comprises an approximately 7000 meter thick sequence of shale, quartzite and conglomerate and is shown in Table 2.1. This sequence of arenaceous and argillaceous, along with subordinate rudaceous units were deposited under fluvial-deltaic conditions in center of the Kaapvaal Craton and have undergone low-grade regional metamorphism (Robb & Meyer, 1995). The Witwatersrand system is divided into a lower, argillaceous unit (West Rand Group) and an upper, arenaceous unit (Central Rand Group). Locally pronounced unconformities separate the Witwatersrand sequence from the underlying Dominion Reef Group. The latter has been proposed as the initial, localized volcanic phase of the Witwatersrand system, (Truswell, 1977).

Table 2. 1: The lithostratigraphy of the Witwatersrand Basin

LITHOSTRATIGRAPHY			
SUPERGROUPS	**GROUPS**		**RELATIVE AGES**
KAROO	Stromberg		ca. 190-180 Ma (Ar/Ar and K/Ar, Fitch and Miller, 1984; Duncan and Marsh, 2007)
	Beaufort		
	Ecca		
	Dwyka		
TRANSVAAL	Pretoria		ca. 2.58- 2.20 Ga (Fitch and Miller, 1984 ; Duncan and Marsh, 2007)
	Chuniespoort		
VENTERSDORP	Pniel		ca. 2729 +/- 19 Ma (igneous-detrial xenotime/zircon aggregate, Kositcin et al., 2003)
	Platberg		ca. 2.72 - 2.63 Ga (Kositcin et al., 2003)
	Klipriviersberg		
WITWATERSRAND	Central Rand	Turffontuin Formation	ca. 2902 – 2849 Ma (Kositcin and Krapez, 2004)
		Johannesberg Formation	
	West Rand	Jeppestown Formation	ca. 2985 - 2809 (Kositcin and Krapez, 2004)
		Government Formation	
		Hospital Hill Formation	
	Dominion		ca. 3074 +/- 6 Ma (single zircon U-Pb SHRIMP, Myers et al., 1989; Armstrong et al., 1991)
ARCHEAN BASEMENT			ca. 3.6 - 3.2 Ga (Poujol et al., 2003)

The approximately 2650 meter thick Dominion Reef Group (ca. 3074 +- 6 Ma; Myers et al., 1989; U-Pb detrital zircon SHRIMP) consists mostly of acid to intermediate volcanics with minor volcano-clastic and clastic sediments (Robb & Meyer, 1995). Few auriferous conglomerate horizons exist in the Dominion Reef Group and have been exploited in the past.

Arenaceous and argillaceous rock in their relative proportions, are the basis of division within the Witwatersrand Supergroup (Robb & Meyer, 1995). Similarly, the West Rand Group (ca. 2985 – 2902 Ma; Kositcin and Krapez, 2004) is subdivided according to these criteria. The West Rand hosts the Hospital Hill, Government- and Jeppestown Formations (Table 2.1). The Crown Formation of the Government Group separates the upper volcanics of the Jeppestown Formation from the underlying shales of the Hospital Hill Formation (Robb & Meyer, 1995). According to Eriksson et al. (1979), the deposition of the Hospital Hill Formation occurred in a subtidal environment and suggested deposition of most of the West Rand occurred under shallow marine conditions. Auriferous conglomerates exist within the Crown Formation and within the basal portions of the Jeppestown sequence but relative to the Central Rand make insignificant contribution to overall gold production in the Witwatersrand Basin (Minter et al, 1993).

The Central Rand (ca. 2902 – 2849 Ma; Kositcin and Krapez, 2004) is subdivided into the Johannesburg- and Turffontein Formations (Table 2.1). It comprises mainly quartzites with several interbedded conglomerates, the latter of which hosts the majority of Witwatersrand gold (Robb & Meyer, 1995). Pretorius (1976) noted the progressive thickening and close spacing of conglomeratic zones stratigraphically upwards, indicative of regressive conditions, thus supporting the supposition that the basin was characterized by progressively increasing instability as it evolved. Cyclic sedimentary units individually resting on either an unconformity or disconformity characterize this sequence (Pretorius, 1976). Each cycle is typically initiated as basal conglomerates are deposited and grade upwards into quartzites. In rare instances these quartzites grade upwards into shale. Each cycle demonstrates a lateral decrease in grain size into the basin (Pretorius, 1976).

The Ventersdorp Supergroup (ca. 2.72 – 2.63 Ga; Manzi et al. 2013) is subdivided into the lower Klipriviersberg-, Platberg Group and upper Pniel Group (Table 2.1). The Klipriviersberg Group hosts five formations namely, the Westonaria, Alberton, Orkney, Jeannette and Edenville Formations (Manzi et al., 2013). The ultra-mafic and mafic metavolcanics of the Kliprivierberg are overlain by the bimodal metavolcanics and clastic metasedimentary constituents of the lower Platberg Group (Crow and Condie, 1988).

The Transvaal Supergroup (ca. 2588 +- 6 Ma; Jolley et al., 2004; Krapez, 1985; Vos, 1975) consists of the basal Black Reef Formation, the Chuniespoort and upper Pretoria Group (Table 2.1). The Black Reef is relatively thin and comprises of lower quartzites with intermittent basal conglomerates, interbedded black carbonaceous shales and upper dolomite units (Robb et al, 1995). The Chuniespoort Group comprises of carbonate, lacustrine deposits and banded iron formations (Eriksson et al., 1995, 2007; Frimmel, 2005). The upper Pretoria Group, mainly comprising of intercalated mudstone-sandstone sequences, minor conglomerate units and andesite, carbonate and diamictite beds, non-conformably overlies the Chuniespoort Group (Eriksson et al., 2007; SACS, 1980).

2.1.4 Structure

Studies conducted by Coward et al. (1995), Beach and Smith (2007), Dankert and Heinn (2010), Jolley et al. (2007) validate the theory that the Witwatersrand basin had undergone more than one episode of deformation. Despite more than a century of gold mining, regional-scale kinematic and structural analysis across the basin is considerably lacking (Dankert and Hein, 2010). However, there is general consensus that the basin experienced inversion tectonics during and subsequent to the deposition of conglomerate (some of which are gold-bearing) and quartzite horizons of the Central Rand Group. Inversion tectonics went from extension to compression i.e. positive inversion (Beach and Smith, 2007; Dankert and Hein, 2010) and then from compression to extension (negative inversion) as the Ventersdorp Supergroup was deposited (Van der Westhuizen et al., 1991). Listric faults in the basin were identified by Coward et al. (1995) and Vermaakt and Chunnet (1994) using gold mine studies in the West Wits Line and West Rand goldfields and by Beach and Smith (2007), Gibson et al. (2000) and Gibson (2004), using

interpreted 3D seismic data. Prominent structural styles including major normal fault zones and the drag folds associated with them were shown, by Beach and Smith (2007), to be attributed to extensional tectonics coeval with the deposition of the Ventersdorp Supergroup (ca. 2709 – 2643). This is possibly coeval with the deposition of the Platberg Group (Beach and Smith, 2007).

Regional faults consist of (1) the WNW-trending extension of the Rietfontein Fault Zone, (2) the Witpoortjie and Roodepoort-Saxon-Panvlakte faults (Mellor, 1911, 1913, 1917b, 1921), (3) the N-trending West Rand fault, and (4) the WSW-trending Doornkop fault and WSW-trending faults south of Westonaria. The West Rand and Saxon-Roodepoort-Panvlakte faults are seemingly laterally displaced by the south Westonaria faults (Mellor, 1911, 1913, 1917b, 1921). Regional folds consist of (1) the NW-trending West Rand Syncline and (2) the NNE-trending Panvlakte Anticline (Mellor, 1911, 1913, 1917b, 1921). The former, is developed exclusively in the meta-sedimentary constituents of the Witwatersrand Supergroup and, according to Toens and Griffith (1964), consists of a refolded doubly-plunging or an asymmetric syncline, as suggested by Pegg (1950), Roering (1968), Myers et al. (1990b) and Killick (1992). The boundary separating the West- and Central Rand goldfields is formed by the syncline.

Manzi et al. 2013, suggest the observed regional faults and folds may be attributed to the following events: (1) formation of fold-faults coeval with the deposition of the Central Rand Group with fold excision; (2) formation of listric faults and/or drag folds (rollover) prior to Klipriviersberg lava emplacement; (3) formation of normal faults and/or rollover folds coeval with the deposition of the Platberg Group (Manzi et al., 2013); (4) formation of thrust-folds coeval with or subsequent to the deposition of the Transvaal Supergroup, and (5) formation of faults coeval with the Vredefort impact event. These events partially correspond with those suggested for the South- and Central-East Rand goldfields (Dankert and Hein, 2010).

2.1.5 Metamorphism

The basin's pressure-temperature metamorphism conditions have been constrained by several authors (Phillips, 1987; Wallmach and Meyer, 1990; Wallmach, et.al, 1990). There is general

consensus that peak metamorphism conditions, attained regionally, were approximately 350 °C and 2.5 kb. Less obvious is whether the metamorphism climax was coincident with a thermal anomaly or burial (or possibly both), and the timing of the peak condition (Robb and Meyer, 1995). Insight into post-depositional metamorphism and alteration is provided by the sequence of geological events which superceded formation of the basin and radiometric age determinations, which reflect the re-setting of isotopes during a particular event (Dankert and Hein, 2010). Age data available from surrounding environs suggest likely re-setting of isotope systems at ca. 2500, 2300 and 2000 Ma (Robb and Meyer, 1995). The basin's rutile and authigenic pyrite yield ages of 2500 and 2578 Ma, respectively (Giusti et al., 1986; Guisti, 1988; Robb et al., 1990a, b) while the Rb-Sr isotope system in West Rand granites have seemingly been reset at 2525 Ma (Barton et al., 1986).

A second generation of pyrite together with bitumen in the basin and nearby granites yields ages of 2260 and 2320 Ma (Allsopp et al., 1986; Guisti et al., 1986; Robb et al., 1994). Ventersdorp lavas and tonalites of the Johannesburg dome have also had their Pb-Pb and Rb-Sr isotope systems reset at 2230 and 2264 Ma, respectively (Van Niekerk and Burger, 1964; Barton et al., 1986; Walraven et al., 1990). Finally, the basin has experienced resetting of uranite at approximately 2040 Ma (Rundle and Snelling, 1977) and shales of the Witwatersrand Supergroup have yielded K-Ar whole rock ages at approximately 1950 Ma (Layer et al., 1988). Clay mineral separates of the Ventersdorp Contact Reef have yielded K-Ar ages of 1888 and 2021 Ma (Zhao et al., 1995).

The ages above, either date the formation of authigenic minerals or record events which have reset isotopes, and thus may reflect metamorphic events within and surrounding the basin. This recognizes at least three metamorphic events at 2500, 2300 and 2000 Ma (Robb and Meyer, 1995). The first two events are thought to reflect progressive burial metamorphism resulting from successive loading of the overlying Ventersdorp and Transvaal sediments, while the 2000 Ma event is likely linked to either the thermal perturbations resulting from the intrusion of the Bushveld Igneous Complex or, the catastrophic tectonism coinciding with the Vredefort impact event, or possibly both (Robb and Meyer, 1995). The correlation between reset age data and the

region's chronostratigraphic-dates provide a framework within which examination of the post-depositional redistribution of Witwatersrand ore is possible (Robb and Meyer, 1995).

2.1.6 Mineralization Processes

2.1.6.1 Origin of Witwatersrand gold

The origin of Witwatersrand gold remains speculative amongst the research community. Pretorius (1991) advocated for the modified placer theory, suggesting the syngenetic introduction and later mobilization of ore while Phillips and Meyer (1989) suggested the epigenetic introduction of ore via precipitation from post-depositional fluids. In-depth microtextural analyses conducted by Liebenberg (1955) and Ramdohr (1955) supported the modified placer theory. These authors suggested that sedimentalogical processes during the deposition of the basin together with post-depositional modification, exhibited crucial control on ore localization. While the bulk of major ore minerals, which include pyrite, gold and uraninite are seemingly allogenic (Schidlowski, 1981; Hallbauer, 1986; Minter et., 1993), approximately half of over 70 ore minerals studied exhibit textural relationships inconsistent with detrital derivation and instead suggest precipitation from hydrothermal fluid (Phillips and Meyer, 1989). Genetically, the assortment of ore textures observed may be explained in terms of a three-stage paragenetic sequence, in which the detrital minerals were initially deposited, followed by the formation of authigenic pyrite and finally, the remobilization of gold and formation of secondary sulphide mineralization (Feather and Koen, 1976).

2.1.6.2 Occurrence of Witwatersrand gold

Witwatersrand gold has been extracted from at least 30 reefs within the basin's meta-sedimentary sequences. Of the exploited reefs, approximately 95% occur within Central Rand conglomerates (Robb et al., 1990). The fluvially-dominated sequences of the Central Rand consist of several dis- and unconformity-bound stratigraphic units. These have accumulated as a result episodic uplift of the basin hinterland, induced by tectono-magmatism (Robb and Meyer, 1995). Reefs showing economic significance occur at six stratigraphic positions within the

Central Rand Group, three of which are hosted by the Johannesburg Sub-group, and the remaining three by the Turffontein Sub-group (Robb et al., 1990a). The West Rand Group comprises three sub-economic reefs, one of which is hosted within the Government Subgroup and two of which are hosted within the Jeppestown Subgroup (Robb and Meyer, 1990a). The reefs generally comprise a range of fluvial lithofacies. These include loosely packed conglomerate, clast-supported oligomitic conglomerate, pebbly arenite or pebble lag surface related to trough-cross bedded quartz-arenite. Ore is rarely hosted within debris-flow lithofacies (Robb and Meyer, 1995).

2.1.6.3 Nature of Witwatersrand gold

Single ore-bodies typically display variable thickness and length, ranging from tens of centimeters to several kilometers (Minter, 1993). Ore bodies seemingly occur between basal surfaces of degradation, generally angular unconformities, and upper planar bedded surfaces marking the contact with siltstones or greywackes above (Minter, 1991). Gravel-associated ore bodies occur mainly as very mature scour-based pebble lag and gravel bar deposits (Minter, 1993). Upper and lower ore-body margins are distinguished by abrupt changes in Au content, ranging from < 20 ppb to several g/t (Minter, 1991). Ore bodies typically occur as lens-like fluvial bar and channel beds with paleo-currents of unimodal direction.

Ore bodies of greater thickness typically occur as multi-channel conglomerate and quartz-arenite sequences (Pretorius, 1974). These are representative of flood and waning stage flows (Robb and Meyer, 1994). The depositional environments hosting ore bodies typically include proximal alluvial fan, braid delta, braid plain, terraced fluvial- and merge into shoreline environments (Robb and Meyer, 1994). Regionally, the distribution of ore bodies is noted primarily along the Central Rand Group margin coincident with the main entries of complex river systems into the original basin (Robb and Meyer, 1994). On mining scales, the highest ore grades are typically found within the channel facies, the highest of which is associated with the thickest channels (Minter, 1991).

There is a spatial association between gold (along with pyrite and uraninite) and detrital minerals such as chromite and zircon (Robb et al., 1990a). These detrital minerals are concentrated on degradation surfaces distinguished by the basal pebble lags of clast-supported conglomerates, as well as on coset boundaries, crossbedded foresets and bottomsets (Smits, 1984). Uranium is present in the form of uraninite, brannerite and leucoxene (Smits, 1984). There is a marked decrease in the uraninite: brannerite ratio up-section, e.g. from 8.7 in the near basal unit of the Welkom District, the Steyn Reef, to exclusively brannerite in the upper Beatrix Reef from the same group, (Smits, 1984). In addition, a systematic trend can be observed in U: Au ratio up-section (e.g. from the highly auriferous reefs of the Central Rand Group to the gold-deficient Dominion Reefs). In the Welkom District, there is a seemingly systematic trend in the U: Au ratios down the paleoslope, where significant uraninite quantities occur in the more distal facies (e.g. from 0.001 on the basin margin to 10 in distal facies; Smits, 1984). Of the iron minerals, pyrite is the most widespread. Iron oxides (predominantly magnetite) occur exclusively in shale facies (Smits, 1984).

Gold is closely associated with carbonaceous matter. The former, occurs as spherical glassy globules within stratabound seams of the latter (Minter, 1993). Carbonaceous seams preferentially occur in environments distal to high energy deposits and are seemingly lacking in proximal environments (Robb et al., 1990a). The carbon seams are found primarily in sandstones and conglomerates comprising rounded pyrite. The seams occur along microfractures and seemingly represent hydrothermal pyrobitumen (Robb and Meyer, 1994). Gold typically occurs in association with carbon and/or pyrite contained within quartz cobble- and pebble conglomerates, orthoquartzites and banded pyrite quartzites (Smits, 1984). Fine gold and uranium may occur in slender bituminous bands within low energy environments of distal fans. Gold occurs in the fore mentioned rocks as (1) fine, free gold in a clastic matrix with quartz, pyrophyllite, sericite, chlorite or fuchsite; (2) with bituminous material such as thucholite; or (3) coatings on pyrite (Smits, 1984).

2.2 Local Geology – The West Rand

The West Rand Group consists of approximately 2300 meters of coarse clastics, 2300 meters of fine clastics and 500 meters of amygdaloidal lava (Crown lava, in the Jeppesetown Subgroup; Camden-Smith, 1980). Stratigraphically, the West Rand consists of three subgroups: the Jeppestown, Government- and Hospital Hill subgroups (Table 2.2; after Camden-Smith, 1980). Sediments of the West Rand represent a more distal, lower energy facies than that typical of the Central Rand (upper Witwatersrand Supergroup). Conglomerates of the West Rand are sparse (Goodwin, 1996). The Hospital Hill Subgroup is dominated by super-mature orthoquartzites while the Government and Jeppestown subgroups are dominated by sub-greywackes (Camden-Smith, 1980).

Table 2. 2: A composite stratigraphic column of the West Rand Group (after Camden-Smith, 1980).

	Subgroup	Formations	Markers
West Rand Group	Jeppestown	Roodepoort	
		Crown Lava	Crown Lava
		Florida Quartzite	
	Government	Witpoortjie	Blue Grit
		Coronation	Government Reef Tillite
		Promise Quartzite	Promise Reef
	Hospital Hill	Brixton	Black Grit
		Parktown Shale	Contorted Bed
		Orange Grove Quartz	

2.2.1 The Hospital Hill Subgroup

The Hospital Hill Subgroup is approximately 1620 meters thick. Although this subgroup contains more arenaceous units than the Central Rand, the ratio of quartzite to shale is similar

(Camden-Smith, 1980). The Orange Grove Quartzite, Parktown Shale and Brixton Formations are well defined by the Orange Grove, Black Grit and Promise Reef lateral markers.

2.2.2 The Government Subgroup

The Government Subgroup is approximately 1300 meters thick (Camden-Smith, 1980). This subgroup consists of three Formations: The Coronation Shale hosting tillite and magnetic marker horizons, the Promise Quartzite and the Witpoortjie Formations (Camden-Smith, 1980). The Blue Grit and Promise Reef are both diamictic markers distinguishing the top and bottom of the Government Subgroup.

2.2.3 The Jeppestown Subgroup

The Jeppestown Subgroup is divided into three formations by the Crown Lava marker (Camden-Smith, 1980). This subgroup consists of three, thick sandstone units, two of which are siltstone units and the third, amygdaloidal lava, all separated by shale (Camden-Smith, 1980).

The West Rand is dominated by extensive outcrop of the Transvaal Supergroup dolomites (Camden-Smith, 1980). Though underlain by various other rock types, the Malmani Subgroup (of the Transvaal Supergroups) dolomites are most significant in terms of extent and management practices (WRDM, 2014). These dolomites serve as aquifers, storing the region's groundwater. Dolomitic areas are susceptible to sinkhole development and karst formation (WRDM, 2014). Consequently, the region is pitted by sinkholes, especially in central sections (WRDM, 2014).

2.3 The Gold One Millsite Slimes Complex study site

The study site for this project is the Gold One Millsite Slimes Complex in the city of Randfontein. The Millsite Slimes Complex forms part of the Gold One tenements and is located close to the Krugersdorp Game Reserve (Van Zyl et al., 2013). The central business district (CBD) of Randfontein is situated between the study site and the Cooke tailings storage facility.

The city of Randfontein is characterized by shale, mudstone or sandstone of the Madzaringwe Formation (Karoo Supergroup) with intrusive dolerites (WRDM, 2014). Archean granite and gneiss of the Halfway House granite underlie the eastern portion of the region, while quartz ridges of the Witwatersrand Supergroup dominate the southern portion (WRDM, 2014).

The Millsite Slimes Complex was established from mining activities on the Main reefs amongst others in the Old Randfontein sections (Van Zyl et al., 2013). These occur north of the Witpoortjie fault. Little information is known about the nature of the Millsite slimes deposits but what is known is that the deposits are formed from quartz pebble conglomerates discarded during the gold mining process (WRMD, 2014). In general, the material is fine-grained and may contain low grade values of gold and uranium which were not effectively recovered during the initial processing operation (WRMD, 2014).

CHAPTER THREE: Methodology

3.1 Preamble

The aim of this study was to understand heavy release from the Gold One Millsite Slimes Complex into the Randfontein area, Witwatersrand. To achieve this, the mineralogical- and geochemical factors controlling metal release were assessed. This chapter provides a general overview of the research methodology and geochemical instrumentation provided for, and used during this study. Data provided for this study include: (i) field investigations and sampling performed by Abegunde (2015) and, (ii) core log appraisal, bulk geochemical data, x-ray diffraction data, paste pH and electrical conductivity (EC) data provided by Abegunde (2015).

Prior to commencing with this research, a desktop study was done to acquire relevant information on the study site, the Witwatersrand environment and the geochemical methods employed. Data generated as part of this study include: (i) core log reappraisal, (ii) petrographic data and the description of trends in the x-ray diffraction data provided, (iii) the description of trends in the bulk geochemical data provided, (iv) sulphide-sulphur determination and (v) selective sequential extraction data.

3.2 Data provided for this study

3.2.1 Field work and sampling

Field investigations and sampling were performed by Abegunde (2015) during September-October, 2012. The Gold One Millsite Slimes Complex (Fig 3.1) was selected as a slimes dam of interest based on its location, easy accessibility (through a network of roads in the Randfontein area), proximity to residential areas and physical state of the slimes dam. After approximately one week of site inspection, three sections were marked for drilling (section T001, T002 and T003). Drilling was performed using a sandrill (Abegunde, 2015). This power-driven auger drill is hydraulically operated and deemed extremely useful in tailings and slimes dams as it is highly efficient and low cost (Bosch, 1987). The sandrill however, does come with limitations as it

cannot penetrate hard materials such as rock. For this reason, sampling was limited to 10.2 meters for section T001, 8.2 meters for section T002 and 8.2 meters for section T003. The location of each drill hole was recorded using GPS coordinates. The holes were constantly measured during drilling using a meter ruler. Slimes samples (of approximately 20 centimeters) were taken at one meter depth intervals for each drill hole. Each of the drill sections were then carefully examined and logged to show colour and grain-size variations downhole. Colour variations and moisture content were the most prominent features of the core logs (Abegunde, 2015). The slimes samples collected were sealed in airtight polythene bags and placed in a dark container to limit any further oxidation. Samples were then transported to the University of the Western Cape, where they were stored for sample preparation and analyses.

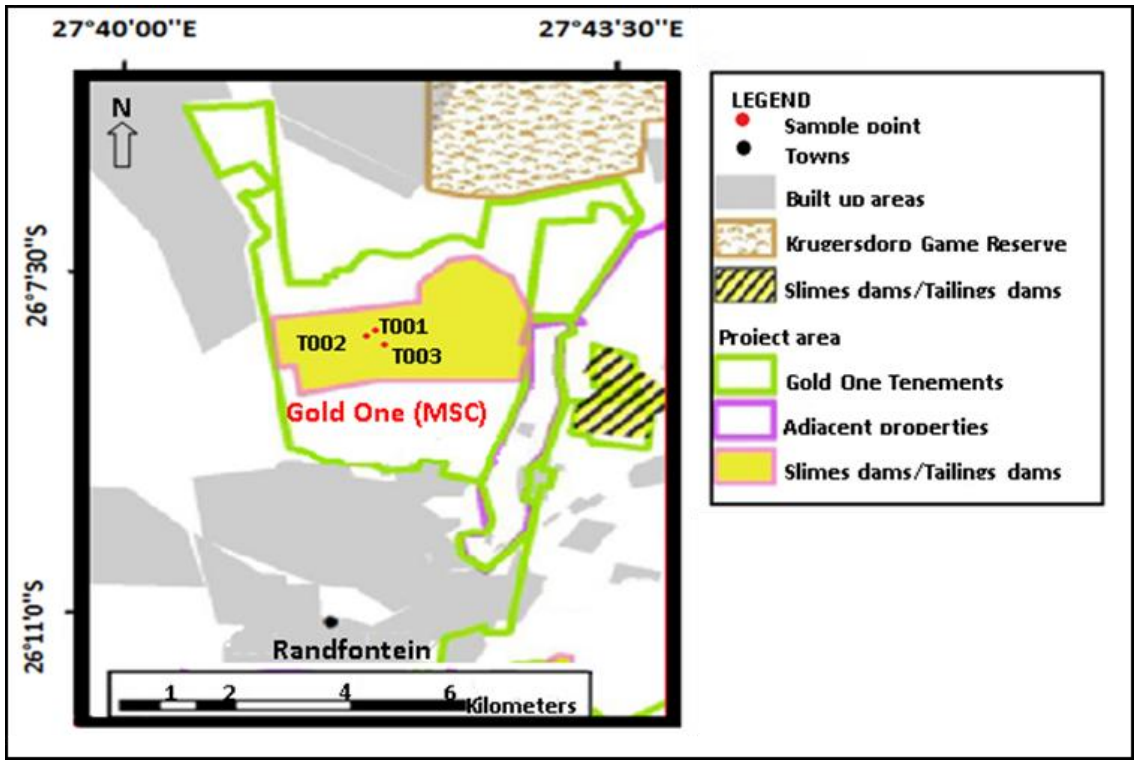

Figure 3. 1: Sampling holes T001, T002 and T003 drilled in the Gold One Millsite slimes complex (MSC) in Randfontein, Witwatersrand.

3.2.2 Appraisal of the core logs

The core logs for sections T001, T002 and T003 were appraised by Abegunde (2015) on the basis of colour and grain-size variation, as these features were most prominent downhole. Abegunde (2015) noted the following: the presence of whitish and light brown fine sand within the first 0.5 meters downhole, light brown fine sand between 1- and 1.2 meters, light brownish yellow fine sand between 2 meters and 4.2 meters, brownish yellow fine sand between 5 meters and 5.2 meters, brownish grey fine sand between 6 meters and 7.2 meters, reddish fine sand between 8 meters and 8.2 meters and dark grey fine sand between 9 meters and 10.2 meters. Core logs for sections T001, T002 and T003 were reappraised as part of this study on the same basis as Abegunde (2015).

3.2.3 Sample preparation for geochemical and x-ray diffraction analysis

Proper sample preparation is crucial prior to any geochemical or mineralogical analysis, as it minimizes the introduction of foreign substances into the sample before proceeding with various analyses. Before the commencement of analyses, slimes samples were dried for approximately 16 hours at a temperature of 40°C (Abegunde, 2015). Samples were then milled to a powder-like consistency using a Dickie and Stockler milling machine (Abegunde, 2015). This was done without sieving as complete elemental analysis was necessary. The milling machine was thoroughly cleaned between uses to avoid sample contamination (Abegunde, 2015). Samples were packaged securely and sent to Acme Analytical Laboratories (Vancouver) Ltd for geochemical analyses, using XRF and LA-ICP-MS, and to Itemba Labs for x-ray diffraction analysis.

3.2.4 Bulk geochemical analyses

A total of 29 prepared slimes samples were sent to Acme Analytical Laboratories (Vancouver) Ltd for bulk geochemical analyses. This included the analysis of loss on ignition and major oxides, total carbon and sulphur, trace- and ultra-trace elements and rare earth elements and additional trace elements.

3.2.4.1 Analysis of loss on ignition (LOI) and major oxides

Loss on ignition and major oxide concentrations were determined using lithium tetraborate/litium metaborate fusion and x-ray fluorescence (XRF). X-ray fluorescence (XRF) is an analytical technique useful in determining the bulk chemical composition of various materials. This technique makes use of an x-ray source (x-ray tube, synchrotron or radioactive material) which excites the sample with x-rays (Bouwer, 2010). Excited elements in the sample emit a unique set of fluorescent x-ray radiation with characteristic energies (Bouwer, 2010). The measurement of the x-rays emitted by the sample allows the determination of elements present while relative element proportions may be determined by measuring the intensity of emitted energies (Bouwer, 2010).

Loss on ignition was determined prior to the major oxides by baking a predetermined weight of sample at 950°C (Abegunde, 2015). Loss on ignition was calculated as a function of weight loss after baking. This was determined by igniting each sample split and then measuring the loss in weight. For the major oxides, 5 g of sample pulp was then baked at 1050°C and fused with commercial lithium tetraborate flux in a platinum-gold crucible (Abegunde, 2015). The molten material was then placed into a platinum mold. The fused discs produced, were analyzed using x-ray fluorescence which was calibrated using certified reference materials (Abegunde, 2015).

In the case of XRF, the use homogeneous glass discs as opposed to pressed powders, minimizes effects associated with mineralogy, particle size and matrices. Thus, better accuracy was achieved with the use of glass discs as opposed to the pressed powder alternative (Abegunde, 2015). The glass discs were prepared using 35% lithium tetraborate/ 65% lithium metaborate as opposed to conventional 100% lithium metaborate to reduce the chances of crystallization. The major oxides analyzed by XRF include; SiO_2, Al_2O_3, Fe_2O_3, CaO, MgO, Na_2O, K_2O, MnO, TiO_2, P_2O_5 and Cr_2O_3 together with LOI.

3.2.4.2 Analysis of total carbon and sulphur

Total carbon and sulphur was determined using Leco analysis (Abegunde, 2015). Total carbon was determined using a Leco carbon analyzer. 0.1 g of each sample was combusted in an

induction furnace at 1350 °C while a stream of oxygen passed through. The carbon dioxide generated was determined by infrared spectroscopic analysis and the total carbon calculated. Total sulphur was determined using Leco sulphur analysis. Similar to that of total carbon, this was determined by the combustion of each sample in an induction furnace at 1350 °C while oxygen passed through. Infrared spectroscopic analysis was used to determine the amount of sulphide dioxide generated and the total sulphur was calculated.

3.2.4.3 Analysis of trace- and ultra-trace elements

Trace and ultra-trace element concentrations were determined by treatment with aqua regia and analysis by ICP-MS (Abegunde, 2015). Aqua regia is a common digestant in multi-element analysis and is made up of a 3:1 ratio of hydrochloric acid and nitric acid. Digestion by aqua regia was done in 250 ml glass beakers, covered with watch glasses. 0.5 g of sample was thoroughly mixed and digested in 12 ml of aqua regia on a hotplate at 110°C and allowed to evaporate for 3 hours. When nearly dry, the sample was diluted with 20 ml of 2 % nitric acid. This solution was then filtered into a 100 ml volumetric flask and diluted with de-ionized distilled water to the 100 ml mark. This solution was then analyzed by ICP-MS. Trace elements analyzed by ICP-MS include: Mo, Cu, Zn, Ag, Ni, As, Au, Cd, Sb, Bi, Hg, Ti and Se.

3.2.4.4 Analysis of rare earth elements and additional trace elements

Rare earth element (REE) concentrations and 16 additional trace element concentrations were determined using a combination of Laser Ablation Inductively Coupled Plasma Mass Spectroscopy (LA ICPMS) and lithium metaborate/tetraborate fusion analysis (Abegunde, 2015). Laser ablation inductively coupled plasma mass spectrometry is a form of plasma spectrometry capable of multi-element trace element detection (Hoffman et al., 1996). This technique makes use of a laser to ablate a sample which is then transported by Ar or an Ar - He mixture to the plasma of the ICP-MS (Hoffman et al., 1996). The ICP-MS plasma produces ions which are subsequently introduced to a mass analyzer (Hoffman et al., 1996). A quadrupole is then used to separate and collect ions based on their mass-charge ratios. ICP-MS by itself is considered relatively unsuitable for direct (in situ) trace element analysis as it requires samples in solution form, where sample introduction is achieved via solution nebulization (Hoffman et al., 1996).

Used together with laser ablation, vaporization of the bulk exposed solid surface occurs upon interaction with a laser beam, making it more suitable for in situ trace element analysis (Hoffman et al., 1996).

Despite this, complete digestion of the sample is still necessary for precise results. This requires the use of a flux, in this case, lithium metaborate/tetraborate fusion (Abegunde, 2015). For the fusion process, 0.2 g of prepared sample was mixed with an equal part $LiBO_2$ /$Li_2B_4O_7$ flux and placed into a graphite crucible. The crucible was placed in an induction furnace and the contents fused at 1150 °C for 30 minutes. The bead was allowed to cool and the resultant fusion bead was dissolved in a solution of 5% nitric acid. Water utilized was deionised water from a Nanopure analytical grade water system. The resultant molten mixture was dissolved with hydrofluoric acid to remove excess silica and release more than 90 % of the flux as gas fluorides. This resulted in clear, steady solutions for analysis by ICP-MS. Rare earth elements and additional trace elements analyzed for include: Ba, Be, Co, Cs, Ga, Hf, Nb, Rb, Sn, Sr, Ta, Th, U, W, Zr and Y.

3.2.5 X-ray diffraction analysis

The mineral composition of 12 slimes samples were determined using a BRUKER AXS D8 Advance X – ray diffraction spectrometry (XRD) machine in locked coupled mode at the Itemba Lab facilities. Samples sent for analysis were selected based on observed variations in colour and texture downhole (Abegunde, 2015). To determine the mineral composition of samples, 1.2 g of each milled sample was placed in the center of the sample holder. The holder consisted of a 20 mm X 20 mm corning glass (specifications include: Tube voltage: 40 kV, Tube current: 40 mA, Slit system: V20 variable slit). Using a circular motion, a microscope glass slide flattened the sample heap until the sample was at the correct height for analysis.

3.2.6 The paste-pH and electrical conductivity (EC) data

To determine paste pH and EC, a multi-meter pH-EC electrode was calibrated using pH 4 and pH 7 buffer solutions (TMH1, 1986; Price, 2009). 5 g of sample was then weighed into a test

tube and 15 ml of distilled water added. This was mixed thoroughly and the sticky solution measured for paste pH and EC.

3.3 Data generated during this study and geochemical instrumentation

3.3.1 Reappraisal of the core logs

Core log reappraisal was performed as part of this study using the core samples collected from each drill hole, i.e. sections T001, T002 and T003. Core log descriptions characterized samples on the basis of colour and grain-size, as these features were most prominent (Abegunde, 2015). Similarly, the reappraisal of core logs for sections T001, T002 and T003 was based on colour and grain-size variations down hole.

3.3.2 Petrographic analysis

The petrographic analysis of selected slimes samples required thorough preparation before the commencement of analysis. The production of thin sections from core slimes samples required similar preparation to that required for rock thin sections but involved impregnation of the sample with a hardening agent (typically resin) prior to cutting, mounding, lapping and polishing. Common resins include epoxy compounds, polystyrene and polyester. As the resin solidifies, a compact block, encompassing the soil sample, is created (FitzPatrick, 1984). Thus, impregnation allows unconsolidated slimes samples to be analyzed microscopically, making mineral characterization possible.

To prepare the slimes samples, three parts epoxy resin and one part hardener was placed into a plastic mould and each loose sample carefully sprinkled into the resin mixture. The moulds (and its contents) were heated for 1-2 hours and allowed to cool overnight. The impregnated soil samples were removed from the mould and cut to the desired thickness. Using resin, the resulting solids were mound to individual thin section slides and allowed to set overnight. Using an LP30 lapping and polishing machine, the slides underwent approximately 1 hour of lapping. The slides

were viewed microscopically every few minutes in order to achieve the desired thickness. After sufficient lapping, slides were polished and analyzed in the microscopy laboratory.

3.3.3 Sulphide-sulphur determination

The aim of this study was to understand the pattern of metal release from slimes into the environment by investigating the mineralogical- and geochemical factors controlling metal release. One of the objectives was to determine sulphide-sulphur (wt %) as it is thought to represent the total reactive sulphur component in samples and may therefore influence metal mobilization. In order to determine sulphide-sulphur, a solution of ammonium oxalate was prepared to extract the sulphate-sulphur (wt %) present in each sample. The sulphate-sulphur (wt %) was then subtracted from the total (leco) sulphur to calculate the sulphide-sulphur (wt %).

To prepare the 0.2 M ammonium oxalate buffer ($(NH_4)_2C_2O_4$. H_2O) at pH 3.0, approximately 28.4 g of $(NH_4)_2C_2O_4$. H_2O was weighed in a 1000 ml measuring cylinder and was topped up to the 1000 ml mark with distilled water. In a second 1000 ml measuring cylinder, 25.2 g of $H_2C_2O_4$ .H_2O (oxalic acid) was weighed and topped to the 1000 ml mark with distilled water. Each cylinder was thoroughly shaken before adding four parts of ammonium oxalate solution and three parts oxalic acid to a 2000 ml measuring cylinder. The solution was thoroughly mixed and the pH adjusted to 3.0 by adding either solution. The solution was checked periodically as the pH changed.

2 g of tailings sample was then weighed into a 100 ml plastic bottle and 45 ml of 0.2 M ammonium oxalate solution (pH 3) added. The samples were placed into a hot water bath and heated at 80 °C for 2 hours. After heating, the samples were allowed to settle for approximately 10 minutes before being filtered into glass beakers. The filtrate was then transferred into 50 ml centrifuge tubes and stored in the refrigerator for ICP – MS analysis.
Sulphide-sulphur (wt %) was also used to determine the acid generating potential of slimes samples, based on acid base accounting. The latter, is one of two basic static tests used to assess acid generating potential of slimes samples. Acid base accounting does so by determining the

balance between acid generating components (AP) and neutralizing components (NP) in each sample.

3.3.4 Partial sequential extraction procedure

The mobilization of heavy metals is strongly associated by the specific bond form of the metal and methods of binding (Lu et al, 2014). Thus, the association of metals with various mineral phases has an influence on their release. The process of selective sequential extraction addresses the partitioning of metals by leaching various mineral phases and thereby the metals bound to them (Tessier et al, 1979). One of the objectives of this project was to determine the leachability of metals from the slimes dam into the environment. For this reason, a four-step sequential extraction procedure was used to release metals associated with four geochemical phases, namely (i) water-soluble, (ii) carbonate, (iii) Mn oxides, (iv) and Fe-oxides (Table 3.1).

Table 3. 1: A summary of the selective sequential extraction.

Step	Targeted phase	Leaching solution	Vol (ml)/wt (g)	Leaching conditions
1	Water-soluble	Double distilled water	90/5	90 mins in a shaker, at room temperature
2	Exchangeable and carbonate	1 M ammonium acetate	90/5	90 mins in a shaker, at room temperature
3	Mn-oxide	0.1 M hydroxylamine hydrochloride	90/5	90 mins in a shaker, at room temperature
4	Fe-oxide	0.25 M hydroxylamine hydrochloride	90/5	90 mins in a shaker, at room temperature

3.3.4.1 The water-soluble phase

Extraction of the water-soluble fraction typically includes the preferential dissolution of secondary sulphates i.e. evaporites (Ribet et al., 1995; Fanfani et al, 1997; Dold, 1999, 2001a, b). The occurrence of secondary minerals in mine waste systems is greatly dictated by prevailing climatic conditions. Under humid climatic conditions, secondary sulfate enrichment may be under developed as a result of extensive leaching. Under more arid and semi-arid climatic conditions, where high evaporation rates prevail, secondary soluble minerals are more strongly developed. Considering the semi-arid climate in Witwatersrand, South Africa, the water-soluble fraction may prove to be of significance. (Lottermoser, 2013).

The partial selective extraction of the water-soluble metals was the first step in the sequential extraction procedure. For this, 5 g of raw (unsieved) slimes sample was weighed into a 100 ml plastic bottle. To this, 90 ml of double distilled water was added. The samples were then placed into the shaker and agitated at room temperature for 90 minutes. The solutions were allowed to settle for approximately 10 minutes and then filtered. The filtrates were recovered in glass beakers and then placed into a 50 ml centrifuge tubes. These were stored in the refrigerator for analysis by GFAAS for Ca, Fe, Mn, Co, Ni, Cu, Zn, Au and Pb. The remaining solid residue was recovered into a 100 ml plastic bottle, using the successive leach, 1M ammonium acetate. 1 M ammonium acetate primarily targets carbonate-bound metals.

3.3.4.2 The carbonate phase

The carbonate phase includes carbonate-bound, surface-sorbed- and exchangeable ions. Metals are extracted by dissolving the soil material at a pH of approximately 5 (Gatehouse et al., 1977; Sondag, 1981; Fonseca and Martin, 1986; Dold and Fontbote, 2001). Extraction of metals generally requires the use of acetic- or sodium-buffered solutions. The metal fraction extracted under these pH conditions may be considered present as co-precipitated with the carbonate fraction but may also be sorbed surficially to Mn/Fe oxyhydroxides, clays and organic matter (Pickering, 1986). In addition, lowering of the pH from 7 (the relative pH of distilled water) to pH 5, promotes extraction of the remainder of specifically-adsorbed metals which escaped the preceding step.

The partial selective extraction of the carbonate-bound metals was the second step in the sequential extraction procedure and required the preparation of 1M ammonium acetate. For this, 77.09 g of ammonium acetate ($NH_4CH_3CO_2$) was weighed into a 1000 ml measuring cylinder and filled to the 1000 ml mark with double distilled water. The solution was buffered with (+- 37 ml) glacial acetic acid, to a pH of 5. The solution was thoroughly shaken prior to extraction. To start the second extraction, 90 ml of the 1M AmAc solution was added to the solid residue recovered from the water extraction and shaken at room temperature for 90 minutes. The solutions were allowed to settle before being filtered. The filtrates were recovered in glass beakers and transferred into 50 ml centrifuge tubes. These were stored in the refrigerator for

analysis by GFAAS for Ca, Fe, Mn, Co, Ni, Cu, Zn, Au and Pb. The remaining solid material was recovered into a 100 ml plastic bottle, with the successive leach, 0.1 M Hydroxylamine hydrochloride. 0.1 M Hydroxylamine hydrochloride targets Mn oxide-bound metals.

3.3.4.3 The Mn-oxide- and Fe-oxide phase

Mn and Fe oxides are renowned scavengers of trace metal ions within soils. Dissolution of nearly all metal-oxide phases may be achieved by controlling the Eh and pH of leach solutions. Reagents which most successfully evaluate the total metal ions in association with hydrous oxides are characterized by both a reducible agent and a ligand capable of retaining extracted ions in a soluble form, the efficiency of which is determined by its reduction potential and ability to attack the various crystalline forms of Mn and Fe oxyhydroxides. The selective digestion of Mn and Fe oxides is typically based on a sequential, progressive increase of the reducing strength of Hydroxylamine Hydrochloride ($NH_2OH.HCl$). Mn oxides are typically effectively extracted by 0.1M $NH_2OH.HCl$ in 0.01 M HNO_3, dissolving only minor quantities of amorphous Fe oxides and negligible crystalline Fe oxides; while hydrous Fe oxides are targeted by increasing the concentration of Hydroxylamine Hydrochloride to 0.25M (Chao, 1972).

The partial selective extraction of Mn oxide - bound metals was the third step in the sequential extraction procedure and required the preparation of 0.1 M hydroxylamine hydrochloride. For this, 6.95 g hydroxylamine hydrochloride ($NH_2OH.HCl$) was weighed into a 1000 ml measuring cylinder and topped with double distilled water to the 1000 ml mark. The solution was buffered with 10 ml of 10 % nitric acid. The latter was prepared by measuring 18.18 ml of 55 % nitric acid into a 100 ml volumetric flask and topping it up to the 100 ml mark.

To start the third extraction, 90 ml of the 0.1 M hydroxylamine hydrochloride solution was added to the solid residue recovered from the carbonate fraction and shaken at room temperature for 90 minutes. The solutions were allowed to settle before being filtered. The filtrates were recovered in glass beakers and transferred into 50 ml centrifuge tubes. These were stored in the refrigerator for analysis by GFAAS for Ca, Fe, Mn, Co, Ni, Cu, Zn, Au and Pb. The remaining solid material was recovered into a 100 ml plastic bottle, with the successive leach, 0.25 M

Hydroxylamine hydrochloride. 0.25 M Hydroxylamine hydrochloride targets Fe oxide-bound metals.

The partial selective extraction of Fe oxide - bound metals was the fourth step in the sequential extraction procedure and required the preparation of 0.25 M hydroxylamine hydrochloride. For this, 17.37 g hydroxylamine hydrochloride ($NH_2OH.HCl$) was weighed into a 1000 ml measuring cylinder and topped with double distilled water to the 1000 ml mark. The solution was buffered with 25 ml of 10 % nitric acid. The latter was prepared by measuring 18.18 ml of 55 % nitric acid into a 100 ml volumetric flask and topping it up to the 100 ml mark.

To start the fourth selective extraction, 90 ml of the 0.25 M hydroxylamine hydrochloride solution was added to the solid residue, recovered from the extraction by 0.1 M hydroxylamine hydrochloride, and shaken at room temperature for 90 minutes. The solutions were allowed to settle before being filtered. The filtrates were recovered in glass beakers and transferred into 50 ml centrifuge tubes. These were stored in the refrigerator for analysis by GFAAS for Ca, Fe, Mn, Co, Ni, Cu, Zn, Au and Pb. The remaining solid material was recovered into the 100 ml plastic bottle, for digestion with hydrofluoric acid and nitric acid.

The analysis of sequential extraction data made use of the GFAAS. Graphite Furnace Atomic Absorption Spectrometry is a quantitative analytical technique based on the measurement of the light absorption of free atoms, at ground state (Schlemmer and Radzuik, 1999). Electromagnetic radiation (from the source) excites ground state atoms which absorb photons having wavelengths equivalent to the excitation energy (Schlemmer and Radzuik, 1999). The amount of energy at the characteristic wavelength absorbed in the furnace is proportional to the concentration of analyte in the sample (Schlemmer and Radzuik, 1999).

In this approach, the sample is injected into a small graphite tube (furnace) and undergoes three stages of heating (Schlemmer and Radzuik, 1999). The initial ‘drying stage’ evaporates the solvent from the liquid sample. A ‘pyrolysis stage’ follows as the furnace temperature is increased and organic material is removed (Schlemmer and Radzuik, 1999). The sample then undergoes a final, ‘atomization stage’ during which temperatures are rapidly increased,

dissociating the analyte into atoms (Schlemmer and Radzuik, 1999). The formation and diffusion of atoms out of the graphite tube produces a peak-shaped absorption signal which can be related to concentration of analyte element present. The sensitivity and comparably lower detection limit of the GFAAS makes it suitable for the quantitative determination of trace metals (Schlemmer and Radzuik, 1999).

3.4 Data evaluation

3.4.1 Quality control and quality assurance

Laboratory quality control and quality assurance measures were included in the (i) bulk geochemical analysis, (ii) sulphide-sulphur analysis and (iii) partial sequential extraction procedures. This was done to ensure adequate quality of the analytical data provided for, and generated during the study.

3.4.1.1 Bulk geochemical analysis

Standard quality control and quality assurance was used during the bulk geochemical analysis and included the use of: standards, reagent blanks, blank samples, pulp duplicates and certified reference materials (Abegunde, 2015). Duplicate data were used to generate precision scatterplots for CaO (Fig. 3.2.1), Fe_2O_3, (Fig. 3.2.2) Cu (Fig. 3.2.3) and Zn (Fig. 3.2.4).

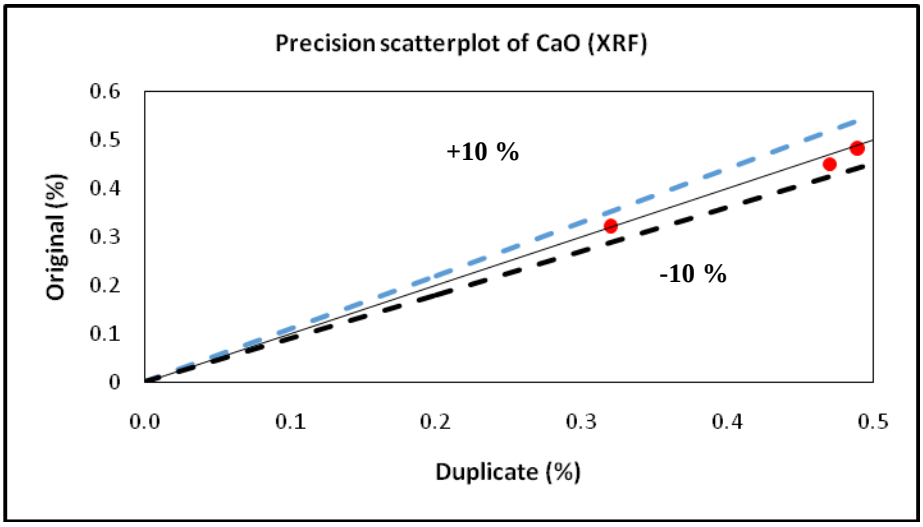

Figure 3.2. 1: A precision scatterplot of CaO, as determined by x-ray fluorescence, showing 10 % error margins.

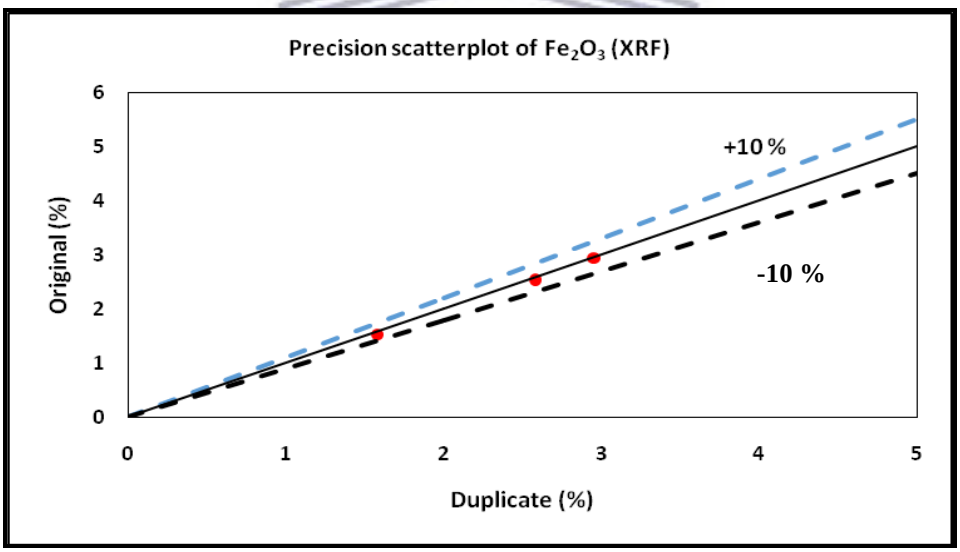

Figure 3.2. 2: A precision scatterplot of Fe_2O_3, as determined by x-ray fluorescence, showing 10 % error margins.

The major oxides (CaO and Fe_2O_3) analyzed by x-ray fluorescence show error percentages within the 10 % error margin (Fig. 3.2.1 and Fig. 3.2.2).

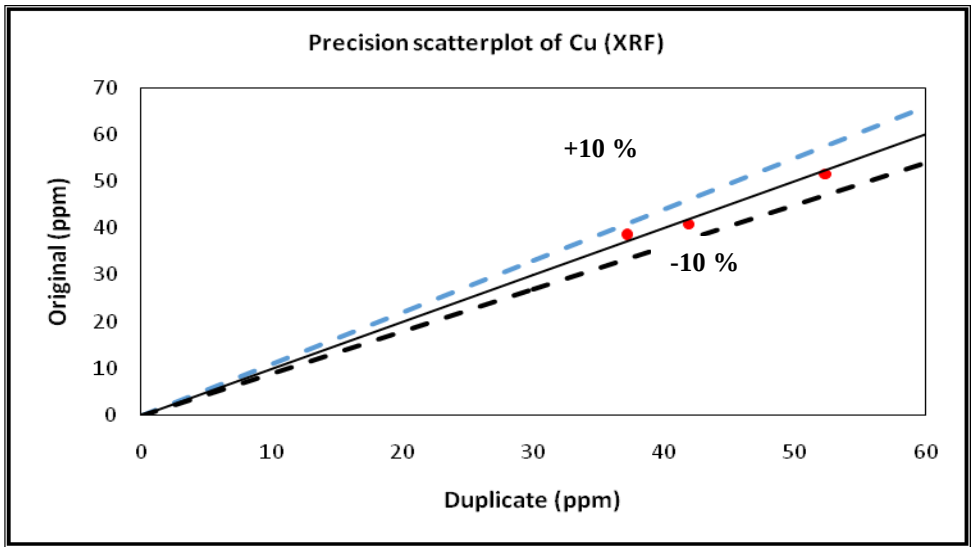

Figure 3.2. 3: A precision scatterplot of Cu, as determined by x-ray fluorescence, showing 10 % error margins.

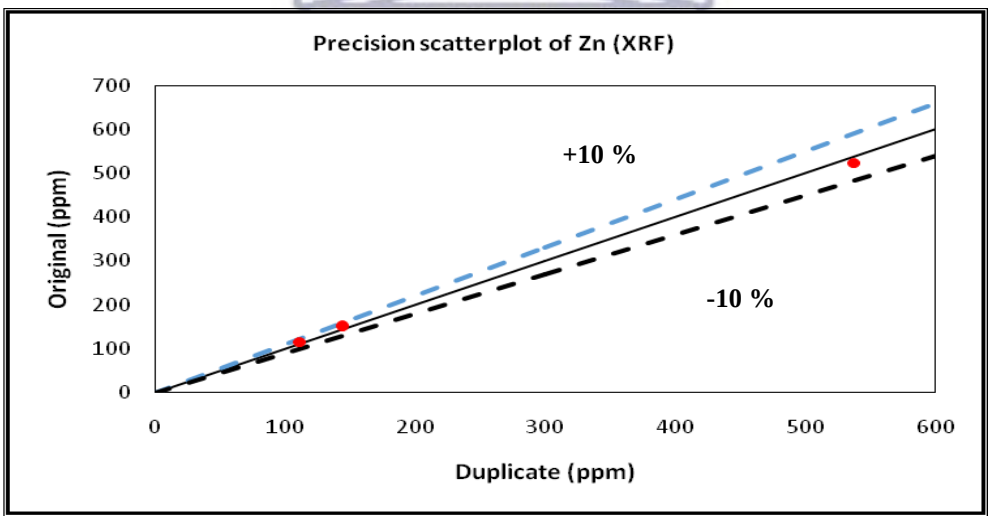

Figure 3.2. 4: A precision scatterplot of Zn, as determined by x-ray fluorescence, showing 10 % error margins.

The trace elements (Cu and Zn) analyzed by x-ray fluorescence show error percentages falling within the 10 % error margin (Fig. 3.2.3 and Fig. 3.2.4)

3.4.1.2 Sulphide-sulphur determination

Sulphide-sulphur was determined by subtracting sulphate-sulphur from the total (Leco) sulphur. Using ICP-MS, sulphate-sulphur was analyzed and duplicate data used to create a precision scatter plot (Fig. 3.2.5).

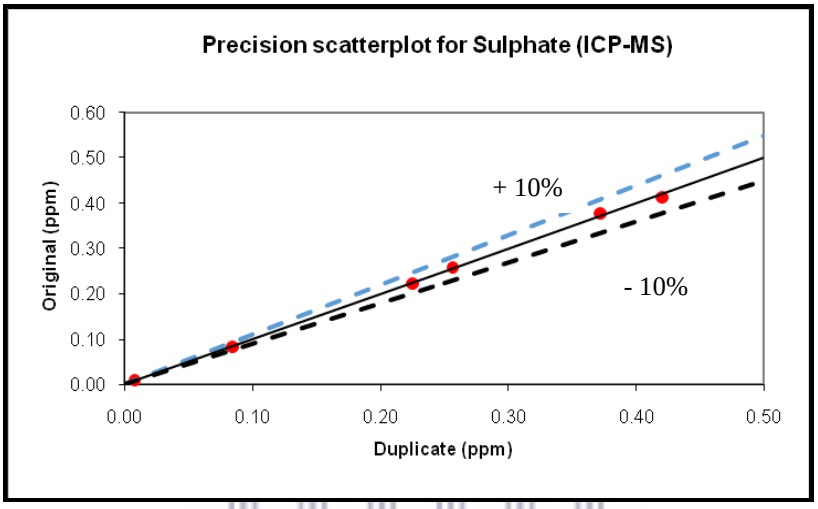

Figure 3.2. 5: A precision scatterplot of sulphate-sulphur, as determined by ICP-MS, showing 10 % error margins.

Sulphate-sulphur analyzed by ICP-MS shows error percentages which fall within the 10 % error range.

3.4.1.3 Partial sequential extraction procedure

Quality control and quality assurance measures used in the graphite furnace analysis included: element standards, blank- and duplicate samples. The element standards include: 1000 ppm Ca, 1000 ppm Zn, 1000 ppm Au and 1000 ppm multi-element (including Fe, Mn, Ni, Co, Co and Pb). The standards were diluted to approximately 50 ppb. Major- and trace elements were measured on the following wavelengths: Ca secondary line (239 nm), Fe primary line (248 nm), Mn primary line (279 nm), Ni primary line (232 nm), Co primary line (240 nm), Cu primary line (324 nm), Zn primary line (213 nm), Pb primary line (217 nm) and Au primary (242 nm). Zn standards were prepared separately from the multi-element standards as not to interfere with the primary wavelength of Cu (324 nm) with which its secondary line nearly overlaps (307 nm).

The graphite furnace parameters for Ca, Fe, Mn, Ni, Co, Cu, Zn, Pb and Au can be found in Appendix Two: D (vi). Blank- samples were included during the analysis to ensure the accuracy of the graphite furnace. Table 3.2, shows the detection limits for the Analytik Jena contraAA. To ensure the precision of measurements, every fifth sample was duplicated during the analysis and used to produce precision scatterplots for Fe and Zn (Fig. 3.2.6 – Fig. 3.2.13). The complete set of precision scatterplots can be found in Appendix Two: D (ii). Table 3.3, provides a general overview of the summary statistics of the error percentages determined for the duplicate samples analyzed by the graphite furnace.

Table 3. 2: Detection limits for the GFAAS (Analalytik Jena contrAA).

Element	Generic Detection Limit_ppb	25% Detection Limit_ppb	25% Detection Limit_*90/5_ppb
Ca	0.005	0.00125	0.0225
Cu	0.02	0.005	0.09
Ni	0.04	0.01	0.18
Co	0.02	0.005	0.09
Zn	0.003	0.00075	0.0135
Pb	0.03	0.0075	0.135
Fe	0.01	0.0025	0.045
Mn	0.006	0.0015	0.027
Au	0.03	0.0075	0.135
U	NA	NA	NA

Table 3. 3: The summary statistics of the error percentages determined for duplicate samples analyzed by graphite furnace

	Double distilled water			1 M ammonium acetate			0.1 M hydroxylamine hydrochloride			0.25 M hydroxylamine hydrochloride		
Element (%)	Min.	Max.	Mean	Min.	Max.	Mean	Min.	Max.	Mean	Min.	Max.	Mean
Ca	0	19	6	0	7	3	0	9	1	0	14	5
Fe	0	11	2	0	14	3	0	5	2	0	4	1
Mn	0	7	2	0	4	2	0	8	3	0	16	5
Co	0	10	3	0	10	2	0	12	5	0	11	4
Ni	0	17	5	0	5	2	0	1	0	0	9	3
Cu	0	11	2	0	5	3	0	7	3	1	13	6
Zn	0	5	1	0	6	2	0	5	2	0	11	3

According to Table 3.3, major oxides extracted by double distilled water show error percentages between 0 % and 19 % and trace elements between 0 % and 17 %. Major oxides extracted by 1

M ammonium acetate show error percentages between 0 % and 14 % and trace elements between 0 % and 10 %. Major oxides extracted by 0.1 M hydroxylamine hydrochloride show error percentages between 0 % and 9 % and trace elements between 0 % and 12 %. Major oxides extracted by 0.25 M hydroxylamine hydrochloride show error percentages between 0 % and 16 % and trace elements between 0 % and 13 %.

Major oxides analyzed by GFAAS show error percentages up to 19 % (Ca extracted by double distilled water) and for trace elements up to 17 % (Ni extracted by double distilled water). The high error percentage for Ca is likely the result of its high contents in the samples relative to that of Fe and Mn. Similarly, Ni was extracted in high quantities relative to Co, Cu and Zn. Thus Ni has the highest error percentage. This is the case because the GFAAS performs optimal measurements of low element (ppb) concentrations. Precision scatterplots were generated (Fig. 3.2.6 – Fig. 3.2.13) as a graphical representation of precision and are presented within 10 percent error margins.

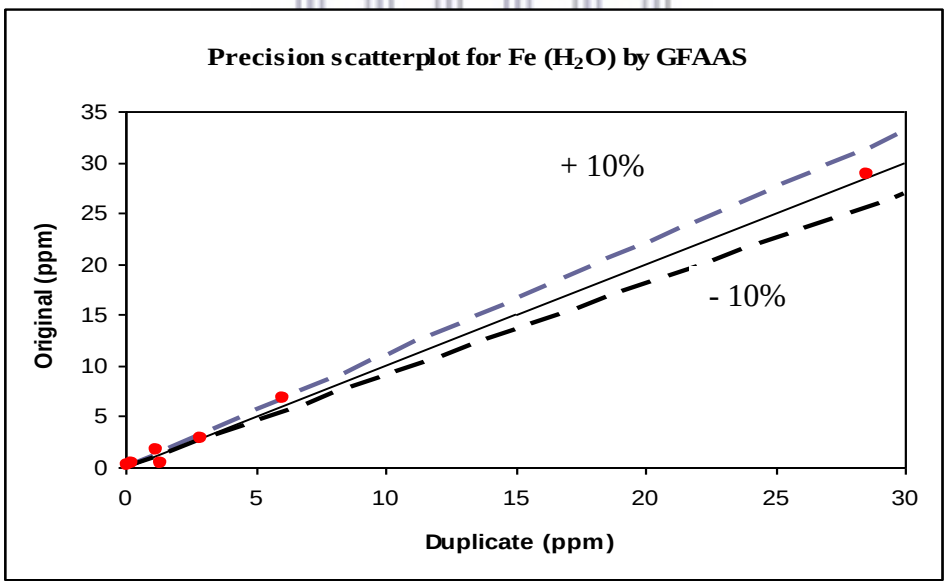

Figure 3.2. 6: A precision scatterplot of Fe extracted by double distilled water, as determined by GFAAS, showing 10 % error margins.

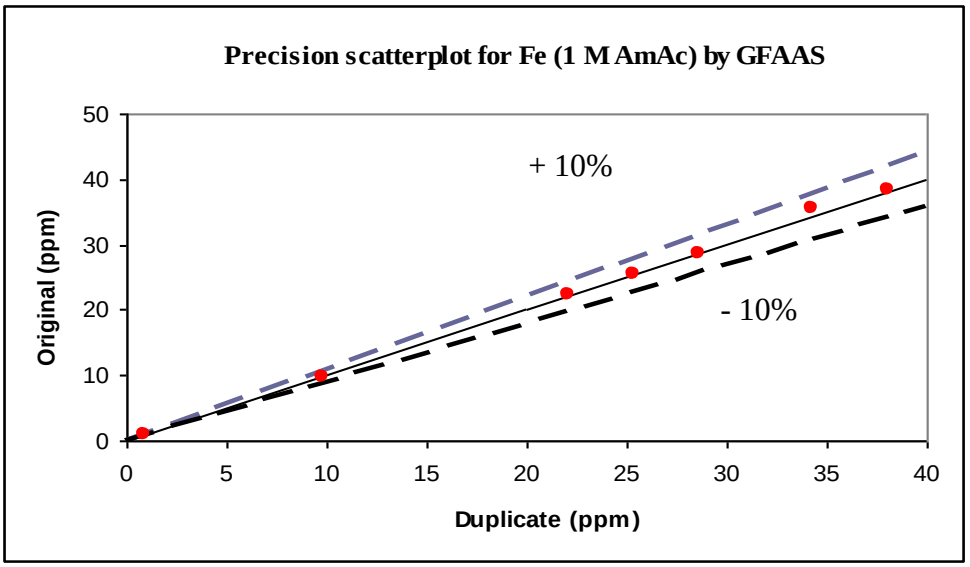

Figure 3.2. 7: A precision scatterplot of Fe extracted by 1 M ammonium acetate (AmAc), as determined by GFAAS, showing 10 % error margins.

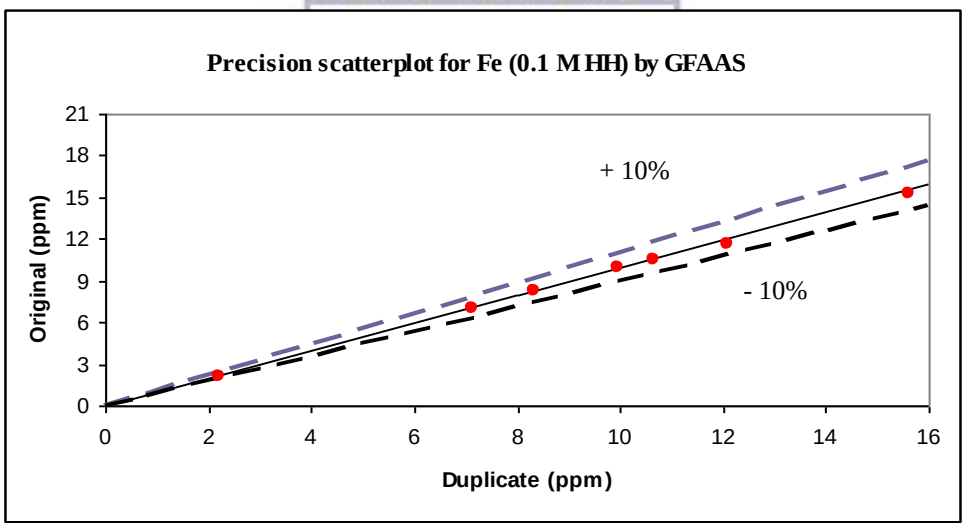

Figure 3.2. 8: A precision scatterplot of Fe extracted by 0.1 M hydroxylamine hydrochloride (HH), as determined by GFAAS, showing 10 % error margins.

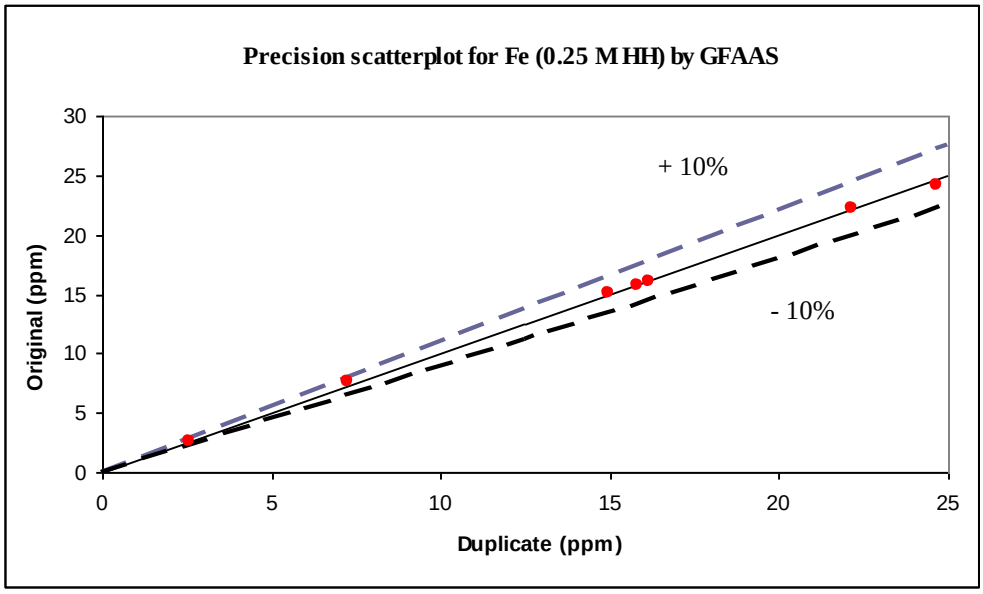

Figure 3.2. 9: A precision scatterplot of Fe extracted by 0.25 M hydroxylamine hydrochloride (HH), as determined by GFAAS, showing 10 % error margins.

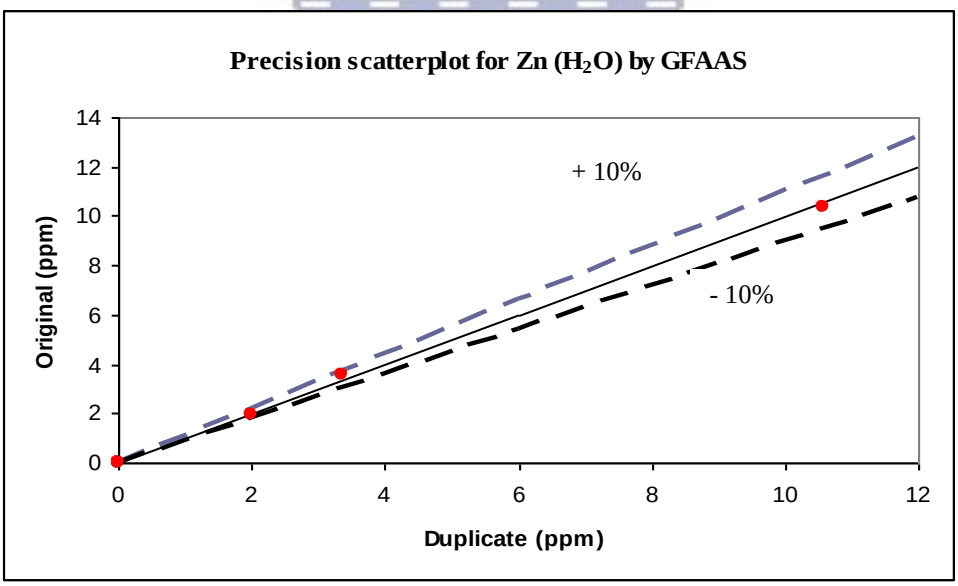

Figure 3.2. 10: A precision scatterplot of Zn extracted by double distilled water, as determined by GFAAS, showing 10% error margins.

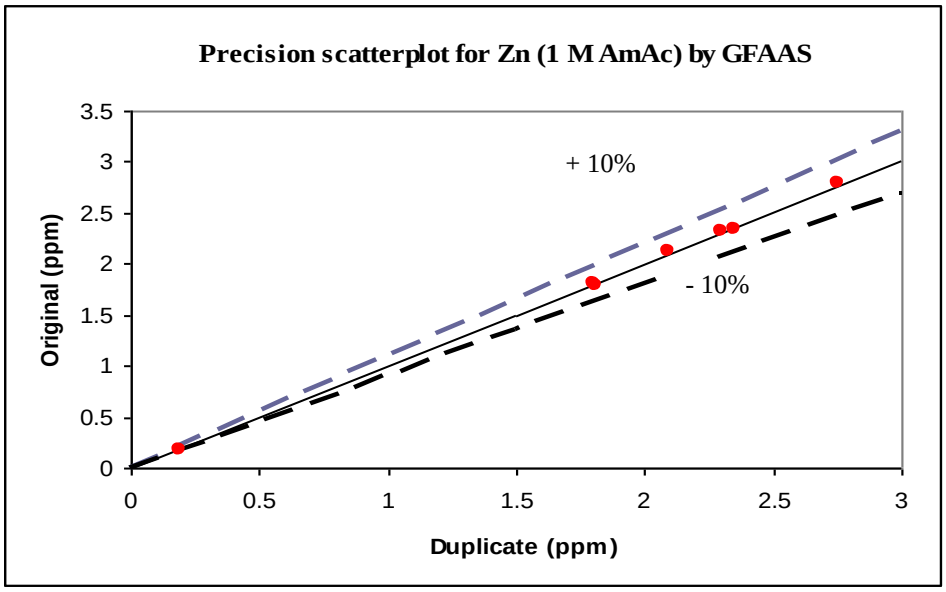

Figure 3.2. 11: A precision scatterplot of Zn extracted by 1 M ammonium acetate, as determined by GFAAS, showing 10 % error margins.

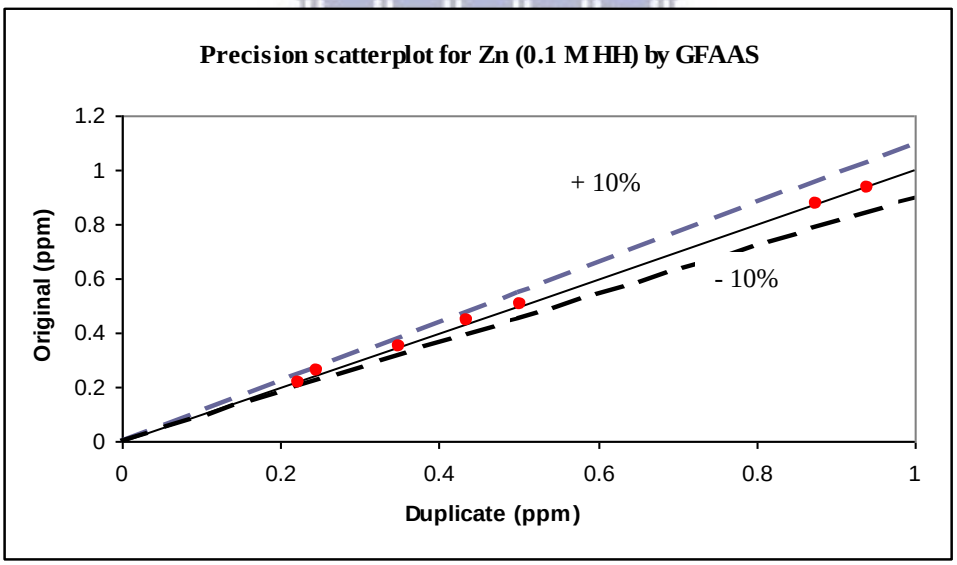

Figure 3.2. 12: A precision scatterplot of Zn extracted by 0.1 M hydroxylamine hydrochloride (HH), as determined by GFAAS, showing 10 % error margins.

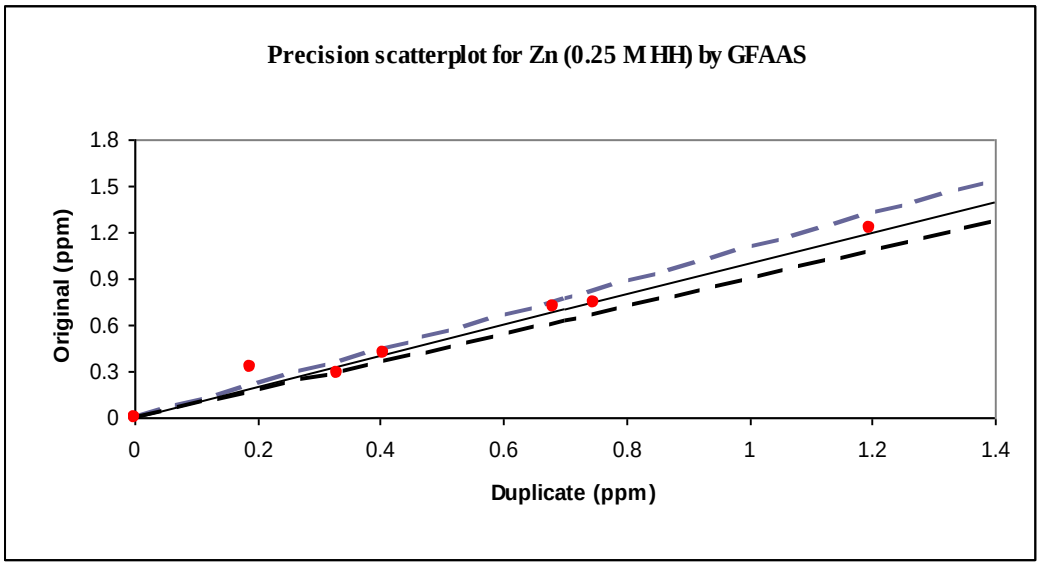

Figure 3.2. 13: Precision scatterplot of Zn extracted by 0.25 M hydroxylamine hydrochloride (HH), as determined by GFAAS, showing 10 % error margins.

The major (Fe) and trace (Zn) elements show error percentages which fall roughly within the 10 % error margins. Exceptions to this are Fe, when extracted by double distilled water and Zn when extracted by 0.25 M hydroxylamine hydrochloride. This is the result of outliers, as shown by the box and whisker plots in Appendix Two: D (iv).

3.4.2 The datasets provided and generated

The datasets provided for this study include: the appraisal of core logs (Appendix One: A), x-ray diffraction data (Appendix One: B), paste pH and electrical conductivity data (Appendix One: C) and bulk geochemical data (Appendix One: D).

The datasets generated as part of this study include: the reappraisal of core logs (Appendix Two: A), petrographic data for section T001 (Appendix Two: B), sulphide-sulphur data (Appendix Two: C) and selective sequential leach data (Appendix Two: D). The sequential extraction dataset includes: (i) bulk geochemical data, (ii) GFAAS precision scatterplots (iii) correlation coefficient analysis, (iv) box and whisker plots (v) Principal Component Analysis statistics, (vi) and graphite furnace parameters.

3.4.3 Statistical analysis

The following statistical analyses were used for the datasets provided for, and those generated by this study:

(i) A summary of descriptive statistics was used to describe the main quantitative features of the bulk geochemical dataset and of each leach dataset. The summary statistics included: min, max, mean and standard deviation. These statistics provided a general overview of the data.

(ii) Cluster and discriminant analyses were used on the bulk geochemical dataset to group the slimes samples based on major oxide chemistry (Abegunde, 2015; Abegunde et al., 2016). Cluster analysis was used to model the weathering zones.

(iii) Box and whisker plots were used to graphically illustrate the distribution range of each leach dataset. These plots were useful in showing the average concentration range of each dataset and the outliers present (Scheinost et al., 2002; Abegunde, 2015; Abegunde et al, 2016; Kennedy et al, 2016).

(iv) Correlation coefficient analysis and principal component analysis was used on each leach dataset to show the relative association between extracted metal concentrations and major oxide phases present (Barona and Romero, 1996; Yangou et al., 2002; Fernández-Caliani et al., 2009; Heikkinen et al., 2009. Huang and Cao, 2016).

3.4.4 Spatial analysis

The bulk geochemical data provided for this study, and sulphide-sulphur- and selective sequential leach data generated during this study underwent spatial analysis using Earthworks® Downhole Explorer (Abegunde, 2015). This software was used to generate plots showing the vertical distribution of elements downhole. The trends in element distribution were described using the downhole plots generated.

CHAPTER FOUR: Results and Interpretation

4.1 Preamble

This chapter provides an overview of the mineralogy and geochemistry determined for samples from the Gold One Millsite Slimes Complex. The investigation of mineralogical and geochemical interactions in slimes/tailings is critical to understand the factors controlling metal distribution in these mine waste environments, and subsequent prevention of metal contamination (Dold, 2005). The mineralogical and geochemical data provided for, and generated during, this study were analyzed in line with the objectives stipulated and includes:

- The assessment of mineralogical influences on metal release through core-log reappraisal and the description of trends in x-ray diffraction data.
- The assessment of geochemical influences on metal release by describing trends in the bulk geochemical data.
- The modeling of weathering zones using cluster and discriminant analysis in order to determine to role of weathering in metal release.
- The calculation of sulphide-sulphur (wt %) and its potential influence on metal mobilization.
- The prediction of the acid generating potential of slimes samples using the calculated sulphide-sulphur (wt %).
- The determination of metal leachability using selective sequential extraction.

4.2 Mineralogical characterization of the weathering zones

The release of metals from slimes into the environment is controlled by the mineralogy of the slimes. The mineralogical data provided for this study included core log data and x-ray diffraction analysis (Abegunde, 2015). Provided core logs were appraised by Abegunde (2015) according to colour, texture and relative grain size. This provided a general description of the slimes core samples while the mineral composition was determined using x-ray diffraction data (Abegunde, 2015). The mineralogical data provided were used to reappraise core logs and

describe trends in the x-ray diffraction data (section 4.2). Petrographic data for section T001 were generated as part of this project to verify trends in slimes descriptions and mineralogy, and are presented in section 4.2.

The core logs for sections T001, T002 and T003 were appraised by Abegunde (2015) on the basis of colour and grain-size variation, as these features were most prominent downhole. Abegunde (2015) noted seven stratigraphic variations downhole namely, (i) whitish brown fine sand, (ii) light brown fine sand, (iii) light brownish yellow fine sand (iv) brownish yellow fine sand (v) brownish grey fine sand (vi) reddish fine sand and (vii) dark grey fine sand. The complete stratigraphic dataset determined by Abegunde (2015) can be found in Appendix One: A.

As part of this study, the core logs were reappraised on the same basis of colour variation and grain-size downhole. This study noted the presence of five stratigraphic variations downhole, namely (i) pale yellow-brown fine sand, (ii) reddish, mottled fine sand, (iii) pale red-brown fine sand, (iv) pale grey-brown fine sand and (v) dark grey-brown fine sand. The complete reappraised stratigraphic dataset can be found in Appendix Two: A. X-ray diffraction data provided for this study determined that slimes samples consist mainly of quartz and lesser quantities of pyrophyllite, pyrite, clinochlore, gypsum and yoshiokaite. The complete x-ray diffraction dataset can be found in Appendix One: B.

Petrographic data for section T001 were generated during this study and described samples on the basis on mineral composition, modal percentages and grain size distribution. The minerals identified and described include quartz (which was the most prominent), pyrophyllite, cryptocrystalline mica, biotite, muscovite and oxides. Cryptocrystalline mica proportions were determined to represent potential clay formation. The complete petrographic dataset can be found in Appendix Two: B

For visual comparison, the stratigraphic-, x-ray diffraction- and petrographic data have been graphically summarized to represent the overall mineralogy of section T001 (Fig. 4.1.1), T002 (Fig. 4.1.2) and T003 (Fig. 4.1.3).

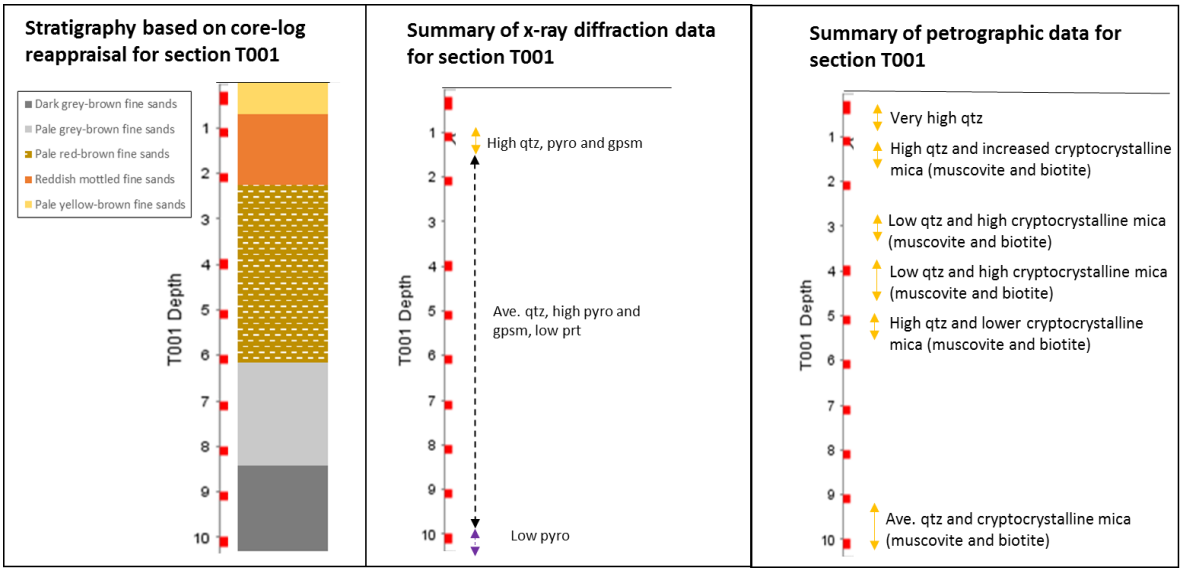

Figure 4.1. 1: The stratigraphy, mineralogy of section T001 based on core log reappraisal, x-ray diffraction data and petrographic data.

Fig. 4.1.1, depicts the stratigraphy, mineralogy and petrography determined for section T001. The first 0.5 m of section T001 are characterized by pale yellow-brown fine sands. The pale yellow-brown fine sands are underlain by reddish mottled fine sands for up to 2.2 meters. X-ray diffraction data between 1- and 2.2 meters show lower quartz and pyrophyllite proportions (approximately 46 % and 2.4 %, respectively) compared to the overlying pale yellow-brown samples. Similar to x-ray diffraction data, petrographic data reveals higher quartz proportions (approximately 58%) within the pale yellow-brown fine sands relative to the underlying reddish mottled fine sands (approximately 45 %). Lower quartz proportions between 0.8 and 1.8 meters are accompanied by increased cryptocrystalline muscovite and biotite proportions (up to 45 %), suggesting potential increased clay proportions.

The red, mottled fine sands between 0.8- and 2.2 meters are underlain by red-brown fine sands for up to 6 meters. X-ray diffraction data for this depth shows average quartz (approximately 46 %), pyrophyllite (approximately 2.4 %) and gypsum (approximately 0.3 – 0.5 %), and low pyrite (approximately 0.12 %). Petrographic data for the same depth, shows slightly higher muscovite and biotite proportions relative to the overlying samples. The relative consistency of mineral proportions between 3.9- and 7.2 meters suggest the red-brown fine sands may represent the transition zone. The red-brown fine sands between 2.2- and 6 meters are underlain by pale grey-

brown fine sands for up to 8.2 meters. Grey-coloured samples at this depth are presumable indicators of the onset of the reduced zone. The pale-grey fine sands between 6- and 8.2 meters are underlain by darker grey-brown fine sands for up to 10.2 meters. An increase in the intensity of grey in samples at this depth suggest a deeper reduced zone. Petrographic data between 10- and 10.2 meters reveal that this depth shows similar oxide proportions to the first 3.6 meters i.e. approximately 3%.

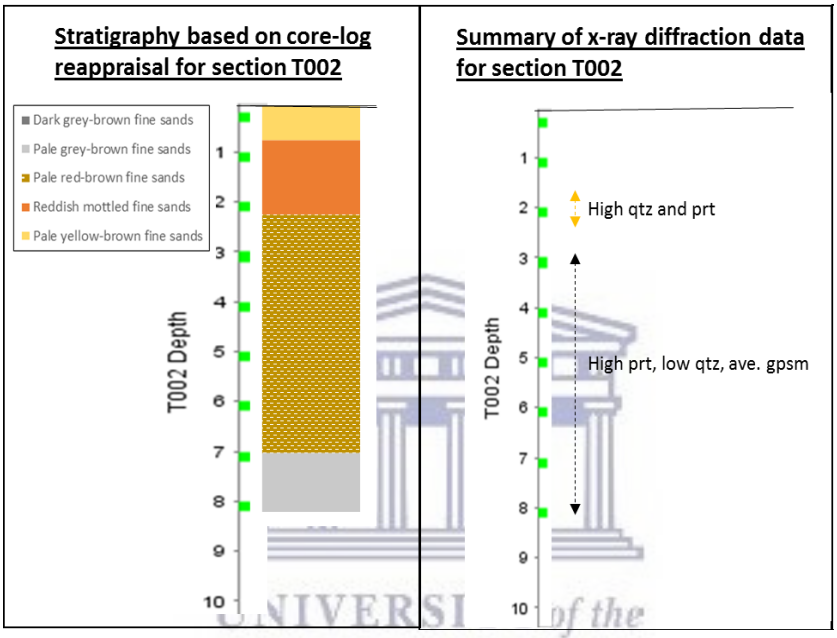

Figure 4.1. 2: The stratigraphy and mineralogy of section T002, based on core-log reappraisal, x-ray diffraction data and petrographic data.

Fig. 4.1.2, depicts the stratigraphy and mineralogy determined for section T002. Similar to section T001, the first 0.5 meters of section T002 is characterized by pale yellow-brown fine sands. Similarly, the latter is underlain by red, mottled fine sands for up to 2.2 meters in section T002.

As for section T001, the x-ray diffraction data at this depth of section T002 reveals slightly lower quartz proportions (approximately 49 %) than overlying pale samples accompanied by higher pyrite (approximately 0.5 %) and lower pyrophyllite (approximately 1 %) and gypsum (0.34 %). Similar to section T001, the red, mottled fine sands are underlain by red-brown fine sands. Unlike section T001, the latter occurs up to 7.2 meters. Relative to section T001, the x-ray

diffraction data for this depth of section T002 shows lower quartz (approximately 41 %), pyrophyllite (approximately 1 %) and gypsum (approximately 0.27 %) and higher pyrite (0.42 %). The consistency of mineral proportions in the red-brown fine sands are presumably indicative of the transition zone. Similar to section T001, the red-brown fine sands of section T002 are underlain by pale-grey fine sands for up to 8.2 meters. As for section T001, the onset of grey sands mark the start of the reduced zone.

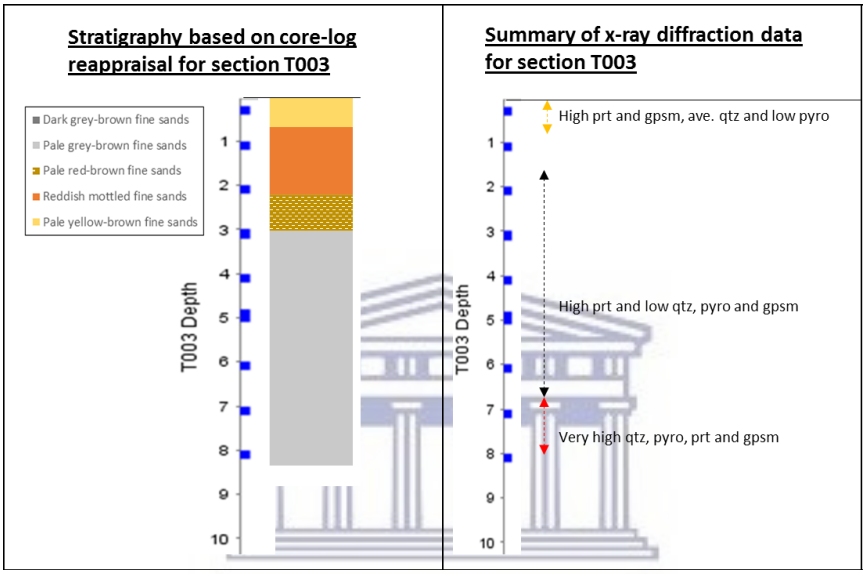

Figure 4.1. 3: The stratigraphy and mineralogy of section T003, based on core log reappraisal, x-ray diffraction data and petrographic data.

Fig. 4.1.3, depicts the stratigraphy and mineralogy determined for section T003. Similar to section T001 and T002, the first 0.8 meters of section T003 is characterized by pale yellow-brown fine sands. According to the x-ray diffraction data, this depth is characterized by average quartz (approximately 46 %), low pyrophyllite (approximately 0.9 %) and high- pyrite (approximately 0.47 %) and gypsum (approximately 0.44 %). Similarly, the pale yellow-brown fine sands are underlain by red, mottled fine sands for up to 2.2 meters in section T003. The red, mottled fine sands are underlain by red-brown fine sands for up to 3.2 meters. Similar to section T002, the x-ray diffraction data for this depth showed low quartz (approximately 41 %), pyrophyllite (approximately 0.8 %) and gypsum (approximately 0.39 %) and higher pyrite (0.42 %). The depth of red-brown fine sands in section T003, is notably shallower than that observed for section T001 and T002. This is likely the result of a shorter transition zone. The red-brown

sands of section T003 are underlain by pale grey-brown fine sands for up to 8.2 meters. This is likely an indicator of a relatively long reduced zone. Unlike section T001 and T002, depths between 8- and 8.2 meters are characterized by peaks in quartz (approximately 63 %), pyrophyllite (approximately 5.8 %), pyrite (approximately 0.6 %) and gypsum (approximately 1.7 %) proportions. This may provide an indication of the relative stability of primary- and secondary minerals at this depth

Trends across sections T001, T002 and T003 show high quartz proportions coincide with pale yellow-brown fine sands in the top portions of each section, suggesting the first 0.8 meters of the slimes dam may be more susceptible to leaching, relative to samples with higher clay contents further down hole. Gypsum proportions in the first 0.8 meters of sections T001 and T002 are notably higher than lower, transition zone samples. This is the result of increased evaporation in the highly oxidized, upper samples of the slimes dam. The relative consistency of mineral proportions in the red-brown fine sands suggest these samples are indicative of the transition zone. According to the distribution of presumably oxidized, transition and reduced samples, section T001 is moderately weathered, section T002 highly weathered and section T003, the least weathered.

4.3 Geochemical characterization of weathering zones using bulk geochemical data

The aim of this study was to understand metal release from the Gold One Millsite Slimes Complex into the Randfontein area, Witwatersrand. To achieve this, the slimes mineralogical data (section 4.2) and bulk geochemical data (section 4.3) was assessed to determine the control of the mineralogical- and geochemical factors on metal release. Bulk geochemical data were provided by Abegunde (2015) and used to (i) model weathering zones using cluster groups (section 4.3.2) and (ii) describe the trends in bulk element chemistry down hole (section 4.3.3). The complete bulk geochemical dataset provided for this study can be found in Appendix One: D. Before the weathering zones could be modeled, cluster analysis was used to group samples based on their major element chemistry (4.3.1).

4.3.1 Cluster and discriminant analysis

Cluster analysis is an exploratory data analysis tool used to sort data into groups based on the extent to which they are associated, i.e. data is placed into a group if its association with that group is maximal and its association to others, minimal (Späth, 1980). Thus, cluster analysis could be used to organize slimes samples into meaningful groups based on bulk element geochemistry (Table 4.1). Hierachical-cluster analysis was performed on major oxide chemistry (LOI, SiO_2, Al_2O_3, Fe_2O_3, CaO, MgO, Na_2O, K_2O, MnO, TiO_2, P_2O_5, Cr_2O_3 and Ba). The analysis produced clusters using Ward's method at an interval of squared Euclidean distance. Cluster analysis identified four different sample groupings (Fig. 4.2.1).

Table 4. 1: The subdivision of slimes samples into cluster groups one, two, three and four.

Cluster 1	Cluster 2	Cluster 3	Cluster 4
48	49	50	55
59	52	53	57
71	54	58	63
75	56	68	64
	60	69	66
	61	70	72
	62		73
	65		
	67		
	74		
	76		

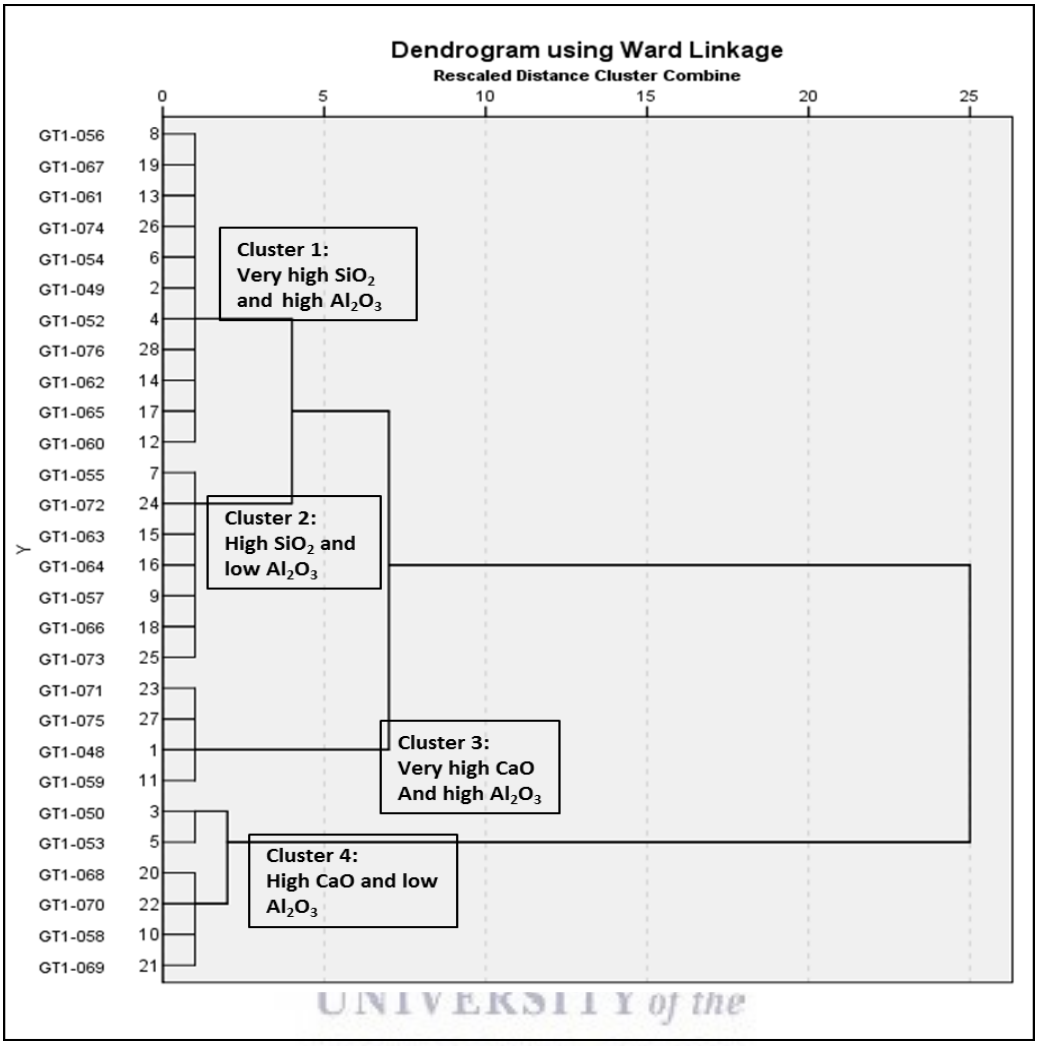

Figure 4.2. 1: A dendogram showing the four sample cluster groups determined by cluster analysis.

While cluster analysis is able to establish structures within data, it does so without providing an explanation as to what the subdivision is based on, i.e. the traits defining the similarity or dissimilarity in samples. Thus, cluster analysis was followed by discriminant analysis.

Discriminant analysis is used to determine which continuous variables discriminate between two or more observed groups (Poulsen and French, 2004). It aims to better understand the data by building a prediction model which allows group membership to be predicted based solely on known interval variables. The model is able to provide insight into the relationship between group membership and the variables used for the prediction of group membership (Poulsen and French, 2004).

Interpretation of discriminant functions is based on standard coefficients (Table 4.2) and the structure matrix (Table 4.3). Each variable in each discriminant function is given a standardized beta coefficient (Poulsen and French, 2004). The greater the standardized coefficient, the greater the contribution of that variable to the discrimination between groups. However, the coeffients fail to provide insight into the groups between which the respective functions discriminate (Poulsen and French, 2004). The nature of discrimination for each discriminate function can be identified by examining the means for the functions across groups. Variation in the location of group means (centroids) display dimensions along which groups vary (Table 4.4). Thus, by plotting the scores of the respective discriminant functions, it is possible to visualize the groups between which the functions discriminate (Fig. 4.2.2).

Table 4. 2: The standardized canonical discriminant functions coefficients which represent the individual contribution of each variable to the discriminant function.

Standardized Canonical Discriminant Function Coefficients			
	Function		
	1	2	3
LOI	4.982	.237	4.260
SiO2	5.184	2.217	3.082
Al2O3	1.043	1.004	1.979
Fe2O3	-.591	2.415	.529
CaO	-1.150	1.317	-.995
MgO	3.940	2.221	2.104
Na2O	1.432	.536	.153
K2O	1.092	1.965	1.177
MnO	.629	-.664	-.499
TiO2	.640	1.115	.784
P2O5	-.284	.458	-.781
Cr2O3	-.490	-.573	-.971
Ba	-1.994	-3.831	-1.108

Standardized canonical discriminant function coefficients (Table 4.2) show that SiO_2 has the largest discriminating ability in the first function. Of the variables defining function two (Al, Mn, K and Na), Al and K show the largest contribution of discriminating ability in function two.

Table 4. 3: The structure matrix representing the simple correlation between the predictor variables and discriminant functions.

Structure Matrix			
	Function		
	1	2	3
SiO2	.567*	.330	-.424
LOI	-.321*	-.143	.212
CaO	-.283*	-.055	-.237
Al2O3	-.207	-.404*	.223
K2O	-.128	-.357*	.164
MnO	-.090	-.339*	.056
Na2O	-.094	-.256*	.015
TiO2	.002	.159*	.094
Ba	-.047	-.155*	.143
P2O5	-.063	-.092*	.055
Fe2O3	-.139	.247	.249*
Cr2O3	-.009	-.153	-.188*
MgO	-.080	-.009	.176*

According to the structure coefficients (Table 4.3) SiO_2 (approximately 0.56) is most strongly correlated with the first function. This is followed by weaker correlation with CaO (approximately - 0.28). The variable showing the strongest correlation with function two is Al_2O_3 (approximately – 0.40). Al is followed closely by K_2O (approximately – 0.35), MnO (approximately – 0.34) and Na (-0.25). Similar to function one, function three is strongly correlated with Si_2O (approximately – 0.42). However, function three is of little use in distinguishing cluster groups and has subsequently been omitted from the canonical discriminant functions (Fig. 4.2.2).

Table 4. 4: The unstandardized canonical discriminant functions evaluated at group means.

Functions at Group Centroids			
	Function		
Ward Method	1	2	3
1	9.637	-2.231	-.610
2	2.982	1.060	.781
3	-8.202	-1.409	.713
4	-3.163	.817	-1.490

Table. 4.4, provides an indication of the canonical linear discriminant functions used to separate cluster groups. In this instance, four cluster groups were identified. Hence, three functions were

calculated as discriminating variables. Each function projects data onto a dimension that best discriminates between the cluster groups. The canonical discriminant functions are given in Fig. 4.2.2.

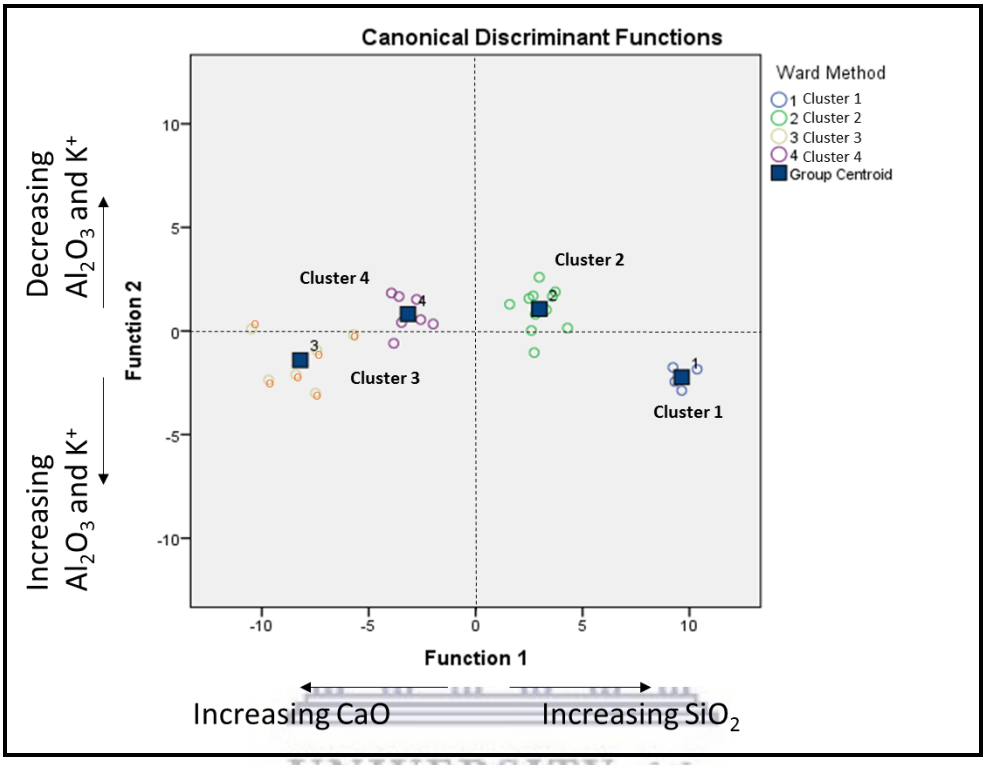

Figure 4.2. 2: The canonical discriminant functions which distinguish between clusters based on major oxide chemistry.

According to Fig. 4.2.2, function one is distinguished by relative SiO_2 and CaO contents and function two, by high/low Al and K^+ contents.

Thus, the cluster groups can be distinguished as follows:

Cluster one: Very high SiO_2 and increasing Al and K^+

Cluster two: High SiO_2 and decreasing Al and K^+

Cluster three: Very high CaO and increasing Al and K^+

Cluster four: High CaO and decreasing Al and K^+

4.3.2 Modeling of weathering zones using cluster analysis

Sample cluster groups (Fig. 4.2.3) were generated as part of this study and used to model the weathering zones in the slimes dam. The slimes samples were grouped using cluster and discriminant analysis and divided into four groups based on their major oxide chemistry. The cluster groups include:

Cluster one: Very high SiO_2 and high Al and K^+
Cluster two: High SiO_2 and low Al and K^+
Cluster three: Very high CaO and high Al and K^+
Cluster four: High CaO and low Al and K^+

K^+ is important as it is readily leached during the formation of clays (Table 1). Under this assumption, high Al and K^+ is representative of lower clay contents and low Al and K^+ higher clay contents. Based on this, cluster two and four samples are expected to represent samples of higher clay contents. Fig. 4.2.3, shows the distribution of sample cluster groups downhole for section T001, T002 and T003.

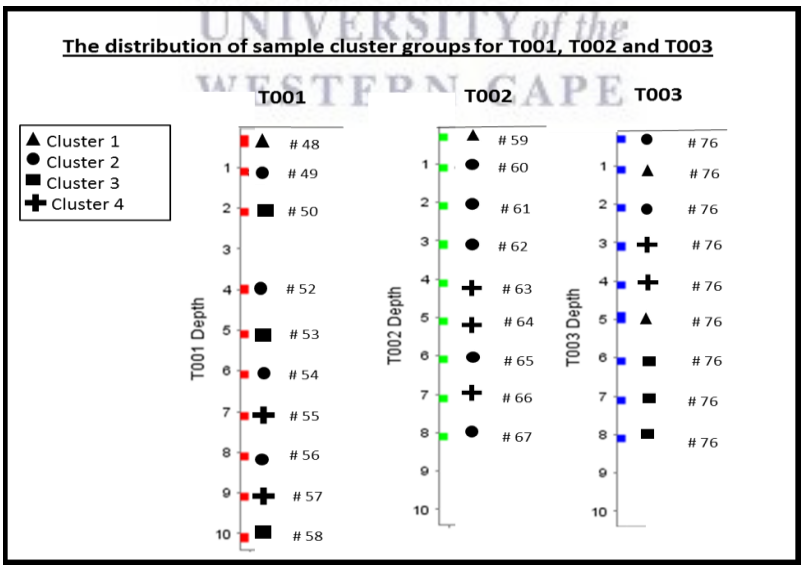

Figure 4.2. 3: The distribution of sample cluster groups in section T001, T002 and T003.

The petrographic data generated during this study were compared with the distribution of sample cluster groups downhole to verify the relationship between K^+ contents and the cryptocrystalline mica (presumable indication of clay formation) for section T001 (Fig. 4.2.4).

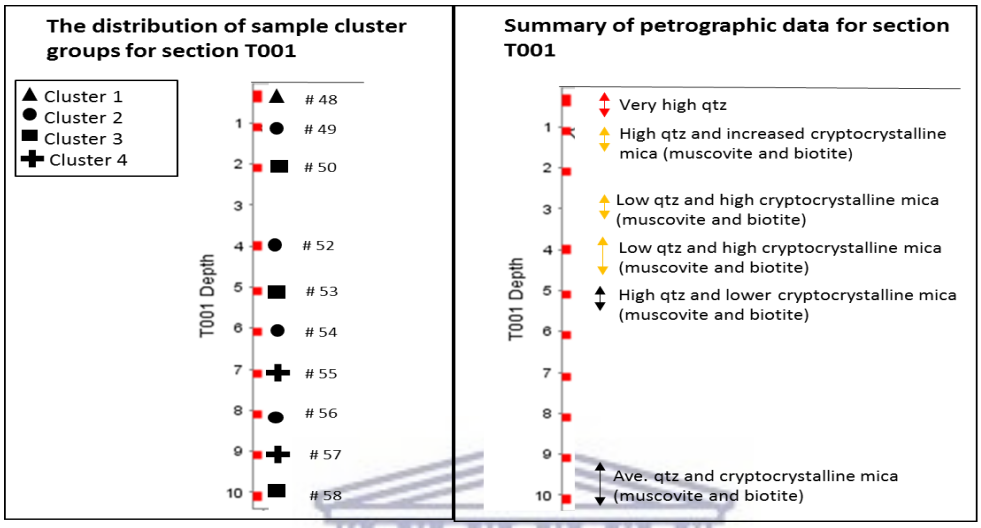

Figure 4.2. 4: A comparison of the distribution of sample cluster groups and the petrographic data for section T001.

Fig. 4.2.4, compares the distribution of sample cluster groups with the petrographic data generated for section T001. As expected, when compared with petrographic analysis, cluster two and four samples (presumably high in clay), coincide with the highest proportions of cryptocrystalline mica observed for section T001. This supports the suggestion that decreases in K^+ are representative of potential clay formation. On the basis of clay contents, section T002 is deemed to have undergone the most hydrolysis, section T001 moderate hydrolysis and section T003, the least hydrolysis. Hydrolysis is a form of chemical weathering which breaks down minerals such as feldspar and mica when reacting with water, to form clays.

The relative CaO contents in samples is also important as this contributes to the neutralizing capacity of samples (Price, 1997). Thus, samples high in CaO (cluster three and four samples) are expected to coincide with neutral or basic paste pH typical of the reduced zone (towards the base of slimes) and samples low in CaO (cluster one and two samples) with more acidic paste pH typical of the oxidized zone (upper zone of the slimes). Paste pH data was supplied by Abegunde

(2015) and used as part of this study to relate the distribution of sample cluster groups to weathering zones (Fig. 4.2.5).

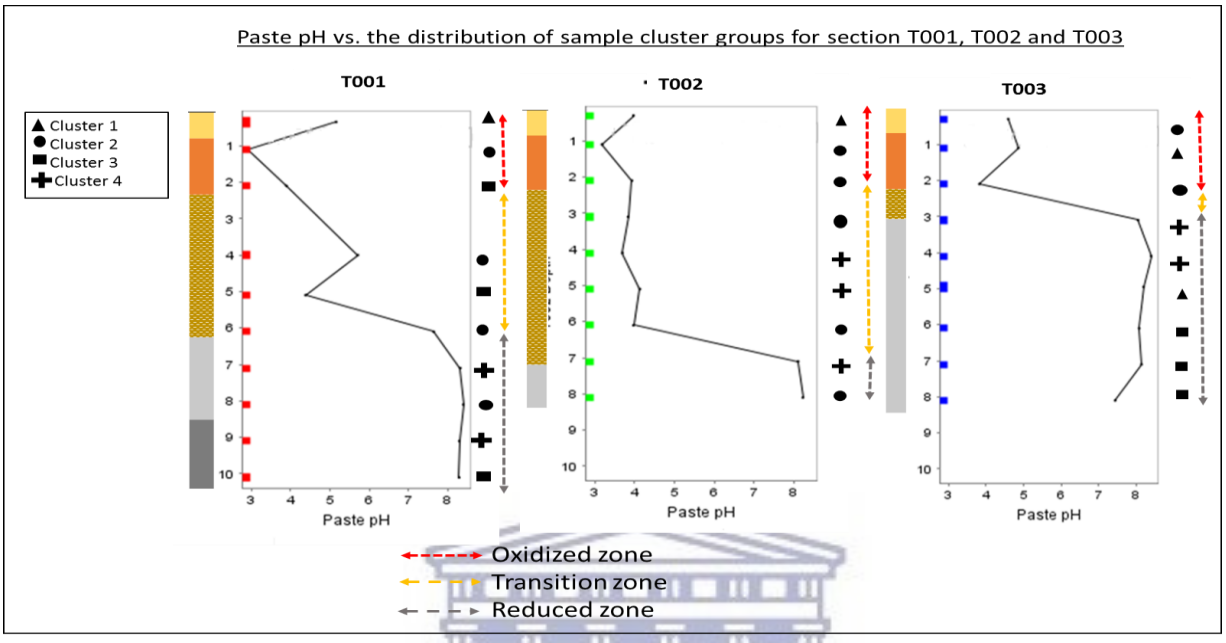

Figure 4.2. 5: The distribution of sample cluster groups and the paste pH data for sections T001, T002 and T003.

Fig. 4.2.5, compares the distribution of sample cluster groups and the paste pH data for sections T001, T002 and T003. As expected, cluster one and two samples (low in CaO and high in SiO_2) dominate the upper portions of the slimes dam. For section T001, cluster one and two samples dominate up to 2 meters. For section T002, cluster one and two samples dominate up to 4 meters. For section T003, cluster one and two samples dominate up to 3 meters. Cluster one samples (very high SiO2) appear to coincident with pale yellow-brown. According to x-ray diffraction and petrographic analysis the pale yellow-brown fine sands show very high quartz. These low CaO and high SiO_2 samples constitute the oxidized zones in each section.

As expected, cluster three and four samples (high in CaO and low in SiO_2) dominate mid- and lower portions of the slimes dam. For section T001, cluster three and four samples dominate between 5- and 10.2 meters. For section T002, cluster three and four samples dominate between 4- and 7.2 meters. For section T003, cluster three and four samples dominate between 3.2- and 8.2 meters. Cluster three and four are coincident with red-brown-, and grey fine sands. Using

CaO to represents alkalinity, the transition zone is marked by the onset, rather than complete dominance, of high-CaO samples downhole. The dominance of high-CaO samples constitute the reduced zones of each section.

Based on the trends in paste pH and the distribution of sample cluster groups (Fig. 4.2.5) for section T001, the oxidized zone occurs up to 2.2 meters, the transition zone between 2.2- and 6 meters and the reduced zone between 6- and 10.2 meters. For section T002, the oxidized occurs up to 2.2 meters, the transition between 2.2- and 7 meters and the reduced zone between 7- and 8.2 meters. For section T003, the oxidized zone occurs up to 2.2 meters, the transition zone between 2.2 and 3.2 meters and the reduced zone between 3.2- and 8.2 meters.

Electrical conductivity (EC) data were supplied by Abegunde, 2015 and used as part of this study to compare to paste pH. The complete electrical conductivity dataset can be found in Appendix One: C. Electrical conductivity is a measurement of a material's ability to carry an electric charge and was compared with paste pH to discern trends between the two (Fig. 4.2.6).

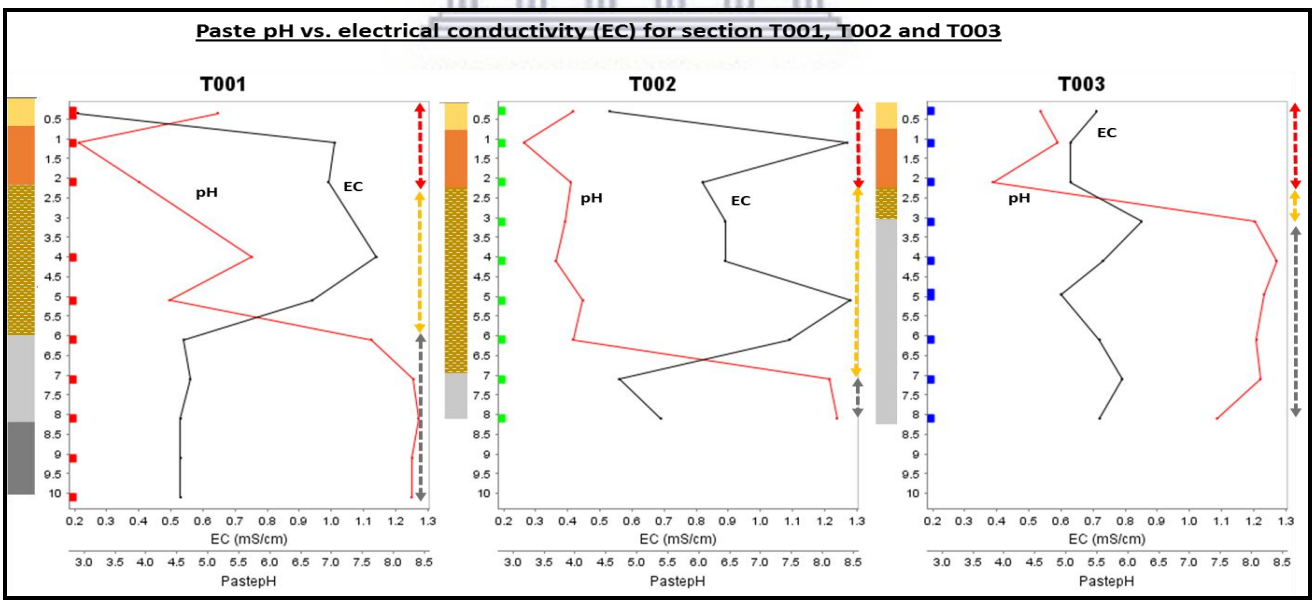

Figure 4.2. 6: Paste pH vs. EC for section T001, T002 and T003.

Fig. 4.2.6, compares paste pH and EC, and shows low pH coincident with high EC in the oxidized zone and high pH coincident with lower EC in the reduced zone. This suggests that

paste pH and EC generally inversely correlated. This is a typical trend in mine waste deposits such as slimes since EC is closely related to the total dissolved salts (TDS). Consequently, low pH is accompanied by high EC because of the increase in ions released into solution under low pH conditions and vice versa under reducing conditions.

The electrical conductivity (EC) of soils is determined by soil texture, drainage conditions, cation exchange capacity, salinity, organic matter contents and subsoil characteristics (Smith and Doran, 1996). In general, sands have low EC, silts have moderate EC and clays have high EC. Thus, electrical conductivity strongly correlates to soil texture and particle size. Based on the EC ranges for section T001 (0.21 – 1.14), T002 (0.23 – 1.28) and T003 (0.6 – 0.85) and the general relationship between EC and grain size, section T003 may host slightly coarser grain sizes. This has implications for the overall rate of oxidation as smaller grains show increased oxidation due to their larger surface area while larger grains show decreased rates of oxidation due to the smaller surface area. Fig 4.2.7, compares the weathering zones, sample cluster groups and slimes stratigraphy for sections T001, T002 and T003.

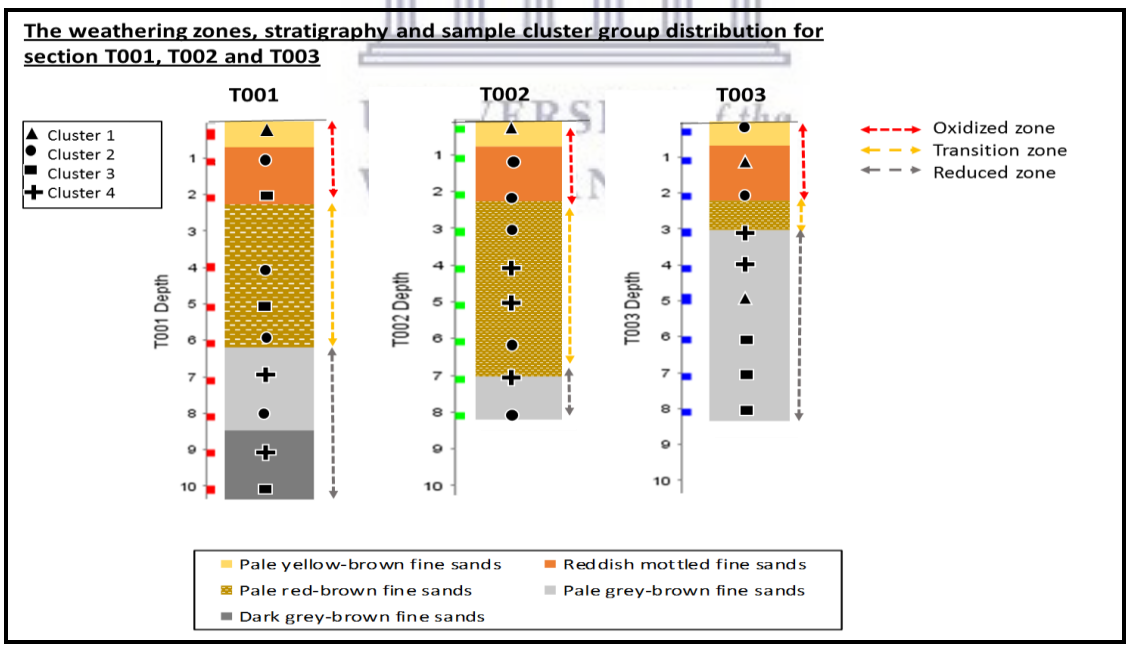

Figure 4.2. 7: A graphical representation of the weathering zones, sample cluster groups and the slimes stratigraphy.

When comparing the weathering zones with stratigraphy for section T001, T002 and T003 (Fig. 4.2.7), the upper oxidized zone is characterized by pale yellow-brown fine and the lower oxidized zone by reddish, mottled fine sand. The transition zone is characterized by pale red-brown fine sand, and the reduced zone by pale- and dark grey-brown sands.

When comparing the distribution of sample cluster groups with stratigraphy, cluster one samples (very high SiO_2 and low clay) coincide with the pale yellow fine sands within the upper oxidized zone of section T001 and T002. Using K^+ loss to represent potential clay formation (as this ion is readily leached during the chemical weathering of feldspars and micas), increasing K^+ within the first 0.5 meters further supports the suggestion that this portion of section T001 and T002 may be highly susceptible to leaching attributed to its low clay and high quartz contents. Clay concentrations are typically well correlated with oxide and metal concentrations, as metals are readily adsorbed to the unsatisfied negative charges on clay surfaces. Thus, this portion of T001 and T002 is expected to be highly leached of oxide and metal contents. For T003, this leached layer occurs between 0.4 meters and 1.2 meters. Fig. 4.2.8, compares the slimes stratigraphy, weathering zones and mineralogy for section T001, T002 and T003.

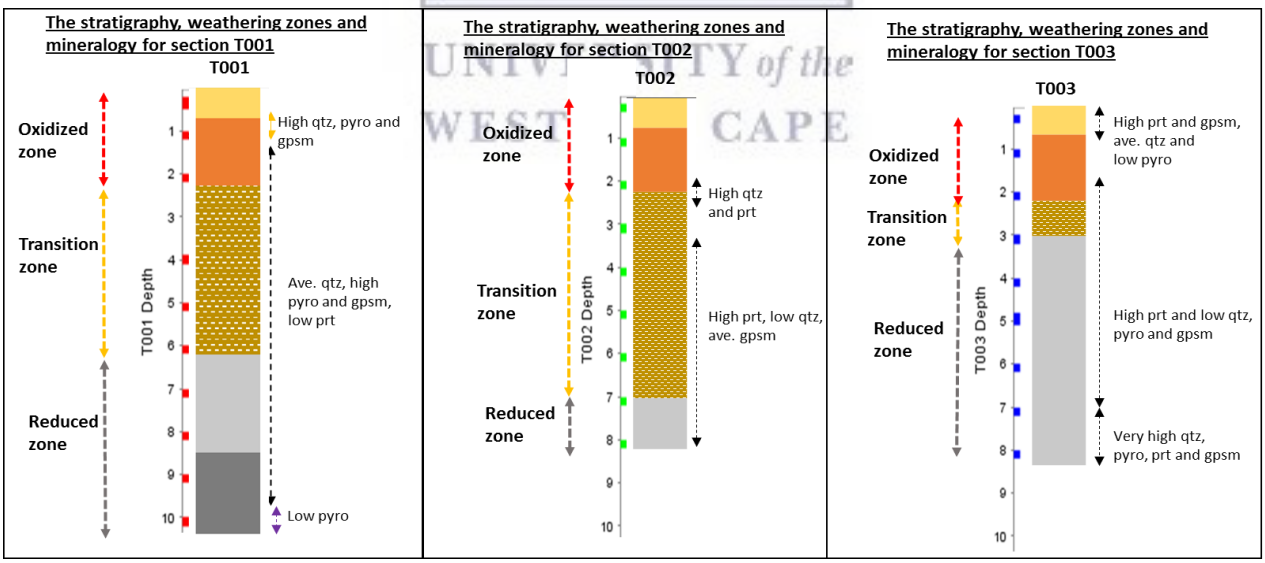

Figure 4.2. 8: The stratigraphy, weathering zones and mineralogy for section T001, T002 and T003.

Fig. 4.2.8, depicts the stratigraphy, weathering zones and mineralogy for section T001, T002 and T003. As expected, mineralogical data for section T001, show higher quartz proportions in the

presumed oxidized zone (approximately 52 %) than the lower transition and reduced zone (approximately 46 %). This supports the notion that high- SiO_2 (cluster one and two) samples dominate the oxidized zone while higher- CaO (cluster three and four) samples dominate the reduced zone of section T001.

Similar to section T001, the mineralogical data for section T002 show higher quartz proportions in the presumed oxidized zone (approximately 49 %) relative to the lower transition and reduced zone (approximately 41 %). Similar to section T001, this supports the notion that high- SiO_2 (cluster one and two) samples dominate the oxidized zone while higher- CaO (cluster three and four) samples dominate the reduced zone of section T002.

Unlike section T001 and T002, the mineralogical data for section T003 suggests that the highest quartz (approximately 63 %), pyrophyllite (up to 5.8 %), pyrite (approximately 0.6 %) and gypsum (approximately 1.8 %) proportions occur between 8- and 8.2 meters. While high pyrite and gypsum proportions are expected at this depth, since weathering is typically minimal here, the high quartz proportion is unexpected. This is possibly the result of human error.

The high contents of soluble salts (K+ and Na+) noted for cluster one slime samples in the upper oxidized zone may not only represent low clay contents as suggested for cluster 3 samples but may also be the result of an upper evaporite (gypsum) layer, as was verified by x-ray diffraction analysis. On the basis of relative pyrite concentrations (Appendix One: B), section T001 is deemed the most oxidized, section T002, moderately oxidized and section T003, the least oxidized.

4.3.3 Bulk element chemistry

One of the objectives of this study was to assess the control of geochemical factors on metal release in slimes samples. To achieve this, bulk geochemical data provided by Abegunde (2015) were used as part of this study to describe the trends in bulk element chemistry downhole. A statistical summary of the bulk element geochemical data is presented in Table 4.5, and provides an overview of selected major oxide- and trace metal concentrations in sections T001, T002 and

T003. This is followed by downhole plots which show the distribution patterns of selected major oxide- (Fig. 4.3.1, Fig. 4.3.3, and Fig. 4.3.5, respectively) and trace metal (Fig. 4.3.2, Fig. 4.3.4, and Fig. 4.3.6, respectively) concentrations in sections T001, T002 and T003. The complete bulk geochemical data can be found in Appendix One: D. Major- and trace element concentrations are displayed separately downhole to ensure consistency in the scaling of the graphs.

Table 4. 5: Summary statistics for selected major oxide- and trace metal concentrations in sections T001, T002 and T003.

	T001				T002				T003			
Element	**Min.**	**Max.**	**Mean**	**Stdev.**	**Min.**	**Max.**	**Mean**	**Stdev.**	**Min.**	**Max.**	**Mean**	**Stdev.**
CaO (wt %)	0.03	1.40	0.79	0.44	0.02	1.02	0.55	0.29	0.25	1.43	0.86	0.43
Fe_2O_3 (wt %)	1.86	4.79	3.02	0.81	1.37	3.59	2.85	0.67	1.73	2.93	2.38	0.42
MnO (wt %)	0.02	0.06	0.03	0.01	0.01	0.03	0.02	0.01	0.00	0.05	0.02	0.02
Co (ppm)	3.70	61.50	26.62	14.76	1.60	56.50	25.67	14.68	18.10	78.00	38.68	22.51
Ni (ppm)	13.20	229.70	73.61	58.36	8.20	96.00	56.33	26.87	38.30	242.20	119.86	78.20
Cu (ppm)	9.80	52.40	33.23	11.13	7.50	50.40	27.49	11.33	28.70	100.50	56.48	22.97
Zn (ppm)	9.00	164.00	91.40	50.24	5.00	109.00	69.11	37.94	25.00	231.00	108.22	80.84
Pb (ppm)	11.40	30.60	21.63	7.42	11.80	26.40	18.32	5.31	13.40	67.50	32.48	18.14
Au (ppb)	59.60	823.30	205.40	235.73	49.00	430.80	145.06	118.97	58.70	812.10	219.86	236.46

According to Table 4.5, the descending order of selected oxide concentrations for section T001 can be given as follows: Fe_2O_3 (approximately 3 %) > CaO (approximately 0.8 %) >> MnO (0.03 %). The descending order of selected trace metal concentrations can be given as follows: Zn (approximately 91 ppm) > Ni (approximately 74 ppm) > Cu (approximately 33 ppm) > Co (approximately 27 ppm) > Pb (approximately 22 ppm) > Au (approximately 205 ppb).

According to Table 4.5, the descending order of selected oxide concentrations in section T002 follow the same pattern as in section T001 and can be given as follows: Fe_2O_3 (approximately 2.9 %) > CaO (approximately 0.6 %) >> Mn (approximately 0.02 %). Similarly, the descending order of selected trace metal concentrations can be given as follows: Zn (approximately 69 ppm) > Ni (approximately 56 ppm) > Cu (approximately 27 ppm) Co (approximately 26 ppm) > Pb (approximately 18 ppm) > Au (approximately 145 ppb). Despite oxide- and trace metal concentrations lower than that of section T001, section T002 shows the same general trend in oxide- and metal proportions.

According to Table 4.5, the descending order of selected major oxide concentrations for section T003 can be given as follows: Fe_2O_3 (approximately 2.4 %) > CaO (approximately 0.9 %) >> MnO (0.02 %). The descending order of selected trace metal concentrations can be given as follows: Ni (approximately 120 ppm) > Zn (approximately 108 ppm) > Cu (approximately 56 ppm) > Co (approximately 37 ppm) > Pb (approximately 32 ppm) > Au (approximately 220 ppb). The trend in the order of selected oxides in section T001, are the same as that of section T001 and T002. Unlike section T001 and T002 where Zn shows the highest concentration of the metals, the trace metal showing the highest concentration in T003 is Ni.

Based on mean (average) concentrations measured across sections T001, T002 and T003 (Table 4.5), section T003 shows the highest overall CaO (approximately 0.86 %), Co (approximately 39 ppm), Ni (approximately 120 ppm), Cu (approximately 56 ppm), Zn (approximately 108 ppm), Pb (approximately 32 ppm) and Au (approximately 220 ppb), while the highest Fe_2O_3 (approximately 3 %) and MnO (approximately 0.03) is observed in section T001. Summary statistics of the bulk geochemical data suggest that of the three sections, T003 is the most mineralized, T002 the least mineralized and section T001 enriched in Fe- and Mn oxides.

Section T003 was determined by core log reappraisal (grey-coloured samples were found to be present at depths as shallow as 3 meters) and x-ray diffraction data (yielding the highest sulphide proportions, indicating the lowest oxidation) as having undergone the least weathering. The summary of the bulk geochemical data further supports this notion as the high CaO- and trace element proportions reported for section T003, show little indication of oxide- and trace element loss to the aqueous phase.

Section T002 was determined by cluster and discriminant analysis as having undergone the most hydrolysis based on the extensive leaching of K^+ and subsequent clay formation. As with section T003, the summary of bulk geochemical data confirms this by showing the lowest oxide- and trace element proportions for section T002. This is the first indication of the crucial role of pH (weathering zones) in metal release. Under acidic conditions, like those dominating up 7 meters in section T002, positive charges develop on the surface of clays and result in metal desorption.

Downhole plots were used to show the distribution patterns of selected major oxide- (Fig. 4.3.1, Fig. 4.3.3, and Fig. 4.3.5, respectively) and trace metal concentrations (Fig. 4.3.2, Fig. 4.3.4, and Fig. 4.3.6, respectively) in sections T001, T002 and T003.

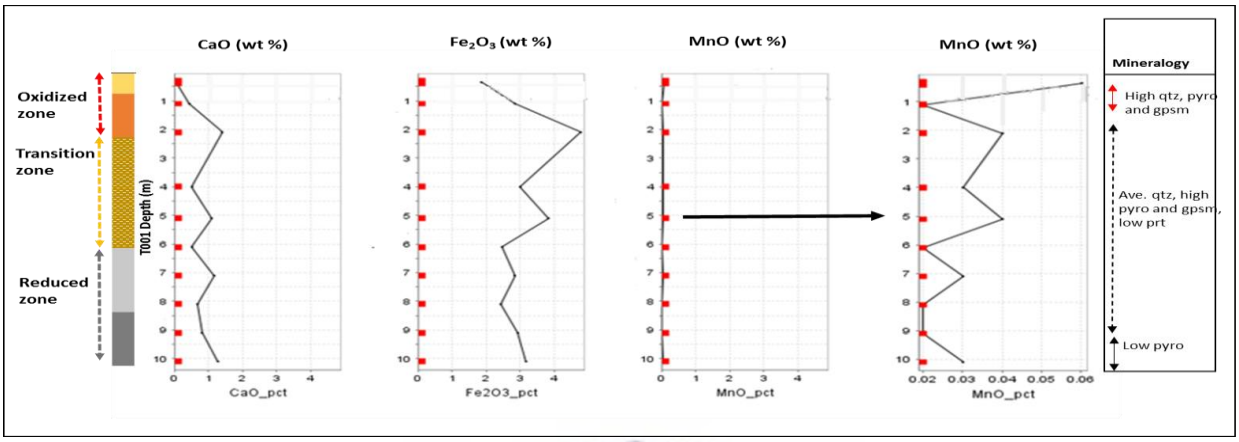

Figure 4.3. 1: Downhole plots showing the distribution patterns of selected trace element concentrations in sections T001.

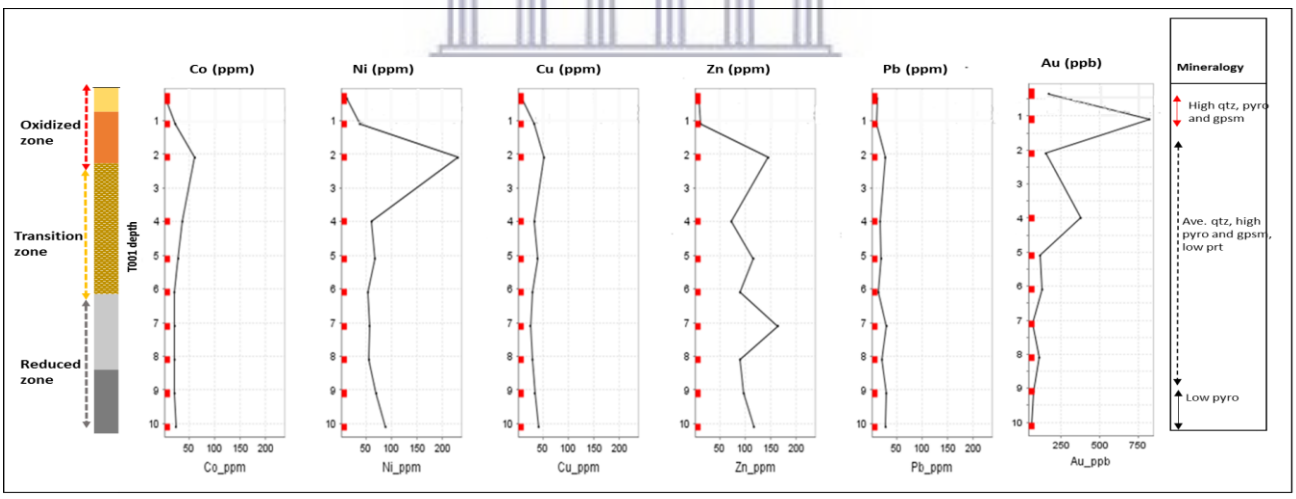

Figure 4.3. 2: Downhole plots showing the distribution patterns of selected trace element concentrations in sections T001.

Fig. 4.3.1 and Fig. 4.3.2, show the downhole distribution of selected major oxide- and trace metal concentrations in section T001. According to Fig 4.4.1 and Fig. 4.4.2, the lowest CaO, Fe_2O_3, Co, Ni, Zn, Au and Pb concentrations occur in the first 0.5 meters. Based on slimes descriptions,

this depth corresponds to pale yellow-brown fine sands and confirms that these pale fine sands are highly leached in major oxide and trace metal contents. The highest oxide- and metal concentration peaks (the most prominent of which is Fe_2O_3) occur between 2- and 2.2 meters. According to slimes descriptions, this depth corresponds to red, mottled fine sands, confirming that the red, mottling is the result of high Fe-oxide contents. Furthermore, the presence of high Ca, Fe, and Mn oxide concentrations in association with high metal concentrations, suggest Ca, Fe and Mn oxides may play a significant role in the retention of trace metals. While Co, Ni and Cu show relatively low and consistent concentration between 4- and 10 meters, Zn and Pb show a second high concentration peak at 7 meters, a depth consistent with pale grey fine sands. Average quartz-, pyrophyllite-, gypsum- and clinochlore proportions at this depth, suggest Zn and Pb concentrations peaks are related to something other than crystalline mineralogy, in this case, Ca oxide which shows a similar concentration peak at 7 meters.

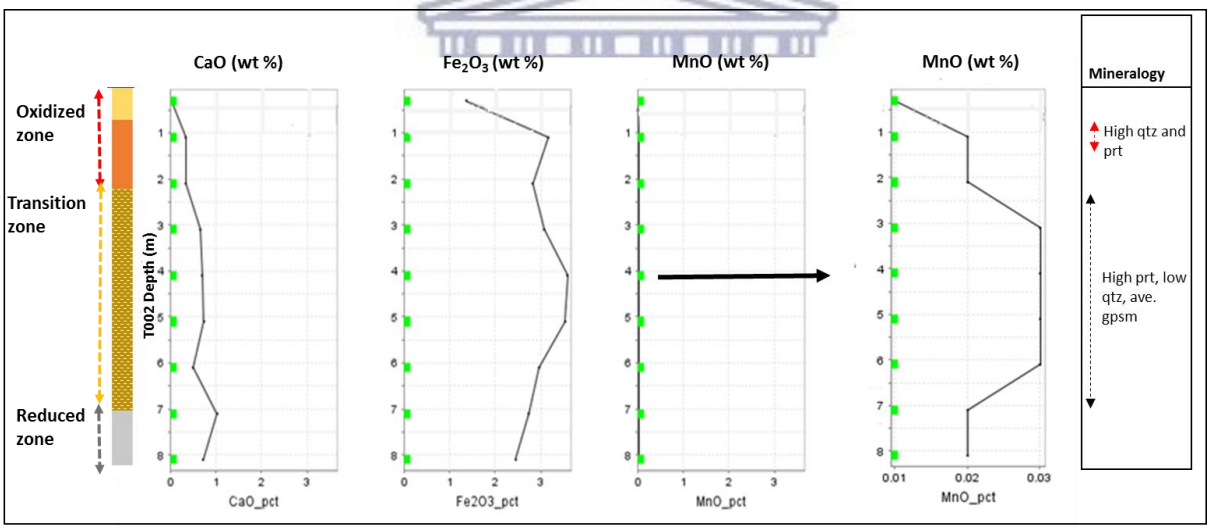

Figure 4.3. 3: Downhole plots which show the distribution patterns of selected major oxide concentrations in sections T002.

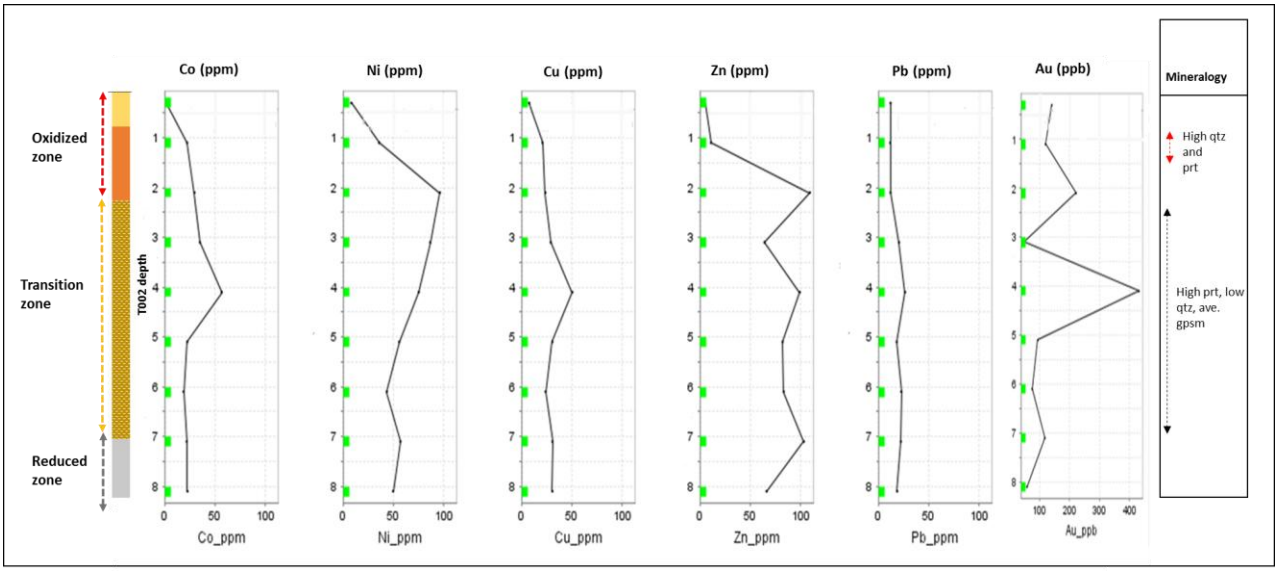

Figure 4.3. 4: **Downhole plots which show the distribution patterns of selected trace element concentrations in sections T002.**

Fig. 4.3.3 and Fig. 4.3.4, show the downhole distribution of selected major oxide- and trace metal concentrations in section T002. Similar to section T001, oxide and metal proportions appear lowest in the first 0.4 meters. Similar to section T001, this depth corresponds to pale yellow fine sands. This confirms that the pale yellow fine sands are considerable lacking in oxide and metal contents. The oxide- and metal concentrations appear to increase towards the transition zone, slightly decreasing when approaching the reduced zone. Ni and Zn show concentration peaks between 2- and 2.2 meters.

Similar to section T001, this depth corresponds to red, mottled fine sands, suggesting Fe oxides play a significant role in the retention of Ni and Zn at this depth. In addition, mineralogical data suggests high quartz, pyrophyllite, pyrite and gypsum proportions at this depth. Further downhole, at approximately 4 meters, concentration peaks are noted for MnO, Fe_2O_3, Co, Cu, Au and Pb, suggesting Mn- and Fe oxides may be responsible for the retention of these metals at this depth.

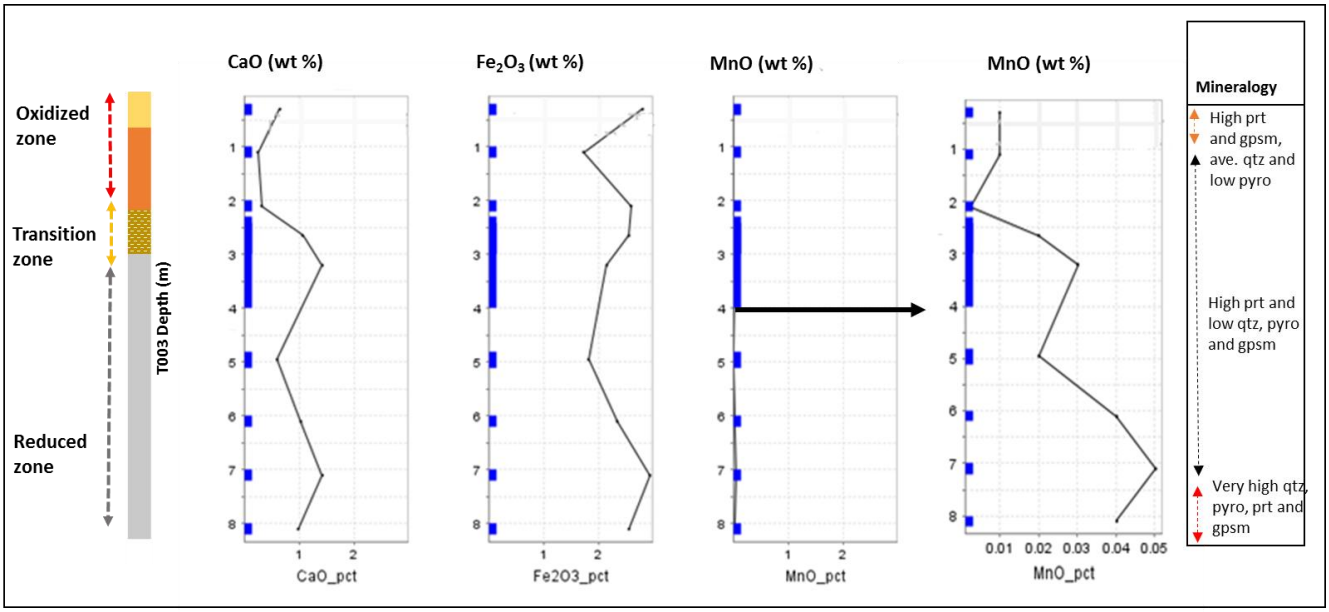

Figure 4.3. 5: Downhole plots which show the distribution patterns of selected major oxide concentrations in sections T003.

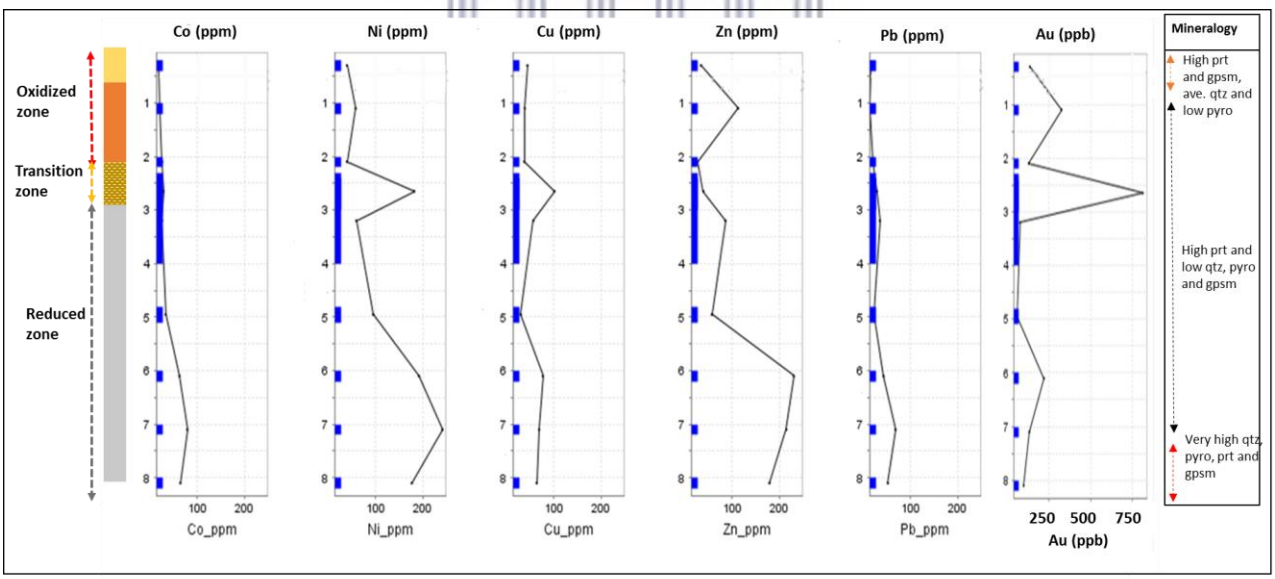

Figure 4.3. 6: Downhole plots which show the distribution patterns of selected trace element concentrations in sections T003.

Fig. 4.3.5 and Fig. 4.3.6, show the downhole distribution of selected major oxide- and trace metal concentrations in section T003. Relatively similar to T001 and T002, the lowest oxide and metal concentrations lie within the first meter of section T003. This depth overlaps with pale yellow-brown sands (between 0.2- and 0.4 meters) and red, mottled fine sands (between 0.4- and 2.2 meters). Prominent concentration peaks occur at 3 meters for Ni, Cu and Au appear in association with Fe oxide. Further downhole Cu and Zn show concentration peaks at 6 meters. These metals are chalcophiles and so behave similarly. Just below this depth, at approximately 7 meters, is a seemingly more common peak present for CaO, MnO, Fe_2O_3, Co, Ni, Zn and Pb. This depth corresponds to pale grey fine sands and according to mineralogical data, very high quartz, pyrophyllite, pyrite, gypsum and clinochlore. This suggests peak oxide and trace element concentrations are the result of a highly mineralized layer.

4.4 Relationship between reactive sulphur (sulphide-sulphur) and heavy metal release

4.4.1 Reactive sulphur (sulphide-sulphur) determination

The aim of this study was to understand the pattern of metal release from slimes into the Randfontein area by investigating the mineralogical and geochemical factors controlling metal release. One of the objectives was to determine the sulphide-sulphur (wt %) in samples. The sulphide-sulphur contents of samples was of interest as sulphide is thought to represent the total reactive sulphur in samples, and may therefore be associated with the mobilization of metals in slimes dams. Sulphide-sulphur was calculated as the difference between total (leco) sulphur and sulphate-sulphur (determined by extraction with ammonium oxalate). Fig. 4.4.1, compares total (leco) sulphur to sulphide-sulphur (wt %). If a quantifiable relationship can be established between the two, the use of total (leco) sulphur as the total reactive sulphur component may suffice for future investigations.

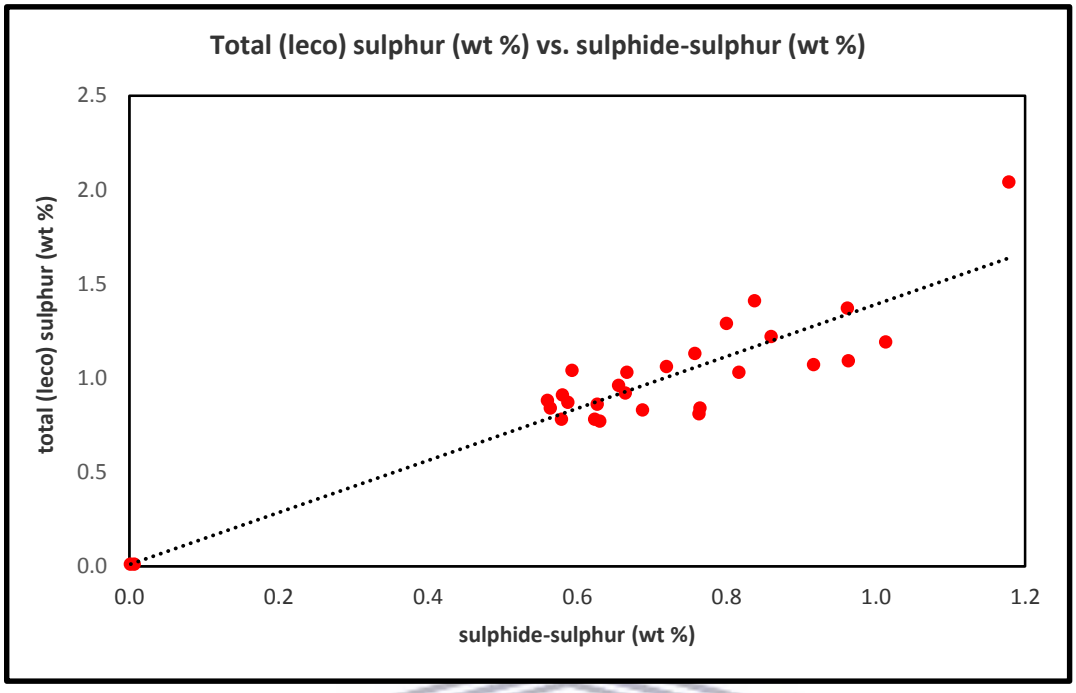

Figure 4.4. 1: A graphical presentation of sulphide-sulphur (wt %) versus total (leco) sulphur for the Gold One Millsite slimes samples.

Fig. 4.4.1, shows a comparison of total (leco) sulphur and calculated sulphide-sulphur (wt %). A line of best fit shows total (leco) sulphur is higher than sulphide-sulphur (wt %). Thus, the total reactive sulphur component in samples may be exaggerated if total (leco) sulphur is used instead of sulphide-sulphur to assess the acid generating potential.

The relationship between sulphide-sulphur and paste pH was of interest since both provide a preliminary indication of the acid generating potential of slimes samples. Fig. 4.4.2, Fig. 4.4.3, and Fig. 4.4.4, compare sulphide-sulphur as a percentage of total (leco) sulphur and paste pH for section T001, T002 and T003, respectively.

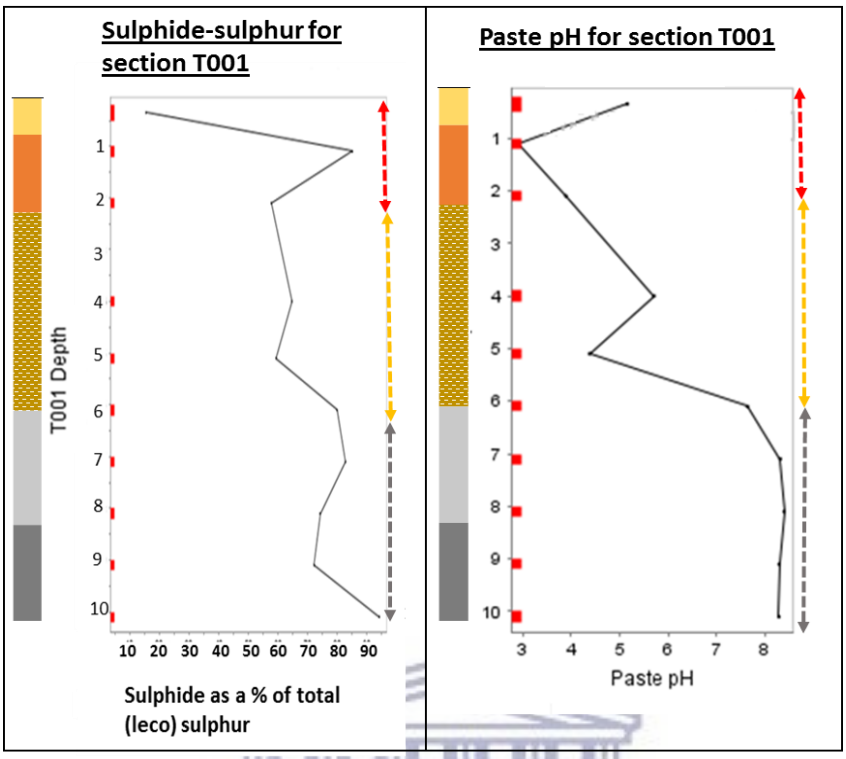

Figure 4.4. 2: A graphical presentation of sulphide-sulphur as a percentage of total (leco) sulphur vs. paste pH for section T001.

Fig. 4.4.2, depicts sulphide-sulphur as a percentage of the total (leco) sulphur, and paste pH for section T001. The first noticeable feature is a sharp increase in sulphide-sulphur percentage from approximately 15 % to 85 % within the first meter (lower oxidized zone). This spike in sulphide-sulphur corresponds with paste pH, showing a drop in pH from approximately 5 to 2.9 at the same depth. Acidic to weakly acidic conditions which follow, occur up to 5.2 m in the transition zone (approximately 3.8 to 5.7) and coincide with sulphide-sulphur values between 57 % and 64 %. Basic conditions represented by pH values of approximately 8 between 6 meters and 10.2 meters coincide with high sulphide-sulphur values between 72 % and 94 %. Under basic conditions, marked by the onset of grey fine sands, such as those prevailing in the reduced zone (6 meters – 10.2 meters), high sulphide-sulphur is expected because of the limited oxidation to form sulphate-sulphur in solution.

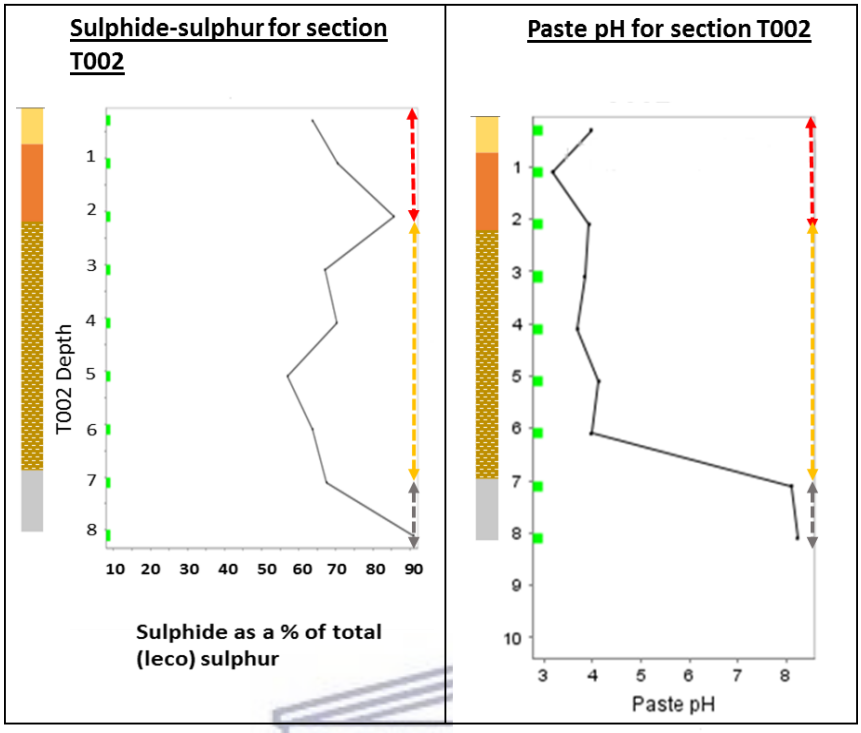

Figure 4.4. 3: A graphical presentation of sulphide-sulphur as a percentage of total (leco) sulphur vs. paste pH for section T002.

Fig. 4.4.3, depicts sulphide-sulphur as a percentage of total (leco) sulphur and paste pH for section T002. Fig. 4.4.3, shows an increase in sulphide sulphur from 63 % to 85 % in the lower oxidized zone coincident with a decrease in pH. These sulphide-sulphur percentages correspond to a decrease in pH to approximately 3.5. Depths between 2.2 m and 5.2 m (in the transition zone) show a zigzag pattern in sulphide-sulphur values although paste pH values remain approximately 3.5. Similar to section T001, the reduced zone (7 meters – 8 meters) shows marked increase in sulphide-sulphur to 91 %. This is because the basic conditions, marked by the onset of grey fine sands, prevailing at this depth limit the oxidation necessary to generate increased sulphate-sulphur.

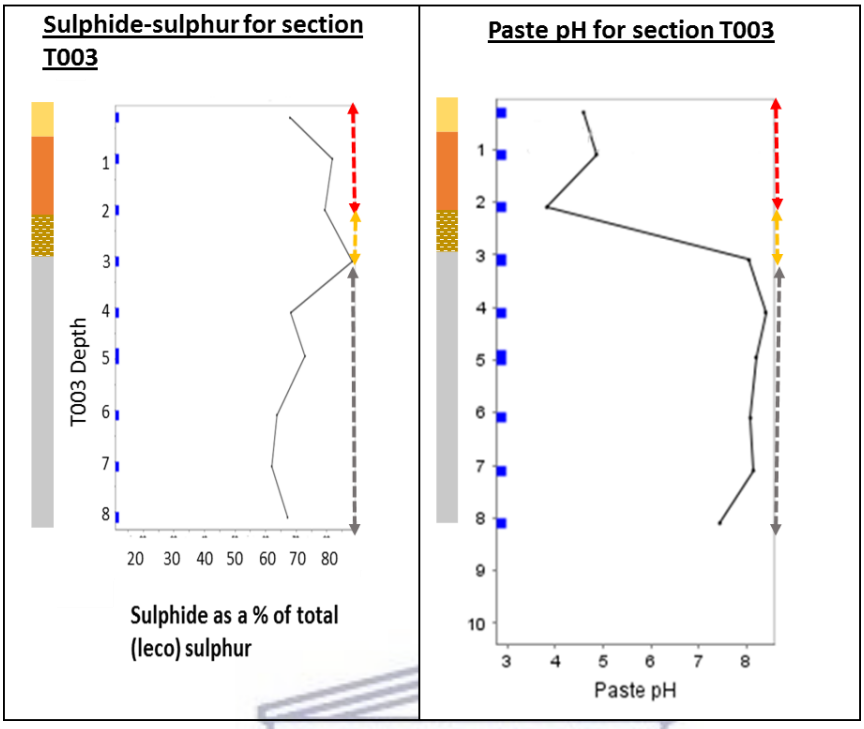

Figure 4.4. 4: A graphical presentation of sulphide-sulphur as a percentage of total (leco) sulphur vs. paste pH for section T003.

Fig. 4.4.4, depicts sulphide-sulphur as a percentage of total (leco) sulphur and paste pH for section T003. Fig. 4.4.4, shows an increase in sulphide-sulphur from 67 % to 88 % in the first 3.2 meters. This correlates well with the onset of the reduced zone at 3.2 meters, noted by the spike in paste pH. At 4 m, sulphide-sulphur values decline to approximately 68 %, showing a slight increase in the next meter to 72 % and ultimately decreases again towards the base of the section to approximately 65 %. Paste pH values of approximately 8.2, show good correlation with near consistent sulphide-sulphur between 5 meters and 8 meters.

To assess the relationship between sulphide-sulphur and metal mobilization, downhole plots were generated to show the trends in trace metal chemistry vs. sulphide-sulphur for section T001, T002 and T003 (Fig. 4.4.5, Fig. 4.4.6 and Fig. 4.4.7, respectively).

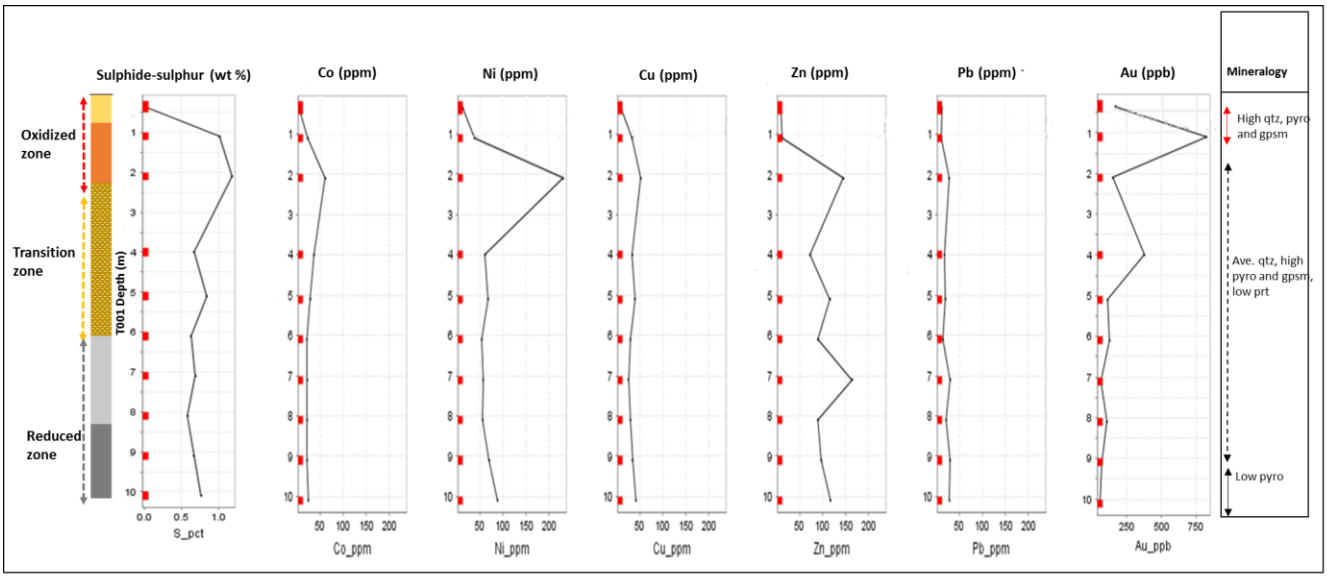

Figure 4.4. 5: A downhole presentation of sulphide-sulphur (wt %) vs. trace element chemistry for section T001.

Fig. 4.4.5, compares the distribution pattern of sulphide-sulphur (wt %) and trace element chemistry for section T001. Similar to the trend in oxide- and metal concentration, section T001 shows that the lowest sulphide-sulphur concentration (< 0.002 wt %) lies within the first 0.5 meters. This is expected since this portion of the slimes dams is highly oxidized and would readily break down pyrite to produce increased SO_4^- and Fe^{2+} (eq. 1). Based on the slime's description, this depth corresponds to pale yellow-brown fine sands. This suggests that pale yellow-brown fine sands are leached in sulphide contents in addition to oxide- and metal contents. According to x-ray diffraction data, the first meter is consistent with high gypsum, suggesting another reason for the low concentration of sulphide-sulphur.

Peaks in sulphide concentration noted between 1- and 2 meters correlate well with the trend observed for metals. According to slimes descriptions, this depth corresponds to red, mottled fine sands. Mineralogical data at this depth shows high pyrite. Thus, the sulphide concentration is influenced by increased pyrite proportions at this depth. Lower sulphide concentration peaks occur at 5 meters in correlation with Cu-, Zn- and Pb peak concentrations at the same depth, and at 7 meters in correlation again with a Pb concentration peak at the same depth. This suggests

that metals such as Zn and Pb may be easily mobilized by sulphide despite the reducing conditions.

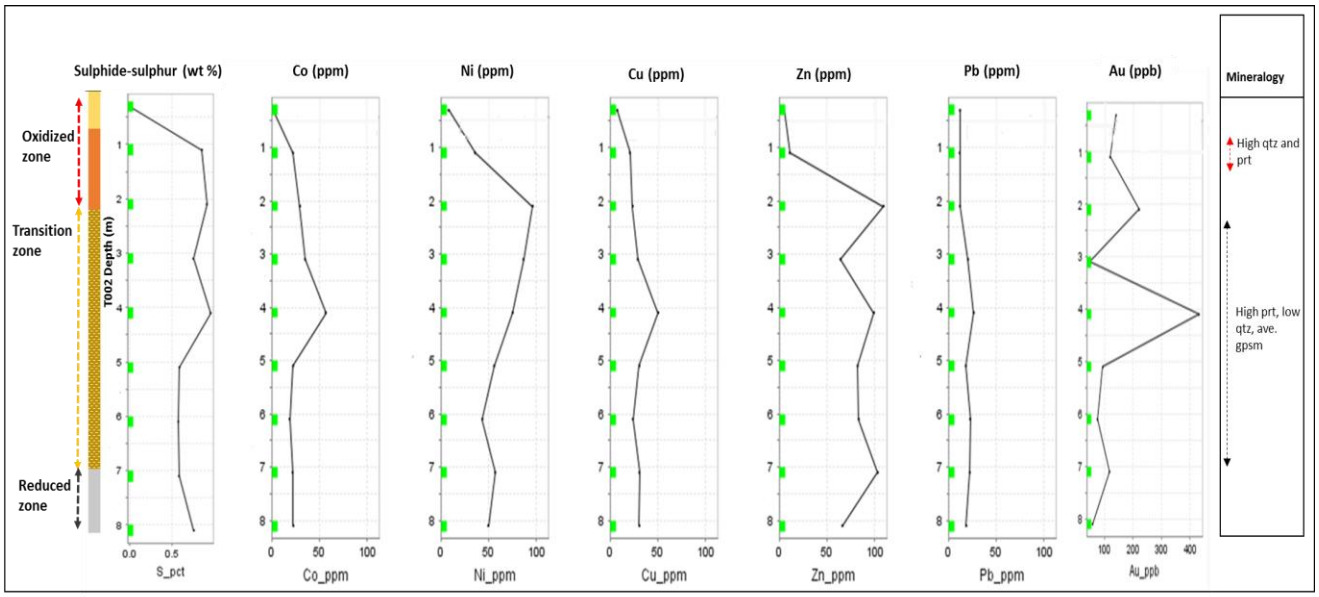

Figure 4.4. 6: A downhole presentation of sulphide-sulphur (wt %) vs. trace element chemistry for section T002.

Fig. 4.4.6, compares the distribution pattern of sulphide-sulphur (wt %) and trace element chemistry for section T002. Similar to T001, section T002 shows the lowest sulphide concentration (approximately 0.006 wt %) in the first 0.4 meters, in association with the lowest oxide- and metal concentrations downhole. This suggests that the pallor of fine sands at this depth is the result of low sulphide contents, in addition to low oxide- and metal contents. As for section T001, very low sulphide-sulphur (wt %) is expected at the very top of the slimes dam as this a highly oxidizing environment which will readily breakdown sulphide minerals for form increased SO_4^- and Fe^{2+} (eq. 1) in solution.

The first sulphide concentration peak occurs at 1 meter, seemingly in association with a concentration peak in Fe oxide at this depth and may therefore correspond to high pyrite proportions. A second sulphide peak can be seen at 2 meters and correlates well with the concentration peaks noted for Ni and Zn at this depth. This suggest that Ni and Zn concentrations at this depth may be the result of mobilization by sulphide. A third sulphide concentration peak can be seen at 4 meters and correlates well with the concentration peaks noted for Co, Cu, Pb and

Au at the same depth. This suggests that metals, even those typically considered relatively immobile (e.g. Pb and Au) may be mobilized by sulphide at this depth.

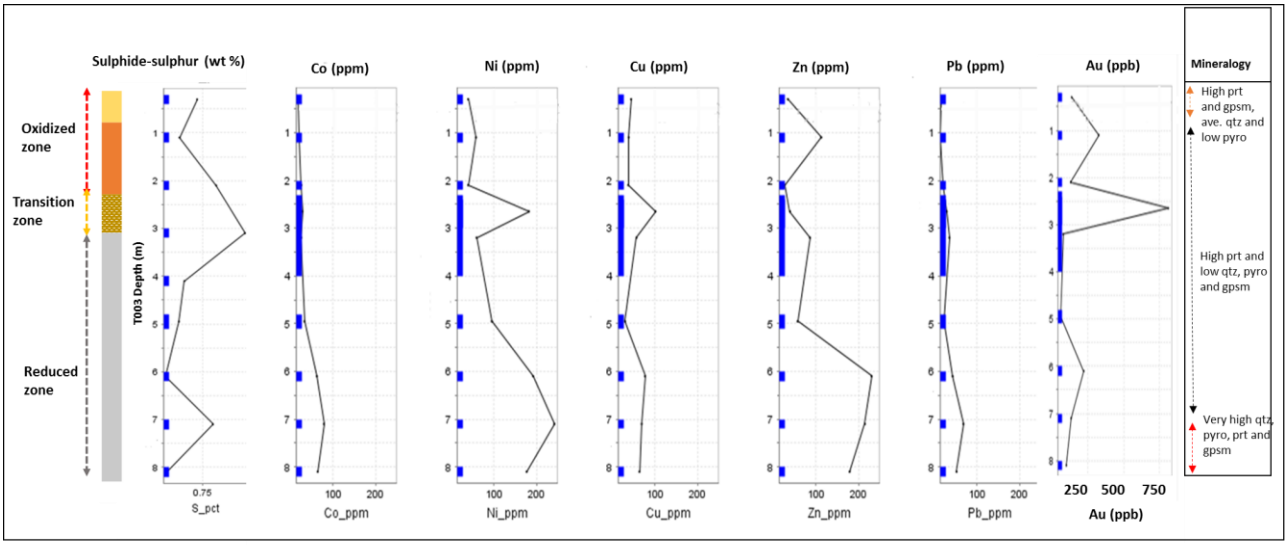

Figure 4.4. 7: A downhole presentation of sulphide-sulphur (wt %) vs. trace element chemistry for section T003.

Fig. 4.4.7, compares the distribution pattern of sulphide-sulphur (wt %) and trace element chemistry for section T003. Unlike section T001 and T002, sulphide-sulphur in the first meter appears higher in sulphide contents (approximately 0.7 wt %). This supports the suggestion that section T003 is the least oxidized of the sections. The first and most prominent sulphide peak occurs at 3 meters. This depth corresponds to the onset of pale grey fine sands i.e. the reduced zone. There is good correlation between this concentration peak and the concentration peaks noted for Ni, Cu and Au at the same depth. Similarly, a second sulphide concentration peak occurs at 7 meters and correlates well with the concentration peaks noted for Co, Ni, Zn and Pb at the same depth. This suggests that metal concentration at this depth may be the result of mobilization by sulphide. Based on the supporting evidence from sections T001, T002 and T003, it is clear that sulphide plays a major role in the mobilization of metals, especially that of heavier metals such as Au and Pb, which would otherwise be considered relatively immobile.

4.4.2 Determination of the acid generating potential of slimes samples

One of the objectives of this study was to predict the acid generating potential of slimes samples using calculated sulphide-sulphur (wt %). The paste pH determined for Millsite slimes samples was useful in determining the present capacity of samples to produce acid. However, to determine the future acid generating potential of samples, it is necessary to assess the relative concentration and reaction rates of acid-generating (AP) and acid-neutralizing (NP) components present. The relative magnitude of the NP and AP is indicated by the ratio of NP/AP (Neutralization Potential Ratio or NPR).

Total carbon was used to represent NP (INAP, 2009), with the assumption that all carbon in the sample is present as calcite ($CaCO_3$):

NP (total carbon content) = % C x 83.3

Sulphide-sulphur was used to represent the total reactive sulphur component in samples (Lawrence, 1990). This method of Modified Acid Base Accounting, assumes that sulfur present as sulfate is not acid producing, and may therefore underestimate the total reactive sulphur if jarosite or other non-acid producing sulfate minerals are present. Theoretically, the relationship between AP (acid generating potential) and reactive sulphur is as follows (INAP, 2009):

AP = reactive sulphur (wt %) x 31.25

31.25 is used to convert sulphur (wt %) to $CaCO_3$/ton so it can be compared with NP (neutralization potential). This is based on the assumption that:

- 1 mole of S produces 2 moles of H^+
- 1 mole of calcite ($CaCO_3$) neutralizes 2 moles of H^+.

FeS_2 (pyrite) + O_2 + $H_2O \rightarrow Fe(OH)_3 + 2\ SO4^{2-} + 4\ H^+$……..eq. 5.
$CaCO_3$ (calcite) + $2H^+ \rightarrow Ca^{2+} + H_2CO_3$……eq. 6.

There is a second neutralization reaction for calcite (eq. 7), which dominates under high pH conditions and requires twice the NP to neutralize each mole of H^+.

$CaCO_3 + H+ \rightarrow Ca^{2+} + HCO_3^-$……eq. 7.

With the first neutralization equation (eq. 6), a net potential ratio (NP/AP) < 1 is required to produce acid mine drainage. With the second neutralization equation (eq. 7), a net potential ration (NP/AP) > 2 is required to mitigate acid mine drainage. The net potential ratio (NPR) of the slimes samples (Fig. 4.4.8) were determined using modified acid base accounting and the results interpreted on the basis of the acid generating potential criteria (Price, 1997). Table 4.6, shows the screening criteria for acid potential based on acid base accounting (Price, 1997).

Table 4. 6: The guidelines for screening criteria based on acid base accounting (Price, 1997).

Potential For Acid Mine Drainage	NPR (AP/NP)Screening Criteria	Interpretation
Likely	< 1	Likely acid-generating
Possibly	Between 1 and 2	Possibly acid-generating if NP is insufficiently reactive or depleted more rapidly than the reactive sulphur.
Low	> 2	Not potentially acid-generating, unless extensive preferential exposure of sulphides along fracture planes or extremely reactive sulphides in combination with insufficient NP.
None	> 4	No further acid-potential testing necessary, unless samples are to be used for alkalinity

The criteria in Table 4.6 was plotted with the NPR data of samples to provide a visual indication of the net acid potential of samples (Fig. 4.4.8).

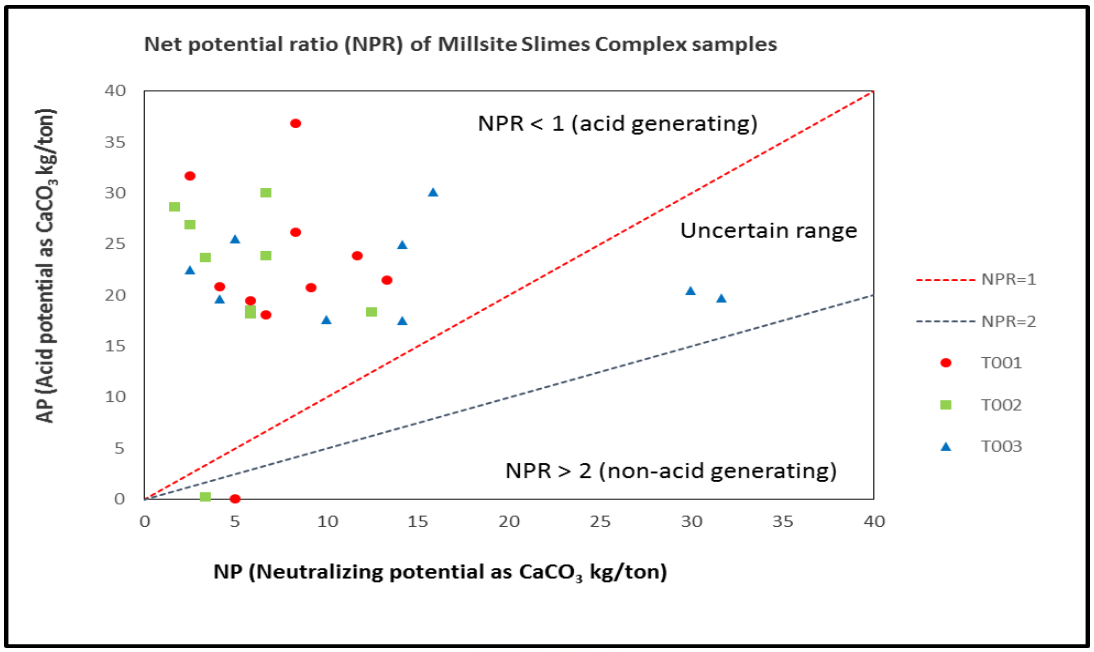

Figure 4.4. 8: Acid potential and neutralization potential graph indicating areas of potential acid generating, uncertain and non-acid generating samples.

According to Fig. 4.4.8, the bulk of samples from sections T001, T002 and T003 show acid generating potential i.e. net potential ratios (NPRs) below one. Samples showing non-acid generating potential are limited to sample 48 (between 0.2 and 0.4 m in section T001) and sample 59 (between 0.2 and 0.5 m in T002). These two potentially non-acid generating samples correspond to the lowest reported sulphide-sulphur percentages (0.002 wt % and 0.006 wt %, respectively). Thus, non-acid generating samples correspond to the sulphide leached, pale fine sands of the upper oxidized zone. Similarly, when calculated as a percentage of the total (leco) sulphur sample 49 is shown to coincide with sulphide-sulphur proportions of approximately 15.5 %, the lowest calculated sulphide-sulphur proportion, while sample 59 coincides with sulphide-sulphur proportions of approximately 63 %. While correlation between sulphide-sulphur and net acid potential is clear in the case of sample 49, direct correlations between sulphide-sulphur and net acid potential are difficult to ascertain since net acid potential is not a reflection of sulphide-sulphur (wt %) alone but rather its proportion relative to the total reactive carbon present.

4.5 Sequential extraction procedures

The release and mobility of metals is strongly dependent on the chemical behaviour of the host minerals. Mineral phases commonly hosting metals include, water-soluble, carbonate, Mn-oxide, Fe oxide and sulphide and silicate (residual) phases. Sequential extraction procedures tie in with the aim of this study as it serves to better understand the release of metals by partitioning the solid-phase metal-hosting phases in the slimes dam. Sequential extraction procedures typically make use of a series of digestants, each designed to extract a specific bonding form, thereby liberating the proportion of metals in that bonding form (Zachmann and Block, 1994).

For the purpose of this study, a four-step sequential extraction procedure was used. Step one, involved treatment of slimes samples with double distilled water in order to liberate water-soluble metal ions. Step two, involved treatment of the residue from the first step with 1 M ammonium acetate in order to liberate metal ions associated with carbonate species. Step three, involved treatment of the residue from step two with 0.1 M hydroxylamine hydrochloride in order to liberate metal ions associated with Mn oxide species. Step four, involved treatment of the residue from step three with 0.25 m hydroxylamine hydrochloride to liberate metal ions associated with Fe oxide species.

The data generated by the sequential extraction procedure include datasets for (i) double distilled water, (ii) 1 M ammonium acetate, (iii) 0.1 M hydroxylamine hydrochloride and (iv) 0.25 m hydroxylamine hydrochloride (section 4.5). The complete sequential extraction dataset can be found in Appendix Two: D (i). The sequential extraction datasets were evaluated using descriptive summary statistics (Table 4.7) to provide an overview of selected major- and trace element concentrations in sections T001, T002 and T003.

4.5.1 Summary of the sequential leach geochemical data

The descriptive summary statistics (min., max., mean and standard deviation) were determined for double distilled water, double distilled water, 1 M ammonium acetate, 0.1 M and 25 M hydroxylamine hydrochloride and are presented (Table 4.7) to give an overview of major oxide and trace element concentrations yielded during the sequential extraction procedure.

Table 4. 7: The descriptive summary statistics of selected major oxide and trace element concentrations for double distilled water, 1 M ammonium acetate, 0.1 M and 25 M hydroxylamine hydrochloride.

	Double distilled water				1 M Ammonium acetate				Hydroxylamine hydrochloride							
									0.1 M				0.25 M			
Element (ppm)	Min.	Max.	Mean	Stdev	Min.	Max.	Mean	Stdev	Min.	Max.	Mean	Stdev	Min.	Max.	Mean	Stdev
Ca	6.18	136.42	57.71	26.44	42.03	797.31	398.56	182.19	20.91	93.65	55.60	21.63	2.78	44.30	13.19	9.65
Mn	0.00	13.23	2.43	3.37	0.36	19.48	7.84	5.01	0.03	4.35	1.75	1.24	0.00	3.34	1.24	1.24
Fe	0.07	61.64	7.50	12.66	0.94	78.71	30.16	16.62	2.10	16.17	9.93	3.17	2.55	25.48	16.63	6.38
Co	0.00	10.38	1.75	2.43	0.06	15.59	4.02	3.45	0.00	3.69	0.80	0.94	0.00	2.15	0.52	0.70
Ni	0.00	25.57	4.00	5.97	0.11	54.96	11.26	12.08	0.00	6.28	1.54	1.71	0.00	6.66	1.58	2.07
Cu	0.00	5.21	1.08	1.60	0.72	17.04	4.93	3.64	0.09	1.14	0.49	0.28	0.32	3.58	1.54	0.98
Zn	0.00	15.86	3.05	3.68	0.18	3.88	1.82	0.89	0.06	1.12	0.55	0.30	0.00	1.66	0.52	0.53
Au	0.00	0.00	0.00	0.00	0.00	0.01	0.00	0.01	0.00	1.26	0.07	0.24	0.00	0.07	0.01	0.02

Based on mean oxide concentrations for double distilled water (Table 4.7), Ca yielded the highest extractable concentrations (approximately 57.71 ppm) and was followed by Fe (approximately 7.51 ppm) and then Mn (2.43 ppm). Amongst the trace elements, Ni yielded the highest extractable concentrations (approximately 4.00 ppm) and was closely followed by Zn (approximately 3.05 ppm), then Co (approximately 1.75 ppm) and Cu (approximately 1.08 ppm). Au and Pb were undetectable. Overall, double distilled water showed selective dissolution of Ca and of the extractions, yielded the highest extractable Zn concentrations.

Based on mean oxide concentrations for 1 M ammonium acetate (Table 4.7), Ca yielded the highest extractable concentrations (ave. 398.56 ppm) and was followed by Fe (ave. 30.16 ppm) and Mn (ave. 7.84 ppm). Amongst the trace metals, Ni yielded the highest extractable concentrations (11.26 ppm) and was followed by Cu (ave. 4.93 ppm), Co (ave. 4.02 ppm), Zn

(1.82 ppm) and Pb (ave. 0.78 ppm). Au yielded the lowest extractable concentrations (ave. 4.47 ppb). Overall, 1 M ammonium acetate showed selective extraction of Ca, yielding nearly 6X that yielded for double distilled water. Relative to the latter, approximately 4X Fe and 3X Mn was extracted by 1 M ammonium acetate. Extractable Ni increased by X3, Cu by X4 and Co by nearly X3. Extractable Zn concentrations were nearly half that yielded for double distilled water.

Based on mean oxide concentrations for 0.1 M hydroxylamine hydrochloride (Table 4.7), Ca yielded the highest extractable concentrations (ave. 55.60 ppm) and was followed by Fe (ave. 9.93 ppm) and Mn (ave. 1.75). Amongst the trace metals, Ni yielded the highest extractable concentration (ave. 1.54 ppm) and was followed by Co (ave. 0.8 ppm), Zn (ave. 0.55 ppm) and Cu (ave. 0.49). Au and Pb yielded the lowest extractable concentrations at 74.56 and 38.64 ppb, respectively. Overall, 0.1M hydroxylamine hydrochloride showed selective extraction of Ca, yielding 6X-less that yielded for 1 ammonium acetate. Relative to 1 M ammonium acetate, 0.1 M hydroxylamine hydrochloride yielded nearly 4 X less extractable Mn, 0.3 X extractable Fe, 4 X less extractable Co, 7 X less extractable Ni, 4 X less extractable Zn and 10 X less extractable Cu proportions.

Based on mean oxide concentrations for 0.25 M hydroxylamine hydrochloride (Table 4.7), Fe yielded the highest extractable concentrations (ave. 16. 63 ppm) and was followed by Ca (ave. 13.19 ppm) and Mn (ave. 1.24 ppm). Amongst the trace metals, Ni yielded the highest extractable concentrations (ave. 1.58 ppm) and was closely followed by Cu (1.54 ppm), then by Zn and Co (ave.0.52 ppm). The lowest extractable concentration was yielded by Au (6.61 ppb). Overall, 0.25 M showed selective extraction of Fe oxides, yielding nearly 2 X that of 0.1 M hydroxylamine hydrochloride. Extractable Mn proportions appear consistent with that of 0.1 M hydroxylamine hydrochloride. Relative to the latter, 0.25 yielded approximately 3X Cu, 3X less Co and near identical Zn and Ni proportions.

4.5.2 Principal component analysis

The sequential extraction datasets were evaluated using principal component analysis (section 4.5.2) to determine element correlation in sections T001, T002 and T003 (Fig. 4.5.1). The complete dataset for Principal Component Analysis can be found in Appendix Two: D (iii - v).

Principal Component Analysis is a method of deconstructing large datasets into only its most crucial (information-bearing) components (Bos and Smilde, 2014). It does so, by reducing data to eigenvectors with corresponding eigenvalues (i.e. principal dimensions of variance) as these are thought to carry the most useful information (Bos and Smilde, 2014). Eigenvectors represent the direction of variance and eigenvalues the amount of variance in the data in that direction (Bos and Smilde, 2014).

Principal Component Analysis of this dataset includes selected major oxide and trace metal data for double distilled water, 1 M ammonium acetate, 0.1 M hydroxylamine hydrochloride and 0.25 M hydroxylamine hydrochloride. The analysis made use of Ca, Mn, Fe, Co, Ni, Cu and Zn concentrations. Thus, the data are divided into seven eigenvectors (PC1 – PC7). Of the eigenvectors, PC1 carries the most useful information and the rest, successively less. Thus, PC1-PC2 eigenvectors were used to display element correlation for double distilled water-, 1 M ammonium acetate-, 0.1 M hydroxylamine hydrochloride- and 0.25 M hydroxylamine hydrochloride (Fig. 4.5.1). The correlation coefficients generated by correlation coefficient analyses are referenced in parenthesis and can be found completed in Appendix Two: D (iii) while box and whisker plots can be found in Appendix Two: D (iv).

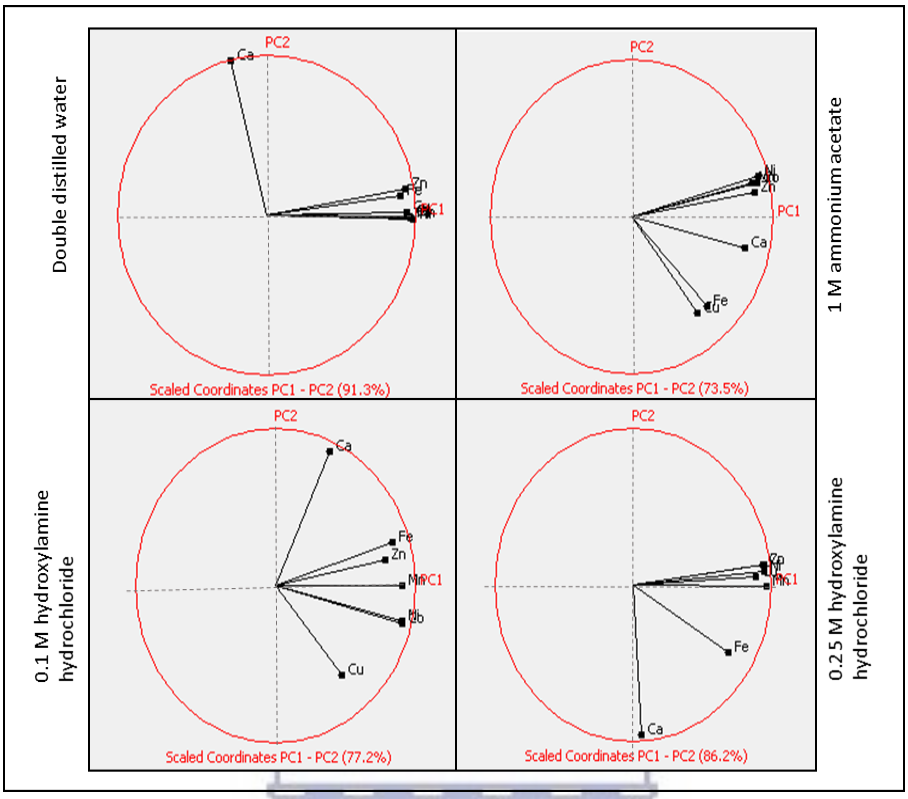

Figure 4.5. 1: A diagrammatic representation of major- and trace element correlation for selective sequential extractions generated by Principal Component Analysis.

Fig. 4.5.1, was determined by Principal Component Analysis and shows a diagrammatic representation of Principal Components one and two determined for double distilled water. Principal Components one and two contain approximately 91.3 % of the information for slimes samples treated with double distilled water and are therefore most useful in determining oxide- and metal associations for this leach. Principal Component one (PC1) is defined by Mn oxide. Strongly positive correlation exists between Principal Component one and Co, Ni and Cu, suggesting a strong association between Co (0.93), Ni (0.93), Cu (0.65) and Mn oxide. Fe oxide appears weakly correlated with Mn (0.26), and strongly correlated with Zn but shows low correlation according to correlation coefficient analysis (0.43). Principal Component two (PC2) is seemingly defined by Ca, to which Co (0.09), Ni (0.10), Cu (-0.04) and Zn (0.12) are very weakly correlated. Thus, strong association exists between Mn, Ni, Co, Cu and Zn, suggesting that Mn oxide is the most significant retainer of these metals for this leach while metals share limited association with Fe oxide and very little association with Ca oxide. When compared to

box and whisker analysis (Appendix Two: D: (iv)), major oxides Ca (40-60 ppm) and Fe (0-8) show narrow distribution ranges as a result of several high outliers. Unlike Ca and Fe, Mn shows a relatively even distribution range with limited high outliers. Of the oxides, Co, Ni, Cu and Zn mimic the distribution trend shown for Mn.

Fig. 4.5.1, was determined by Principal Component Analysis and shows a diagrammatic representation of Principal Components one and two determined for 1 M ammonium acetate. Principal Components one and two contain approximately 73.5 % of the information for slimes samples treated with 1 M ammonium acetate and are therefore most useful in determining oxide- and metal associations for this leach. Similar to that observed for double distilled water, Principal Component one (PC1) is defined by Mn oxide. Strongly positive correlation exists between Principal Component One and Co, Ni and Zn, suggesting a strong association between Co (0.73), Ni (0.74), Zn (0.74) and Mn oxide. Principal Component two is seemingly defined by Fe, which shows weak correlation with Cu (0.25). Thus, when treated with 1 M ammonium acetate, metals appear to be in strongest association with Mn, suggesting that Mn oxide is the most significant retainer of these metals for this leach. Relative to Mn, metals (Co, Ni, Cu and Zn) show less association with Ca (0.54, 0.57, 0.4 and 0.76, respectively) and the least association with Fe oxide overall (0.47, 0.41, 0.25 and 0.23, respectively). When compared to box and whisker analysis (Appendix Two: D (iv)), metal distributions are narrowly confined to lower concentration ranges, with several high outliers. Mn shows an even distribution range with no outliers, suggesting metals show stronger association with Mn when extracted with double distilled water than when extracted by 1 M ammonium acetate.

Fig. 4.5.1, was determined by Principal Component Analysis and shows a diagrammatic representation of Principal Components one and two determined for 0.1 M hydroxylamine hydrochloride. Principal Components one and two contain approximately 77.2 % of the information for slimes samples treated with 0.1 M hydroxylamine hydrochloride and are therefore most useful in determining oxide and metal associations for this leach. Similar to that observed for double distilled water and 1 M ammonium acetate, Principal Component one (PC1) is defined by Mn oxide. Strongly positive correlation exists between Principal Component one and Co and Ni, suggesting a strong association between Co (0.71), Ni (0.70), and Mn oxide.

Principal Component two (PC2) is seemingly defined by Ca, to which metals (Co, Ni, Cu and Zn) are very weakly correlated (0.15, 0.19, -0.12 and 0.40, respectively). Thus, when treated with 0.1 M hydroxylamine hydrochloride metals appear in closest association with Mn, seemingly less association with Fe oxide and the least association with Ca oxide overall. When compared to box and whisker analysis (Appendix Two: D (iv)), Co and Ni show narrow distribution ranges, seemingly confined to low concentration ranges. Cu and Zn show near even distribution ranges. This suggests that metals show the strongest association with Mn when extracted by double distilled water, relative to 0.1 M hydroxylamine hydrochloride.

Fig. 4.5.1, was determined by Principal Component Analysis and shows a diagrammatic representation of Principal Components one and two determined for 0.25 M hydroxylamine hydrochloride Principal Components one and two contain approximately 86.2 % of the information for slimes samples treated with 0.25 M hydroxylamine hydrochloride and are therefore most useful in determining oxide and metal associations for this leach. Similar to that observed for double distilled water, 1 M ammonium acetate and 0.1 M hydroxylamine hydrochloride, Principal Component one (PC1) is defined by Mn oxide. Metals (Co, Ni, Cu and Zn) show strong correlation with Principal Component one, suggesting strong association between Co (0.81), Ni (0.87), Cu (0.74), Zn (0.80) and Mn. Principal Component two (PC2) is defined by Ca, to which metals (Co, Ni, Cu and Zn) are very weakly correlated (-0.05, 0.05, 0.05 and -0.06, respectively). Thus, when treated with 0.25 M hydroxylamine hydrochloride metals appear in closest association with Mn, less association with Fe oxide and the least association with Ca oxide overall. When compared to box and whisker analysis (Appendix Two: D (iv)), metals show distribution ranges mimicking that of Mn, suggesting metals show strongest association with Mn when extracted by double distilled water and 0.25 M hydroxylamine hydrochloride.

4.5.3 Downhole distribution of elements

Selected major element and trace metal concentrations determined by selective sequential extraction were plotted using Earthworks Downhole Explorer®. This form of spatial analysis was used to describe trends in selected major- and trace element concentrations downhole. The downhole sequential extraction patterns for section T001 (Fig. 4.5.2, 4.5.3, 4.5.4, 4.5.5) are presented first and are followed by the sequential extraction patterns for section T002 (Fig. 4.5.6, 4.5.7, 4.5.8, 4.5.9) and T003 (Fig. 4.5.10, 4.5.11, 4.5.12, 4.5.13).

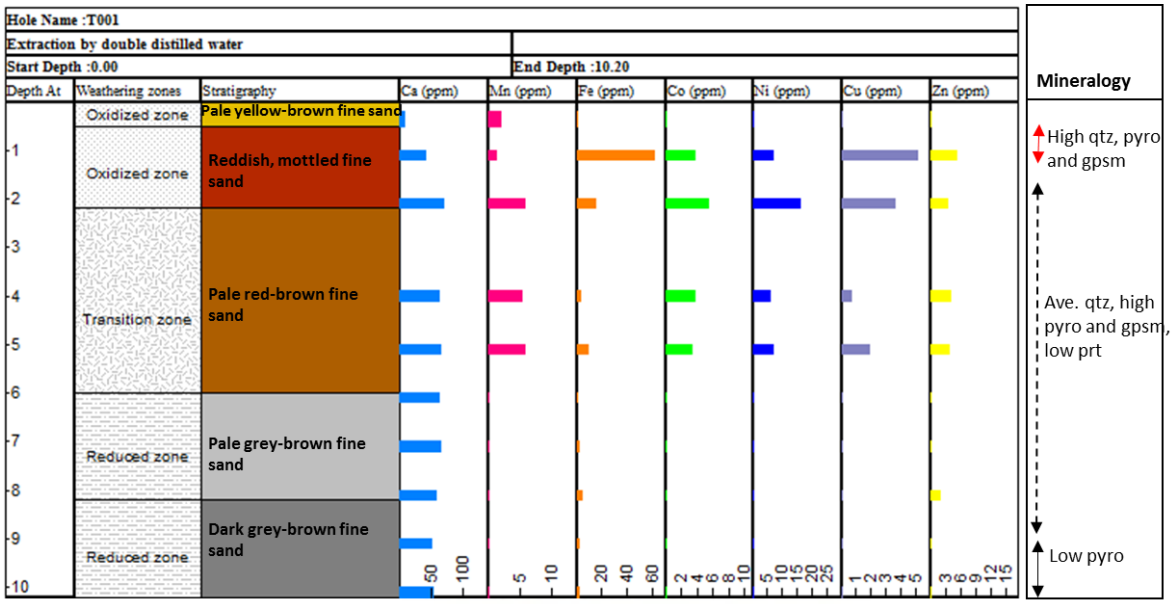

Figure 4.5. 2: The downhole distribution of selected major- and trace elements extracted by double distilled water for section T001.

Fig. 4.5.2, shows the downhole distribution of selected major- and trace element concentrations extracted by double distilled water for section T001. Similar to the bulk element geochemical data for section T001, Ca, Fe, Co, Ni, Cu and Zn concentrations extracted by double distilled water in the first 0.4 meters appear very low (near below detection) while Mn is high. According to slimes stratigraphy, this depth corresponds to leached, pale yellow-brown fine sands. Peak Mn (up to 5.7 ppm)-, Fe (up to 61 ppm)-, Co (up to 5 ppm)-, Ni (up to 15 ppm)-, Cu (up to 5 ppm)- and Zn (up to 5 ppm) concentrations occur between 1- and 2.2 meters. According to the weathering zones, this depth corresponds to the lower oxidized zone and based on slimes

descriptions, corresponds to red, mottled fine sands. The high concentration of Fe oxide content at this depth, accounts for the red, mottled appearance of slimes at this depth, and suggest that metal concentrations occur largely in association with Fe. When compared with x-ray diffraction data, this depth also corresponds to low pyrite proportions. Thus, high Fe contents may also be the result of extensive sulphide weathering at this depth. Ca and Mn show similar concentrations between 4 and 5 meters while Fe, Co, Ni and Cu appear subdued. Based on paste pH data, this depth is consistent with transitional pH conditions. This accounts for the decrease in extractable oxide and metal concentrations. At depths between 6 meters and 10.2 meters, all but Ca show very low, near undetectable, concentrations. According to the weathering zones, this depth is consistent with the reduced zone. Low extractable concentrations are expected since metal ions are likely bound to Mn- and Fe oxide under these reduced conditions. Thus, metals are less available for extraction by water.

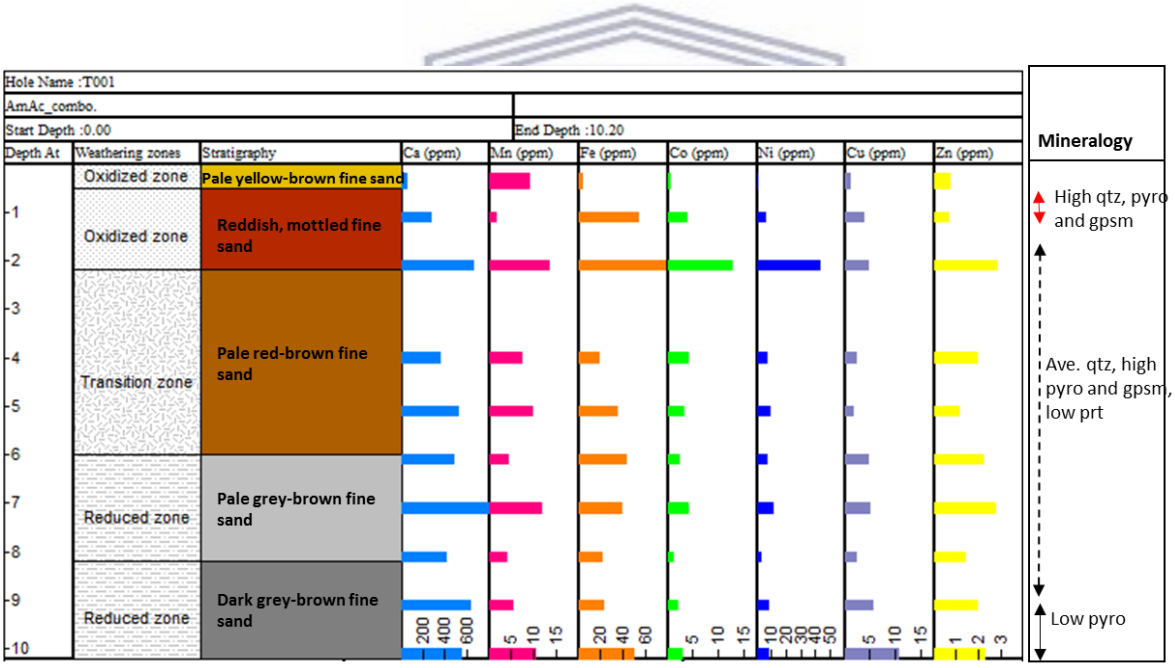

Figure 4.5. 3: The downhole distribution of selected major- and trace elements extracted by 1 M ammonium acetate for section T001.

Fig. 4.5.3, shows the downhole distribution of selected oxide- and metal concentrations extracted by 1 M ammonium acetate for section T001. Similar to the bulk element geochemical data for section T001, Ca, Fe, Co, Ni, Cu and Zn concentrations extracted by 1 M ammonium acetate within the first 0.4 meters appear very low and Mn, seemingly high. According to slimes

stratigraphy, this depth corresponds to leached, pale yellow-brown fine sands. Peak concentrations are noted between 2 meters and 2.2 meters for Ca (approximately 645 ppm), Mn (approximately 13.4 ppm), Fe (approximately 78 ppm), Co (approximately 12.8 ppm), Ni (approximately 42.7 ppm) and Zn (approximately 2.8 ppm), coincident with Fe-mottled fine sands of the lower oxidized zone. Although higher in overall oxide and metal concentration, this trend resembles that for double distilled water. Peak metal concentrations at this depth are the result of increased Mn and Fe oxide contents. As stated before, high Fe concentrations can be attributed to extensive sulphide oxidation at this depth. The oxide concentrations remain relatively high between 4 and 7 meters, and metal concentrations minor. Decreased Mn and Fe proportions between 8 and 10 meters are accompanied by similar decreases in Co and Ni. According to the weathering zones, this depth is associated with reduced pH conditions. Under reducing conditions, metals are readily bound to Mn and Fe oxides, making them less available for extraction by 1 M ammonium acetate.

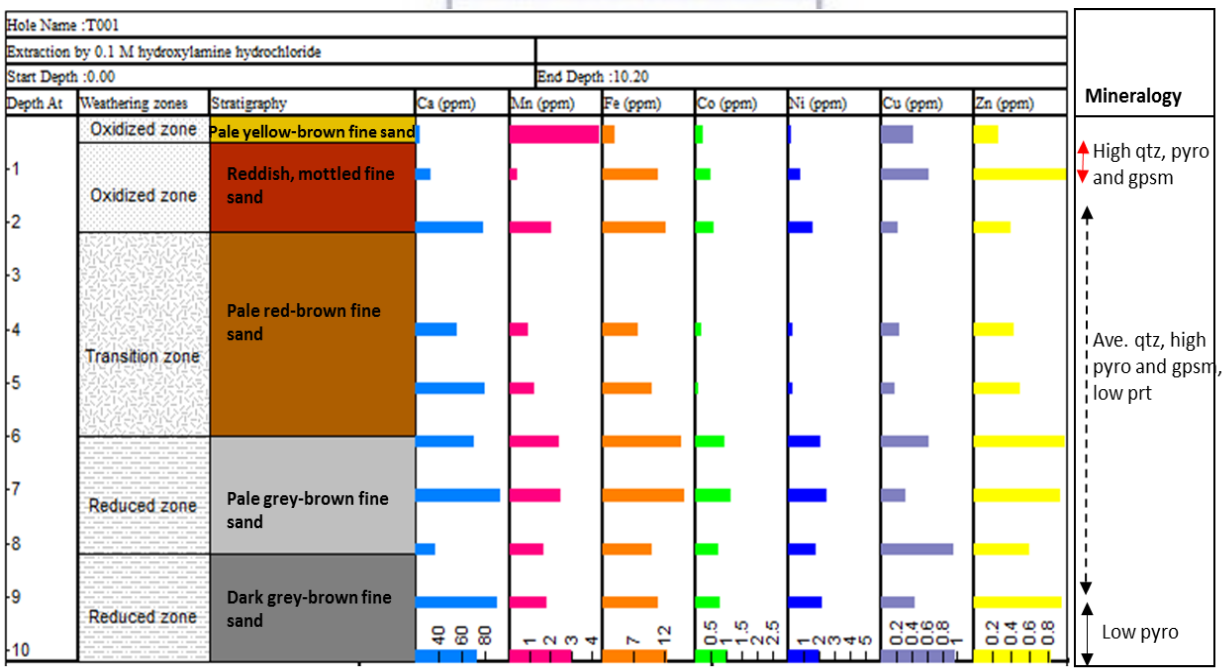

Figure 4.5. 4: The downhole distribution of selected major- and trace elements extracted by 0.1 M hydroxylamine hydrochloride for section T001.

Fig. 4.5.4, shows the downhole distribution of selected oxide- and metal concentrations extracted by 0.1 M hydroxylamine hydrochloride for section T001. Similar to the bulk element

geochemical data for section T001, Ca, Fe, Co, Ni, Cu and Zn concentrations extracted by 0.1 M hydroxylamine hydrochloride within the first 0.5 meters appear very low and Mn, high. According to slimes stratigraphy, this depth corresponds to leached, pale yellow-brown fine sands. Peaks in Fe concentration are noted between 1 and 2.2 meters in reddish mottled fine sands and are accompanied by Cu and Zn peak concentrations. This suggests that Cu and Zn concentrations are influenced by increased Fe oxide contents. Unlike the trend seen for double distilled water, the oxides and metals show peak concentrations between 6 meters and 10.2 meters. According to the weathering zones, this depth is consistent with reducing conditions. Under reducing conditions, metals are readily bound to Mn- and Fe oxides, making them increasingly available for extraction by 0.1 M hydroxylamine hydrochloride. Overall, there is a clear association between Fe, Cu and Zn and between Mn, Co and Ni. These relationships were defined by Principal Component Analysis and are evident downhole.

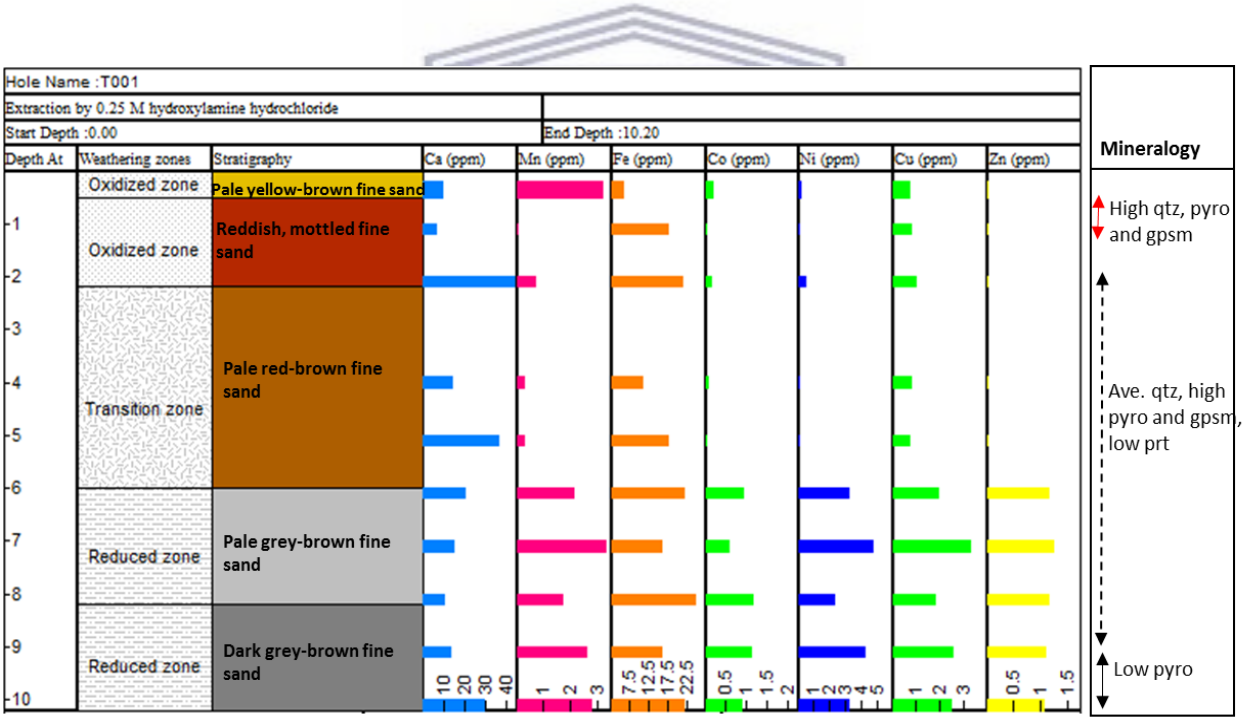

Figure 4.5. 5: The downhole distribution of selected major- and trace elements extracted by 0.25 M hydroxylamine hydrochloride for section T001.

Fig. 4.5.5, shows the downhole distribution of selected oxide- and metal concentrations extracted by 0.25 M hydroxylamine hydrochloride for section T001. Similar to the bulk element geochemical data for section T001, Ca, Fe, Co, Ni, Cu and Zn concentrations extracted by 0.1 M

hydroxylamine hydrochloride within the first 0.5 meters are very low and Mn, high. According to slimes stratigraphy, this depth correspond to leached, pale yellow-brown fine sands. Peaks in Fe concentration are noted between 1 and 2.2 meters in reddish mottled fine sands, with no corresponding peaks in metal concentration. While Fe remains relatively high between 1 meter and 5 meters, Mn appears very low. Metal ions mimic this trend in low concentration for the same depth. Similarly, peaks in Mn concentration between 6 meter and 10.2 meters are accompanied by peaks in Co, Ni, Cu and Zn concentrations. This suggests that metals are most intimately associated with Mn oxides (verifying Principal Component Analysis). According to the weathering zones, this depth is consistent with reducing conditions. Under reducing conditions, metals are readily bound to Mn- and Fe oxides, making them increasingly available for extraction by 0.25 M hydroxylamine hydrochloride.

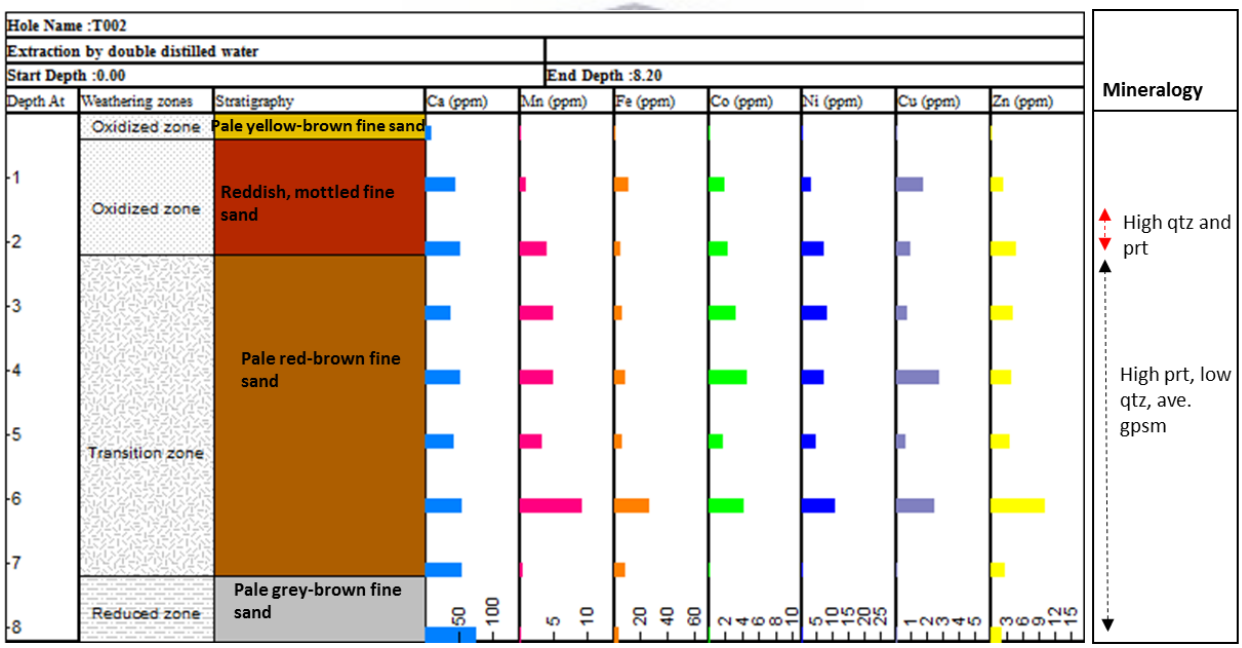

Figure 4.5. 6: The downhole distribution of selected major- and trace elements extracted by double distilled water for section T002.

Fig. 4.5.6, shows the downhole distribution of selected oxide- and metal concentrations extracted by double distilled water for section T002. Similar to the bulk element geochemical data for section T002, Ca, Fe, Mn, Co, Ni, Cu and Zn concentrations extracted by double distilled water in the first 0.5 meters are very low (near below detection). Similar to T001, this depth corresponds to pale yellow-brown fine sands. Very low oxide and metal concentrations, suggest

a reason for the pallor appearance of fine sands within the first 0.5 meters. With the exception of 5 meters, relatively consistent Ca (approximately 35 – 55 ppm) Mn (approximately 3 – 4 ppm), Fe (approximately 4 – 6 ppm), Co (approximately 1 – 4 ppm), Ni (approximately 3 – 7 ppm), Cu (approximately 0.5 – 2 ppm) and Zn (approximately 3 – 4 ppm) concentrations occur between 2 meters and 6 meters. Based on slimes descriptions, this depth coincides with pale red-brown fine sands. According to paste pH data, depths from 2- to 6 meters are characterized by pH values between 3.6 and 3.9, with the exception of 5 meter which has a higher paste pH of 4.2. The slightly more basic conditions at 5 meters are the reason for a slight decrease in Mn, Co, Ni and Cu. Zn is uninfluenced by the decrease in Mn at this depth, suggesting that Zn is more closely associated with Fe oxide. The intimate relationship between Fe and Zn was defined by Principal Component Analysis and is evident downhole.

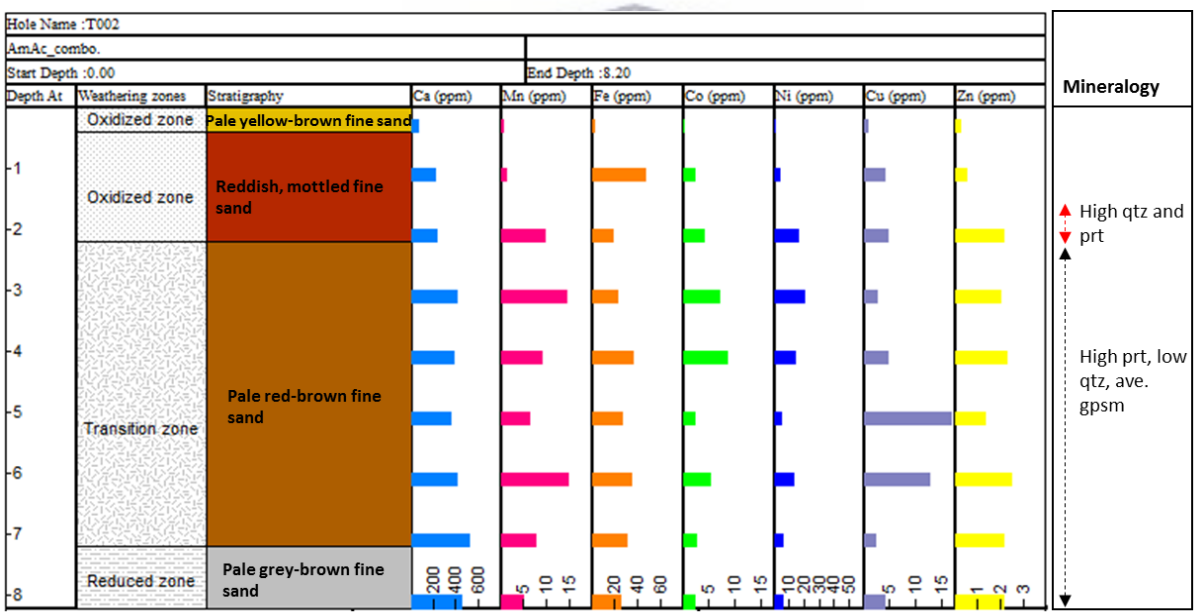

Figure 4.5. 7: The downhole distribution of selected major- and trace elements extracted by 1 M ammonium acetate for section T002.

Fig. 4.5.7, shows the downhole distribution of selected oxide- and metal concentrations extracted by 1 M ammonium acetate for section T002. Similar to the bulk element geochemical data for section T002, Ca, Fe, Mn, Co, Ni, Cu and Zn concentrations extracted by 1 M ammonium acetate in the first 0.5 meters are very low. This depth corresponds to leached, pale yellow-brown fine sands. Fe concentrations seemingly peak between 1- and 1.2 meters. According to slimes

descriptions, this depth coincides with red, mottled fine sands. High Fe concentrations encountered at this depth account for red, mottled appearance of fine sands. Despite this peak in Fe, metal (Co, Ni, Cu and Zn) concentrations remain low, in association with low Mn at the same depth. Peak Cu concentrations occur between 5- and 6.2 meters and peak Zn concentrations between 6 meters and 6.2 meters, in association with Mn concentrations. Metal concentrations decrease between 7- and 8 meters. According to slimes descriptions, this depth corresponds with reduced grey fine sands. Under reduced conditions metal are readily bound to Mn- and Fe oxides and thus less available for extraction by 1 M ammonium acetate, which targets Ca oxides.

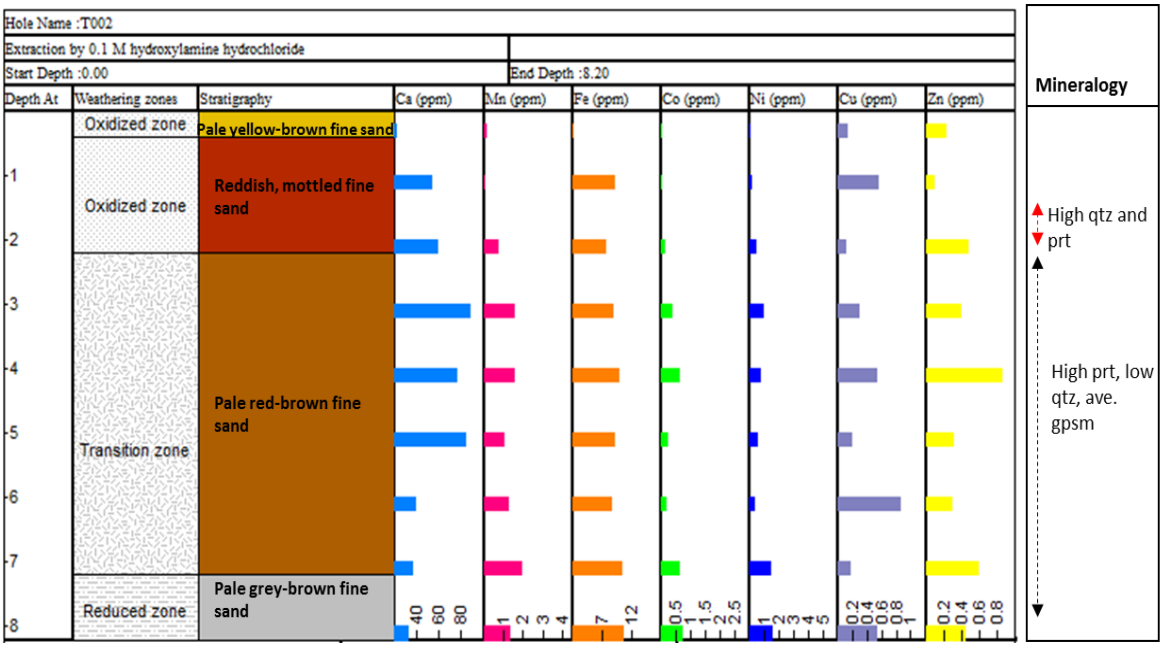

Figure 4.5. 8: The downhole distribution of selected major- and trace elements extracted by 0.1 M hydroxylamine hydrochloride for section T002.

Fig. 4.5.8, shows the downhole distribution of selected oxide- and metal concentrations extracted by 0.1 M hydroxylamine hydrochloride for section T002. Similar to the bulk element geochemical data for section T002, Ca, Fe, Mn, Co, Ni, Cu and Zn concentrations extracted by 0.1 M hydroxylamine hydrochloride are very low in the upper oxidized zone. Very low oxide and metal concentrations, suggest a reason for the pallor of fine sands within the first 0.5 meters downhole. Compared to that of 1 M ammonium acetate, 0.1 M hydroxylamine hydrochloride is distinguished by considerably lower oxide- and metal contents. Co and Ni concentrations remain nearly consistent between 2 and 6.2 meters, in association with Mn. Cu and Zn concentration

peaks at various depths downhole, in association with Fe. Co and Ni concentrations peak between 7- and 8. According to the weathering zones, this depth corresponds to reduced conditions. Under reduced conditions metal are readily bound to Mn oxides making metals increasingly available for extraction by 0.1 M hydroxylamine hydrochloride.

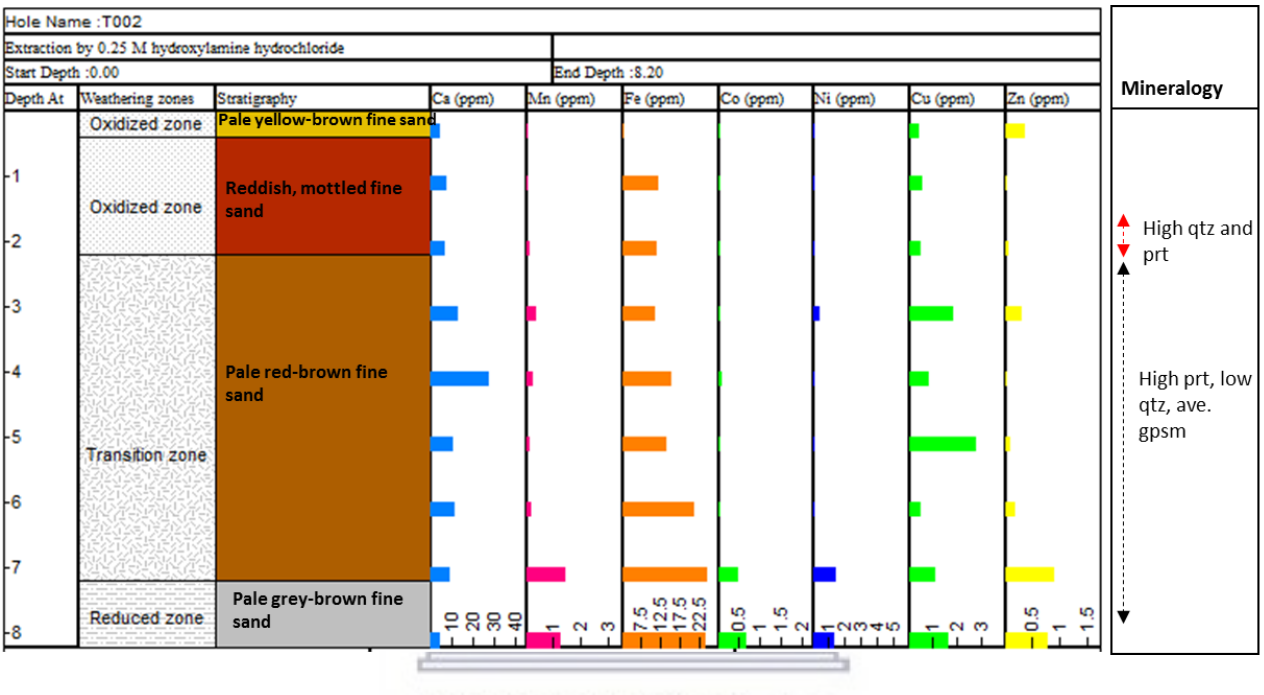

Figure 4.5. 9: The downhole distribution of selected major- and trace elements extracted by 0.25 M hydroxylamine hydrochloride for section T002.

Fig. 4.5.9, shows the downhole distribution of selected oxide- and metal concentrations extracted by 0.25 M hydroxylamine hydrochloride for section T002. Similar to the bulk element geochemical data for section T002, Ca, Fe, Mn, Co, Ni, Cu and Zn concentrations extracted by 0.25 M hydroxylamine hydrochloride are very low in the upper oxidized zone. Similar to 0.1 M hydroxylamine hydrochloride, 0.25 M hydroxylamine hydrochloride yielded considerably low oxide and metal concentrations. The relationship between Co, Ni, Zn and Mn is evident for 0.25 M hydroxylamine hydrochloride, while Cu concentrations show some association with Fe. These relationships were defined by principal component analysis and are clear downhole. Peak Mn, Fe, Co, Ni, Zn concentrations occur between 7- 8 meters. This depth corresponds to reduced conditions. Under reduced conditions metal are readily bound to Mn oxides making metals increasingly available for extraction by 0.25 M hydroxylamine hydrochloride.

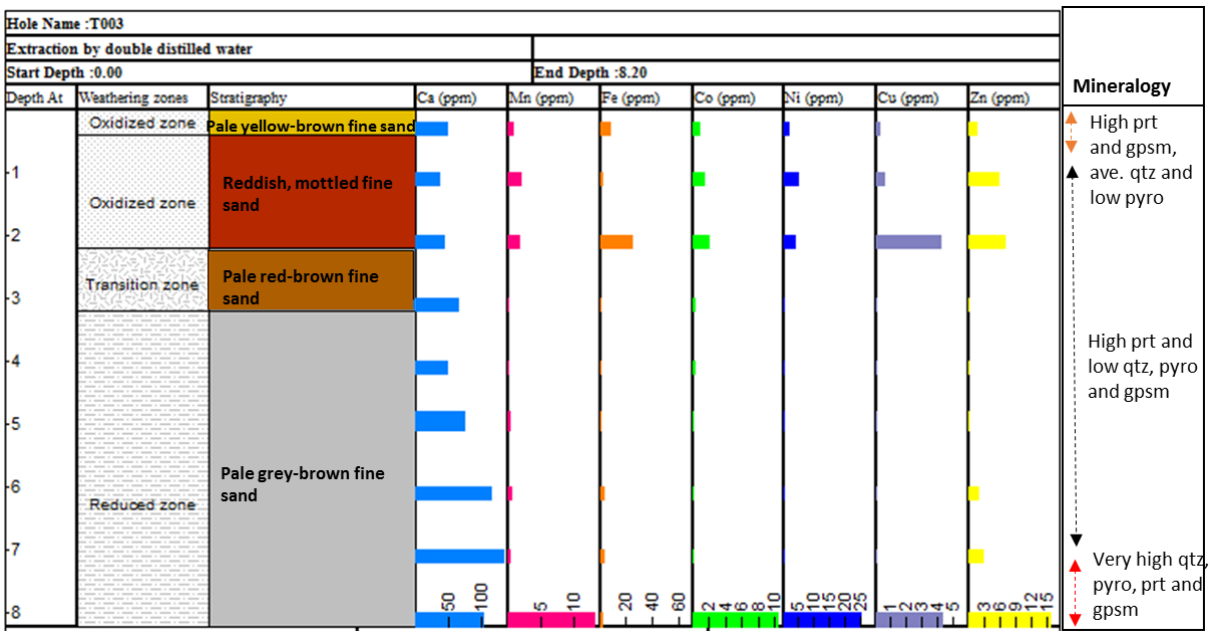

Figure 4.5. 10: The downhole distribution of selected major- and trace elements extracted by double distilled water for section T003.

Fig. 4.5.10, shows the downhole distribution of selected oxide- and metal concentrations extracted by double distilled water for section T003. Unlike that of sections T001 and T002, the bulk element geochemical data for section T003 show minor oxide and metal concentrations up to 2.2 meters. Metal concentrations at this depth are attributed to high gypsum, as shown by x-ray diffraction data. According to the weathering zones, this depth corresponds with the oxidized zone. Depths between 3 and 7 meters show very low, near undetectable, oxide and metal concentrations for all but Ca, which shows a general increase with depth. According to the weathering zones, this depth is consistent with the transition zone and reduced zone. Under reducing conditions, metals are likely bound to Mn and Fe oxides, rendering them less available for extraction by water. Peak metal concentrations occur between 8- and 8.2 meters, in association with Mn oxides. According to paste pH, this depth is consistent with near neutral pH (7.4), rendering metals more available for extraction by water.

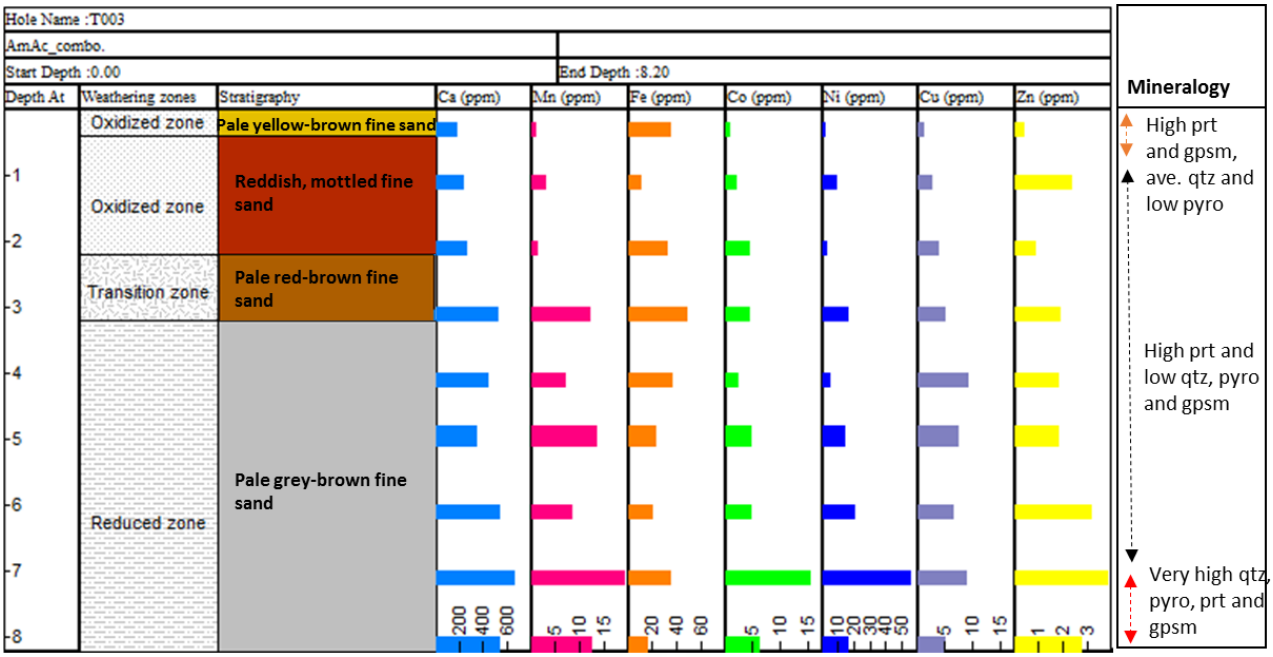

Figure 4.5. 11: The downhole distribution of selected major- and trace elements extracted by 1 M ammonium acetate for section T003.

Fig. 4.5.11, shows the downhole distribution of selected oxide- and metal concentrations extracted by 1 M ammonium acetate for section T003. Similar that of double distilled water, extraction by 1 M ammonium acetate yielded minor Mn, Co and Ni but increased Fe, Cu and Zn concentrations in the first 2.2 meters. This depth corresponds to the oxidized zone and is distinguished from lower zones by low Co and Ni concentrations, in association with Mn. Extraction by 1 M ammonium acetate yielded peak concentrations between 3- and 7 meters. According to the weathering zones, this depth is consistent with reducing conditions. Under reduced conditions, metals are increasing bound to oxides and thus available for extraction by 1 M ammonium acetate. The oxide- and metal concentrations decrease between 7- and 8.2 meters. According to x-ray diffraction data, this depth is distinguished from the rest of the reduced zone by very high pyrite, pyrophyllite and gypsum. This suggests that a large proportion of major and trace elements are present in primary minerals and therefore less available for extraction by 0.1 M hydroxylamine hydrochloride.

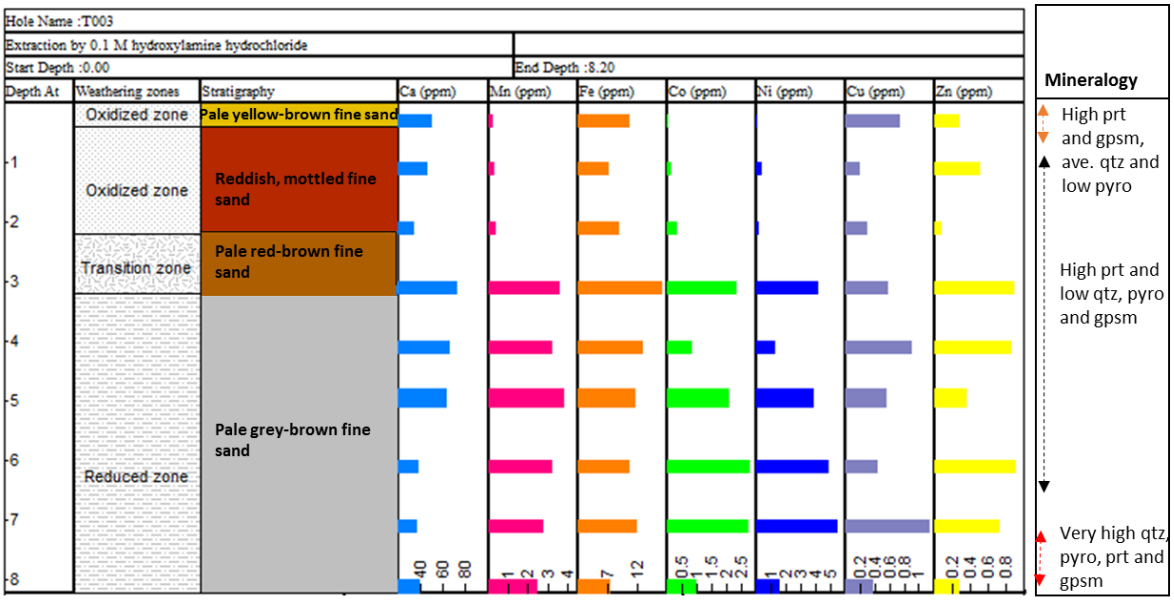

Figure 4.5. 12: The downhole distribution of selected major- and trace elements extracted by 0.1 M hydroxylamine hydrochloride for section T003.

Fig. 4.5.12, shows the downhole distribution of selected oxide- and metal concentrations extracted by 0.1 M hydroxylamine hydrochloride for section T003. Similar to that of double distilled water and 1 M ammonium acetate, extraction by 0.1 M hydroxylamine hydrochloride yielded low Mn, Co and Ni concentrations within the first 2.2 meters (the oxidized zone). Very low Co (0.02 – 0.2 ppm) and Ni (0.02 – 0.3 ppm) concentrations at this depth, occur in association with very low Mn (0.1 -0.2 ppm) concentrations while Cu and Zn show concentrations in association with Fe at the same depth. Similar to that of 1 M ammonium acetate, extraction by 0.1 M hydroxylamine hydrochloride yielded peak concentrations between 3- and 7 meters. According to the weathering zones, this depth the transition zone and reduced zone. Under reduced conditions, metals are increasing bound to oxides and thus available for extraction by 0.1 M hydroxylamine hydrochloride. Similar to results for 0.1 M hydroxylamine hydrochloride, concentrations decrease between 7- and 8 meters.

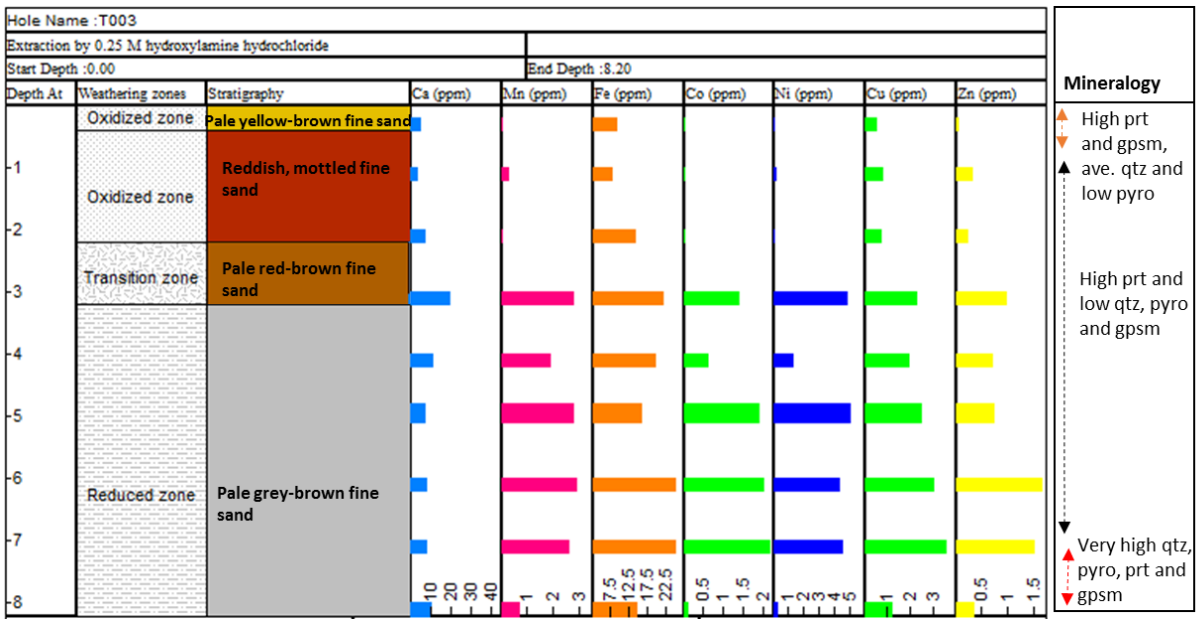

Figure 4.5. 13: The downhole distribution of selected major- and trace elements extracted by 0.25 M hydroxylamine hydrochloride for section T003.

Fig. 4.5.13, shows the downhole distribution of selected oxide- and metal concentrations extracted by 0.25 M hydroxylamine hydrochloride for section T003. Similar to that of double distilled water and 1 M ammonium acetate, and 0.1 M hydroxylamine hydrochloride, extraction by 0.25 M hydroxylamine hydrochloride yielded low Mn, Co and Ni concentrations within the first 2.2 meters (the oxidized zone). Similar to 0.1 M hydroxylamine hydrochloride, very low, near undetectable, Co (approximately 0.09 – 6 ppb) and Ni (approximately 0.01 ppb – 0.1 ppm) occur in close association with very low Mn (approximately 50 ppb – 0.25 ppm) at this depth. Cu (approximately 0.5 – 0.7 ppm) and Zn (approximately 0.03 – 0.2 ppm) concentrations occur in close association with Fe (approximately 7 – 13 ppm). Similar to that of 1 M ammonium acetate and 0.1 M hydroxylamine hydrochloride, extraction by 0.25 M hydroxylamine hydrochloride yielded peak concentrations between 3- and 7 meters. According to the weathering zones, this depth is consistent with the transition zone and the reduced zone. Under reduced conditions, metals are increasing bound to oxides and thus available for extraction by 0.25 M hydroxylamine hydrochloride. Similar to 1 M ammonium acetate and 0.1 M hydroxylamine hydrochloride, concentration decreases noted between 7- and 8.2 meters are attributed to the presence of stable primary host minerals.

While the extraction of water-soluble metals in section T001 shows peak concentrations in the reddish mottled sands of the lower oxidized zone, metal concentrations extracted by 1 M ammonium acetate, 0.1 M hydroxylamine hydrochloride and 0.25 M hydroxylamine hydrochloride show peak metal concentrations in the pale grey-brown sands and dark grey-brown sands of the reduced zone. This is the result of metal desorption dominating the oxidized zone and metal adsorption dominating the reduced zone.

Similar to T001, water-extractable oxide and metal concentration in section T002 are limited to the lower oxidized- and transition zone. Relative to the reddish mottled sands of T001, section T002 shows no pronounced metal peaks. Unlike section T001, section T002 shows near consistent concentrations for 1 M ammonium acetate and 0.1 M hydroxylamine hydrochloride between 1 – 8 m while similar to T001, 0.25M hydroxylamine hydrochloride shows noticeable metal and oxide increases in the reduced zone.

Similar to section T001 and T002, water-extractable oxide (barring Ca) and metal concentrations in section T003 are limited to the oxidized zone, with the exception of the lowest layer of pale grey-brown sands of the reduced zone. Onset of the reduced zone is very pronounced, exhibiting oxide and metal concentration increases for 1 M ammonium acetate, 0.1 M hydroxylamine hydrochloride and 0.25 M hydroxylamine hydrochloride. As with section T001, this is the result of metal desorption dominating the oxidized zone and metal adsorption dominating the reduced zone.

4.6 Summary of the results

4.6.1 Mineralogical results

- The slimes mineralogy was determined to consist of mainly high quartz and minor pyrophyllite, pyrite, chlinochlore, gypsum and yoshiokaite proportions. Of the slimes sections, section T003 showed the highest mineral proportions.
- Cluster and discriminant analysis grouped samples into the following groups: Cluster one (very high SiO_2 and increasing Al and K^+), cluster two (High SiO_2 and decreasing Al and K^+), cluster three (Very high CaO and increasing Al and K^+) and cluster four (High CaO

and decreasing Al and K^+). Here, K^+ represents relative clay contents. SiO_2- groups were shown to dominate the top of the slimes dam and CaO-rich samples, the middle and bottom of the slimes.

- Based on cluster groups, the slimes samples were divided into an oxidized zone (up to 2.2 meters), 1 – 5 meter transitions zone and 1 – 4 meter reduced zone. The oxidized zone is characterized by upper pale fine sands and lower mottled fine sand while the transition zone is characterized by red-brown fine sands and the reduced zone by grey fine sands.
- Petrographic data showed that high quartz proportions dominate the upper oxidized zone, while clayish proportions appear highest in the lower oxidized zone (between 0.8 meters and 2.2 meters) and the reduced zone (between 8.2 meters to 10.2 meters).

4.6.2 Geochemical results

- The upper oxidized zone is characterized by subdued major-oxide and trace elements while the lower oxidized- and reduced zone are enriched.
- Paste pH and sulphide-sulphur show good correlation. In general, the oxidized zone is characterized by low pH and sulphide-sulphur while the reduced zone is characterized by high pH and sulphide-sulphur.
- The role of sulphide-sulphur in metal mobilization was evident as metals, even those conventionally considered immobile (Zn, Pb and Au) showed distribution patterns similar to that of sulphide-sulphur.
- Acid base accounting characterized the slimes as largely acid-generating, hosting only two non-acid generating samples in the upper oxidation zone, coincident with near undetectable sulphide-sulphide, likely in response to extensive oxidation at the surface.
- Selective sequential extraction determined that weathering zones (pH) have significant impact on the release and mobilization of metals as water- and carbonate- related extractions yielded the highest concentrations in the oxidized zone while oxide-related extractions yielded the highest concentrations in the reduced zone.
- Of the metals leached by selective sequential extraction, Ni, Cu, Co and Zn showed the highest concentrations (approximately 11 ppm, 5 ppm, 4 ppm and 3 ppm) in the water-

soluble, exchangeable- and carbonate phases, rendering these metals considerable bioavailable threats.

- Of the metal-sorbing phases, metals appeared most intimately associated with Mn-oxides, suggesting that Mn oxides play a significant role in metal release.

CHAPTER FIVE: Discussion

This chapter discusses the results obtained in line with the study's aims and objectives. The aim of this study was to understand heavy metal release from the Gold One Millsite Slimes Complex into the Randfontein area, Witwatersrand. To achieve this, several objectives were outlined. These were as follows:

- To assess the influence of mineralogical- and geochemical factors on heavy metal release.
- To determine and model the weathering zones using cluster analysis.
- To determine sulphide-sulphur (wt %) and its potential influence on metal mobilization.
- To determine the leachability of metals using selective sequential extraction.
- To predict the acid generating potential of slimes samples using the calculated sulphide-sulphur (wt %).

5.1 Findings

5.1.1 Mineralogy, geochemistry and stratigraphy

Mineralogy of the Witwatersrand gold tailings is limited to a seemingly narrow compositional range, typically comprising of approximately 70 – 90 % quartz, approximately 10 – 30 % sericite, including minor chlorite, pyrophyllite and chloritoid, approximately 3 – 4 % pyrites, approximately 1 – 2 % other sulphides, approximately 1 – 2 % heavy detrital minerals including zircon, rutile, uraninite and chromite and approximately 1 % uraniferous kerogen (Liebenberg, 1957; Förstner and Wittmann 1976; Rösner et al., 2001). A study by Rösner et al., 2001 determined that minor pyrophyllite-, chlorite- and muscovite proportions accompany quartz fractions in gold tailings.

Slimes however, although still dominated by quartz, show considerable proportions of phyllosilicates (approximately 15 % illite clays, 20 % muscovite and 20 % pyrophyllite, clinchlore and kaolinite) with trace amounts of pyrite and other sulphide minerals (Stanley,

1987). In general, mineral proportions in the Witwatersrand gold tailings show good correlation with the composition of the gold-bearing conglomerates of the Witwatersrand according to (Table 5.1, after Stanley, 1987).

Table 5. 1: The mineralogical composition of auriferous Witwatersrand conglomerates (after Stanley, 1987)

Mineral	Proportions
Quartz	70 - 90 %
Phyllosilicates (Clays)	10 - 30 %
Pyrites	3 - 4 %
Other sulphides	1 - 2 %
Grains of primary minerals	1 - 2 %
Gold	approx. 45 ppm

X-ray diffraction data provided for this study, showed slimes mineralogy to consist mainly of quartz (approximately 41 % - 63 %) and minor pyrophyllite (approximately 0.8 % - 5.9 %), pyrite (approximately 0.12 % - 0.6 %), clinochlore (approximately 0.2 % – 0.4 %), gypsum (approximately 0.3 % - 1.8 %) and yoshiokaite (approximately 0.08 % - 0.4 %) proportions. Overall, these findings show good correlation with the auriferous Witwatersrand conglomerates but show lower quartz and pyrite proportions relative to that of Witwatersrand- conglomerates (Table 5.1) and gold tailings (Liebenberg, 1957; Förstner and Wittmann 1976; Rösner et al., 2001). This is the result of increased weathering in slimes. Relative to tailings dams (approximately 75 µm – 500 µm; USEPA, 2009), slimes dams consists of finer material (approximately 45 µm – 75 µm; USEPA, 2009) considered to undergo increased oxidation related to their larger reactive surfaces (Bezuidenhout and Rousseau, 2006).

Gypsum was determined as the dominant water-soluble phase in the upper oxidized zone and in certain samples from the reduced zone, with elevated gypsum and quartz proportions dominating the upper oxidized zone (0.2 – 0.5 m) of the slimes. Increased secondary sulphate (e.g. gypsum) concentrations are often encountered on mine waste surfaces (in semi-arid/arid climates), where

excessive evaporation concentrates mobile ions, forming highly water-soluble, heavy metal-enriched salts at the top of mine waste dams (Hammastrom et al., 2005; Smuda et al., 2007). Investigations of tailings geochemistry performed by Rosner (2000), Abegunde (2015), Abegunde et al., (2016) found that tailings geochemistry was dominated by high SiO_2. Similarly, bulk geochemical data provided for this study, for sections of the Gold One Millsite Slimes Complex, suggest that the geochemistry of Witwatersrand slimes dams is largely dominated by SiO_2, most of which occur as quartz (approximately 41 wt. % - 64 wt. %), based on x-ray diffraction analysis. Similar to x-ray diffraction data, the bulk geochemical data provided for this study show good correlation with the composition of the Witwatersrand conglomerates.

Stratigraphy within the Witwatersrand basin constitutes an upper (ochre) oxidized zone, a transition zone and basal (grey), reduced zone (Nengovhela et al., 2006). Enhanced permeability of the Witwatersrand sand dumps, relative to slimes dumps, typically renders them more susceptible to oxidation. In general, the oxidized zones in tailings sands extend up to 5 m depths, while oxidized zones in slimes tailings extend to approximately 2 m depths (Marsden, 1986). Similarly, this investigation distinguished three major weathering zones, namely an oxidized zone, transition zone and reduced zone. The oxidation zone includes an upper layer (0 – 0.5 meters) characterized by pale yellow-brown fine sands and a lower layer (1 – 2.2 meters) characterized by reddish, mottled fine sands. The upper pale sands of the oxidized zone appear significantly leached of both metal, oxide and sulphide contents. The lower mottled fine sands of the oxidized zone (1 – 2.2 m) are distinguished from upper pale sands by significant metal enrichment. The transition zone is below the oxidized zone and is characterized by pale, red brown fine sands (1 – 5 meters). The reduced zone is below the transition zone and is characterized by light- and dark grey fine sands (2 – 4).

5.1.2 The weathering zones

Cluster and discriminant analyses was used to determine and model the weathering zones in the slimes dam. The analysis grouped slimes samples into four groups based on relative SiO_2, CaO and clay (Al and K^+)-related contents. Samples were placed into cluster one if they showed very high SiO_2 and high (Al and K^+), into cluster two if they showed high SiO_2 and low (Al and K^+),

into cluster three if they showed very high CaO and high (Al and K^+) and into cluster four if they showed high CaO and low (Al and K^+).

The upper portions of the slimes sections were dominated by low CaO and high-SiO_2 samples while mid- to lower portions of the dam were dominated by high-CaO and low-SiO_2. These parameters were used to distinguish the SiO_2-rich oxidized zone from the CaO-rich reduced zone. The transition zone was marked by the onset of CaO-rich samples while the reduced zone showed near dominance of CaO-rich samples and was verified by basic pH values. Based on x-ray diffraction data (Appendix One: B), samples showing the lowest reported quartz proportions (< 42 %) correlate well with samples indicating potential clay formation based on leached K^+ contents (distinguishing cluster groups two and four). This verifies that K^+ provides some preliminary indication of clay formation.

Of the slimes sections investigated, T003 was determined as having undergone the least weathering. Evidence for this includes:

(i) X-ray diffraction analysis which showed the highest pyrite proportions (0.42 wt. % - 0.64 wt. %) for section T003. The presence of high, seemingly preserved, pyrite proportions are a result of low oxygen levels within this section and thus, limited oxidation (Rosner, 2000).

(ii) Core-log reappraisal which showed the onset of grey-coloured, reduced samples as shallow as 3 meters and up to 8.2 meters. Here, the early onset of reduced samples and overall extent of the reduced zone suggests the presence of limited oxygen and thus, limited oxidation within section T003

(iii) Paste pH data which shows high paste pH values (approximately 8.1) encountered at 3 meters persisting up to 8.2 meters. Similar to the core-log reappraisal, the onset of reduced conditions as shallow as 3 meters suggests low oxygen levels up to 8.2 meters.

(iv) Bulk geochemical analysis which showed the highest CaO and trace element concentrations in section T003. Acidic, oxidizing conditions are thought to liberate trace elements into the

aqueous solution. Thus, the retention of trace element concentrations in solid phase can be attributed to low oxygen levels and the reduced conditions dominating between 3- and 8.3 meters in section T003.

(v) Calculated sulphide-sulphur within the first meter of the slimes shows higher sulphide-sulphur (0.7 wt %) yielded for section T003, compared to sections T001 (< 0.002 wt %) and T002 (0.006 wt %). This suggests that even at this depth, where the slimes dam is thought to experience the greatest exposure to the atmosphere, the degree of oxidation in T003 is considerably lower than that determined for section T001 and T002.

(vi) Cluster and discriminant analysis which, based on K^+ proportions (presumably related to the formation of clays), determined that section T003 hosted the least number of samples indicating potential clay formation. Since clay formation is a product of chemical weathering, the lower clay proportions suggested section T003 is the least weathered.

Of the slimes sections investigated during this study, section T001 was determined as having undergone the most oxidation. Evidence for this includes:

(i) X-ray diffraction analysis which showed the lowest pyrite proportions (0.12 wt. % - 0.13 wt. %) reported for section T001. The loss of pyrite is a consequence of sulphide oxidation when exposed to the atmosphere and water. Low pyrite proportions up to 10.2 meters suggests section T001 is considerably oxidized.

(ii) Calculated sulphide-sulphur which shows the lowest sulphide-sulphur (< 0.002 wt %) yielded for section T001, compared to sections T002 (0.006 wt %) and T003 (0.7 wt %). This mimics the trend observed for pyrite. The lowest sulphide-sulphur noted for section T001 correlates well with the lowest percentage of sulphide (approximately 15 %) observed when calculated as a percentage of the total (leco) sulphur. The lowest proportions of sulphide-sulphur are typically expected in the very top zones of the oxidized zone as this is a highly oxidizing environment.

5.1.3 Metal mobilization and retention in the weathering zones

The distribution of metal concentrations under surficial conditions is largely related to weathering processes and the relative stability of primary and secondary minerals at the surface (Smuda et al., 2014). In general, the processes controlling metal mobilization in tailings and slimes include: (i) flushing/leaching by infiltrating surface waters and (ii) oxidation/reduction processes (iii) hydrolysis and subsequent clay formation and (iv) the precipitation of mineral-oxides and hydroxides (Carlsson et al., 2002) and subsequent metal adsorption related to oxide species (Acero et al., 2007). The role of these processes in metal mobilization/retention were evident during this study.

(i) Leaching of upper oxidized layers by infiltrating rainwater

Metal mobilization in the upper zones of tailings/slimes can often occur in the form of flushing/leaching by infiltrating rainwaters as was noted during this investigation (Evans and Banwart, 2006). Subdued, near undetectable metal concentrations determined for the upper oxidized zone (first 0.5 meters) of section T001 and T002, are the result of extensive leaching. Samples at this depth are characterized by pale, yellow-brown fine sands. The x-ray diffraction and petrographic data determined for this depth, showed the highest reported quartz proportions downhole. The high quartz proportions render the upper oxidized zone more susceptible to metal leaching relative to the lower oxidized zone. Abegunde et al, (2016), noted a similar occurrence in the Mongale tailings dam in the Witwatersrand, where high silica samples in the oxidized zone were associated with intensive metal flushing. These findings verify the poor correlation determined for SiO_2 and trace elements (Abegunde et al, 2016).

(ii) Oxidation and reduction processes

The oxidation process of greatest environmental concern in slimes and tailings, is the oxidation of pyrite. Pyrite in slimes/tailings is readily oxidized in the presence of air and water and is responsible for the generation of acid mine drainage (Jambor and Blowes, 1998). The resulting formation of sulphuric acid can result in acidic solutions. Most metals are soluble under acidic

conditions. Thus, metal mobilization in tailings may be closely related to sulphide contents (Nordstrom and Alpers 1999, Younger et al. 2002, Banks 2004). The process of sulphide oxidation in tailings/slimes is a self-sustaining one, and therefore may persist long after the cessation if mining operations (Nordstrom, 1979; Moses et al., 1987; Blowes et al., 1998).

To this end, this study assessed the potential relationship between sulphide and metal mobilization in the slimes dam. This was achieved by calculating sulphide-sulphur (wt. %) for the slimes samples and comparing the distribution patterns thereof to that of trace elements (XRF data). Consequently, this study determined strong correlation between sulphide- and metal distribution and concluded that even fairly immobile metals (Zn, Pb and Au) may be mobilized by sulphide-sulphur. Using the sulphide-sulphur contents, acid base accounting methods were used to determine the relative acid generating/consuming potential of slimes by relating acidity to total pyrite content and neutralization to total carbon content (Lawrence, 1990). The dissolution of pyrite (FeS_2) is a significant acid generating reaction because of the nearly ubiquitous presence of minor pyrite concentrations in coal enrichments and the surrounding rocks of most metalliferous mines (Pope et al., 2010).

Acid base accounting methods applied during this investigation suggest all but samples 48 and 59 (0.2 – 0.4 m), are net acid producing. Net acid neutralizing samples (48 and 59) correspond to the pale yellow-brown sands of the upper oxidized zone in T001 and T002 and are both characterized, according to discriminant analysis, by high SiO_2, Al and K^+. These samples correlate well with calculated sulphide-sulphur, accounting for the lowest reported sulphide-sulphur (< 0.002 wt. % and 0.006 wt. %, respectively). Thus, results determined by acid base accounting for sample 48 and 59 (between 0.2 and 0.4 meters), are attributed to extremely low, leached sulphide-sulphur (wt %) concentrations. Very low sulphide-sulphur can be expected within the upper zones of the slimes dam where oxygen diffusion is rapid as a result partial water saturation, causing an acceleration of the rate of sulphide oxidation. Furthermore, the oxidation of sulphides in slimes is catalyzed by bacterial activity, further promoting the release of reaction products into solution at the surface (Bezuidenhout and Rousseau, 2006). Silicate minerals may contribute to neutralization potential by supplying soluble base cations and in some rocks, may exhibit neutralization effects exceeding that of carbonates (Weber et al. 2005). This suggests that

neutralization between 0.2 – 0.4 m may be the result of extensive sulphide oxidation at the surface, combined with enhanced neutralization resulting from the high silica proportions at the surface.

(iii) Clay formation

Relatively high muscovite (up to 20 %) and illite clay (up to 20 %) proportions determined for Witwatersrand slimes, suggest slimes show good potential for clay formation (Stanley, 1978). Cluster and discriminant analysis distinguished sample groups based on relative SiO_2, CaO and clay-related contents. Clay-rich samples were determined throughout the slimes sections, the largest percentage of which occur in section T002, and the lowest of which occur in section T003. Clay minerals are common products of chemical weathering, typically forming in response to the hydrolysis (reaction with water) of feldspars and micas. Charges often develop on clay surfaces as result of the hydrolysis of broken Si-O and Al-OH along the surfaces of clay lattices (Greenland and Mott, 1978). This charge is largely pH dependent (Gallez et al., 1976). At relatively low pH, clays typically behave as anion exchangers, resulting from surplus H^+. At relatively high pH, clay species typically behave as cation exchanger, resulting from surplus OH^- (Greenland and Mott, 1978).

(iv) The precipitation of oxide minerals and hydroxide minerals and related metal adsorption

Metals are largely soluble under acidic conditions but can be precipitated by increasing the pH. Typically, the resulting products are oxide and oxyhydroxides (Ibanez et al., 2008). Alkali- and alkali earth elements typically precipitate in pH solutions above the range determined for natural waters while transition elements precipitate within the pH range of natural waters. The reaction of water (hydrolysis) with solid metal oxides results in oxide hydration, consequently forming a monolayer hydroxyl groups (Ibanez et al., 2008). Depending on pH, this layer may be protonated or deprotonated. Similar to clays, the amphoteric nature of oxides allows oxide particles to develop either positive (as a result of protonation) or negative (as the result of deprotonation) electrical charges (Ibanez et al., 2008).

A state known as Point of Zero Proton Charge (pzpc) describes the pH conditions at which the electrical charge density on the oxide surface equates to zero (Ibanez et al., 2008). At a pH lower than that required to attain the pzpc, the surficial sites become protonated, resulting in the development of excess positive charges on the oxide surface (attributed to surplus H^+). Thus, under low pH conditions, such as those encountered in the oxidized zones of T001, T002 and T003, oxides develop an anion exchange capacity (Ibanez et al., 2008). The inverse takes place at pH values higher than the pzpc, typical of the reduced zones of sections T001, T002 and T003, resulting in excess negative charges on the oxide surface (attributed to surplus OH^-) where the oxide develops cation exchange capacity (Ibanez et al., 2008). Metals are attracted- and bond to the positive and negative charges on oxide surfaces. This form of surface bonding is called adsorption. Metals are readily adsorbed to carbonate-, Mn-oxide- and Fe-oxide- species under reduced conditions, and readily desorbed under oxidizing conditions as is evident from this study. Thus, the distribution of metal concentrations is controlled by weathering (pH).

As noted by selective sequential extraction, metal concentrations occur largely in association with Mn oxides. Under reduced conditions metals are readily adsorbed to the negative surface charges on the Mn oxides as a result of surplus OH^-, making metals increasingly available for selective extraction. Under more oxidizing conditions, metals are readily desorbed from the surface of the Mn oxides as a result of surplus H^+ and enter the aqueous phase, rendering metals unavailable for selective extraction.

5.1.4 Metal speciation

Rosner and van Schalkwyk (2000) investigated several case study sites near Johannesburg and found that the topsoils were highly acidic, containing elevated metal proportions (Ni, Co and Zn in particular). While the study concluded that most of these metals were non-bioavailable, they considered the possibility of these metals being leached into the groundwater system long term. Bioavailable fractions includes water-soluble and exchangeable forms and potentially, oxide-, carbonate- and organic-matter-associated forms; while residual forms are considered non-bioavailable (Pickering, 1986).

This study investigated the chemical speciation of possible contaminants using a four-step selective sequential extraction procedure. The selective sequential extraction procedure was used to leach the metals associated with the (i) water-soluble phase (double distilled water), (ii) exchangeable and carbonate phase (using 1 M ammonium acetate), (iii) Mn oxide- phase (using 0.1 M hydroxylamine hydrochloride) and (iv) Fe oxide- phase (using 0.1 M hydroxylamine hydrochloride).

Overall, double distilled water yielded the highest extractable Zn concentrations, suggesting Zn may be easily mobilized by infiltrating rainwater. 1 M ammonium acetate yielded the highest metal concentrations, removing 3 X Ni, 4 X Cu and nearly 3 X Co, relative to double distilled water. Extractable Zn concentrations were nearly half that yielded for double distilled water. 1 M ammonium acetate targets exchangeable- and pH-sensitive fractions (Tessier et al, 1979). It therefore represents the portion of metals susceptible to changes in the ionic composition of water and changes in pH. This suggests that Ni, Cu, Co and Zn pose a future threat of contamination as sulphide oxidation in the slimes continues overtime, as suggested by Rosner and Schalkwyk (2000). Relative to 1 M ammonium acetate, 0.1 M hydroxylamine hydrochloride yielded nearly 4 X less Co, 7 X less Ni, 4 X less Zn and 10 X less Cu proportions. Relative to 0.1 M hydroxylamine hydrochloride, 0.25 yielded M hydroxylamine hydrochloride approximately 3X Cu, 3X less Co and near identical Zn and Ni proportions. Hydroxylamine hydrochloride (in 0.1 M- and 0.25 M concentrations) targets redox sensitive fractions, suggesting only a minor portion of metals will be leached as a result of drastic changes in redox conditions.

Of the metal-sorbing phases, metals are most intimately associated with Mn oxide, suggesting that this secondary mineral exerts the most significant control on metal retention and transport. Its relatively high crustal abundance and physical/chemical traits explain why Mn is so closely associated with heavy metal concentration. Mn is readily oxidized in surficial environments and typically occurs in association with Fe, Mg, Ni and Co (Hall, 1998). Small metal ions easily substitute for Mn^{4+} in manganese oxides while larger substituted ions occupy tunnel and interlayer areas present in its many different crystalline structures (Hall, 1998). In addition, Mn oxides have characteristically high cation exchange capacity (CEP), further enhanced by

increased surface area (Hall, 1998). The latter, is attributed to the generally fine-grained- and poorly crystalline form of Mn oxides.

5.2 Recommendations for further studies

While selective sequential extraction procedures provide a means of assessing short term metal leachabilty, leach column testing is able to provide an assessment of metal leaching in the long term (McGowen and Basta, 2001). Leach column testing allows the leachate to flow through sampling material under controlled laboratory conditions instead of subjecting the samples to agitation (as in the case of selective extraction). Typically, layers of tailings/slimes material are placed into columns and various leachates added to the top, allowing the leachate to drain through the column, towards the bottom. The contents is then monitored, collected and tested (McGowen and Basta, 2001). Extracting reagents mimic various pH conditions encountered in the environment. Leach testing may prove useful in simulating long term, in situ leaching under controlled, laboratory conditions.

Furthermore, the Witwatersrand Supergroup hosts higher proportions of uranium than gold (Coetzee et al., 2006). As a result, Witwatersrand tailings/slimes often contain high proportions of uranium, including other radioactive constituents such as thorium, radium, polonium and a number of lead isotopes (Coetzee et al., 2006). In addition to metals, acid mine drainage readily transports these toxic, radioactive elements into the groundwater system rendering them potentially unsafe for irrigation and human consumption. An attempt was made to include the analysis of uranium in the sequential extraction procedures. However, the dynamic range of uranium proved difficult to achieve using the GFAAS. The relatively high uranium proportions found in Witwatersrand tailings/slimes and the potentially fatal consequences of contamination, suggest why further studies would benefit from an assessment of uranium migration from mine waste dumps into the environment. Several works have assessed the role of mining in the region's uranium pollution problem (Winde et al., 2004; Winde and Sandham, 2004; Tutu, 2006) but do not address the chemical partitioning of uranium in surrounding soils.

CHAPTER SIX: Conclusion

The city of Randfontein hosts several tailings and slimes storage facilities which pose potential threat to the environment through the generation of acid mine drainage. The sulphuric acid formed, readily scavenges heavy metals in transit, potentially compromising the region's water supply resources and subsequently environmental- and human health. The aim of this study was to understand metal release from the Gold One Millsite Slimes Complex into the Randfontein area, Witwatersrand. To achieve this, the mineralogical- and geochemical factors controlling metal release were assessed using the data provided by Abegunde (2015), including core-log appraisal, x-ray diffraction data and bulk geochemical data and data generated as part of this study (core-log reappraisal, description of trends in x-ray diffraction- and bulk geochemical data, determination of sulphide-sulphur data and selective sequential extraction data).

This study distinguished three major weathering zones, namely an oxidized zone (consisting of upper pale fine sands and lower mottled fine sands), a transition zone (consisting of pale red-brown fine sands) and reduced zone (consisting of grey fine sands). The mineralogy of the slimes dam was determined to consist of mainly quartz and minor pyrophyllite, pyrite, chlinochlore, gypsum and yoshiokaite fractions, and together with petrographic analysis, determined elevated quartz and gypsum fractions dominating the first few centimeters of the oxidized zone. The major element chemistry was dominated by SiO_2. Slimes mineralogy and major element geochemistry were found to correlate well with the mineral and geochemical composition of the gold-bearing conglomerates of the Witwatersrand.

The upper oxidized zone is distinguished form the lower weathering zones by subdued oxide and trace element concentrations. This is attributed to leaching by infiltrating surface waters. Acid base accounting characterized the slimes dam as largely acid generating, hosting only two non-acid generating samples in the upper oxidized zone, out of a total of twenty nine. The distribution patterns of sulphide-sulphur suggest sulphide shows strong potential for metal mobilization, even for fairly immobile metals such as Zn, Pb and Au. The four-step sequential extraction procedure determined that the role of pH (weathering zones) is crucial in metal release. Water-soluble

extractions appeared most efficient in the oxidized zone while Mn- and Fe- selective extractions appeared most efficient in the reduced zone. Under reduced conditions metals are readily adsorbed to the negative surface charges on oxides as a result of surplus OH^-, making metals increasingly available for selective extraction. Under more oxidizing conditions, metals are readily desorbed from the surface of oxides as a result of surplus H^+ and enter the aqueous phase, rendering metals unavailable for selective extraction.

Of the metals extracted, Ni, Cu, Co, Zn yielded the highest concentrations (approximately 11 ppm, 5 ppm, 4 ppm and 3 ppm, respectively) in the water-soluble, exchangeable and carbonate phases, suggesting these pose the largest bioavailable threat to the surrounding environment. Of the metal-adsorbing phases, metals appear most intimately associated with Mn oxide, suggesting Mn as a major control on metal distribution in the slimes dam. Since the results yielded by selective extraction provide an indication of metal leachabilty only for the given period of selective extraction (approximately 90 minutes), future studies would benefit from leach column testing which simulate in situ metal leaching in the laboratory, to provide an indication of long term metal leachabilty in slimes.

LIST OF REFERENCES

A

Abegunde, O.A., (2015). Geological and geochemical assessment of acid mine drainage and heavy metals contamination in the West Rand, Witwatersrand Basin, South Africa. Master's thesis, University of the Western Cape, Cape Town, 182 pp.

Abegunde, O.A, Okujeni, C.D., Wu, C., Siad, A. (2016). Distribution patterns of contaminants in the Mongale Gold tailings dam: a case study from South Africa. Environmental Earth Sciences, 75: 1365.

Acero, P., Ayora, C., Carrera, J. (2007). Coupled thermal, hydraulic and geochemical evolution of pyritic tailings in unsaturated column experiments. Geochimica et Cosmochimica Acta 71 (22), 5325 pp.

Adler R., and Rascher, J. (2007). A Strategy for the Management of Acid Mine Drainage from Gold Mines in Gauteng. CSIR report Number CSIR/NRE/PW/ER/2007/0053/C.Pretoria: CSIR.

Allsopp, H.L., Evans, I.B., Giusti, L., Hallbauer, D.K., Jones, M.Q.W. and Were, H.J. (1986). U-Pb dating and isotopic characterization of carbonaceous components of Witwatersrand reefs. Ext. Abstr., Geocongress '86, Johannesburg, pg. 85-88.

Armstrong, R.A., Compston, W., Retief, E.A., Williams, I.S., Welke, H.J., (1991). Zircon ion microprobe studies bearing on the age and evolution of the Witwatersrand triad. Precambrian Research 53, 243–266.

B

Banks, D. (2004). Geochemical processes controlling minewater pollution. In: G. Prokop, P. Younger, and K.E. Roehl, (Eds). Groundwater management in mining areas. Proceedings of the 2nd IMAGE-TRAIN Advanced Study Course. Vienna, pg. 17–44.

Barona, A., and Romero, F. (1996). Distribution of metals in soils and relationship among fractions by principal component analysis. Journal of Soil Technology. Vol. 8 (4), pg. 303 – 319.

Barton, E.S., Barton, J.M., Jr., Callow, M.J., Allsopp, H.L., Evans, I.B. and Welke, H.J. (1986). Emplacement ages and implications for the source region of granitoid rocks associated with the Witwatersrand Basin: Ext. Abstr. Geocongress, 86, pg. 93-97.

Beach, A., Smith, R. (2007). Structural geometry and development of the Witwatersrand Basin, South Africa. In: Ries, A.C., Butler, R.W.H., Graham, R.H. (Eds.), Deformation of the Continental Crust: The Legacy of Mike Coward: Geological Society, London, Special Publications, 272, pg. 533–542.

Bezuidenhout, N. and Rosseau, P.D.S. (2006). Investigations into the depth and rate of weathering of Witwatersrand gold tailings dam surfaces as key information for long-term ARD risk assessment. In: R.I. Barnhisel (Ed.). 7th International Conference on Acid Rock Drainage. American Society of Mining and Reclamation, pg. 128-140.

Bigham, J.M. and Nordstrom, D.K. (2000). Iron and aluminium hydroxysulfates from acid sulfate waters. In: Alpers, C.N., Jambor, J.L., and Nordstrom, D.K. (Eds) Sulphate minerals: Crystallography, Geochemistry and Environmental Significance. Reviews in Mineralogy and Geochemistry, Vol 40, pg. 351-403.

Blight, G.E. and Caldwell, J.A. (1984). The abatement of pollution from abandoned gold residue dams. Journal of South African Institute of Mining and Metallurgy, 84, pg. 1-9.

Blowes, D.W., and Ptacek, C.J. (1994). Acid-neutralization Mechanisms in Inactive Mine Tailings, In Jambor, J.L. and Blowes, D.W. (Eds). The Environmental Geochemistry of Sulphide

Mine-Wastes. Mineralogical Association of Canada, Short Course Handbook, Vol. 22, pg. 271-292.

Blowes, D. W., Ptacek, C.J., Benner, S. G., Waybrant, K. R., Bain, J. G. (1998). Permeable reactive barriers for the treatment of mine tailings drainage water, Proceedings of the International Conference and Workshop on Uranium Mining and Hydrogeology, Freiberg, Germany, Vol.2, pg. 113-119.

Bosch, D.W. (1987). Retreatment of residues and waste rock. Extraction of Metallurgy Gold South Africa, pg. 707 -743.

Bos, R. and Smilde, A.K. (2014). Principal Component Analysis. Analytical Methods, Vol 6, pg. 2812-2831.

Bouwer, P. N. (2010). Theory of XRF. PANanalytical B.V., Almelo, The Netherlands.

Burke, K., Kidd, W.S.F., Kusky, T.M. (1986). Archean foreland basin tectonics in the Witwatersrand, South Africa. Tectonics 5, pg. 439–456.

C

Caboi, R., Cidu, R., Cristini, A., Fanfani, L., Massoli-Novalli, R., Zuddas, P. (1993). The abandoned Pb-Zn mine of Ingurtosa, Sardinia (Italy). Eng. Geol. 34, pg. 211-218.

Camden-Smith, P.M. (1980). The sedimentology, geochemistry and diagenesis of the West Rand Group sediments in the Heidelberg area, Transvaal, MSc Thesis, University of Cape Town, 380 pp.

Carlsson, E., Thunberg, J., Ohlander, B., Holmstrom, H. (2002). Sequential extraction of sulfide-rich tailings remediated by the application of till cover, Kristineberg mine, northern Sweden. The Science of the Total Environment 299 (1–3), pg. 207–226.

Chao, T.T. (1972). Selective dissolution of manganese oxides from soils and sediments with acidified hydroxylamine hydrochloride. Soil Science Society of America, 36, pg. 764–768.

Cheney, E.S. (1995). Plate tectonic significance of supersequences in the 2.7 to 2.1 Ga Transvaal succession of the Kaapvaal Province of Africa. Ext. Abstr. Geocongress '95. Geol. Soc. S. Afr., Johannesburg, pg. 867-870.

Clarke, L. (1996). Coal mining and water quality. Journal of Mines Metals and Fuels 44, pg. 181–183.

Clendenin, C.W., Charlesworth, E.G., Maske, S. (1988). An early Proterozoic three stage rift system, Kaapvaal Craton, South Africa. Tectonophysics 145, pg. 73–86.

Clevenger, T.E. (1990). Use of sequential extraction to evaluate the heavy metals in mining wastes. Water, Air and Soil Pollution 50, pg. 241-254.

Coetzee, H., Winde, F., Wade, P.W. (2006). An assessment of sources, pathways, mechanisms and risks of current and potential future pollution of water and sediments in gold-mining areas of the Wonderfonteinspruit catchment. Report No. 1214/06. Water Research Commission, Pretoria.

Coward, M.P., Spencer, R.M., Spencer, C.E. (1995). Development of the Witwatersrand Basin, South Africa. In: Coward, M.P., Ries, A.C. (Eds.), Early Precambrian Processes: Geological Society, London, Special Publications, 95, pg. 243–269.

Crow, C., Condie, K.C. (1988). Geochemistry and origin of Late Archaean volcanics from the Ventersdorp Supergroup, South Africa. Precambrian Research 42, pg. 19–37.

D

Dankert, B.T., Hein, K.A.A. (2010). Evaluating the structural character and tectonic history of the Witwatersrand Basin. Precambrian Research 177, pg. 1–22.

De la Winter, H. R. (1987). A cratonic foreland model for Witwatersrand Basin development in a continental back-arc plate tectonic setting. S. Afr. J. Geol., 90, pg. 409-427.

De Wit, M.J., De Ronde, C.E.J., Tredoux, M., Roering, C., Hart, R.J., Armstrong, R.A., Green, R.W.E., Peberdy, E., Hart, R.A. (1992). Formation of an Archaean continent. Nature 357, pg. 553–562.

Dold, B. (1999). Mineralogical and geochemical changes of copper flotation tailings in relation to their original composition and climatic settings – implications for acid mine drainage and element mobility. PhD thesis. Terre and Environment, University of Geneva, Geneva, 230 pp.

Dold, B. (2001a). A 7-step sequential extraction for geochemical studies of copper sulphide mine waste, securing the future. International Conference of Mining and the Environment. Skelleftea, Sweden, pg. 158-170.

Dold, B. (2001b). Dissolution kinetics of schwertmannite and ferrihydrate, securing the future. International Conference of Mining and the Environment. Skelleftea, Sweden, pg. 171-181.

Dold, B. (2003). Speciation of the most soluble phases in a sequential extraction procedure adapted for geochemical studies of copper sulphide mine waste. Journal of Geochemical Exploration 80, pg. 55 – 68.

Dold, B. (2005). Basic concepts of environmental geochemistry of sulfide mine-waste. Mineralogía, geoquímica y geomicrobiología para el manejo ambiental de desechos mineros.XXIV Curso Latinoamericano de Metalogenia, vol. 22, pg. 1-36.

Dold, B., Fontbote´, L. (2001). Element cycling and secondary mineralogy in porphyry copper tailings as a function of climate, primary mineralogy and mineral processing. Special Issue: geochemical studies of mining and the environment. Journal of Geochemical Exploration 74 (1–3), pg. 3– 55.

Dold, B., Fontbote´, L. (2002). A mineralogical and geochemical study of element mobility in sulfide mine tailings of the Fe oxide Cu–Au deposits from the Punta del Cobre district, northern Chile. Chemical Geology 189, pg. 135–163.

Duncan, A.R., Marsh, J.S. (2007). The Karoo Igneous Province. In: Johnson, M.R., Anhaeusser, C.R., Thomas, R.J. (Eds.), The Geology of South Africa. Geological Society of South Africa/Council for Geoscience, Johannesburg, Pretoria, pg. 501–520.

E

Eby, G.N. (2004). Acid mine drainage, In Dodson, K. (Ed.): Principles of Environmental Geochemistry. Brookes/Cole, pg. 352-358.

El-Demerdashe, S., Dahdoh, M.S.A., Hassan, F.A. (1995). Sequential extraction of nine trace elements from sludge amended soils. Fertilizer Res. 41, pg. 77-85.

Eriksson, K.A., Turner, B.R., Vos, R.G. (1979). Evidence of tidal processes from the lower part of the Witwatersrand Supergroup, South Africa. Irf. Circ. Econ. Geol. Res. Unit, Univ. Witwatersrand, Johannesburg, 140, 9 pp.

Eriksson, P.G., Hattingh, P.J., Altermann,W. (1995). An overviewof the geology of the Transvaal Sequence and Bushveld Complex, South Africa.Mineralium Deposita 30, pg. 98–111.

Eriksson, P.G., Altermann, W., Hartzer, F.J. (2007). The Transvaal Supergroup and its precursors. In: Johnson, M.R., Anhaeusser, C.R., Thomas, R.J. (Eds.), The Geology of South Africa. Geological Society of South Africa, Johannesburg/Council for Geoscience, Pretoria, pg. 237–260.

Evans, K.A., Banwart, S.A. (2006). Rate controls on the chemical weathering of natural polymineralic material. I. Dissolution behaviour of polymineralic assemblages determined using batch and unsaturated column experiments. Applied Geochemistry, 21 (2), 352 pp.

F

Fanfani, L., Zuddas, P., Chessa, A. (1997). Heavy metals speciation analysis as a tool for studying mine tailings weathering. J. Geochem. Explor 58, pg. 241-248.

Favas, P.J., Pratas, J. Gomes, M.E.P., Cala, V. (2011). Sequential chemical extraction of heavy metals in tailings and soils contaminated by mining activity: Environmental implications. Journal of Geochemical Exploration 111, pg. 160 – 171.

Feather, C. E. and Koen, G.M. (1976). The mineralogy of the Witwatersrand Reefs. Miner. Sci. Eng., pg. 187-224.

Fernández-Caliani, J.C, Barba-Brioso, C., González, I., Galan, E. (2009). Heavy Metal Pollution in Soils Around the Abandoned Mine Sites of the Iberian Pyrite Belt (Southwest Spain). Water, Air and Soil Pollution. Vol. 200 (1-4), pg. 211 – 226.

Filipek, L.H., Hatton, C., Gusek, J., Tsukamoto, T. (2003). Passive treatment of acid rock drainage (ARD): state of the practice. In: Proceedings of the Tenth International Conference on Tailings and Mine Waste, October, 2003, Colorado, USA, pg. 293–303.

Fitch, F.J., Miller, J.A. (1984). Dating Karoo igneous rocks by the conventional K-Ar 40Ar/39Ar age spectrum methods. In: Erlank, A.J. (Ed.), Petrogenesis of the Volcanic Rocks of the Karoo Province. Geological Society of South Africa Special Publication, pg. 247–266.

FitzPatrick, E.A. (1984). Principles of thin section preparation. In FitzPatrick, E.A., (Ed.) Micromorphology of soils. Springer Netherlands. pg. 1 – 5.

Fonseca, E. and Martin, H. (1986). The selective extraction of Pb and Zn in selected mineral and soil samples, application in geochemical exploration (Portugal). J. Geochem. Explor., 26, pg. 231-248.

Förstner U., Wittmann G.T.W. (1976). Metal accumulation in acidic waters from gold mines in South Africa. Geoforum, 7, pg. 44-49.

Frimmel, H.E. (2005). Archaean atmospheric evolution evidence from the Witwatersrand gold fields, South Africa. Earth-Science Reviews 70, pg. 1–46.

Fyson, A., Kalin, M., Adrian, L.W. (1994). Arsenic and nickel removal by wetland sediments. In: Proceedings of the International Land Reclamation and Mine Drainage Conference and Third International Conference on the Abatement of Acidic Drainage, vol. 1. Pittsburgh, PA, pg. 109–118.

G

Gallez, A., Juo, A.S.R., Herbillon, A.J. (1976). Surface and charge characteristics of selected soils in the tropics. Soil Science Society American Journal. Vol. 40, pg. 601-608.

Gatehouse, S., Russel, D.W. and van Moort, J.C. (1977). Sequential soil analyses in exploration geochemistry. J. Geochem. Explor., 8, pg. 483-494.

Giusti, L, Hallbauer, D.K., Allsopp, H.L., Evans, I.B. and Welke, H.J. (1986). Dating and isotopic characterization of components of Witwatersrand conglomerates and possible source rocks. Ext. Abstr. Geocongress' 86. Geol. Soc. S. Afr., Johannesburg, pg. 123-127.

Giusti, L. (1988). U-Pb isotopic data for sulfides of the Varkenskraal granite (Western Transvaal, South Africa) and their bearing on the age and origin of uranium mineralization in the Witwatersrand basin. Chem. Geol., 72, pg. 311-328.

Gibson, M.A.S., Jolley, S.J., Barnicoat, A.C. (2000). Interpretation of the Western Ultra Deep Levels 3D seismic survey. The Leading Edge 19, pg. 730–735.

Gibson, M.A.S. (2004). Goldfields KEA 3D Seismic Project: Final Report. Unpublished report to Gold Fields Mining, 52 pp.

Goodwin, A.M. (1996). Principles of Precambrian Geology: The Dynamic Evolution of the Continental Crust, Academic Press, 327 pp.

Greenland, D.J. and Mott, J.B. (1978). Surfaces of soil particles. In (Eds.) D.J. Greenland and M.H.B. Hayes): The Chemistry of Soil Constituents. John Wiley & Sons. New York, pg. 321-354.

Groves, J.E., (1974). Reclamation of mining degraded land. South African Journal of Science, 70, pg. 296-29.

H

Hall, G.E.M. (1998). Analytical perspective on trace element species of interest in exploration. Journal of Geochemical Exploration, 61, pg. 1–19.

Hallbauer, D.K. (1986). The mineralogy and geochemistry of Witwatersrand pyrite, gold, uranium and carbonaceous matter. In: C.R. Anhaeusser and S. Maske (Eds), Mineral Deposits of southern Africa, I. GeoL Soc. S. Afr., pg. 731-752,

Hammarstrom, J.M., Seal, R.R., Meier, A.L., Kornfeld, J.M. (2005). Secondary sulfate minerals associated with acid drainage in the eastern US: recycling of metals and acidity in surficial environments. Chemical Geology 215 (1–4), pg. 407–431.

He, Z.L., Yang, X.E, Stoffellab, P.J. (2005). Trace elements in agroecosystems and impacts on the environment. Review. J. Trace Elem. Med. Biol. 19, pg. 125-140.

Heikkinen, P.M. (2009). Active sulphide mine tailings impoundments as sources of contaminated drainage: controlling factors, methods of characterization and geochemical constraints for mitigation. Geological Survey of Finland. Espoo, 38 pp.

Heikkinen, P.M., Räisänen, M.L., Johnson, R.H. (2009). Geochemical Characterization of Seepage and Drainage Water Quality from Two Sulphide Mine Tailings Impoundments: Acid Mine Drainage versus Neutral Mine Drainage. Mine Water and the Environment. Vol. 28 (1), pg. 30 – 49.

Hoffmann, E., Ludke, C., Stephanowitz, H. (1996). Application of laser-ICP-MS in environmental analysis, Fresinius Journal of Analytical Chemistry, 355, pg. 900-903.

Huang, X., Cao, G. (2016). Hydrogeochemical signatures and evolution of groundwater impacted by Bayan Obo tailing pond in northwest China. Science of the Total Environment. Vol. 543 (A), pg. 357 – 372.

I

Ibanez, J.G., Hernandez-Esparza, M., Doria-Serrano, C., Signh, M.M. (2008). The point of zero charge. Environmental Chemistry, pg. 70-78.

Iliso (Consulting Ltd.). (2008). Wonderfonteinspruit catchment area remediation plan. Report to Department of Water Affairs and Forestry and National Nuclear Regulator, 1st draft.

INAP (The International Network for Acid Prevention). (2009). GARD (Global Acid Rock Drainage) Guide, http://gardguide.com/index, accessed August 2017.

J

Jaeckel, P., Kroner, A., Wendt, I.J., Brandl, G. and Todt, W. (1995). The Limpopo Belt, South Africa: new evidence from zircon ages for extended late Archaean to early Proterozoic evolution. TerraAbstr., EUG8, Strassbourg, 102 pp.

Jambor, J. L. and Blowes, D. W. (1998). Theory and applications of mineralogy in environmental studies of sulfide-bearing mine waste. In: Cabri, L. J. and Vaughan, D. J. (eds.): Short Course Handbook on Ore and Environmental Mineralogy. Mineralogical Association of Canada, Nepean, Vol. 27, pg. 367-401.
James, A.L. (1966). Stabilizing mine dumps with vegetation. Endevour, 25, pg. 154-157.

Jolley, S.J., Freeman, S.R., Barnicoat, A.C., Phillips, G.M., Knipe, R.J., Pather, A., Fox, N.P.C., Strydom, D., Birch,M.T.G., Henderson, I.H.C., Rowland, T.W. (2004). Structural controls on Witwatersrand gold mineralisation. Journal of Structural Geology 26, pg. 1026–1086.

Jolley, S.J., Stuart, G.W., Freeman, S.R., Knipe, R.J., Kershaw, D.,McAllister, E., Barnicoat, A.C., Tucker, R.F. (2007). Progressive deformation of a Late Orogenic Thrust System, from duplex development to extensional reactivation and disruption: Witwatersrand Basin, South Africa. Geological Society, London, Special Publications, 272, pg. 543–569.

K

Kennedy, C.B., Day, S.J., Anglin,C.D. (2016). Geochemistry of Tailings from the Mount Polley Mine, British Columbia. Proceedings Tailings and Mine Waste 2016, pg. 857 - 868.

Killick, A.M. (1992). Pseudotachylites of the West Rand Goldfield, Witwatersrand Basin, South Africa. PhD Thesis, Rand Afrikaans University, Johannesburg, 273 pp.

Kleinmann, R. L. P., Crerar, D. A. & Pacelli, R. R. (1981). Biogeochemistry of Acid Mine Drainage and a Method to Control Acid Formation. Mining Engineering, March 1981, pg. 300–305.

Kleinman, R.L.P. (1990). Acid mine drainage, US bureau of mines researches and develops: control methods for both coal and metal mines. Environmental Science and Technology 24 (9), pg. 1278–1285.

Kositcin, N., Krapež, B. (2004). Relationship between detrital zircon age-spectra and the tectonic evolution of the Late Archaean Witwatersrand Basin, South Africa. Precambrian Research 129, pg.141–168.

Krapež, B. (1985). The Ventersdorp Contact placer: a gold–pyrite placer of stream and debris-flow origins from the Archaean Witwatersrand Basin of South Africa. Sedimentology 32, pg. 223–234.

Kuyucak, N. (2002). Acid mine drainage prevention and control options. CIM Bulletin 95 (1060), pg. 96–102.

L

Lawrence, R. (1990). Prediction of the Behavior of Mining and Processing Wastes in the Environment. In Doyle, F. (Ed) Proc. Western Regional Symposium on Mining and Mineral Processing Wastes. Edited by Fiona Doyle, Published by the Society for Mining, Metallurgy, and Exploration, Inc., Littleton, CO.

Layer, P.A., Kr6ner, A. McWilliams, M. and Clauer, N. (1988). Regional magnetic overprinting of Witwatersrand Supergroup sediments, South Africa. J. Geophysical Res., 93, pg. 2191-2200.

Leinz, R.W., Sutley, S.J., and Briggs, P.H. (1999). The use of sequential extractions for the chemical speciation of mine wastes, in Tailings and Mine Waste '99 - Proceedings of the Sixth International Conference on Tailings and Mine Waste, Fort Collins, Colorado, January 24-27, 1999: Rotterdam, A.A. Balkema, pg. 555-561.

Leinz, R.W., Sutley, S.J., Desborough, G.A., and Briggs, P.H. (2000), An investigation of the partitioning of metals in mine wastes using sequential extractions, in ICARD 2000: Proceedings from the Fifth International Conference on Acid Rock Drainage, Denver, Colorado, May 21-24, 2000: Society for Mining, Metallurgy, and Exploration, Inc., pg. 1489-1499.

Liebenberg, W.R. (1955). The occurrence and origin of gold and radioactive minerals in the Witwatersrand System, the Dominion Reef, the Ventersdorp Contact Reef and the Black Reef. Trans. Geol. S. Aft., 58, pg. 101-227.

Liebenberg, W.R.A. (1957). A mineralogical approach to the development of uranium extraction processes practiced on the Witwatersrand. J. S. Afr. Inst. Min. Metall., vol 57 (4), pg. 153 – 208.

Lottermoser, B.G. (2013). Mine wastes Characterization, Treatment and Environmental Impacts. Springer-Verlag Berlin Heidelberg, 271 pp.

Lu, J., Alakangas, L., Wanhainen, C. (2014). Metal mobilization under alkaline conditions in ash-covered tailings. Journal of Environmental Management. 139, pg. 38 – 49.

M

Manzi, M.S.D., Hein, K.A.A, King, N., Durrheim, R. (2013). Neoarchaean tectonic history of the Witwatersrand Basin and Ventersdorp Supergrou: New constraints from high-resolution 3D seismic reflection data. Tectonophysics 590, pg. 94-105.

Marsden, D.D. (1986). The current limited impact of Witwatersrand gold mine residues on water pollution in the Vaal River system. Journal of the South African Institute of Mining and Metallurgy 86, pg. 481–504.

McCarthy, T.S. (2011). The impact of acid mine drainage in South Africa. South African Journal of Science. 107 (5/6), Art #712. Doi:10.4102/sajs.v10715/6.712, 7 pp.

McGowen, S.L., and Basta, N.T. (2001) Heavy metal solubility and transport in soil contaminated by mining and smelting. Heavy metals release in soils. In: Selim, H.M., and Sparks, D.L. (Eds.) Heavy metals release in soils. Lewis Publishers, CRC Press LLC. pg. 89 – 108.

McGrath, S.P., Cegarra, J. (1992). Chemical extractability of heavy metals during and after long-term applications of sewage sludge to soil. J. Soil Sci. 43, pg. 313-321.

McGregor, R.G., Blowes, D.W., Robertson, W.D. (1995). The application of chemical extractions to sulphide tailings at the Copper Cliff tailings area, Sudbury, Ontario. Sudbury '95 Proceedings 3, pg.1133– 1142.

Mellor, E.T. (1911). Some structural features of the Witwatersrand System on the Central Rand, with a note on the Rietfontein Series. Transactions of the Geological Society of South Africa 14, pg. 24–41.

Mellor, E.T. (1913). Structural features of the western Witwatersrand. Transactions of the Geological Society of South Africa 16, pg. 1–32.

Mellor, E.T. (1917b). The Geology of the Witwatersrand. An Explanation of the Geological Map of the Witwatersrand Goldfield. Special Publication, Pretoria, 46 pp.

Mellor, E.T. (1921). The Geology of the Country Surrounding Johannesburg. Special Publication, Pretoria, 41 pp.

Minter, W.E. L. and Loen,J.S. (1991). Palaeocurrent dispersal patterns of Witwatersrand gold placers: In S. Afr. J. Geol. v94, pg. 70-85.

Minter, W.E.L., Goedhart, M., Knight, J. and. Frimmel, H.E. (1993). Morphology of Witwatersrand gold grains from the Basal Reef: evidence for their detrital origin. Econ. Geol., 88, pg. 237-248.

Molden, D. and Merrey, D. (2002). Managing Water from Farmers' Fields to River Basins: Implications of Scale. In: Turton, A. and Henwood, A. Hydropolitics (Eds.) in the Developing World. A Southern African Perspective. Pretoria: AWIRU, University of Pretoria.

Moses, C. O., Nordstrom, D. K., Herman, J. S. and Mills, A. L. (1987). Aqueous pyrite oxidation by dissolved oxygen and by ferric iron. Geochimica et Cosmocimica Acta, Vol. 51, pg. 1561-1571.

Mphephu, N.F. and Viljoen, M.J. (2002). Rehabilitation and cleaning of abandoned mining sites: the case of the Central Rand Goldfield, Johannesburg, South Africa. Proceedings of the conference on environmental management in Southern Africa. Johannesburg, South Africa, 27 - 30 August 2002. CD.

Myers, R.E., McCarthy, T.S., Stanistreet, I.G. (1989). A tectono-sedimentary reconstruction of the development of the Witwatersrand Basin, with particular emphasis on the Central Rand Group. Economic Geology Research Unit Information Circular, No. 216, pg. 497–540.

Myers, R.E., McCarthy, T.S., Stanistreet, I.G. (1990b). A tectono-sedimentary reconstruction of the development and evolution of the Witwatersrand Basin, with particular emphasis on the Central Rand Group. South African Journal of Geology 93, pg. 180–201.

N

Naicker, K., Cukrowska, E., McCarth, T.S. (2003). Acid mine drainage arising from gold mining activity in Johannesburg, South Africa and environs. Environmental Pollution 122, pg. 29 – 40.

Nengovhela, A.C., Yibas, B., Ogola, J.S. (2006). Characterization of gold tailings dams of the Witwatersrand Basin with reference to their acid mine drainage potential.Water SA vol. 32 (4), pg. 499 – 506.

Nordstrom, D. K., Jenne, E. A. and Ball, J. W. (1979). Redox equilibria of iron in acid mine waters. In: Jenne, E.A. (Ed.): Chemical modeling in aqueous systems. Am. Chem. Soc. Symp. Washington, D.C., Series 93, pg. 51-79.

Nordstrom, D. K. (1982). Aqueous Pyrite Oxidation and the Consequent Formation of Secondary Iron Minerals. In: Kittrick, J. A., Fanning, D. S., Hossner, L. R., Kral, D. M. & Hawkins, S. (Eds) Acid sulfate weathering, proceedings of a symposium. Soil Science Society of America, Special Publication 10, pg. 37–56.

Nordstrom, D.K., and Alpers, C.N. (1999). Geochemistry of acid mine waters. In G.S. Plumlee and M.J. Logson, (Eds). The environmental geochemistry of mineral deposits. Reviews in Economic Geology, Vol 6A. Littleton: Society of Economic Geologists, pg. 133-160.

P

Pegg, C.W. (1950). A contribution to the geology of the West Rand Area. Transactions of the Geological Society of South Africa 53, pg. 209–227.

Phillips, G.N. (1987). Metamorphism of the Witwatersrand goldfields: conditions during peak metamorphism. J. Metamor. Geol., 5, pg. 307-322.

Phillips, G.N., Myers, R.E. (1989). Witwatersrand goldfields: Part II: an origin for Witwatersrand gold during metamorphism and associated alteration. Economic Geology Monograph 6, pg. 598–608.

Pickering, W.F. (1986). Metal ion speciation – soils and sediments (a review). Ore. Geol. Rev. 1, pg. 83-146.

Plumlee, G. S. (1999). The Environmental Geology of Mineral Deposits. In: Plumlee, G. S. & Logsdon, M. J. (Eds), The Environmental Geochemistry of Mineral Deposits. Part A: Processes, Techniques, and Health Issues. Reviews in Economic Geology, Vol. 6A, pg. 71–116.

Pope, J., Weber, P., Mackenzie, A., Newman, N. and Rait, R. (2010). Correlation of acid base accounting characteristics with the Geology of commonly mined coal measures, West Coast and Southland, New Zealand, New Zealand Journal of Geology and Geophysics, 53: 2, pg. 153 — 166.

Poujol, M., Robb, L.J., Anhaeusser, C.R., Gericke, B., (2003). A review of the geochronological constraints on the evolution of the Kaapvaal Craton, South Africa. Precambrian Research 127, 181–213.

Poulsen, J. and French, A. (2004). Discriminant Function Analysis (DA*).* San Francisco State University, Available at: http://userwww.sfsu.edu/efc/classes/bio710/discrim/discrim.pdf (Accessed September 2016)

Pretorius, D.A. (1974). The nature of the Witwatersrand gold-uranium deposits. In: Wolf, K.H. (Ed.), Handbook of Strata-bound and Stratiform Ore Deposits. II. Regional Studies and Specific Deposits. Elsevier, Amsterdam, pg. 29–88.

Pretorius, D.A. (1976). The nature of Witwatersrand gold-uranium deposits: In Wolf, K.H. , (Ed.), Handbook of Stratabound and stratiform ore deposits, Vol. 7, Elsevier Publishing Co., Amsterdam, pg. 29-88 pg.

Pretorius D A. (1991) - The sources of Witwatersrand gold and uranium: A continued difference of opinion (extracts): *in Econ Geol.* Monograph 8 pg. 139-145.

Pretorius, D.A., Brink, W.C.J., Fouche, J. (1986). Geological map of the Witwatersrand Basin. In: Anhaeusser, C.R., Maske, S. (Eds.), Mineral Deposits of Southern Africa, vol. I. Geological Society of South Africa, Johannesburg.

Price, W. A. (1997). Draft Guidelines and Recommended Methods for the Prediction of Metal Leaching and Acid Rock Drainage at Minesites in British Columbia. Reclamation Section, Energy and Minerals Division; British Columbia Ministry of Employment and Investment. Pages

at http://www.mndm.gov.on.ca/mines/mg/leg/BC%201997%20Draft%20Guideline.pdf. Accessed October 2016, 159 pp.

Price, W. (2009). Prediction Manual for Drainage Chemistry from Sulphidic Geological Materials. MEND Report 1.20. 1, Natural Resources Canada.

R

Ramdohr, P. (1955). Neue Beobachtungen an Erzen des Witwatersrandes in Siidafrika and ihre geoetische Bedeatung. Abh. Dtsch. Akad. Wiss. Berlin, Kl. Chem. Biol., 5, pg. 160-163

Ribet, I., Ptacek, C.J., Blowes, D.W., Jambor, J.L. (1995). The potential for metal release by reductive dissolution of weathered mine tailings. Journal of Contaminant Hydrology 17 (3), pg. 239 – 273.

Robb, L.J., Meyer, F.M., Ferraz, M.F. and Drennan, G.R. (1990a). The distribution of radioelements in Archaean granites of the Kaapvaal Craton, with implications for the force of uranium in the Witwatersrand Basin. S. Afr. J. Geol., 93 (1), pg. 5--40.

Robb, L.J., Davis, D.W. and Kamo, S.L. (1990b). U-Pb ages on single detrital zircon grains from the Witwatersrand Basin, South Africa: constraints on the age of sedimentation and on the evolution of granites adjacent to the basin. J. Geol., 98, pg. 311-328.

Robb, L.J., Davis, D.W., Kamo, S.L. (1991). Chronological framework for the Witwatersrand basin and environs: towards a time-constrained depositional model. South African Journal of Geology 94, pg. 86–95.

Robb, L.J., Landais, P., Meyer, F.M. and Davis, D.W. (1994). Nodular hydrocarbons in granites: implications for the origim of kerogen in the Witwatersrand Basin, South Africa. Explor. Min. Geol., 3, pg. 219-230.

Robb, L.J., Meyer, F.M. (1994). Geological environment and mineralization processes during the formation of the Witwatersrand Au-U deposits: *in* XVth CMMI Congress, Johannesburg, *SAIMM*, v3, pg. 3-18.

Robb, L.J., and Meyer, F.M. (1995). The Witwatersrand Basin, South Africa: Geological framework and mineralization processes. Ore Geology Reviews 10, pg. 67 – 94.

Robb, L.J., Robb, V.M. (1998). Gold in the Witwatersrand basin. In: Wilson, M.G.C., Anhaeusser, C.R. (Eds.), The Mineral Resources of South Africa. : Handbook, 16. Council for Geoscience, Pretoria, pg. 294–349.

Roering, C. (1968). The Tectonics of the West Rand Syncline—A Field Study of Brittle Failure in the Witwatersrand Basin, Information Circular. Economic Geology Research Unit, University of the Witwatersrand, Johannesburg, South Africa, pp. 28.

Rosner, T., van Schalkwyk, A. (2000). The environmental impact of gold mine tailings footprints in the Johannesburg region, South Africa. Bull. Eng. Geol. Env., v59, pg. 137–148.

Rösner, T., Boer, R., Reyneke, R., Aucamp, P., Vermaak, J. (2001). A preliminary assessment of pollution contained in the unsaturated and saturated zone beneath reclaimed gold – Mine residue deposits. WRC report No. 797/1/01.

Rundle, C.C., and Snelling, N.J. (1977). The geochronology of uraniferous minerals in the Witwatersrand triad; an interpretation of new U-Pb data on rock and minerals from the Dominion Reef, Witwatersrand and the Ventersdorp Supergroups, Philos. Trans. R. Soc. London. A286, pg. 567-583.

S

SACS, South African Committee for Stratigraphy. (1980). Stratigraphy of South Africa. Part 1: Lithostratigraphy of the Republic of South Africa. South West Africa/Namibia and the Republics

of Bophuthatswana, Transkei and Venda, Geological Survey of South Africa Handbook, Pretoria, 8, 690 pp.

Sami, K., and Druczinski, A.L. (2003). Predicted spatial distribution of naturally occurring arsenic, selenium and uranium in groundwater in South Africa – reconnaissance survey. Water Research Commission, Pretoria, WRC report no. 1236/1/03, 84 pp.

Scheinost, A.C., Kretzschmar, R., Pfister, S., Roberts, D.R. (2002). Combining Selective Sequential Extractions, X-ray Absorption Spectroscopy, and Principal Component Analysis for Quantitative Zinc Speciation in Soil. Journal of Environmental Science and Technology. 36 (23), pg. 5021 – 5028.

Schidlowski, M. (1981). Uraniferous constituents of the Witwatersrand conglomerates: Ore-microscopic observations and implications for the Witwatersrand metallogeny. U.S. Geol. Surv., Prof. Pap., 1161-N, 23 pp.

Schlemmer, G. and Radzuik, B. (1999). Analytical Graphite Furnace Atomic Absorption Spectrometry: A Laboratory Guide. Birkhauer, 291 pp.

Singer, P. C. and Stumm W. (1970). Acid mine drainage: rate determining step, *Science* 167, pg.1121-1123.

Smits, G. (1984). Mineral modifications observed in uranium-bearing reefs of the Witwatersrand, South Africa: in S. Afr. J. Geol. v87, pg. 245-256.

Smuda, J., Dold, B., Friese, K., Morgenstern, P., Glaesser, W. (2007). Mineralogical and geochemical study of element mobility at the sulfide-rich Excelsior waste rock dump from the polymetallic Zn–Pb–(Ag–Bi–Cu) deposit, Cerro de Pasco, Peru. Journal of Geochemical Exploration 92 (2–3), pg. 97–110.

Smuda, J.; Dold, B.; Spangenberg, J.E.; Friese, K.; Kobek, M.R.; Bustos, C.A.; Pfeifer, H.-R. (2014). Element cycling during the transition from alkaline to acidic environment in an active porphyry copper tailings impoundment, Chuquicamata, Chile. J. Geochem. Explor.,140, pg. 23–40.

Sondag, F. (1981). Selective extraction procedures applied to geochemical prospecting in an area of old mine workings. J. Geochem. Explor 15, pg. 645-652.

Späth, H. (1980). Hierachical cluster algorithms. In Horwood, E. (Ed): Cluster analysis algorithms for data reduction and classification of objects. New York, Halsted Press, 226 pp.

Stanistreet, I.G., McCarthy, T.S. (1991). Changing tectonosedimentary. Scenarios relevant to the development of the Late Archaean Witwatersrand Basin. Journal of African Earth Sciences 13, pg. 65–81.

Stanley, G.G. (1987). The Extraction Metallurgy of Gold In south Africa, The South African Institute of Mining and Metallurgy Monograph Series M7, The Chamber of Mines South Africa, Vol. 1 & 2.

T

Tessier, A., Campbell, P.G.C. and Bisson, M. (1979). Sequential extraction procedure for the speciation of particulate trace metals. Anal. Chem., 51, pg. 645 – 652.

TMH1. (1986), Standard Methods of Testing Road Construction Materials - Technical Methods for Highways TMH1, National Institute for Transport and Road Research of the Council for Scientific and Industrial Research (CSIR), Second edition.

Toens, P.D., Griffith, G.H. (1964). The geology of the West Rand. In: Haughton, S.H. (Ed.), The Geology of Some Ore Deposits in Southern Africa. Geological Society of South Africa, Johannesburg, pg. 283–322.

Truswell, J.F. (1977). The geological evolution of South Africa. Purnel, Cape Town, 218 pp.

Tutu, H. (2006). Determination and Geochemical Modeling of the Dispersal of Uranium in gold-Mine Polluted Land on the Witwatersrand. PhD Thesis, University Witwatersrand, Johannesburg.

U

USEPA. (2009). Integrated Science Assessment (ISA) for Particulate Matter (Final Report, Dec, 2009). U.S. Environmental. Protection Agency, Washington, DC, EPA/6000/R-08/139F.

V

Van De Venter, P.W. (2002) Rehabilitation of tailings dams: Rock-cladding in perspective. At: http://www.envirogreen.co.za/rock.htm. 2002/09/10.

Van der Westhuizen, W.A., De Bruiyn, H., Meintjes, P.G. (1991). The Ventersdorp Supergroup: an overview. Journal of African Earth Sciences 13, pg. 83–105.

Van Niekerk, C.B., and Burger, A.J. (1964). The age of the Ventersdorp system, South African Geol. Surv. Annals. 3, pg. 75-86.

Van Zyl, A., Mostert, M., Dixon, R. (2013). Gold One International technical assessment and valuation report. SRK consulting (South Africa) Pty Ltd.

Vermaakt, D.T., Chunnett, I.E. (1994). Tectono-sedimentary processes which controlled the deposition of the Ventersdorp Contact Reef within the West Wits Line. In: XVth CMMI Congress, SAIMM, Johannesburg, pg. 117–130.

Vos, R.G. (1975). An alluvial plain and lacustrine model for the Precambrian Witwatersrand deposits of South Africa. Journal of Sedimentary Petrology 45, pg. 480–493W**W**

W

Wallmach, T. and Meyer, F.M. (1990). A petrogenetic grid for metamorphosed alumineous Witwatersrand shales. S. Aft. J. Geol., 93, pg. 93-102.

Wallmach, T., Meyer, F.M., Schweitzer, J.K. and Henkel, J. (1990). The stability of chloritoid, andalusite and pyrophyllite during very low grade metamorphism in metasediments of the Witwatersrand. Ext. Abstr. Geocongress '90, UCT, Cape Town.

Walraven, F., Armstrong, R.A., Kruger, F.J. (1990). A chronostratigraphic framework for the north-central Kaapvaal craton, the Bushveld Complex and the Vredefort structure. Tectonophysics 171, pg. 23–48.

Weber, P.A., Thomas, J.E., Skinner, W.N., Smart, R.S.C. (2005). A methodology to determine the acid-neutralization capacity of rock samples. The Canadian Mineralogist 43, pg. 1183-1192.

White, W. W. III, Lapakko, K. A. & Cox, R. L. 1999. Static-test Methods most commonly used to Predict Acid Mine Drainage: Practical Guidelines for Use and Interpretation. In: Plumlee, G.S. & Logsdon, M. (Eds) The Environmental Geochemistry of Mineral Deposits. Part A: Processes, Techniques, and Health Issues. Reviews in Economic Geology, Vol. 6A, pg. 325–338.

Winde, F., Sandham, L.A. (2004). Uranium pollution of South African streams – an overview of the situation in gold mining areas of the Witwatersrand. Geo Journal 61, pg. 131-149.

Winde, F., Wade, P., van der Walt, I.J. (2004). Gold tailings as a source of water-borne uranium contamination of streams – the Koekemoerspruit (South Africa) as a case study. Water SA 30, pg. 219–239.

WRDM (West Rand District Municipality) Spatial Framework. (2014). At: http://www.wrdm.gov.za. pp. 134.

Y

Yaldwyn, R. Maake, L., Roode, C. Smithen, A., Shepherd, P., van Zyl, A. (2013). Gold One Cooke Surface operations, Gauteng, South Africa, Independent Technical Report. SRK Consulting (South Africa) (Pty) Ltd.

Yangou, T., Shijun, N., Xianguo, T., Chengjiang, Z., Yuxiao, M. (2002). Geochemical baseline and trace metal pollution of soil in Panzhihua mining area. Chinese Journal of Geochemistry. Vol. 21 (3), pg. 274 – 281.

Younger, P.L., Banwart, S.A. and Hedin, R.N., (2002). Mine water: hydrology, pollution, remediation. Dordrecht: Kluwer Academic, 464 pp.

Z

Zachmann, D.W., Block, R. (1994). Studies of the availability of toxic heavy elements in soils and sediments in the vicinity of a lead smelting site (Germany). Water, Air and Soil Pollution 78, pg. 317-334.

Zhao, B., Meyer, F.M., Robb, L.J., Toulkeridis, T., Zwingmann, H. and Clauer, N. (1995). Thermal history of gold mineralization in the Ventersdorp Contact Reef, Witwatersrand Basin, South Africa. Abstr., EUG8, Strasbourg, 292 pp.

APPENDIX

Appendix One (A): Core-log appraisal

Sample #	Sample ID	Depth from (M)	Depth to (M)	Lithology
48	T001	0.2	0.5	whitish and light brown fine sand
49	T001	1	1.2	light brown fine sand
50	T001	2	2.2	light brownish yellow fine sand
52	T001	3.9	4.1	light brownish yellow fine sand
53	T001	5	5.2	brownish yellow fine sand
54	T001	6	6.2	brownish grey fine sand
55	T001	7	7.2	brownish grey fine sand
56	T001	8	8.2	reddish fine sand
57	T001	9	9.2	dark grey fine sand
58	T001	10	10.2	dark grey fine sand
59	T002	0.2	0.4	whitish and light brown fine sand
60	T002	1	1.2	light brown fine sand
61	T002	2	2.2	light brownish yellow fine sand
62	T002	3	3.2	light brownish yellow fine sand
63	T002	4	4.2	brownish yellow fine sand
64	T002	5	5.2	brownish grey fine sand
65	T002	6	6.2	brownish grey fine sand
66	T002	7	7.2	reddish fine sand
67	T002	8	8.2	dark grey fine sand
68	T003	0.2	0.4	whitish and light brown fine sand
69	T003	1	1.2	light brown fine sand
70	T003	2	2.2	light brownish yellow fine sand
71	T003	3	3.2	light brownish yellow fine sand
72	T003	4	4.2	brownish yellow fine sand
73	T003	4.8	5.1	brownish grey fine sand
74	T003	6	6.2	brownish grey fine sand
75	T003	7	7.2	reddish fine sand
76	T003	8	8.2	dark grey fine sand

Appendix One (B): X-ray diffraction data

Sample No	Sample ID	Depth from (M)	Depth to (m)	Quartz SiO_2	Pyrophyllite $Al_2Si_4O_{10}(OH)_2$	Pyrite FeS_2	Clinochlore $(Mg, Fe)_6(Si,Al)_4O_{10}(OH)_8$	Gypsum $CaSO_4.2H_2O$	Yoshiokaite $Ca(Al,Si)_2O_4$
GT1-048	T001	0.2	0.5						
GT1-049	T001	1	1.2	52.13	2.71	0.13	0.18	0.49	0.09
GT1-050	T001	2	2.2						
GT1-052	T001	3.9-4	4.1	46.75	2.43	0.12	0.16	0.44	0.08
GT1-053	T001	5	5.2						
GT1-054	T001	6	6.2						
GT1-055	T001	7	7.2	46.68	2.43	0.12	0.16	0.44	0.08
GT1-056	T001	8	8.2						
GT1-057	T001	9	9.2						
GT1-058	T001	10	10.2	46.68	0.91	0.12	0.27	0.44	0.08
GT1-059	T002	0.2	0.4						
GT1-060	T002	1	1.2						
GT1-061	T002	2	2.2	49.28	1.18	0.5	0.28	0.34	0.13
GT1-062	T002	3	3.2						
GT1-063	T002	4	4.2						
GT1-064	T002	5	5.2	41.67	1	0.42	0.24	0.27	0.15
GT1-065	T002	6	6.2						
GT1-066	T002	7	7.2						
GT1-067	T002	8	8.2	41.67	1	0.42	0.37	0.27	0.37
GT1-076	T003	0.2	0.4	46.68	0.91	0.47	0.27	0.44	0.08
GT1-075	T003	1	1.2						
GT1-074	T003	2	2.2						
GT1-073	T003	3	3.2	41.75	0.81	0.42	0.24	0.39	0.08
GT1-072	T003	4	4.2						
GT1-071	T003	4.8	5.1						
GT1-070	T003	6	6.2						
GT1-069	T003	7	7.2	41.67	3.84	0.42	0.24	1.16	
GT1-068	T003	8	8.2	63.65	5.87	0.64	0.37	1.77	

Appendix One (C): Paste pH and electrical conductivity (EC) data.

Sample ID	Depth from (M)	Depth to (M)	Paste pH	EC (µ /cm)
T001	0.2	0.5	5.16	0.21
T001	1.0	1.2	2.92	1.01
T001	2.0	2.2	3.89	0.99
T001	3.9	4.1	5.71	1.14
T001	5.0	5.2	4.38	0.94
T001	6.0	6.2	7.64	0.54
T001	7.0	7.2	8.32	0.56
T001	8.0	8.2	8.40	0.53
T001	9.0	9.2	8.30	0.53
T001	10.0	10.2	8.29	0.53
T002	0.2	0.4	3.97	0.53
T002	1.0	1.2	3.18	1.27
T002	2.0	2.2	3.93	0.82
T002	3.0	3.2	3.84	0.89
T002	4.0	4.2	3.69	0.89
T002	5.0	5.2	4.13	1.28
T002	6.0	6.2	3.97	1.09
T002	7.0	7.2	8.11	0.56
T002	8.0	8.2	8.23	0.69
T003	0.2	0.4	4.59	0.71
T003	1	1.2	4.86	0.63
T003	2	2.2	3.82	0.63
T003	3	3.2	8.05	0.85
T003	4	4.2	8.40	0.73
T003	4.8	5.1	8.20	0.60
T003	6	6.2	8.08	0.72
T003	7	7.2	8.14	0.79
T003	8	8.2	7.44	0.72

Appendix One (D): Bulk geochemical data

Sample No	Sample ID	Depth from (M)	Depth to (M)	LOI (%)	SiO_2 (%)	Al_2O_3 (%)	Fe_2O_3 (%)	CaO (%)	MgO (%)	Na_2O (%)	K_2O (%)
GT1-048	T001	0.2	0.5	1.40	91.58	4.44	1.86	0.03	0.19	0.00	0.14
GT1-049	T001	1.0	1.2	2.78	89.38	3.96	2.85	0.43	0.26	0.00	0.11
GT1-050	T001	2.0	2.2	5.63	82.45	4.73	4.79	1.40	0.34	0.02	0.15
GT1-051	T001										
GT1-052	T001	3.9	4.1	2.54	89.17	3.90	3.00	0.51	0.34	0.00	0.12
GT1-053	T001	5.0	5.2	4.29	84.96	4.25	3.84	1.08	0.38	0.01	0.13
GT1-054	T001	6.0	6.2	1.97	90.38	3.90	2.47	0.51	0.28	0.00	0.12
GT1-055	T001	7.0	7.2	3.40	86.46	4.86	2.84	1.16	0.36	0.02	0.16
GT1-056	T001	8.0	8.2	2.42	89.78	3.98	2.43	0.67	0.25	0.01	0.12
GT1-057	T001	9.0	9.2	2.84	87.57	4.64	2.93	0.80	0.31	0.02	0.15
GT1-058	T001	10.0	10.2	3.94	81.44	7.82	3.17	1.28	0.81	0.14	0.51
GT1-059	T002	0.2	0.4	0.68	93.29	3.75	1.37	0.02	0.24	0.01	0.11
GT1-060	T002	1.0	1.2	3.14	88.47	3.90	3.16	0.33	0.27	0.00	0.11
GT1-061	T002	2.0	2.2	2.12	89.68	3.75	2.82	0.33	0.26	0.00	0.11
GT1-062	T002	3.0	3.2	3.07	88.77	3.82	3.07	0.65	0.27	0.00	0.12
GT1-063	T002	4.0	4.2	3.49	86.97	4.24	3.59	0.69	0.30	0.02	0.13
GT1-064	T002	5.0	5.2	3.50	86.66	4.37	3.53	0.73	0.36	0.00	0.14
GT1-065	T002	6.0	6.2	2.81	88.57	3.93	2.96	0.49	0.31	0.02	0.13
GT1-066	T002	7.0	7.2	2.96	87.87	4.30	2.73	1.02	0.31	0.02	0.13
GT1-067	T002	8.0	8.2	2.45	89.98	3.79	2.45	0.71	0.23	0.02	0.12
GT1-076	T003	0.2	0.4	2.70	89.68	3.81	2.80	0.65	0.24	0.01	0.13
GT1-075	T003	1.0	1.2	2.01	91.99	3.40	1.73	0.25	0.14	0.04	0.16
GT1-074	T003	2.0	2.2	2.41	89.68	3.76	2.59	0.32	0.15	0.04	0.20
GT1-073	T003	3.0	2.3	3.45	87.47	4.30	2.55	1.06	0.13	0.04	0.19
GT1-072	T003	4.0	2.4	3.80	86.76	5.03	2.15	1.43	0.13	0.06	0.22
GT1-071	T003	4.8	5.1	2.30	92.39	2.74	1.82	0.60	0.10	0.01	0.12
GT1-070	T003	6.0	6.2	4.08	83.75	7.80	2.34	1.03	0.19	0.07	0.32
GT1-069	T003	7.0	7.2	5.29	81.44	7.40	2.93	1.43	0.35	0.04	0.29
GT1-068	T003	8.0	8.2	4.15	84.56	6.58	2.55	0.98	0.16	0.04	0.29

Sample No	Sample ID	Depth from (M)	Depth to (M)	MnO (%)	TiO_2 (%)	P_2O_5 (%)	Cr_2O_3 (%)	Ba (%)	SUM (%)	TOT/C (%)	TOT/S (%)
GT1-048	T001	0.2	0.5	0.06	0.29	0.02	0.05	0.00	100.00	0.06	0.01
GT1-049	T001	1.0	1.2	0.02	0.26	0.02	0.05	0.00	100.00	0.03	1.19
GT1-050	T001	2.0	2.2	0.04	0.24	0.02	0.07	0.00	100.00	0.10	2.04
GT1-051	T001										
GT1-052	T001	3.9	4.1	0.03	0.24	0.02	0.05	0.00	100.00	0.05	1.03
GT1-053	T001	5.0	5.2	0.04	0.25	0.02	0.06	0.00	100.00	0.10	1.41
GT1-054	T001	6.0	6.2	0.02	0.25	0.01	0.05	0.00	100.00	0.07	0.78
GT1-055	T001	7.0	7.2	0.03	0.26	0.02	0.06	0.00	100.00	0.16	0.83
GT1-056	T001	8.0	8.2	0.02	0.29	0.01	0.06	0.00	100.00	0.08	0.78
GT1-057	T001	9.0	9.2	0.02	0.25	0.02	0.05	0.00	100.00	0.11	0.92
GT1-058	T001	10.0	10.2	0.03	0.29	0.03	0.06	0.01	100.00	0.14	0.81
GT1-059	T002	0.2	0.4	0.01	0.24	0.01	0.05	0.00	100.00	0.04	0.01
GT1-060	T002	1.0	1.2	0.02	0.28	0.05	0.05	0.00	100.00	0.03	1.22
GT1-061	T002	2.0	2.2	0.02	0.30	0.01	0.05	0.00	100.00	0.02	1.07
GT1-062	T002	3.0	3.2	0.03	0.24	0.02	0.05	0.00	100.00	0.04	1.13
GT1-063	T002	4.0	4.2	0.03	0.26	0.02	0.06	0.00	100.00	0.08	1.37
GT1-064	T002	5.0	5.2	0.03	0.25	0.02	0.06	0.00	100.00	0.07	1.04
GT1-065	T002	6.0	6.2	0.03	0.25	0.01	0.06	0.00	100.00	0.07	0.91
GT1-066	T002	7.0	7.2	0.02	0.25	0.02	0.05	0.00	100.00	0.15	0.87
GT1-067	T002	8.0	8.2	0.02	0.27	0.02	0.05	0.00	100.00	0.08	0.84
GT1-076	T003	0.2	0.4	0.01	0.24	0.02	0.06	0.00	100.00	0.03	1.06
GT1-075	T003	1.0	1.2	0.01	0.25	0.02	0.09	0.00	100.00	0.38	0.77
GT1-074	T003	2.0	2.2	0.00	0.29	0.02	0.05	0.00	100.00	0.06	1.03
GT1-073	T003	3.0	2.3	0.02	0.30	0.02	0.07	0.00	100.00	0.19	1.09
GT1-072	T003	4.0	2.4	0.03	0.24	0.03	0.06	0.00	100.00	0.36	0.96
GT1-071	T003	4.8	5.1	0.02	0.22	0.02	0.05	0.00	100.00	0.05	0.86
GT1-070	T003	6.0	6.2	0.04	0.27	0.03	0.06	0.00	100.00	0.17	0.88
GT1-069	T003	7.0	7.2	0.05	0.23	0.03	0.05	0.00	100.00	0.17	1.29
GT1-068	T003	8.0	8.2	0.04	0.25	0.03	0.06	0.00	100.00	0.12	0.84

Sample No	Sample ID	Depth from (M)	Depth to (M)	Ba (ppm)	Be (ppm)	Co (ppm)	Cs (ppm)	Ga (ppm)	Hf (ppm)	Nb (ppm)	Rb (ppm)
GT1-048	T001	0.2	0.5	53.00	1.00	3.70	0.60	3.80	3.30	4.00	5.80
GT1-049	T001	1.0	1.2	20.00	0.25	23.10	0.30	4.00	4.60	3.90	3.40
GT1-050	T001	2.0	2.2	34.00	0.25	61.50	0.50	4.60	5.00	3.90	4.60
GT1-051	T001										
GT1-052	T001	3.9	4.1	24.00	0.25	37.00	0.20	3.50	4.40	3.40	3.40
GT1-053	T001	5.0	5.2	30.00	0.25	28.90	0.50	3.60	4.20	3.80	4.20
GT1-054	T001	6.0	6.2	26.00	0.25	21.50	0.40	3.50	4.00	3.20	3.60
GT1-055	T001	7.0	7.2	40.00	0.25	22.10	0.50	4.20	3.90	3.70	4.80
GT1-056	T001	8.0	8.2	27.00	2.00	22.00	0.40	3.90	4.70	3.50	4.00
GT1-057	T001	9.0	9.2	37.00	0.25	21.90	0.50	4.60	4.30	3.70	4.90
GT1-058	T001	10.0	10.2	107.00	1.00	24.50	1.40	8.20	3.80	3.70	18.70
GT1-059	T002	0.2	0.4	25.00	1.00	1.60	0.30	4.00	4.90	3.70	3.70
GT1-060	T002	1.0	1.2	23.00	0.25	22.30	0.30	5.50	4.90	3.80	3.40
GT1-061	T002	2.0	2.2	22.00	0.25	29.60	0.30	4.10	4.90	4.10	3.50
GT1-062	T002	3.0	3.2	38.00	1.00	35.00	0.30	4.20	4.70	4.40	3.90
GT1-063	T002	4.0	4.2	38.00	0.25	56.50	0.50	4.60	4.80	3.80	4.70
GT1-064	T002	5.0	5.2	31.00	0.25	22.50	0.40	4.90	4.50	3.80	4.30
GT1-065	T002	6.0	6.2	31.00	2.00	18.80	0.40	4.10	4.50	3.70	4.30
GT1-066	T002	7.0	7.2	38.00	0.25	22.00	0.50	5.00	4.70	4.20	4.40
GT1-067	T002	8.0	8.2	31.00	0.25	22.70	0.40	4.70	3.80	3.60	4.50
GT1-076	T003	0.2	0.4	22.00	0.25	18.10	0.30	3.20	3.20	3.40	4.10
GT1-075	T003	1.0	1.2	29.00	0.25	18.90	0.40	3.40	3.60	4.60	5.10
GT1-074	T003	2.0	2.2	39.00	0.25	24.80	0.40	3.70	4.10	4.60	7.80
GT1-073	T003	3.0	2.3	35.00	0.25	27.20	0.60	4.50	4.60	5.00	7.40
GT1-072	T003	4.0	2.4	40.00	0.25	24.50	0.60	4.90	2.90	4.60	7.30
GT1-071	T003	4.8	5.1	27.00	0.25	31.90	0.30	2.60	3.30	4.30	3.70
GT1-070	T003	6.0	6.2	55.00	0.25	61.30	0.90	7.40	3.30	5.70	11.50
GT1-069	T003	7.0	7.2	57.00	2.00	78.00	1.10	7.00	3.90	4.10	9.20
GT1-068	T003	8.0	8.2	58.00	0.25	63.40	1.00	7.50	4.70	5.00	9.70

Sample No	Sample ID	Depth from (M)	Depth to (M)	Sn (ppm)	Sr (ppm)	Ta (ppm)	Th (ppm)	U (ppm)	V (ppm)	W (ppm)	Zr (ppm)
GT1-048	T001	0.2	0.5	2.00	13.70	0.50	3.60	4.00	40.00	1.00	156.00
GT1-049	T001	1.0	1.2	1.00	14.30	0.60	6.70	8.30	30.00	1.20	193.00
GT1-050	T001	2.0	2.2	1.00	19.70	0.60	8.20	35.80	34.00	1.30	184.10
GT1-051	T001										
GT1-052	T001	3.9	4.1	2.00	14.10	0.50	5.10	20.60	31.00	1.00	166.30
GT1-053	T001	5.0	5.2	0.25	18.90	0.60	5.80	21.20	33.00	1.30	168.40
GT1-054	T001	6.0	6.2	0.25	16.00	0.60	4.70	15.80	28.00	1.40	163.80
GT1-055	T001	7.0	7.2	1.00	22.90	0.60	6.10	18.90	32.00	2.70	177.00
GT1-056	T001	8.0	8.2	0.25	16.30	0.50	5.60	15.30	26.00	1.10	175.20
GT1-057	T001	9.0	9.2	0.25	23.20	0.60	6.60	20.70	28.00	1.40	159.00
GT1-058	T001	10.0	10.2	2.00	39.10	0.60	7.90	31.20	44.00	1.30	143.20
GT1-059	T002	0.2	0.4	0.25	13.60	0.70	3.00	4.80	31.00	1.00	170.20
GT1-060	T002	1.0	1.2	1.00	15.20	0.60	8.80	9.60	31.00	1.20	201.90
GT1-061	T002	2.0	2.2	0.25	14.70	0.70	5.00	16.30	33.00	1.30	203.40
GT1-062	T002	3.0	3.2	0.25	17.80	0.80	5.70	21.70	40.00	1.20	183.30
GT1-063	T002	4.0	4.2	2.00	20.90	0.70	6.30	23.80	37.00	1.20	187.70
GT1-064	T002	5.0	5.2	3.00	18.40	0.60	6.10	18.30	37.00	0.90	181.20
GT1-065	T002	6.0	6.2	3.00	19.30	0.60	5.60	14.50	33.00	1.30	176.70
GT1-066	T002	7.0	7.2	1.00	21.70	0.70	6.50	18.70	30.00	1.60	178.10
GT1-067	T002	8.0	8.2	1.00	17.70	0.60	6.10	16.20	33.00	1.20	184.00
GT1-076	T003	0.2	0.4	1.00	16.40	0.50	4.90	8.30	36.00	1.00	126.80
GT1-075	T003	1.0	1.2	1.00	19.50	0.70	4.30	45.10	28.00	0.80	135.50
GT1-074	T003	2.0	2.2	2.00	21.50	1.00	5.80	6.10	33.00	1.00	181.80
GT1-073	T003	3.0	2.3	1.00	26.20	0.60	5.00	10.30	37.00	1.20	173.90
GT1-072	T003	4.0	2.4	2.00	33.00	0.50	5.60	14.80	36.00	1.30	134.30
GT1-071	T003	4.8	5.1	0.25	21.50	0.50	3.70	14.70	26.00	1.00	133.90
GT1-070	T003	6.0	6.2	2.00	44.00	0.70	8.90	52.40	45.00	1.30	141.70
GT1-069	T003	7.0	7.2	2.00	40.00	0.70	10.90	56.50	41.00	1.20	151.50
GT1-068	T003	8.0	8.2	3.00	36.80	0.70	9.00	37.10	43.00	1.20	169.00

Sample No	Sample ID	Depth from (M)	Depth to (M)	Y (ppm)	La (ppm)	Ce (ppm)	Pr (ppm)	Nd (ppm)	Sm (ppm)	Eu (ppm)	Gd (ppm)
GT1-048	T001	0.2	0.5	6.60	13.20	27.00	2.64	9.90	1.68	0.36	1.41
GT1-049	T001	1.0	1.2	7.40	15.40	27.30	2.89	9.60	1.98	0.40	1.57
GT1-050	T001	2.0	2.2	9.60	18.90	34.60	3.72	14.00	2.40	0.54	2.20
GT1-051	T001										
GT1-052	T001	3.9	4.1	7.50	14.70	28.00	3.09	10.80	2.06	0.46	1.71
GT1-053	T001	5.0	5.2	7.70	16.00	30.30	3.38	11.80	2.05	0.44	1.79
GT1-054	T001	6.0	6.2	7.70	15.40	28.30	3.18	11.70	1.86	0.45	1.55
GT1-055	T001	7.0	7.2	9.00	18.60	34.70	3.72	13.40	2.27	0.52	1.88
GT1-056	T001	8.0	8.2	8.40	16.40	29.50	3.28	12.30	1.97	0.46	1.87
GT1-057	T001	9.0	9.2	8.80	17.40	32.10	3.75	14.80	2.32	0.49	2.00
GT1-058	T001	10.0	10.2	10.70	23.80	43.70	4.81	18.30	2.90	0.66	2.55
GT1-059	T002	0.2	0.4	7.10	14.80	28.00	3.02	10.70	1.82	0.40	1.59
GT1-060	T002	1.0	1.2	7.60	15.30	28.50	3.21	11.20	2.00	0.44	1.66
GT1-061	T002	2.0	2.2	8.30	16.50	30.10	3.21	11.00	2.04	0.45	1.85
GT1-062	T002	3.0	3.2	8.90	18.20	33.40	3.58	13.00	2.24	0.50	2.15
GT1-063	T002	4.0	4.2	8.70	17.80	32.80	3.67	13.90	2.16	0.51	1.98
GT1-064	T002	5.0	5.2	8.60	17.20	31.00	3.55	12.10	2.20	0.52	1.88
GT1-065	T002	6.0	6.2	8.10	16.30	29.70	3.40	12.30	1.97	0.48	1.83
GT1-066	T002	7.0	7.2	8.60	18.00	32.30	3.63	13.30	2.23	0.54	2.05
GT1-067	T002	8.0	8.2	8.40	16.30	31.20	3.56	14.30	2.09	0.46	1.78
GT1-076	T003	0.2	0.4	6.20	13.90	25.30	2.92	10.70	1.71	0.37	1.37
GT1-075	T003	1.0	1.2	8.20	18.00	33.80	3.81	14.40	2.40	0.52	1.77
GT1-074	T003	2.0	2.2	7.60	15.70	30.80	3.44	11.20	2.04	0.43	1.60
GT1-073	T003	3.0	2.3	9.90	20.20	38.20	4.21	14.80	2.34	0.54	2.19
GT1-072	T003	4.0	2.4	9.80	22.00	38.60	4.45	15.60	2.36	0.56	2.30
GT1-071	T003	4.8	5.1	7.90	17.50	33.00	3.66	13.60	2.24	0.53	1.92
GT1-070	T003	6.0	6.2	15.40	34.20	67.30	7.47	26.80	4.79	1.02	4.25
GT1-069	T003	7.0	7.2	16.70	38.00	69.60	8.32	31.10	4.73	1.22	4.41
GT1-068	T003	8.0	8.2	15.10	31.20	60.30	6.91	23.60	4.04	1.01	3.77

Sample No	Sample ID	Depth from (M)	Depth to (M)	Tb (ppm)	Dy (ppm)	Ho (ppm)	Er (ppm)	Tm (ppm)	Yb (ppm)	Lu (ppm)	Mo (ppm)
GT1-048	T001	0.2	0.5	0.18	1.29	0.25	0.67	0.11	0.69	0.11	6.60
GT1-049	T001	1.0	1.2	0.23	1.36	0.26	0.73	0.11	0.84	0.12	5.90
GT1-050	T001	2.0	2.2	0.30	1.85	0.33	1.06	0.15	0.98	0.16	7.50
GT1-051	T001										
GT1-052	T001	3.9	4.1	0.24	1.58	0.26	0.78	0.12	0.82	0.12	6.40
GT1-053	T001	5.0	5.2	0.24	1.47	0.25	0.71	0.12	0.83	0.12	8.10
GT1-054	T001	6.0	6.2	0.22	1.38	0.25	0.67	0.11	0.79	0.12	5.40
GT1-055	T001	7.0	7.2	0.28	1.74	0.31	0.96	0.14	0.90	0.15	4.60
GT1-056	T001	8.0	8.2	0.23	1.54	0.28	0.78	0.12	0.82	0.13	6.20
GT1-057	T001	9.0	9.2	0.27	1.72	0.26	0.84	0.14	0.81	0.13	4.30
GT1-058	T001	10.0	10.2	0.34	1.84	0.37	1.10	0.17	0.99	0.15	4.80
GT1-059	T002	0.2	0.4	0.21	1.22	0.26	0.77	0.10	0.67	0.11	7.40
GT1-060	T002	1.0	1.2	0.23	1.32	0.27	0.81	0.12	0.86	0.13	6.60
GT1-061	T002	2.0	2.2	0.23	1.37	0.24	0.77	0.12	0.94	0.12	7.10
GT1-062	T002	3.0	3.2	0.28	1.69	0.29	0.85	0.15	1.05	0.15	6.70
GT1-063	T002	4.0	4.2	0.28	1.63	0.28	0.89	0.14	0.87	0.14	8.20
GT1-064	T002	5.0	5.2	0.25	1.60	0.26	0.85	0.13	0.84	0.12	8.90
GT1-065	T002	6.0	6.2	0.24	1.46	0.26	0.79	0.13	0.81	0.13	8.60
GT1-066	T002	7.0	7.2	0.26	1.68	0.29	0.79	0.13	0.83	0.13	6.30
GT1-067	T002	8.0	8.2	0.25	1.68	0.31	0.80	0.13	0.91	0.13	6.10
GT1-076	T003	0.2	0.4	0.19	0.89	0.23	0.60	0.09	0.67	0.11	9.40
GT1-075	T003	1.0	1.2	0.27	1.47	0.30	0.85	0.12	0.99	0.14	8.10
GT1-074	T003	2.0	2.2	0.22	1.24	0.23	0.86	0.10	0.76	0.11	7.50
GT1-073	T003	3.0	2.3	0.30	2.03	0.35	0.96	0.12	0.90	0.13	9.20
GT1-072	T003	4.0	2.4	0.29	1.88	0.33	0.83	0.12	0.96	0.14	9.40
GT1-071	T003	4.8	5.1	0.25	1.39	0.29	0.67	0.11	0.89	0.11	9.10
GT1-070	T003	6.0	6.2	0.55	2.98	0.55	1.47	0.21	1.23	0.20	6.60
GT1-069	T003	7.0	7.2	0.54	3.38	0.57	1.55	0.23	1.52	0.22	4.20
GT1-068	T003	8.0	8.2	0.46	2.83	0.44	1.36	0.20	1.27	0.20	8.50

Sample No	Sample ID	Depth from (M)	Depth to (M)	Cu (ppm)	Pb (ppm)	Zn (ppm)	Ag (ppm)	Ni (ppm)	As (ppm)	Au (ppb)	Cd (ppm)
GT1-048	T001	0.2	0.5	9.80	12.60	9.00	0.03	13.20	27.00	169.10	0.03
GT1-049	T001	1.0	1.2	33.50	11.40	13.00	0.10	38.10	189.70	823.30	0.03
GT1-050	T001	2.0	2.2	52.40	28.20	145.00	0.03	229.70	191.40	149.30	0.60
GT1-051	T001										
GT1-052	T001	3.9	4.1	34.10	18.00	73.00	0.03	61.30	92.70	375.70	0.20
GT1-053	T001	5.0	5.2	39.80	20.10	116.00	0.03	67.70	130.30	112.10	0.20
GT1-054	T001	6.0	6.2	30.10	14.80	90.00	0.03	54.10	87.40	125.70	0.20
GT1-055	T001	7.0	7.2	25.80	30.60	164.00	0.03	57.20	127.10	62.40	0.10
GT1-056	T001	8.0	8.2	30.10	21.70	90.00	0.03	56.10	108.70	107.00	0.03
GT1-057	T001	9.0	9.2	34.60	30.10	97.00	0.03	70.20	122.30	69.80	0.03
GT1-058	T001	10.0	10.2	42.10	28.80	117.00	0.03	88.50	114.80	59.60	0.20
GT1-059	T002	0.2	0.4	7.50	12.10	5.00	0.03	8.20	21.70	140.40	0.03
GT1-060	T002	1.0	1.2	20.90	11.80	11.00	0.03	35.80	700.20	119.60	0.03
GT1-061	T002	2.0	2.2	23.70	12.10	109.00	0.03	96.00	94.30	221.40	0.20
GT1-062	T002	3.0	3.2	29.00	20.50	64.00	0.03	86.40	95.30	49.00	0.20
GT1-063	T002	4.0	4.2	50.40	26.40	99.00	0.03	75.00	113.50	430.80	0.10
GT1-064	T002	5.0	5.2	30.60	18.30	82.00	0.03	55.80	102.10	94.00	0.03
GT1-065	T002	6.0	6.2	24.00	22.80	83.00	0.03	43.40	93.60	75.10	0.10
GT1-066	T002	7.0	7.2	30.70	22.30	103.00	0.03	56.80	115.90	117.20	0.03
GT1-067	T002	8.0	8.2	30.60	18.60	66.00	0.03	49.60	108.80	58.00	0.03
GT1-076	T003	0.2	0.4	43.20	15.40	33.00	0.03	38.40	155.80	134.10	0.03
GT1-075	T003	1.0	1.2	37.20	13.40	112.00	0.10	56.80	67.60	324.00	0.80
GT1-074	T003	2.0	2.2	36.20	19.00	25.00	0.03	38.30	84.60	127.80	0.03
GT1-073	T003	3.0	2.3	100.50	28.00	38.00	0.10	182.00	91.30	812.10	0.03
GT1-072	T003	4.0	2.4	55.70	34.20	85.00	0.20	58.40	83.00	75.50	0.20
GT1-071	T003	4.8	5.1	28.70	21.90	56.00	0.03	94.20	56.20	58.70	0.20
GT1-070	T003	6.0	6.2	75.90	41.80	231.00	0.20	191.80	103.70	219.00	0.70
GT1-069	T003	7.0	7.2	68.10	67.50	215.00	0.30	242.20	132.90	130.40	0.70
GT1-068	T003	8.0	8.2	62.80	51.10	179.00	0.10	176.60	100.30	97.10	0.30

Sample No	Sample ID	Depth from (M)	Depth to (M)	Sb (ppm)	Bi (ppm)	Hg (ppm)	Ti (ppm)	Se (ppm)
GT1-048	T001	0.2	0.5	0.40	0.40	0.06	0.03	0.13
GT1-049	T001	1.0	1.2	0.70	0.50	0.20	0.03	0.13
GT1-050	T001	2.0	2.2	1.20	1.10	0.42	0.03	1.20
GT1-051	T001							
GT1-052	T001	3.9	4.1	0.80	0.60	0.25	0.03	0.13
GT1-053	T001	5.0	5.2	0.80	0.60	0.46	0.03	0.13
GT1-054	T001	6.0	6.2	0.60	0.50	0.20	0.03	0.13
GT1-055	T001	7.0	7.2	0.90	0.80	0.67	0.03	0.13
GT1-056	T001	8.0	8.2	0.80	0.60	0.25	0.03	0.13
GT1-057	T001	9.0	9.2	1.00	0.90	0.29	0.03	0.13
GT1-058	T001	10.0	10.2	0.70	0.70	0.39	0.03	0.13
GT1-059	T002	0.2	0.4	0.50	0.40	0.17	0.03	0.13
GT1-060	T002	1.0	1.2	0.80	0.90	0.19	0.03	1.20
GT1-061	T002	2.0	2.2	0.70	0.50	0.15	0.03	1.50
GT1-062	T002	3.0	3.2	0.90	0.70	0.19	0.03	0.13
GT1-063	T002	4.0	4.2	0.90	0.70	0.41	0.03	0.90
GT1-064	T002	5.0	5.2	0.70	0.50	0.35	0.03	0.60
GT1-065	T002	6.0	6.2	0.80	0.50	0.37	0.03	0.13
GT1-066	T002	7.0	7.2	0.80	0.70	0.27	0.03	0.50
GT1-067	T002	8.0	8.2	1.00	0.60	0.40	0.03	0.13
GT1-076	T003	0.2	0.4	0.70	0.70	0.29	0.03	0.70
GT1-075	T003	1.0	1.2	0.60	0.70	0.21	0.03	0.13
GT1-074	T003	2.0	2.2	0.70	0.80	0.75	0.03	0.70
GT1-073	T003	3.0	2.3	0.90	1.10	0.78	0.03	1.00
GT1-072	T003	4.0	2.4	1.00	1.30	3.38	0.03	1.30
GT1-071	T003	4.8	5.1	0.70	0.90	0.55	0.03	0.70
GT1-070	T003	6.0	6.2	1.10	1.60	8.26	0.03	0.90
GT1-069	T003	7.0	7.2	1.00	1.30	4.37	0.03	0.13
GT1-068	T003	8.0	8.2	0.90	1.00	5.39	0.03	0.70

Appendix Two (A): Core log reappraisal based on sample colour, texture and grainsize

Sample #	Sample ID	Depth from (M)	Depth to (M)	Description
48	T001	0.2	0.5	Pale yellow - brown fine sand
49	T001	1	1.2	Reddish mottled fine sand
50	T001	2	2.2	Reddish mottled fine sand
52	T001	3.9	4.1	Pale red - brown fine sand
53	T001	5	5.2	Pale red - brown fine sand
54	T001	6	6.2	Pale grey - brown fine sand
55	T001	7	7.2	Pale grey - brown fine sand
56	T001	8	8.2	Pale grey - brown fine sand
57	T001	9	9.2	Dark grey - brown fine sand
58	T001	10	10.2	Dark grey - brown fine sand
59	T002	0.2	0.4	Pale yellow - brown fine sand
60	T002	1	1.2	Reddish mottled fine sand
61	T002	2	2.2	Reddish mottled fine sand
62	T002	3	3.2	Pale red - brown fine sand
63	T002	4	4.2	Pale red - brown fine sand
64	T002	5	5.2	Pale red - brown fine sand
65	T002	6	6.2	Pale red - brown fine sand
66	T002	7	7.2	Pale grey - brown fine sand
67	T002	8	8.2	Pale grey - brown fine sand
76	T003	0.2	0.4	Pale yellow - brown fine sand
75	T003	1	1.2	Reddish mottled fine sand
74	T003	2	2.2	Reddish mottled fine sand
73	T003	3	3.2	Pale grey - brown fine sand
72	T003	4	4.2	Pale grey - brown fine sand
71	T003	4.8	5.1	Pale grey - brown fine sand
70	T003	6	6.2	Pale grey - brown fine sand
69	T003	7	7.2	Pale grey - brown fine sand
68	T003	8	8.2	Pale grey - brown fine sand

Appendix Two (B): Petrographic data for section T001.

Sample depth	Mineral	Modal %	Grainsize distribution	Thin section description
0.2m - 0.8m	Quartz	58%	3mm - 2.5cm	Variable, fine - medium grainsize with sharp edges and minor roundness
	Hydromuscovite	17%	1mm - 4mm	Very fine flecks
	Hydrobiotite	12%	2mm - 2cm	Very fine
	Pyrophilite	5%	0.5cm - 1.5cm	Fine
	Muscovite	3%	0.5cm - 1cm	Fine, elongate
	Biotite	2%	0.5cm - 1.5cm	Fine, elongate, variable grainsize distribution
	Oxides	3%	2mm - 2cm	Two types: matte and sharp edged and red tinge, sericitised looking
1.6m	Quartz	45%	3mm - 1.2cm	Relatively equidimensional fine grains with sharp egdes and minor roundness
	Hydromuscovite	25%	1mm - 3mm	Very fine flecks
	Hydrobiotite	20%	2mm - 1.5cm	Very fine, seemingly enclosing quartz grains
	Pyrophilite	2%	5mm - 1cm	Fine
	Muscovite	3%	1cm - 1.5cm	Fine, elongate
	Biotite	2%	1cm - 1.5cm	Fine, elongate, variable grainsize distribution
	Oxides	3%	2mm - 2cm	Two types: matte and sharp edged and red tinge, sericitised looking
3.6m	Quartz	40%	0.1cm - 0.8cm	Mostly very fine, with some fine grains, larger sharp edged grains
	Hydromuscovite	35%	1mm - 3mm	Very fine flecks
	Hydrobiotite	15%	2mm - 3.5cm	Very fine, some aggregated, some isolated
	Muscovite	3%	0.5cm - 1.5cm	Fine, elongate
	Biotite	3%	0.5cm - 1.5cm	Fine, elongate, variable grainsize distribution
	Pyrophilite	1%	0.5cm - 1.5cm	Fine
	Oxides	3%	0.1cm - 0.1cm	Two types: matte and sharp edged and red tinge, sericitised looking
4.2m - 4.5m	Quartz	40%	0.1cm - 0.5cm	Very fine, near equidimensional, both some and round edged
	Hydromuscovite	30%	1mm -4mm	Very fine flecks
	Hydrobiotite	15%	2mm - 1.5cm	Very fine, partially enclosing fine quartz grains
	Pyrophilite	3%	0.5cm - 1.5cm	Fine
	Muscovite	5%	1cm - 2cm	Fine, elongate
	Biotite	4%	0.5cm - 2cm	Fine, variable grainsizes
	Oxides	3%	1mm - 1cm	Two types: matte and sharp edged and red tinge, sericitised looking

Sample depth	Mineral	Modal %	Grainsize distribution	Thin section description
5.7m	Quartz	48%	0.1cm - 0.4cm	Fine-very fine, fine grains near equidimensional and sharp-edged
	Hydromuscovite	30%	1mm - 3mm	Very fine flecks
	Hydrobiotite	10%	2mm - 2cm	very fine, amongst fine quartz grains
	Muscovite	5%	1cm - 1.5cm	Fine, elongate
	Biotite	3%	1cm - 1.5cm	Fine, elongate
	Pyrophilite	2%	0.5cm - 1.5cm	Fine
	Oxides	2%	1mm - 3mm	Two types: matte and sharp edged and red tinge, sericitised looking
10.2m	Quartz	45%	0.1cm - 0.3cm	Very fine
	Hydromuscovite	35%	1mm - 2mm	Very fine flecks
	Hydrobiotite	10%	1mm - 4mm	Very fine aggregates
	Muscovite	2%	0.1cm - 0.3cm	Fine
	Biotite	2%	0.1cm - 0.3cm	Fine
	Pyrophilite	3%	0.5cm - 1.5cm	Fine
	Oxides	3%	0.1cm -1cm	Two types: matte and sharp edged and red tinge, sericitised looking

Appendix Two (C): Sulphide-sulphur data and net potential ratios

Sample #	Sulphate in 1ml (ppm)	Sulphate*V/g (45/2) in ppm	% sulphate-sulphur	% total sulphur (leco)	% sulphide-sulphur	AP	% total carbon	NP	NPR = NP/AP
48	3.76	84.54	0.01	0.01	0.00	0.05	0.06	5.00	103.44
49	78.58	1768.16	0.18	1.19	1.01	31.66	0.03	2.50	0.08
50	382.88	8614.87	0.86	2.04	1.18	36.83	0.10	8.33	0.23
52	161.59	3635.74	0.36	1.03	0.67	20.83	0.05	4.17	0.20
53	254.48	5725.70	0.57	1.41	0.84	26.17	0.10	8.33	0.32
54	69.52	1564.11	0.16	0.78	0.62	19.49	0.07	5.83	0.30
55	63.39	1426.18	0.14	0.83	0.69	21.48	0.16	13.33	0.62
56	89.29	2008.96	0.20	0.78	0.58	18.10	0.08	6.66	0.37
57	113.51	2553.94	0.26	0.92	0.66	20.77	0.11	9.16	0.44
58	20.78	467.47	0.05	0.81	0.76	23.85	0.14	11.66	0.49
59	1.61	36.28	0.00	0.01	0.01	0.20	0.04	3.33	16.73
60	160.05	3601.15	0.36	1.22	0.86	26.87	0.03	2.50	0.09
61	68.05	1531.20	0.15	1.07	0.92	28.65	0.02	1.67	0.06
62	165.41	3721.81	0.37	1.13	0.76	23.68	0.04	3.33	0.14
63	181.31	4079.44	0.41	1.37	0.96	30.06	0.08	6.66	0.22
64	198.69	4470.61	0.45	1.04	0.59	18.53	0.07	5.83	0.31
65	146.54	3297.22	0.33	0.91	0.58	18.13	0.07	5.83	0.32
66	125.54	2824.54	0.28	0.87	0.59	18.36	0.15	12.50	0.68
67	33.57	755.41	0.08	0.84	0.76	23.89	0.08	6.66	0.28
68	122.57	2757.82	0.28	0.84	0.56	17.63	0.12	10.00	0.57
69	217.79	4900.18	0.49	1.29	0.80	25.00	0.17	14.16	0.57
70	142.12	3197.76	0.32	0.88	0.56	17.51	0.17	14.16	0.81
71	103.58	2330.66	0.23	0.86	0.63	19.59	0.05	4.17	0.21
72	135.42	3047.01	0.30	0.96	0.66	20.48	0.36	29.99	1.46
73	56.24	1265.42	0.13	1.09	0.96	30.11	0.19	15.83	0.53
74	94.74	2131.70	0.21	1.03	0.82	25.53	0.06	5.00	0.20
75	62.11	1397.49	0.14	0.77	0.63	19.70	0.38	31.65	1.61
76	151.18	3401.64	0.34	1.06	0.72	22.49	0.03	2.50	0.11

Appendix Two (D): Sequential extraction data

i) Raw sequential extraction data

Geochemical dataset generated for Gold One Millsite slimes complex samples, following extraction by double distilled water.

Sample	Ca_ppm	Mn_ppm	Fe_ppm	Co_ppm	Ni_ppm	Cu_ppm	Zn_ppm	Au_ppb	Pb_ppm
48	8.12	2.05	0.07	0.00	0.00	0.00	0.00	0.14	0.00
49	42.40	1.27	61.64	3.61	7.00	5.21	5.16	0.14	0.00
50	70.84	5.78	14.45	5.29	15.88	3.60	3.40	0.14	0.00
51	35.09	9.28	28.76	6.29	14.38	3.80	10.38	0.14	0.00
52	62.14	5.22	3.01	3.57	5.69	0.67	4.00	0.14	0.00
53	64.94	5.75	8.37	3.22	6.79	1.92	3.69	0.14	0.00
54	64.14	0.00	0.49	0.00	0.00	0.02	0.00	0.14	0.00
55	65.09	0.04	1.69	0.00	0.00	0.00	0.00	0.14	0.00
56	58.30	0.11	3.58	0.00	0.00	0.02	1.85	0.14	0.00
57	50.44	0.00	1.00	0.00	0.00	0.00	0.00	0.14	0.00
58	52.87	0.05	0.70	0.00	0.00	0.00	0.00	0.14	0.00
59	6.18	0.10	0.15	0.00	0.00	0.00	0.00	0.14	0.00
60	43.20	0.83	10.04	1.69	2.77	1.69	2.12	0.14	0.00
61	50.54	3.90	4.25	2.11	6.83	0.82	4.53	0.14	0.00
62	35.67	4.83	4.69	3.14	7.85	0.64	3.92	0.14	0.00
63	52.06	4.79	6.77	4.33	6.55	2.68	3.53	0.14	0.00
64	42.22	3.13	5.14	1.61	3.92	0.51	3.42	0.14	0.00
65	53.60	9.19	25.70	3.95	10.48	2.36	9.92	0.14	0.00
66	53.74	0.30	6.73	0.01	0.02	0.04	2.35	0.14	0.00
67	76.18	0.09	2.90	0.00	0.01	0.04	1.96	0.14	0.00
68	104.47	13.23	1.42	10.38	25.57	4.38	15.86	0.14	0.00
69	136.42	0.13	2.74	0.05	0.03	0.01	2.67	0.14	0.00
70	117.42	0.43	2.89	0.03	0.07	0.01	1.77	0.14	0.00
71	74.66	0.24	0.35	0.01	0.00	0.00	0.00	0.14	0.00
72	47.59	0.02	0.33	0.14	0.00	0.02	0.00	0.14	0.00
72.1	69.64	0.00	0.09	0.71	0.00	0.00	0.00	0.14	0.00
73	65.36	0.09	0.42	0.15	0.00	0.00	0.00	0.14	0.00
73.1	58.44	0.06	0.33	0.05	0.03	0.00	0.00	0.14	0.00
74	43.08	1.77	24.70	1.85	3.85	4.26	6.85	0.14	0.00
75	36.66	1.99	1.44	1.33	4.85	0.50	5.73	0.14	0.00
76	47.45	0.78	7.58	0.80	1.37	0.26	1.40	0.14	0.00

Geochemical dataset generated for Gold One Millsite slimes complex samples, following extraction by 1 M ammonium acetate.

Sample	Ca_ppm	Mn_ppm	Fe_ppm	Co_ppm	Ni_ppm	Cu_ppm	Zn_ppm	Au_ppb	Pb_ppm
48	42.03	8.97	2.99	0.16	0.36	0.92	0.67	12.83	1.41
49	267.21	1.24	53.71	3.52	5.72	3.72	0.61	0.14	0.08
50	645.30	13.50	78.71	12.81	42.71	4.50	2.85	10.92	0.11
51	325.98	9.37	28.66	3.99	10.08	2.32	1.81	0.14	0.03
52	347.22	7.41	17.86	3.98	6.48	2.21	1.94	11.58	0.10
53	508.68	9.64	35.11	3.08	7.81	1.43	1.12	12.90	0.02
54	468.45	4.32	43.27	2.17	6.41	4.67	2.19	11.05	1.09
55	797.31	11.69	38.39	3.98	10.45	4.73	2.79	0.14	0.92
56	402.12	3.96	20.75	0.94	2.55	2.24	1.41	0.14	2.22
57	625.32	5.16	22.47	1.90	6.80	5.56	1.94	0.14	2.12
58	534.42	10.26	49.26	2.76	7.46	10.54	2.30	10.80	1.35
59	52.11	0.36	0.94	0.06	0.11	0.72	0.18	0.14	0.16
60	208.08	1.01	47.39	2.10	3.14	3.80	0.48	0.14	0.19
61	224.91	9.62	18.13	4.04	15.72	4.53	2.18	0.14	0.04
62	403.20	14.60	22.10	7.02	19.63	2.48	2.04	0.14	0.06
63	369.54	9.18	35.45	8.52	13.14	4.52	2.31	11.51	0.11
64	350.37	6.19	25.94	2.11	4.61	17.04	1.34	0.14	0.08
65	402.30	14.99	34.45	5.13	11.97	12.60	2.47	0.14	0.09
66	510.30	7.67	30.92	2.39	5.28	2.17	2.18	0.14	0.70
67	442.62	4.84	25.36	2.14	5.11	3.94	2.12	0.14	1.38
68	527.76	12.34	14.94	6.06	15.56	4.99	2.79	0.14	0.43
69	656.55	19.48	35.04	15.59	54.96	8.87	3.88	0.14	1.85
70	533.07	8.43	19.28	4.52	19.54	6.48	3.19	0.14	1.26
71	330.66	13.61	22.19	4.56	13.49	7.27	1.79	0.14	0.00
72	426.51	6.96	35.92	2.14	4.16	9.06	1.79	10.46	1.25
72.1	633.15	11.18	47.25	7.64	28.12	6.99	2.21	10.26	0.57
73	510.12	12.22	49.06	4.33	15.69	4.97	1.87	10.23	1.47
73.1	173.78	0.52	3.64	0.25	1.18	2.69	0.53	11.78	2.62
74	245.70	1.06	31.19	4.19	1.90	3.54	0.84	0.14	0.02
75	226.62	2.77	9.86	1.87	7.86	2.30	2.33	0.14	0.08
76	163.97	0.53	34.62	0.69	0.90	1.03	0.36	0.14	0.06

Geochemical dataset generated for Gold One Millsite slimes complex samples, following extraction by 0.1 M hydroxylamine hydrochloride.

Sample	Ca_ppm	Mn_ppm	Fe_ppm	Co_ppm	Ni_ppm	Cu_ppm	Zn_ppm	Au_ppb	Pb_ppm
48	22.09	4.35	3.76	0.19	0.12	0.40	0.26	4.58	0.00
49	32.08	0.27	10.86	0.46	0.70	0.60	0.99	50.52	0.05
50	78.72	1.97	12.15	0.57	1.56	0.21	0.38	7.24	0.01
51	39.62	1.14	8.26	0.22	0.56	0.34	0.26	0.14	0.00
52	55.16	0.86	7.56	0.16	0.23	0.22	0.41	10.82	0.01
53	79.28	1.16	9.91	0.07	0.19	0.17	0.49	1.15	0.00
54	69.98	2.34	14.57	0.92	2.03	0.62	0.97	114.27	0.11
55	93.65	2.40	15.28	1.13	2.40	0.29	0.93	0.14	0.00
56	35.71	1.57	9.90	0.71	1.68	0.94	0.58	256.95	0.26
57	90.32	1.78	10.95	0.75	2.09	0.42	0.94	0.14	0.00
58	72.44	2.97	12.53	1.01	1.93	0.96	0.82	0.14	0.00
59	20.91	0.10	2.10	0.00	0.00	0.11	0.22	0.14	0.00
60	53.54	0.03	9.17	0.01	0.06	0.54	0.09	0.14	0.00
61	59.03	0.69	7.65	0.09	0.42	0.09	0.47	0.14	0.00
62	88.58	1.51	8.76	0.35	0.92	0.28	0.39	0.14	0.00
63	77.12	1.55	9.89	0.62	0.72	0.53	0.86	0.14	0.00
64	85.32	1.00	9.00	0.19	0.52	0.17	0.31	0.14	0.00
65	38.37	1.24	8.61	0.16	0.30	0.86	0.28	1261.44	1.26
66	36.37	1.88	10.30	0.60	1.40	0.17	0.59	0.14	0.00
67	32.18	1.33	10.55	0.72	1.53	0.54	0.44	0.14	0.00
68	39.11	2.47	7.43	0.98	1.55	0.37	0.26	69.34	0.07
69	36.50	2.74	11.84	2.73	5.49	1.14	0.73	502.47	0.50
70	37.10	3.23	10.51	2.78	4.91	0.42	0.91	0.14	0.00
71	63.60	3.82	11.65	2.08	3.90	0.55	0.35	0.14	0.00
72	65.95	3.22	12.87	0.83	1.21	0.90	0.86	0.14	0.00
72.1	75.56	3.64	14.53	3.69	6.28	0.68	1.12	0.14	0.00
73	72.86	3.61	16.17	2.35	4.21	0.56	0.90	0.14	0.00
73.1	43.24	0.64	4.65	0.12	0.53	0.78	0.37	29.81	0.03
74	34.19	0.27	8.82	0.28	0.10	0.29	0.06	0.14	0.00
75	45.80	0.20	6.97	0.09	0.32	0.18	0.50	0.14	0.00
76	49.35	0.15	10.51	0.00	0.03	0.74	0.26	0.14	0.00

Geochemical dataset generated for Gold One Millsite slimes complex samples, following extraction by 0.25 M hydroxylamine hydrochloride.

Sample	Ca_ppm	Mn_ppm	Fe_ppm	Co_ppm	Ni_ppm	Cu_ppm	Zn_ppm	Au_ppb	Pb_ppm
48	9.23	3.21	5.73	0.16	0.08	0.67	0.00	4.36	0.00
49	6.58	0.00	17.80	0.00	0.02	0.74	0.00	0.14	0.00
50	44.30	0.69	21.61	0.11	0.42	0.99	0.00	22.63	0.02
51	17.51	0.44	22.18	0.02	0.16	2.01	0.42	0.14	0.00
52	14.38	0.27	10.89	0.02	0.01	0.78	0.00	3.90	0.00
53	36.79	0.27	17.71	0.00	0.02	0.67	0.00	0.14	0.00
54	20.30	2.14	21.82	0.90	3.25	1.93	1.15	0.14	0.00
55	14.67	3.34	15.72	0.55	4.76	3.30	1.23	44.68	0.04
56	9.98	1.69	25.16	1.12	2.31	1.80	1.14	0.14	0.00
57	13.54	2.64	16.11	1.08	4.23	2.54	1.09	0.14	0.00
58	29.57	2.76	21.82	0.86	3.19	2.46	1.07	0.14	0.00
59	3.79	0.00	2.55	0.00	0.00	0.32	0.33	0.14	0.00
60	7.31	0.00	11.77	0.00	0.00	0.49	0.01	0.14	0.00
61	6.34	0.07	10.95	0.00	0.03	0.39	0.02	0.14	0.00
62	12.12	0.28	10.91	0.00	0.34	1.82	0.26	55.74	0.06
63	26.93	0.17	15.11	0.02	0.03	0.74	0.00	70.25	0.07
64	9.87	0.08	13.63	0.00	0.01	2.76	0.05	0.14	0.00
65	11.29	0.10	20.94	0.00	0.00	0.45	0.14	0.14	0.00
66	8.75	1.41	24.66	0.45	1.39	1.05	0.87	0.14	0.00
67	3.89	1.18	24.21	0.64	1.30	1.56	0.74	0.14	0.00
68	10.23	0.69	14.63	0.08	0.19	1.21	0.32	0.14	0.00
69	8.14	2.62	25.48	2.15	4.57	3.58	1.52	0.14	0.00
70	8.18	2.94	25.33	1.99	4.31	3.08	1.66	0.14	0.00
71	7.29	2.77	16.12	1.88	5.08	2.48	0.72	0.14	0.00
72	10.54	1.90	19.94	0.57	1.22	1.95	0.70	0.14	0.00
72.1	14.41	3.21	21.94	1.90	6.66	2.93	1.26	0.14	0.00
73	19.29	2.82	21.98	1.36	4.90	2.27	0.96	0.14	0.00
73.1	9.43	0.35	8.29	0.11	0.42	0.89	0.00	0.14	0.00
74	6.75	0.01	14.00	0.00	0.00	0.68	0.20	0.14	0.00
75	2.78	0.25	7.57	0.01	0.10	0.77	0.29	0.14	0.00
76	4.77	0.00	8.97	0.00	0.00	0.50	0.04	0.14	0.00

Appendix Two (D): Sequential extraction data

ii) GFAAS precision scatterplots

Precision scatterplots for double distilled water

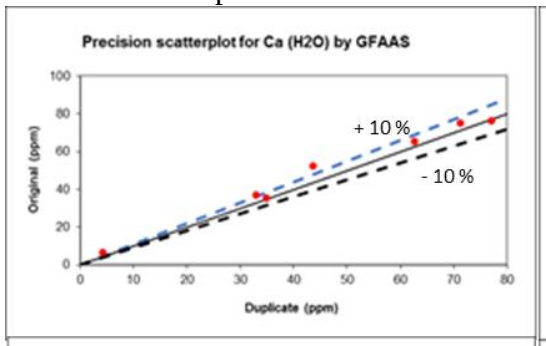

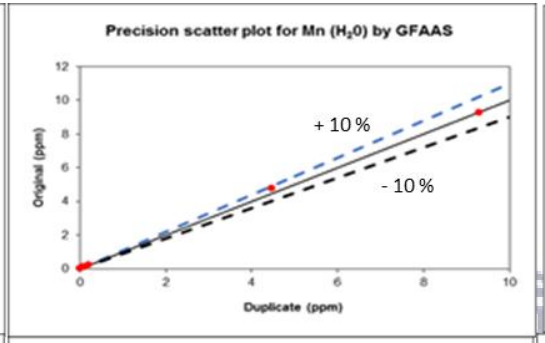

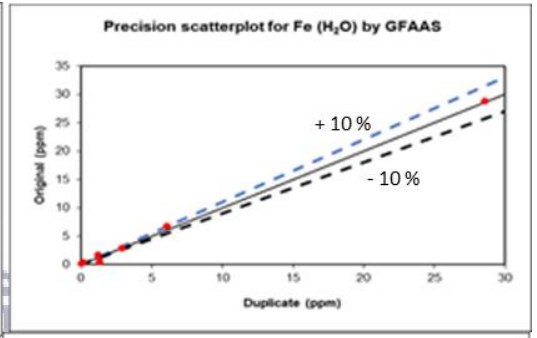

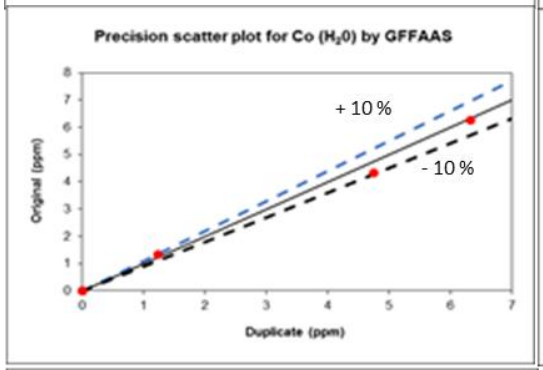

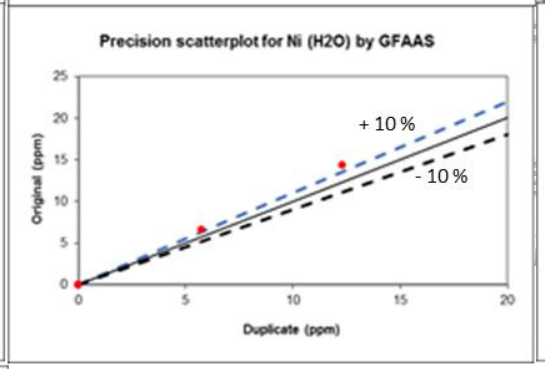

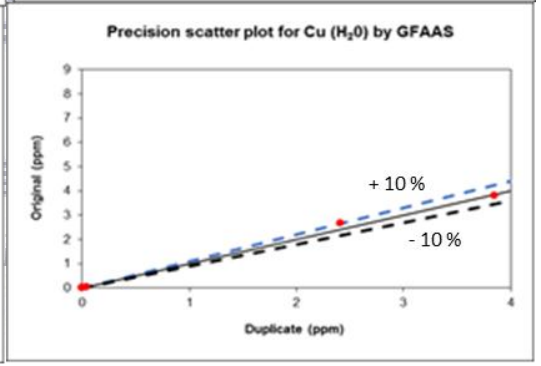

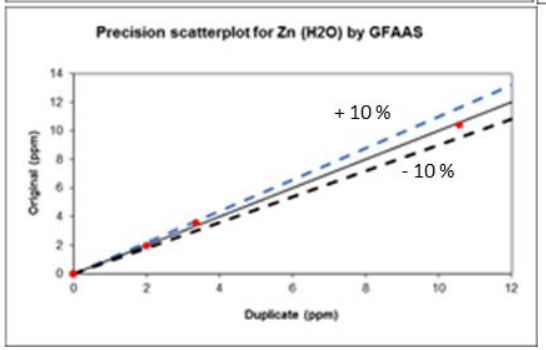

Precision scatterplots for 1 M ammonium acetate

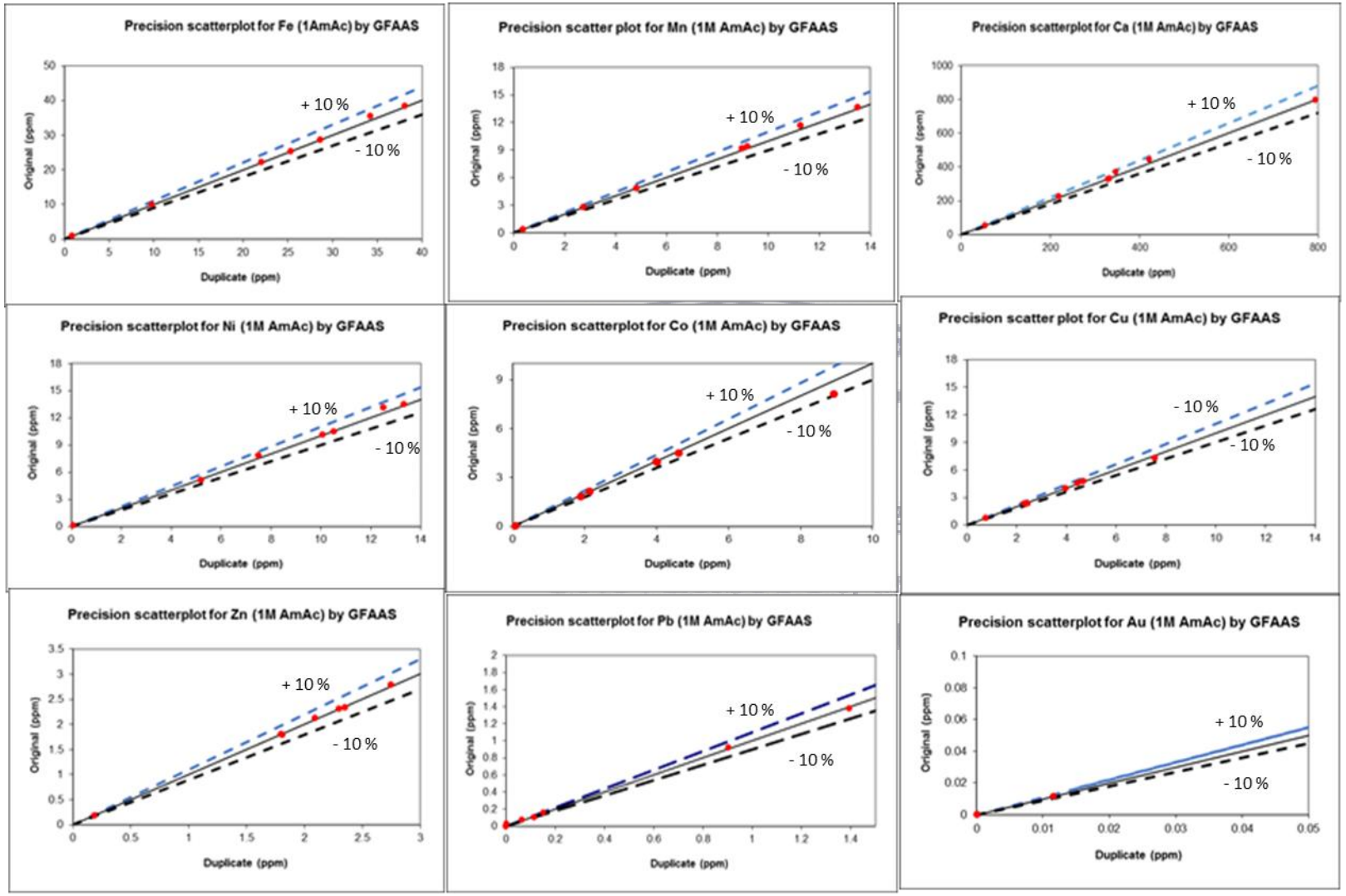

Precision scatterplots for 0.1 M hydroxylamine hydrochloride

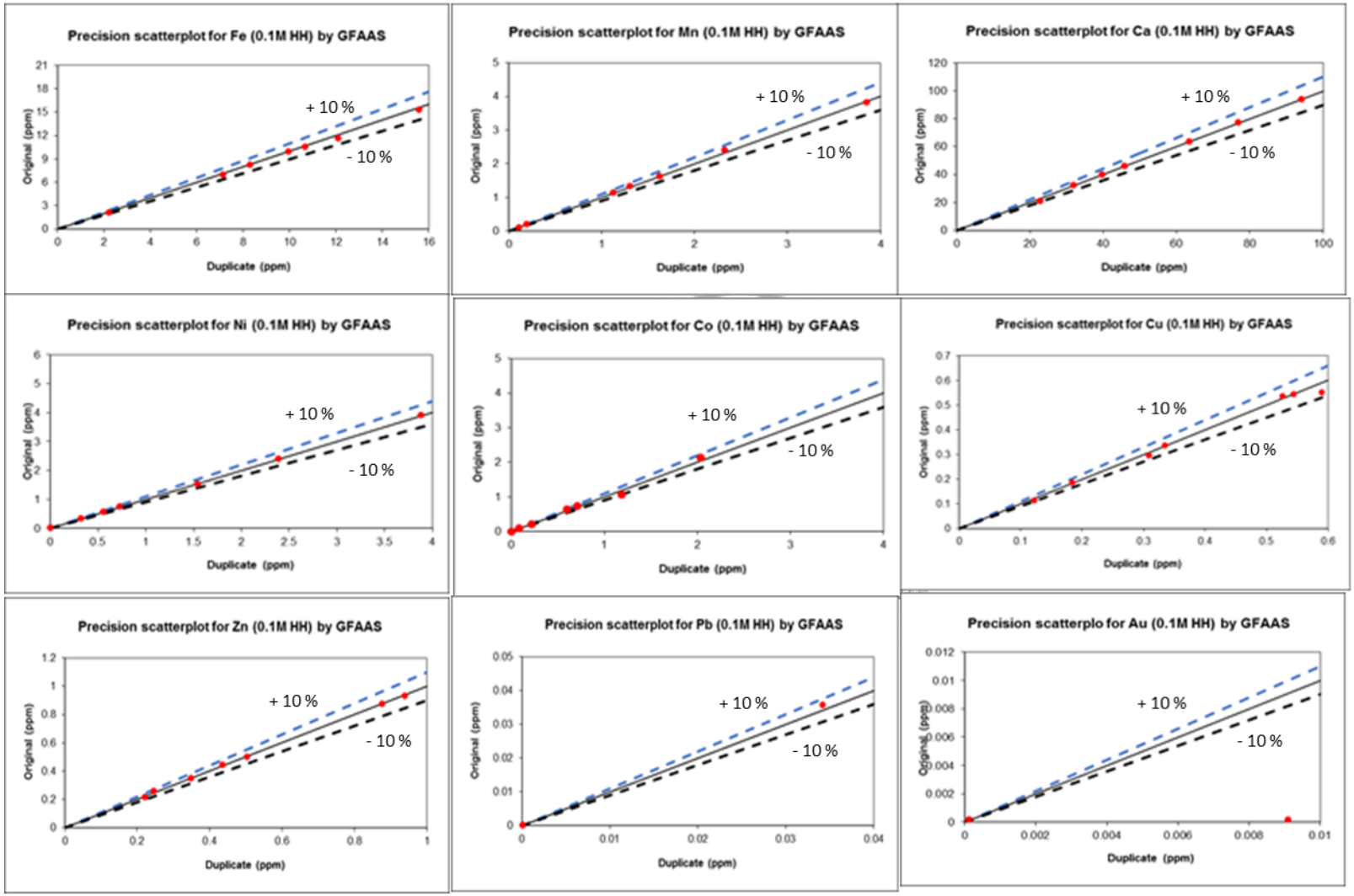

Precision scatterplots for 0.25 M hydroxylamine hydrochloride

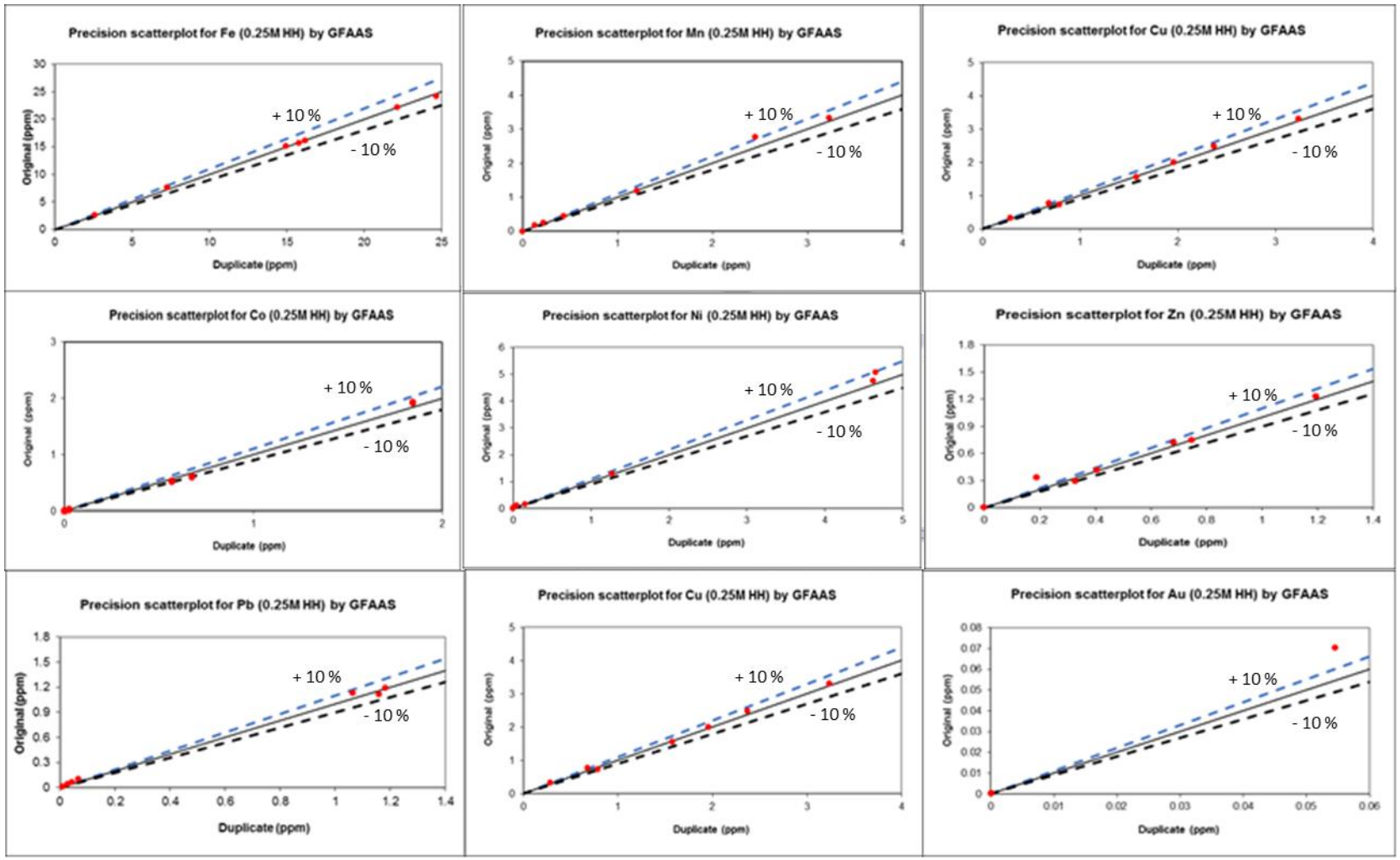

Appendix Two (D): Sequential extraction data

iii) Correlation coefficient analysis

Correlation coefficients for double distilled water, showing the relative association between extracTable Ca, Mn, Fe, Co, Ni, Cu, Zn, Au and Pb.

Element (ppm)	Ca	Mn	Fe	Co	Ni	Cu	Zn
Ca	1.00	0.05	-0.18	0.09	0.10	-0.04	0.12
Mn	0.05	1.00	0.26	0.93	0.93	0.65	0.88
Fe	-0.18	0.26	1.00	0.39	0.35	0.77	0.43
Co	0.09	0.93	0.39	1.00	0.98	0.81	0.87
Ni	0.10	0.93	0.35	0.98	1.00	0.77	0.88
Cu	-0.04	0.65	0.77	0.81	0.77	1.00	0.75
Zn	0.12	0.88	0.43	0.87	0.88	0.75	1.00

Correlation coefficients for 1 M ammonium acetate, showing the relative association between extracTable Ca, Mn, Fe, Co, Ni, Cu, Zn, Au and Pb.

Element (ppm)	Ca	Mn	Fe	Co	Ni	Cu	Zn	Au	Pb
Ca	1.00	0.59	0.51	0.54	0.57	0.34	0.76	0.07	0.07
Mn	0.59	1.00	0.24	0.73	0.74	0.38	0.74	0.10	0.10
Fe	0.51	0.24	1.00	0.47	0.41	0.25	0.23	0.23	0.23
Co	0.54	0.73	0.47	1.00	0.94	0.24	0.69	0.05	0.05
Ni	0.57	0.74	0.41	0.94	1.00	0.25	0.72	0.03	0.03
Cu	0.34	0.38	0.25	0.24	0.25	1.00	0.37	-0.07	-0.07
Zn	0.76	0.74	0.23	0.69	0.72	0.37	1.00	-0.05	-0.05
Au	0.07	0.10	0.23	0.05	0.03	-0.07	-0.05	1.00	1.00
Pb	0.07	0.10	0.23	0.05	0.03	-0.07	-0.05	1.00	1.00

Correlation coefficients for 0.1 M hydroxylamine hydrochloride, showing the relative association between extracTable Ca, Mn, Fe, Co, Ni, Cu, Zn, Au and Pb.

Element (ppm)	Ca	Mn	Fe	Co	Ni	Cu	Zn	Au	Pb
Ca	1.00	0.20	0.57	0.15	0.19	-0.12	0.40	-0.24	-0.24
Mn	0.20	1.00	0.46	0.71	0.70	0.31	0.46	-0.02	-0.02
Fe	0.57	0.46	1.00	0.60	0.62	0.35	0.68	-0.02	-0.02
Co	0.15	0.71	0.60	1.00	0.99	0.38	0.60	0.02	0.02
Ni	0.19	0.70	0.62	0.99	1.00	0.38	0.61	0.03	0.03
Cu	-0.12	0.31	0.35	0.38	0.38	1.00	0.32	0.45	0.45
Zn	0.40	0.46	0.68	0.60	0.61	0.32	1.00	-0.09	-0.09
Au	-0.24	-0.02	-0.02	0.02	0.03	0.45	-0.09	1.00	1.00
Pb	-0.24	-0.02	-0.02	0.02	0.03	0.45	-0.09	1.00	1.00

.

Correlation coefficients for 0.25 M hydroxylamine hydrochloride showing the relative association between extracTable Ca, Mn, Fe, Co, Ni, Cu, Zn, Au and Pb).

Element (ppm)	Ca	Mn	Fe	Co	Ni	Cu	Zn	Au	Pb
Ca	1.00	0.08	0.31	-0.05	0.05	0.05	-0.06	0.33	0.33
Mn	0.08	1.00	0.43	0.81	0.87	0.74	0.80	-0.06	-0.06
Fe	0.31	0.43	1.00	0.59	0.51	0.54	0.65	-0.13	-0.13
Co	-0.05	0.81	0.59	1.00	0.92	0.78	0.87	-0.20	-0.20
Ni	0.05	0.87	0.51	0.92	1.00	0.82	0.87	-0.07	-0.07
Cu	0.05	0.74	0.54	0.78	0.82	1.00	0.81	0.04	0.04
Zn	-0.06	0.80	0.65	0.87	0.87	0.81	1.00	-0.13	-0.13
Au	0.33	-0.06	-0.13	-0.20	-0.07	0.04	-0.13	1.00	1.00
Pb	0.33	-0.06	-0.13	-0.20	-0.07	0.04	-0.13	1.00	1.00

iv) Box and whisker plots

Box and whisker plots for double distilled water, showing the relative distribution ranges of Ca, Mn, Fe, Co, Ni, Cu, Zn, Au and Pb.

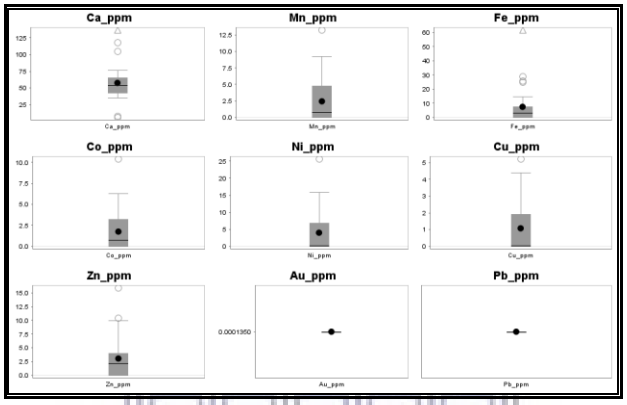

Box and whisker plots for 1 M ammonium acetate, showing the relative distribution ranges of Ca, Mn, Fe, Co, Ni, Cu, Zn, Au and Pb.

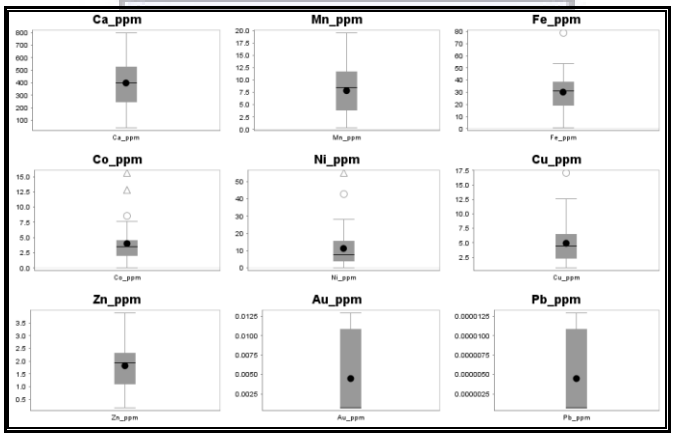

Box and whisker plots for 0.1 M hydroxylamine hydrochloride, showing the relative distribution ranges of Ca, Mn, Fe, Co, Ni, Cu, Zn, Au and Pb.

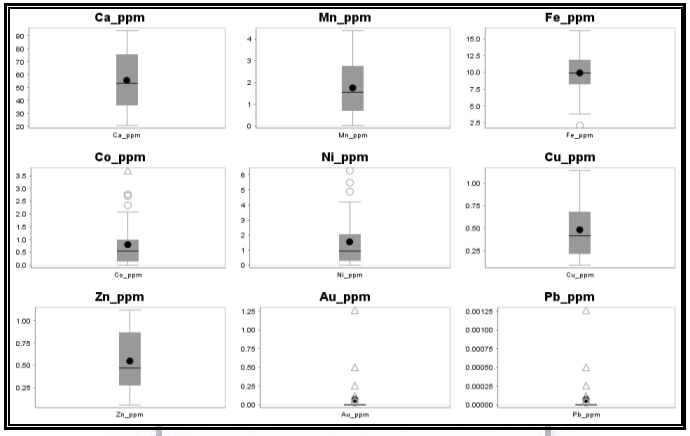

Box and whisker plots for 0.25 M hydroxylamine hydrochloride, showing the relative distribution ranges of Ca, Mn, Fe, Co, Ni, Cu, Zn, Au and Pb.

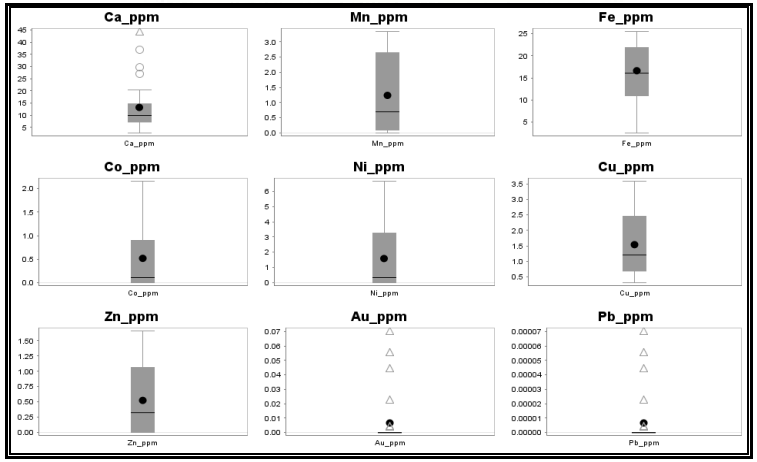

v) Principal Component statistics

The seven eigenvectors and the element correlation trends for double distilled water.

Eigenvectors	PC1	PC2	PC3	PC4	PC5	PC6	PC7
Ca	-0.10	0.98	-0.14	0.07	0.06	0.01	0.06
Mn	0.41	-0.01	-0.27	-0.22	0.68	-0.49	-0.03
Fe	0.38	0.12	0.78	0.08	0.34	0.32	0.00
Co	0.41	-0.01	-0.44	0.24	0.00	0.51	-0.57
Ni	0.42	-0.02	-0.27	-0.18	-0.14	0.35	0.76
Cu	0.40	0.02	0.07	0.70	-0.33	-0.47	0.12
Zn	0.40	0.16	0.16	-0.60	-0.54	-0.22	-0.29

Eigenvectors and corresponding eigenvalues (variance) in percentage and cumulative percentage for double distilled water.

	Eigenvalues	Percent	Cumulative %
PC1	5.41	77.34	77.34
PC2	0.98	13.94	91.27
PC3	0.28	4.03	95.30
PC4	0.22	3.11	98.41
PC5	0.07	0.97	99.38
PC6	0.03	0.40	99.78
PC7	0.02	0.22	100.00

The seven eigenvectors and the element correlation trends for 1 M ammonium acetate.

Eigenvectors	PC1	PC2	PC3	PC4	PC5	PC6	PC7
Ca	0.39	-0.21	0.03	-0.70	-0.01	0.55	-0.11
Mn	0.41	0.23	-0.24	0.09	0.84	-0.06	0.04
Fe	0.26	-0.59	0.65	0.06	0.18	-0.34	0.11
Co	0.43	0.23	0.23	0.37	-0.21	0.10	-0.72
Ni	0.44	0.27	0.16	0.30	-0.28	0.29	0.68
Cu	0.23	-0.63	-0.62	0.37	-0.15	0.09	-0.01
Zn	0.42	0.16	-0.26	-0.37	-0.34	-0.69	0.04

Eigenvectors and corresponding eigenvalues (variance) in percentage and cumulative percentage for 1 M ammonium acetate.

	Eigenvalues	Percent	Cumulative %
PC1	4.22	60.32	60.32
PC2	0.92	13.15	73.47
PC3	0.87	12.46	85.93
PC4	0.56	8.02	93.95
PC5	0.25	3.56	97.51
PC6	0.12	1.74	99.24
PC7	0.05	0.76	100.00

The seven eigenvectors and the element correlation trends for 0.1 M hydroxylamine hydrochloride

Eigenvectors	PC1	PC2	PC3	PC4	PC5	PC6	PC7
Ca	0.19	0.76	-0.16	-0.33	0.42	0.27	-0.03
Mn	0.44	0.00	0.19	-0.34	0.12	-0.80	0.02
Fe	0.41	0.25	-0.28	-0.07	-0.83	0.07	0.00
Co	0.44	-0.22	0.37	-0.02	0.06	0.33	-0.71
Ni	0.45	-0.20	0.35	-0.03	0.08	0.38	0.70
Cu	0.23	-0.51	-0.74	-0.27	0.24	0.10	-0.01
Zn	0.39	0.15	-0.23	0.84	0.23	-0.16	0.01

Eigenvectors and corresponding eigenvalues (variance) in percentage and cumulative percentage for 0.1 M hydroxylamine hydrochloride.

	Eigenvalues	Percent	Cumulative %
PC1	4.14	59.18	59.18
PC2	1.26	18.04	77.21
PC3	0.74	10.58	87.80
PC4	0.43	6.11	93.90
PC5	0.25	3.51	97.41
PC6	0.17	2.40	99.81
PC7	0.01	0.19	100.00

Seven eigenvectors and the element correlation trends for 0.25 M hydroxylamine hydrochloride

Eigenvectors	PC1	PC2	PC3	PC4	PC5	PC6	PC7
Ca	0.03	-0.90	0.38	0.05	0.02	-0.22	0.04
Mn	0.44	0.00	0.22	0.14	0.35	0.41	-0.67
Fe	0.31	-0.40	-0.81	-0.04	-0.09	0.26	0.04
Co	0.42	0.12	-0.01	0.36	-0.63	-0.46	-0.25
Ni	0.43	0.08	0.31	0.29	-0.11	0.44	0.65
Cu	0.40	0.04	0.19	-0.87	-0.21	-0.03	0.01
Zn	0.43	0.12	-0.14	0.04	0.65	-0.55	0.24

Eigenvectors and corresponding eigenvalues (variance) in percentage and cumulative percentage for 0.25 M hydroxylamine hydrochloride

	Eigenvalues	Percent	Cumulative %
PC1	4.88	69.76	69.76
PC2	1.15	16.39	86.15
PC3	0.50	7.14	93.29
PC4	0.25	3.52	96.81
PC5	0.13	1.92	98.73
PC6	0.07	0.98	99.70
PC7	0.02	0.30	100.00

(vi) The graphite furnace (Analytik Jena) parameters

	Ca	Fe	Mn	Ni	Co	Cu	Zn	Pb	Au
Tube Type	wall	platform	platform	platform	platform	platform	platform	platform	platform
Pyrolysis Temperature (°C)	1200	1100	1200	1050	1200	1100	300	800	800
Atomization Temperature (°C)	2550	2000	2000	2300	2100	2000	1300	1500	2000
Ramp Rate for Atomization (°C)	1500	1500	1500	1500	1500	1500	1500	1500	1500